University of Canterbury

Department of Civil and Natural Resources Engineering

Identification of Cost-Effective Retrofit and/or Rehabilitation Strategies for Steel Buildings

ENEQ690 Thesis

Thesis for Master's Degree

Candidate:

Fransiscus Asisi Arifin

91631731

Supervisors:

Associate Professor Timothy J. Sullivan

Associate Professor Gregory A. MacRae

Earthquake Engineering Programme

University of Canterbury

Christchurch, New Zealand

2017

Abstract

Recently developed performance-based earthquake engineering framework, such as one provided by PEER (Deierlein et al. 2003), assist in the quantification in terms of performance such as casualty, monetary losses and downtime. This opens up the opportunity to identify cost-effective retrofit/rehabilitation strategies by comparing upfront costs associated with retrofit with the repair costs that can be expected over time. This loss assessment can be strengthened by learning from recent earthquakes, such as the 2010 Canterbury and 2016 Kaikoura earthquakes.

In order to investigate which types of retrofit/rehabilitation strategies may be most cost-effective, a case study building was chosen for this research. The Pacific Tower, a 22-storey EBF apartment located within the Christchurch central business district (CBD), was damaged and repaired during the 2010 Canterbury earthquake series. As such, by taking hazard levels accordingly (i.e. to correspond to the Christchurch CBD), modelling and analysing the structure, and considering the vulnerability and repair costs of its different components, it is possible to predict the expected losses of the aforementioned building. Using this information, cost-effective retrofit/rehabilitation strategy can be determined.

This research found that more often than not, it would be beneficial to improve the performance of valuable non-structural components, such as partitions. Although it is true that improving such elements will increase the initial costs, over time, the benefits gained from reduced losses should be expected to overcome the initial costs.

Aftershocks do increase the predicted losses of a building even in lower intensities due to the fact that non-structural components can get damaged at such low intensities. By comparing losses computed with and without consideration of aftershocks for a range of historical earthquakes, it was found

that the ratio between losses due to main shock with aftershocks to the losses due to the main shock only tended to increase with increasing main shock magnitude. This may be due to the fact that larger magnitude earthquakes tend to generate larger magnitude aftershocks and as those aftershocks happen within a region around the main shock, they are more likely to cause intense shaking and additional damage. In addition to this observation, it was observed that the most significant component of loss of the case study building was the non-structural partition walls.

Keywords: PEER-PBEE, loss estimation, retrofit or rehabilitation, steel buildings, aftershocks.

Acknowledgements

Firstly, I would like to thank my professors, Tim Sullivan and Greg MacRae, for having agreed to be my supervisors for this research and giving lots of feedback and guidance throughout my research. They lead the way on my research and helped me a lot along the way. Without their teaching and patience, I would have never completed this research and thesis. I have learned a lot during my study and research from both of them, especially on performance based design.

Secondly, to my sponsor, Lembaga Pengelola Dana Pendidkan, for giving me the opportunity to study here in the University of Canterbury, one of the best universities in the world. Through this Indonesian Government scholarship, I was able to complete my studies, albeit extended for a short period of time. Not only did they cover my studies here, they also provided me with moral support throughout the thesis and research.

This research is part of the smart earthquake engineering retrofit (SMERET) Project in collaboration with Disaster Prevention Research Institute, Kyoto University. As such, I would like to acknowledge them for giving me this amazing opportunity to work on this project. Especially Professor Kurata from Kyoto University for his help and guidance throughout my research, particularly during my stay in Japan. He gave me a lot of suggestions and ideas to think about regarding the differences of design in Japan and New Zealand which opened my thoughts.

I wish to give a special thanks to Tadahisa Takeda, my research partner on the SMERET Project, who became one of my best friends. He took a really good care of me during my stay in Japan as I was collecting data for this research and gave me lots of moral support during my research. He also assisted me during my research in providing translations for Japanese papers and books.

Without his aid, I would not have gained as much experience as I have at this point.

I would like to acknowledge Sean Gardiner, a calibre engineer who provided valuable information on the Pacific Tower and its performance during the 2010 Canterbury Earthquakes and on the costing of EBF repairs. This information helped this research reach its goals.

A special mention to Trevor Yeow for supplying me with the ground motions selected to represent the hazard level of Christchurch central business district. Thank you for your help in this research.

Special thanks also to my mother, Lilianny Arifin, father, John Arifin and sister, Maria Arifin for supporting me throughout this master's degree. Because without their help, prayer and support, I will never be where I am today. Thanks Mom and Dad.

I would also like to thank my friends and colleagues, Gerry Tirtawidjaja, Tim Sibaev, Jainesh Prasad, Amir Rezanejad, Amir Orumiyehei, Helmy Hermawan, Boney Bun, Rendy Putra, Emir Hartato, Danny Hermawan, Pien Schutte, Lei Zhang, Angella Jusuf, Stephani Devina and others that I cannot mention one by one for their help during my study here in University of Canterbury.

Last but not least, I would like to mention the administration staff here at the University of Canterbury, Elizabeth Ackermann and Leigh Davidson for helping me ease my study and research.

Table of Contents

Table of Figures

Table of Tables

1. Introduction

1.1. Background

During an earthquake, the ground motion can cause damage to structural and/or non-structural elements. A very intense shaking event may even cause collapse of the structure. Such disastrous events can be mitigated by construction in accordance with seismic codes that prepare structures for earthquakes using various processes and designs. However, even though a structure may be designed in compliance with codes, the after effects of the earthquake, such as the cost to repair the damaged structure, may still be a big issue (Poland et al. 1995). Therefore, structural designs should not only consider the seismic codes' life safety objective but also the cost-efficiency of the building regarding seismic risk. Furthermore, traditional structural analysis results, such as an element's inner forces and deformations, are not direct indicators of performance and tend to be hard to interpret, sometimes even misunderstood. Hence, expressing performance in terms of monetary losses may assist with the communication of seismic risk.

One approach that attempts to enable the quantification of alternative performance measures, such as monetary losses and downtime, is the Pacific Earthquake Engineering Research Performance-Based Earthquake Engineering (PEER-PBEE) framework (Deierlein et al. 2003), explained in section 2.1. The PEER-PBEE framework aims to utilize a complete assessment process to quantify alternative performance measures with adequate treatment of uncertainties. A disadvantage of the PEER-PBEE process is the amount of time it consumes compared to current "traditional" practice. Furthermore, not all structures, both past and present constructions, were constructed with PEER-PBEE considerations. This results in many existing buildings adopting less cost-effective seismic design and retrofit strategies and thus being susceptible to more losses.

Even though a rigorous application of the PEER-PBEE framework is time consuming, currently there are various tools to simplify the rigorous PEER-PBEE process. Software, such as Performance Assessment Calculation Tool (PACT), shown in Figure 1.1, from FEMA P-58.3, can speed up the building performance calculations.

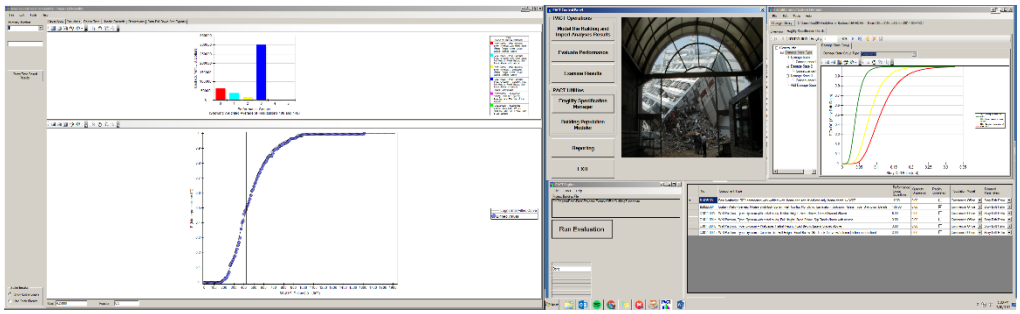

Figure 1.1. Performance Assessment Calculation Tool (FEMA P-58.3)

Other simplified approaches have also been proposed in recent years (Bradley et al. 2008; Porter & Beck 2004; Welch et al. 2014; Zareian & Krawinkler 2006) and as such, it is expected that the feasibility of evaluating expected monetary losses in practice will continue to improve.

As the ability for engineers to estimate likely monetary losses improves, this opens up the possibility of identifying cost-effective retrofit and/or rehabilitation strategies. This is the subject of this research, which specifically investigates the case of steel framed office (or mixed-use) buildings typical of New Zealand construction practice. This research endeavours to benefit from recent observations about seismic performance in both the Canterbury and Kaikoura earthquakes.

1.2. Objectives

This research investigates the cost-efficiency of different retrofit and rehabilitation strategies for steel-framed buildings considering seismic risk in terms of expected annual loss (EAL). Therefore, the main objective of this research is to:

"Identify cost-effective retrofit and/or rehabilitation strategies for typical steel office buildings in New Zealand"

A key aspect of this research is to assess the potential impact of aftershocks (AS) when selecting effective retrofit or rehabilitation strategies. This is motivated by the observations (reported in discussions with local engineers) of repeated damage to non-structural elements observed in buildings following the Canterbury earthquakes.

To account for aftershocks, analyses is conducted in two phases. The first phase considers loss assessments without aftershocks (i.e. a "conventional" loss assessment procedure to give an EAL), and the second phase considers main shocks and aftershocks, explained in chapter 3.

2. Literature Review

2.1. Performance Based Earthquake Engineering

The Structural Engineers Association of California (1995) defined, in a Vision 2000 document, Performance-Based Earthquake Engineering as "consisting of the selection of design criteria, appropriate structural systems, layout, proportioning and detailing for a structure and its non-structural components and contents, and the assurance and control of construction quality and long-term maintenance, such that at specified levels of ground motion and with defined levels of reliability, the structure will not be damaged beyond certain limiting states or other usefulness limits". The Vision 2000 Project also stated that the achievement of performance objectives is never guaranteed but is expected. The earthquake performance levels defined in The Vision 2000 Project can be seen in Figure 2.1,

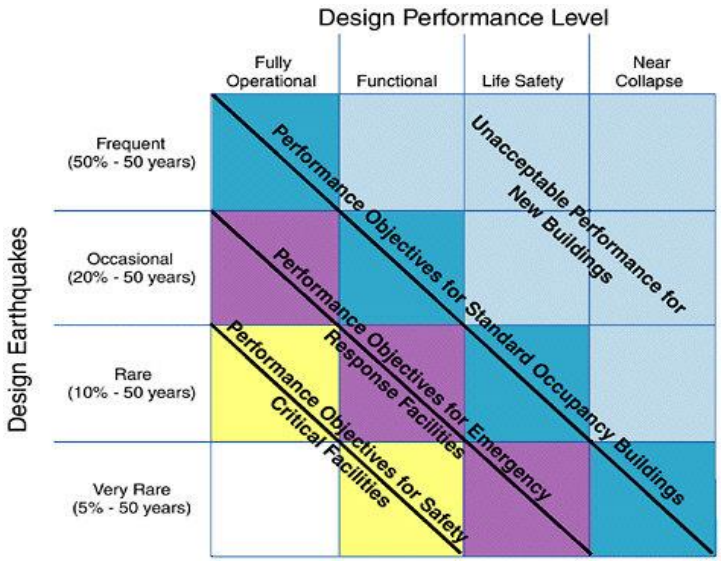

Figure 2.1. Earthquake Performance Levels (National Research Council 2003)

A shortcoming with the SEAOC PBEE approach in is that it is an approach that only considers a pre-determined performance level at a limited number of intensity levels, i.e. frequent, occasional, rare and very rare. Ideally,

seismic performance should be expressed in probabilistic terms since the performance levels are uncertain and intensity of shaking at a site during a given period is variable. Another drawback with the SEAOC vision is the difficulty in communicating global system performance as well as incorporating stakeholders in the decision process due to the binary type performance criteria (i.e. satisfies the code or not) (Porter 2003). Hence, a new version of PBEE developed by the Pacific Earthquake Engineering Research (PEER) Centre was proposed.

The PEER-PBEE (Deierlein et al. 2003) approach focuses on more universally understood parameters known as the 3 D's, which are Dollars, Deaths and Downtime. The framework of PEER-PBEE, seen in Figure 2.2, incorporates the use of a ground motion Intensity Measure (IM), such as the Mean Seismic Hazard Curve (McGuire et al. 2005), as a means of loading for non-linear computer analyses which will produce the Engineering Demand Parameters (EDP).

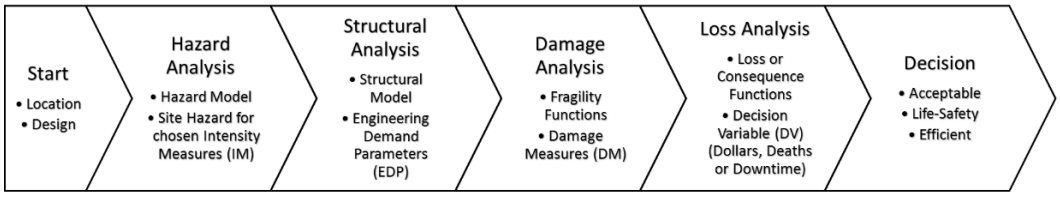

Figure 2.2. PEER-PBEE Framework

These EDPs are structural analysis results such as maximum inter-storey drifts and peak transient floor accelerations, which can be related to physical damage of structural and non-structural components known as Damage Measures (DM). The damage of a structure can then be categorized to damage states or other consequences (e.g. a panel with major cracks is categorized as Damage State 3), using fragility curves. These damage states will be linked with relevant decision variables (DVs) such as repair costs expected after a certain intensity earthquake. Relevant DVs might also be the expected downtime and deaths. Summing the integration of hazard analysis, damage analysis and loss

analysis of every structural and non-structural component results in an expected annual loss (EAL) which could be useful when deciding whether or not a structure should be retrofitted and/or rehabilitated. The definition of retrofit and rehabilitation is explained in section 2.4.

2.1.1. Hazard Analysis

This research does not cover the process of hazard analysis. However, it will use the hazard levels given for the Christchurch Central Business District. As a part of the hazard analysis, a set of ground motions are used for the structural analysis to represent the hazard.

There are various ground motion selection processes spanning from simple methods to rigorous and complex methods. The selection of ground motions is an important process in the dynamic analyses or assessment of structures. This is due to the fact that the structural site response, which is affected by the ground motions, is critical to the structural response and can create bias if not done properly. Hence, in order to avoid bias, a rigorous ground motion selection process is needed. Complex methods include the Mean Seismic Hazard Curve (McGuire et al. 2005), which accounts for the epistemic uncertainties by using logic trees and Probabilistic Seismic Hazard Analyses (Cornell 1968), see Figure 2.3 and Figure 2.4.

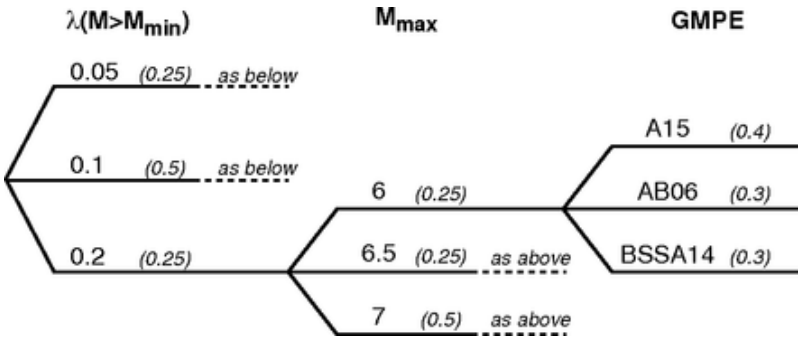

Figure 2.3. Logic Tree Example (Baker & Gupta 2016)

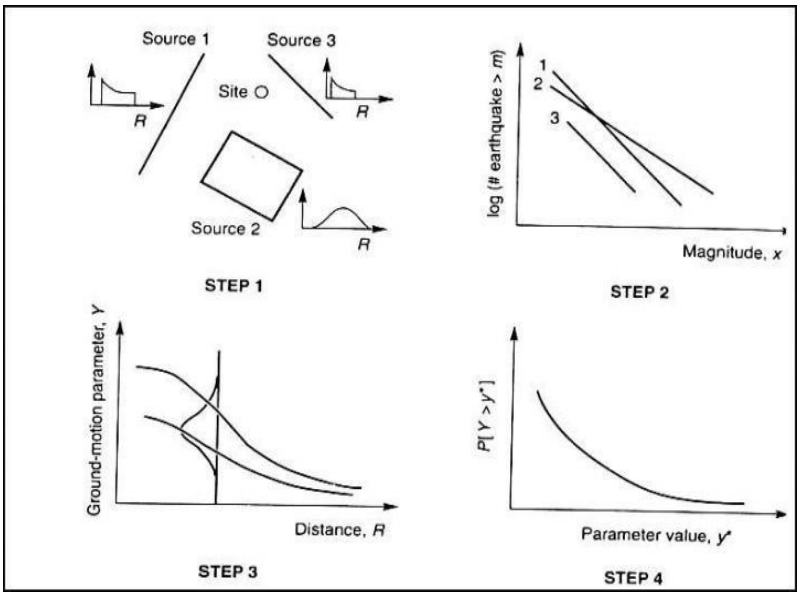

Figure 2.4. Probabilistic Seismic Hazard Analyses Process (Reiter 1991)

It is a fact that earthquakes are uncertain and thus seismic hazard is defined in terms of probabilities. This emphasizes the need for seismic risk of a structure nowadays to be defined in terms of probabilities as well. Ground motion selections that are compatible with Uniform Hazard Spectra (UHS) (McGuire 1995) have been popular in the past. However, the UHS has its limitations as it still creates bias for individual earthquake scenarios (Bommer et al. 2000; McGuire 1995; Naeim & Lew 1995). Besides UHS, another alternative for ground motion selection is the Conditional Mean Spectra (CMS), which is considered an improvement over the UHS. CMS derives its target spectrum for a target intensity measure at a given site with considerations for the corresponding magnitude, distance and *epsilon* values (Baker & Cornell 2006). This method, however, still poses a bias due to the fact that CMS only accounts for ground motion characteristics represented by spectral accelerations (Bradley 2010).

Hence, the Generalized Conditional Intensity Measure (GCIM) method, illustrated in Figure 2.5, was developed by Bradley (2010).

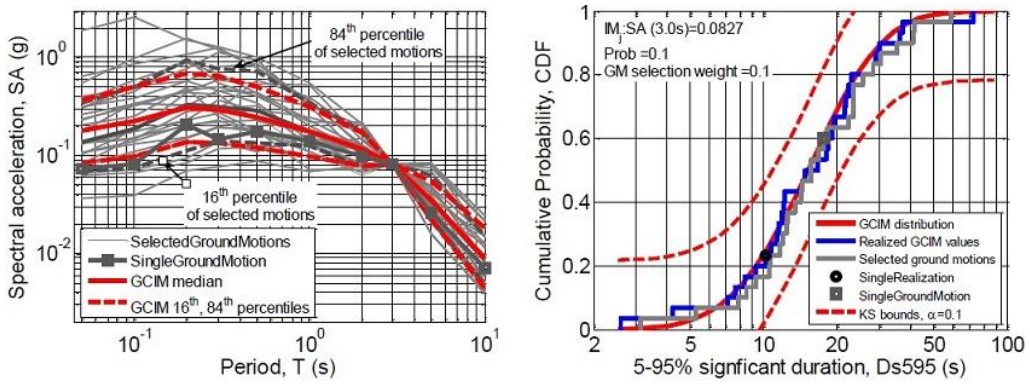

Figure 2.5. GCIM Illustration (Bradley 2010)

The GCIM selects ground motions that are compatible with a conditional multivariate distribution of an intensity measure given any other intensity measure ($IM_i = im_i$) (Bradley 2010). The selected scaled ground motions are then used as 'loads' which will represent the site response, thus representing a compatible loading to the structure. An example of this process can be seen in the paper by Yeow et al. (2016).

2.1.2. Structural Analysis

A structural model can be created as a detailed model with all non-structural elements and distributed loads defined by finite element models, such as discussed in Hanganu et al. (2002). However, the amount of time and expertise needed to analyse a detailed model is certainly larger compared to a simplified model. Hence, a simplified model is preferred as running a 3D analyses with a series of ground motions (multi-stripe non-linear response history analyses) is time consuming. A simplified model can contain only the main lateral load resisting frames, as discussed in Kappos et al. (2002) (Figure 2.6).

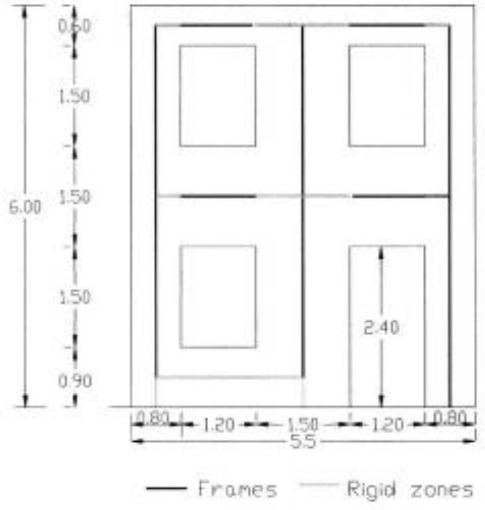

Figure 2.6. Example of a simplified lateral resisting frame model (Kappos et al. 2002)

Besides the structural model, the analyses themselves can be done as simplified elastic analyses (i.e. with initial stiffness and specified ductility capacity), such as response spectrum analyses, explained in Gupta (1992). However, using this method has shortcomings such as the discrepancies due to the use of displacement-equivalent assumption and the specification of ductility according to structural type only while it should also consider structural geometry and material properties (Priestley et al. 2007). For a simplified loss assessment, Welch et al. (2014) suggest that the structural analysis phase could instead be conducted using a displacement-based assessment procedure.

For PEER-PBEE, structural analysis results of interest are EDPs, for example peak transient floor acceleration and maximum inter-storey drifts. In order to obtain these parameters, the structural model should ideally have all relevant information, which would include the structural stiffness, seismic mass, inelastic structural behaviour or response during an earthquake as well as the performance of non-structural elements. To fulfil these requirements, the model needs to incorporate the floor masses (lumped or distributed) and structural elements that have inelastic properties as needed. Moreover, the model may also

need to be modelled in three dimensions if the structure is expected to twist or has irregular shapes.

Verifying a model can be done in many stages of creating the structural model. A few simple checks such as Modal Analysis and Model Integrity can be used during the modelling process. Some more advanced checks, such as comparing response predictions of experimental test specimens with test results, can also be used. However, owing to the time required and limited number of test specimens available, this approach is not commonly used.

Another option is to use recorded data from instrumented or observed buildings and compare this with predictions from analytical models. Due to the massive number of elements in real buildings, including non-structural elements, as well as given the uncertainty in foundation and soil behaviour, it is difficult to obtain exact results compared to the actual data from previous earthquakes. Hence, even though it is still a viable option, the verification via 'matching' damage patterns of a structure after a previous earthquake is often only used to gain some confidence that the response is at least similar (Lang et al. 2012).

2.1.3. Damage Analysis

The damage measure states the condition of the structural or non-structural elements of a building after an imposed demand (e.g. drift or acceleration). Nowadays, the design of structural elements allows for a controlled distribution of damage, e.g. designing mid-level beams to yield before columns, due to capacity design (Priestley & Paulay 1992). Hence, buildings are less-likely to be damaged to a state that it needs structural repairs. This is important to note because repairing a structural element is not an easy task due to inaccessibility and difficulty of repair (Newman 2001). Non-structural elements are more prone to damage, and while they may be easily

accessible and repairable to a certain extent, they tend to contribute most to earthquake losses (Bradley et al. 2008).

In order to analyse non-structural elements, different parameters need to be accounted for. This is due to the fact that non-structural elements respond differently compared to one another. For example, a window pane (facades) is sensitive to inter-storey drift, while a hanging ceiling is prone to floor accelerations. This results in the need for different engineering demand parameters to gauge the likely performance of different elements. Fortunately, since the mass of non-structural elements are typically much smaller compared to structural elements, one option is to post-process the structural analysis results to evaluate the likely response of non-structural elements (i.e. a cascade type of analysis).

Assessing non-structural elements is also difficult due to the variety of non-structural elements and the demands they are sensitive to. Hence, options such as the use of visual indicators (Baird et al. 2011) shown in Figure 2.7., may be used.

Figure 2.7. Visual Indicators of Damage States (Baird et al. 2011)

The damage states defined can be related to the cost of repair which is an important decision value (Deierlein et al. 2003). For a simple deterministic example, first take a case of a partition wall that suffers visible major cracks and connection damage, classified as damage state 3. This type of damage requires

a total replacement of the partition walls. This damage state certainly has its own rehabilitation procedures (i.e. total replacement) which comes with the cost and time to rehabilitate it. Secondly, take the same case of the partition wall but assume the partition wall had been retrofitted (i.e. improved). The damage probably would not have reached damage state 3, say damage state 2: minor cracks, which only require the replacement of the gypsum boards. This would not cost as much to rehabilitate compared to the first case. However, the retrofit process has an initial installation cost. As such, the sum of all costs to retrofit to reduce the damage, including the implementation costs, and repair costs to rehabilitate the damage post-earthquake should be considered to make a decision (DV) as part of a cost-benefit analysis.

The PEER-PBEE loss estimation process is a probabilistic procedure. Hence, the loads, damage states and costs are expressed in probabilistic terms. The loads incorporate probability by the use of Probabilistic Seismic Hazard Analysis (PSHA) as mentioned in section 2.1.1. While for damage states, engineering demand parameters (EDPs) and a random sampling of probabilities are used to sample the probabilities of certain damage states via fragility curves such as those shown in Figure 2.8, (from Lupoi et al. (2006)).

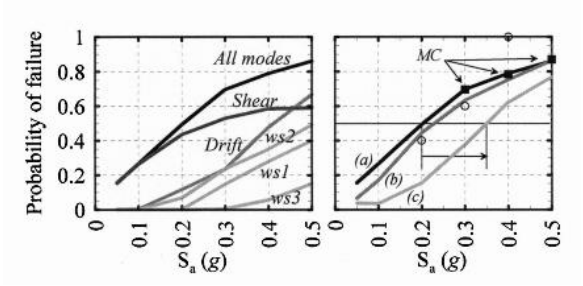

Figure 2.8. Fragility Curves Example (Lupoi et al. 2006)

2.1.4. Loss Analysis

Damage states obtained from fragility curves can be translated to losses via consequence functions with a range of possible losses for a given damage state, i.e. it needs to be treated via a probabilistic method. Another option is to

use deterministic costs for certain damage states as mentioned in Mitrani-Reiser (2007). There are a number of papers on the cost of structural and non-structural damage cost such as interior partitions and exterior glazing discussed in Mitrani-Reiser (2007), ceilings (Paganotti et al. 2011) as well as computers and printers (office components) discussed in Buchan (2007).

For each case of analysis, a ground motion with a chosen intensity level is used as a load for the structural analysis. From the engineering demand parameters that are generated by this analyses, a random sampling of probability is used to obtain a damage state which can be translated to losses via consequence functions or deterministic values. The cost from each case can be summed up (by integration) to calculate the expected annual loss (EAL) of all cases, which can be used to make a decision either to retrofit a structure and/or rehabilitate it (Bradley et al. 2008). An example of EDP to damage state and damage state to repair cost curves is shown in Figure 2.9.

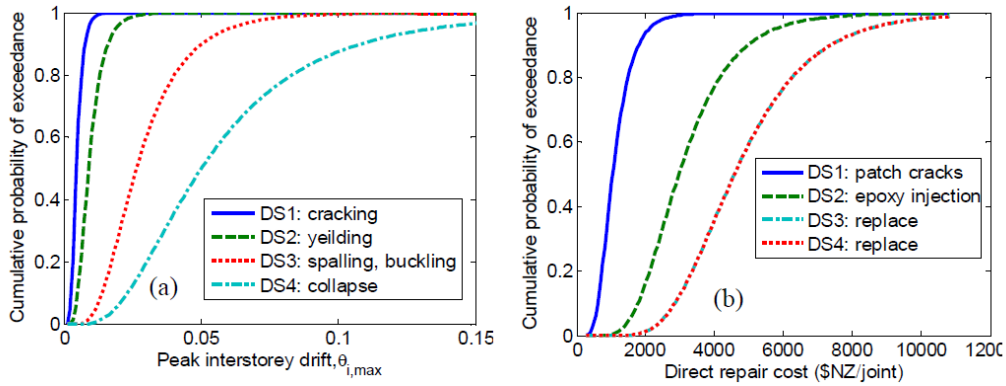

Figure 2.9. Seismic Loss Estimation Process Example (Bradley et al. 2008)

2.1.5. Previous Studies of Relevance

The development of PBEE in the past few years can be summarized as the PEER methodology as stated by Porter (2003). In this work, Porter underlines the importance of performance based earthquake engineering as well as showing a few issues that still arise with the PEER-PBEE. This includes the

uncertainty in intensity measures used as well as the number of structural analyses needed.

In 2006, a paper by Bommer and Crowley (2006) states the significance of incorporating uncertainties such as seismicity input and vulnerability characteristics of the building. The work suggests to use Monte-Carlo simulations (MCS) to simulate the magnitude-location scenario occurrences. Another interesting point that this work raises is the difficulty to validate loss models by comparing predicted and actual damage or loss.

The work by Mitrani-Reiser (2007) shows the importance of a performance based analysis by developing and implementing an analytical approach for PBEE to a new reinforced-concrete moment-frame office building. This work also shows both direct (repair costs) and indirect losses (downtime and deaths) as well as a simplified methodology to estimate building downtime in the aftermath of an earthquake.

Another work that stresses the importance of PBEE is the work by Bradley et al. (2008). This paper shows the role of PBEE in efficient decision making for stakeholders by quantifying the risk of a specific site. An example of this process was shown and the benefits of the method, such as consistent communication and rational decision making, was presented. An interesting point in that work is that non-structural components and contents' monetary loss is significant. Moreover, the paper also shows an example of retrofit influence on the expected annual loss (EAL).

In terms of damage and loss analysis, the importance of fragility and loss functions cannot be neglected, as mentioned in section 2.1. Hence, to help with the objective of this research, a few relevant papers on this matter are mentioned here. The work on damage and loss analysis used for this research is mainly focused on recent works (Badillo-Almaraz et al. 2007; Davies et al. 2011; FEMA P-58.3 ; O'Reilly & Sullivan 2016) as well as New Zealand based works (Baird 2014; Buchan 2007; Dhakal et al. 2016; Paganotti et al. 2011) to ensure

the details, damages and costs represents structures which are also based in New Zealand, refer to section 3.2

Work by Dhakal et al. (2016) proposes simplified seismic loss functions for suspended ceilings and drywall partitions. This includes developing generalized loss functions for both typical New Zealand suspended ceilings and drywall partitions. The generalized loss functions are derived by analysing the distribution of ceilings and partitions in office areas. Using this distribution and previous works on ceiling and partition loss functions, such as partitions by Porter et al. (2001) and ceilings by Paganotti et al. (2011), a generalized loss function based on floor area was established. Finally, a few case studies were done for both ceilings and partitions to show that the generic loss functions accurately predicts actual loss to a certain level of significance, 90% confidence level for ceilings and less than 2% difference for partitions.

Another work that investigates partition fragilities is the one by Davies et al. (2011). In this work, analysis tools for modelling non-structural partition walls was developed. This included experimental testing of partition walls which resulted in a fragility database for different configurations of partition walls. Due to the rigorous experimental testing and similarity in detailing with common New Zealand practice, as presented in Figure 2.10, this work is considered suitable for this research. Furthermore, the fragility functions obtained from this work and the one from PACT FEMA P-58 compare relatively well with one another.

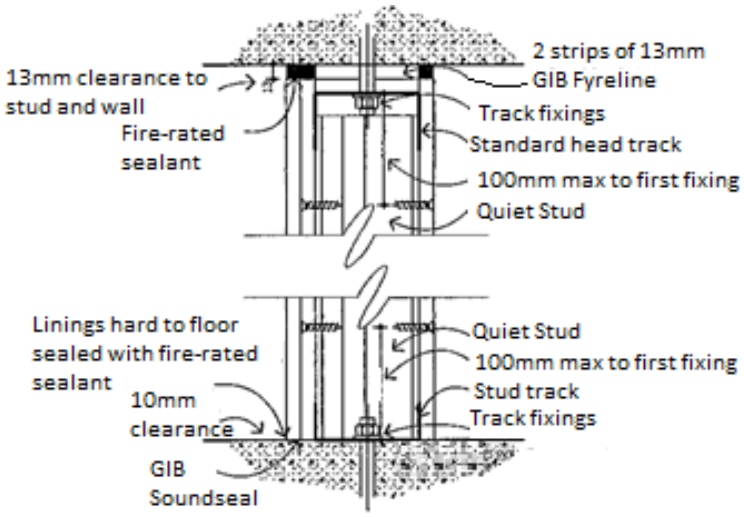

Figure 2.10. Common New Zealand Partition Fixing (taken from Christchurch City Council (2016a))

For claddings, Baird (2014) undertook work relevant to New Zealand. Fragility and loss functions for a few types of cladding panels and their connections were developed by experimental work. However, the cladding connections were not compatible with the connections found in the case study building (explained in section 3.2) examined in this research. Hence, another approach will be used to obtain fragility and loss functions for the cladding connection, explained in section 4.3.2.

Although an important focus of this research will be on non-structural elements, one could expect some damage in eccentrically braced frame (EBF) links. Therefore, fragility and loss functions for EBFs are also of interest to this research. Recent work on EBF fragilities to this extent is that by O'Reilly and Sullivan (2016). The main advantage of this work is the fact that it proposes the use of inter-storey drift as an engineering demand parameter (EDP) instead of plastic chord rotations, which was previously used as EDPs for EBFs, since drifts are more common to be discussed in structural response as compared to plastic chord rotations. This paper developed a set of MATLAB (MathWorks 2005) codes to generate EBF fragility functions based on a few important

parameters such as storey height, link section size, link length and bay width. The level of uncertainty (i.e. dispersion) can be reduced the more information is known. Loss functions can instead be determined for EBFs from information on costs obtained from within PACT (FEMA P-58.3) itself and modifying the costs according to information from engineers and contractors, more details in section 4.3.7.

For other items, such as elevators, sprinklers and piping, fragility and loss functions available in PACT (FEMA P-58.3) are considered for this research, noting that these components are not expected to contribute significantly to losses.

2.2. Data Collection

The data collection process involves geographical surveys, site visits as well as literature reviews. With regard to the subject to interest of this research, the surveyed buildings are mostly steel structures.

2.2.1. Typical Office Buildings in New Zealand

A typical office or mixed use building in New Zealand is summarized as a 3 to 4 storey building with eccentrically braced frames as means of lateral support.

Historically, reinforced concrete structures have been preferred in New Zealand over steel structures due to cheap concrete aggregates and labour disputes with the steel construction industry in 1970. However, recently steel structures has increased in par with reinforced concrete / precast concrete structures (Clifton et al. 2011).

Table 2-1 summarizes a few buildings of significance in Christchurch that suffered the 2010 – 2011 Canterbury earthquakes. From these buildings, most concrete structures suffered more severe damage compared to steel structures. This is attributed to the fact that most steel structures were designed with the latest seismic provisions (Clifton et al. 2011). And from the steel structures, mostly use EBFs as lateral resisting system, which shows a trend towards the use of EBFs in future buildings. While there are a few mid to high-rise buildings such as the Pacific Tower and Club Tower, the majority of office buildings in Christchurch only have 3 to 4 floors.

Table 2-1. Summary of representative sample buildings in Christchurch area after the February 2011 earthquake (Canterbury Earthquakes Royal Commission 2011)

Name	Lateral Resisting System	Floors	Condition
Central Library Building	Reinforced concrete MRF	4	Demolished
Hotel Grand Chancellor	Reinforced concrete Shear Walls	26	Demolished
Christchurch Civic Building	Reinforced concrete MRF + Concrete Filled Steel for Extension	7	Open
Clarendon Tower	Reinforced concrete MRF	17	Demolished
Radio Network House	Reinforced concrete MRF	14	Demolished
Pyne Gould Corporation	Reinforced concrete Shear Walls	4	Collapsed
Forsyth Building	Reinforced concrete MRF	18	Collapsed
Police Tower	Reinforced concrete MRF	15	Demolished
Westpac Tower	Reinforced concrete MRF	13	To be demolished
Craig's Investment House Building	Reinforced concrete MRF	10	Unknown
Bradley Nuttal House Building	Reinforced concrete Shear Walls	7	Repairing
Novotel Christchurch Building	Reinforced concrete Shear Walls	14	Open
Oxford Apartments	Reinforced concrete Shear Walls	12	Closed
Westfield Shopping Mall Parking Garage	EBF	3	Open
Christchurch Hospital Carpark Building	EBF	3	Open
Pacific Tower	EBF & Steel MRF	22	To be repaired
Club Tower	EBF & Steel RF	12	Open
Christchurch Women's Hospital	EBF & Steel MRF	9	Open
BreakFree on Cashel Christchurch	CBF & Shear Walls	7	Open
161 Hereford Suites	Steel MRF	10	To be repaired

2.2.2. Typical Office Buildings in Japan

From discussion with researchers from Japan and literature reviews during a field study in Japan, a typical office building in Japan is summarized as a 3 to 4 storey office building with moment resisting frames as the primary lateral resisting system. A book published by the Japan Building Disaster Prevention Association (2011) shows a recommended structural plan for an office building in Japan, shown in Figure 2.11 and Figure 2.12.

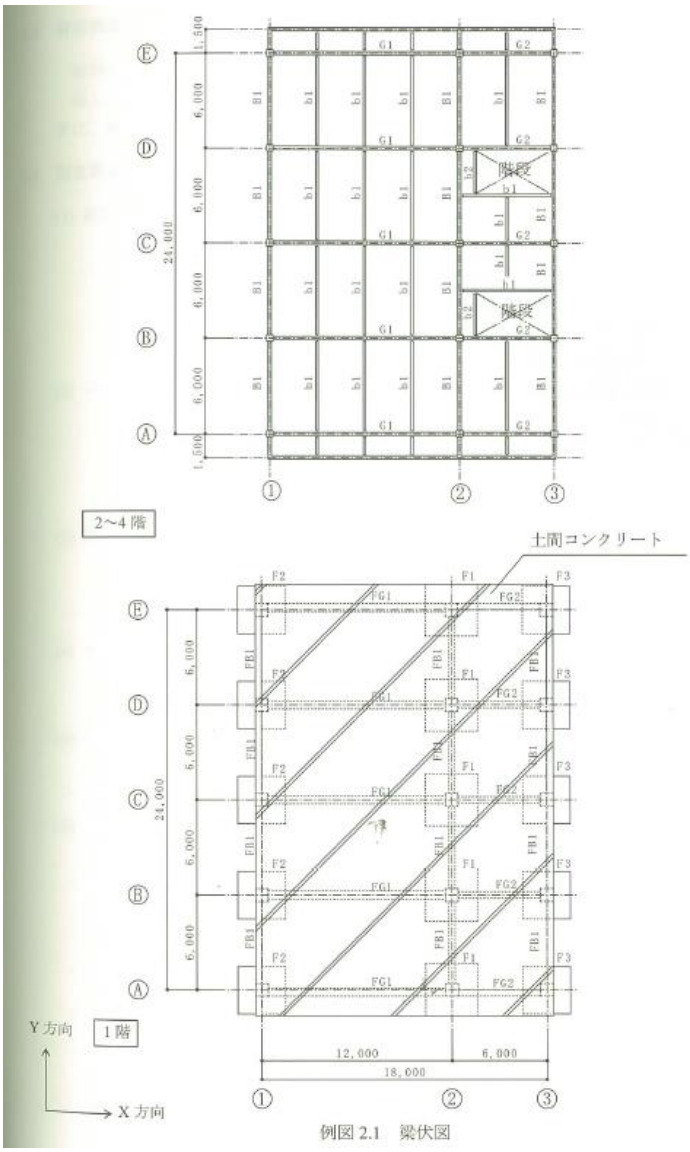

Figure 2.11. Typical Structural Plan for Office Buildings (Japan Building Disaster Prevention Association 2011)

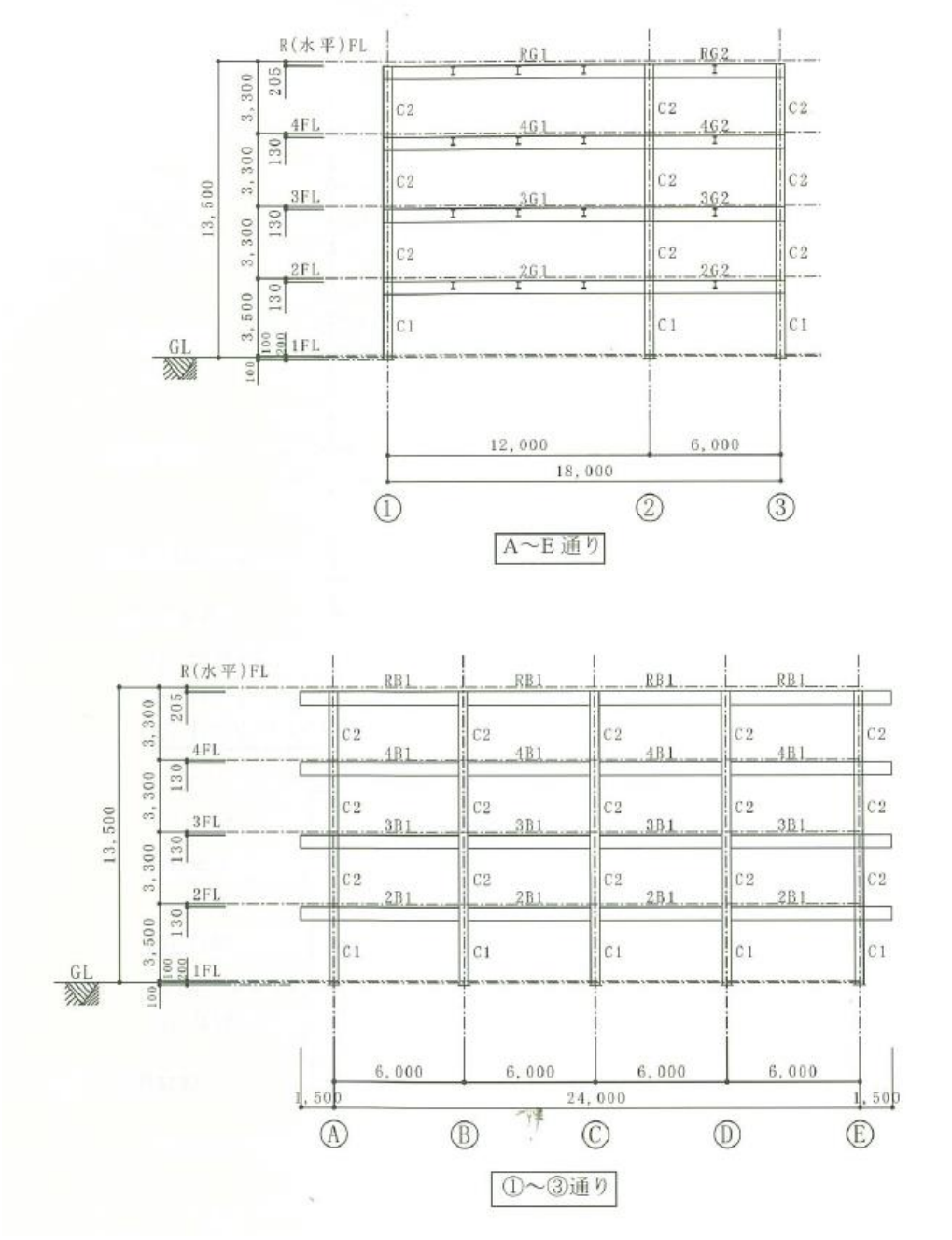

Figure 2.12. Typical Elevation Plan for Office Buildings (Japan Building Disaster Prevention Association 2011)

2.3. Comparison of Loss Estimation with Actual Data

Comparing analytical and experimental data in building seismic loss is not an easy task. Mainly, this is due to the fact that in order to obtain experimental data, an earthquake of different intensities should take place in the same site. Other difficulties include the availability and accuracy of fragilities developed, large uncertainties in the hazards and the availability of damage or loss reports on buildings that suffered from different intensity earthquakes.

2.3.1. Previous Studies on Comparing Loss Estimates

Not a lot of work has been done in comparing loss estimation with observed damage. A work by Spence et al. (2003) discusses this matter in the 1999 Kocaeli Earthquake in Turkey. This was possible due to the availability of several detailed damage surveys regarding the earthquake. The work underlined that currently, loss estimations tend to over predict the damages and suggests to use displacements approach as compared to intensity-based models. Another interesting point is the need of more instrumentation in buildings in order to carry more comparative studies as such.

Work by Lang et al. (2012) states the difficulties in doing this comparisons. This includes the availability and accuracy of vulnerability information and the uncertainties involving ground motion values.

2.4. Selection of Effective Strategies for Retrofit/Rehabilitation

In Newman's Structural Renovation of Buildings (Newman 2001), a retrofit is an upgrading of certain building systems, such as mechanical, electrical, or structural, to improve performance, function, or appearance. In the case of this study, the focus of retrofit is on the upgrade of non-structural elements to improve performance. While rehabilitation involves the 'repair' of a structure after damage has occurred but the word rehabilitation is used to recognize that a part of the structure that is damaged may not need to be repaired

as part of the rehabilitation strategy. Sometimes, another part of the structure can be strengthened or modified to account for the decrease of capacity or function of the damaged element.

There are a few retrofit or possibly rehabilitation strategies that can be used to modify a structure to meet the present needs of performance level, such as:

- Retrofitting a vulnerable component by increasing its strength and/or stiffness
- Rehabilitate by increasing strength and/or stiffness in a damaged component or other parts of the structure to account for the reduced capacity due to the damage;
- Retrofit by increasing deformation capacity of a vulnerable component;
- Retrofit or rehabilitate by reducing seismic demands via addition of energy dissipation devices or reducing seismic mass.

These retrofit/rehabilitation strategies are applied differently to different types of structures, e.g. steel frames, concrete frames or walls. Each type of structure has its own retrofit/rehabilitation techniques to apply these retrofit/rehabilitation strategies. For example, in a moment resisting concrete frame, retrofit techniques such as applying fibre reinforced polymer (FRP) wrappings to RC columns, as discussed in (Roy et al. 2009), can be used to increase its local deformation (displacement) capacity and strength. While for steel structures, modifications such as reinforcing by welding, creating a composite action or even thermal pre-stressing of steel structures can be done to increase the strength of the structure (Newman 2001). Another option is the use of a reduced beam section (RBS) to reduce the total mass of the structure hence, reducing the demands (Civjan et al. 2000). Non-structural elements can

also be retrofitted/rehabilitated to reduce the damage, such as anchoring the non-structural elements to a structural floor or wall or bracing the item to a structural element (FEMA 2011).

Each retrofit/rehabilitation strategy has its own advantages and disadvantages. For example, by reducing seismic demand on the structure, e.g. via base isolation, the structure will most likely not need further repairs in other parts even after the next earthquake. However, reducing the seismic demand can be costly and difficult to do in some structures. While increasing the strength of the elements can be less costly and easier to install, it may not be the best option for an unpredictable earthquake in the future. In conclusion, there are no "perfect" solutions to this matter, but there are cost effective solutions that are expected to be the most cost effective solution over the current situation.

2.4.1. Previous Studies on Effective Retrofit/Rehabilitation

Determining an effective retrofit/rehabilitation option requires a cost-benefit and life-cycle cost analysis. A work by Kappos and Dimitrakopoulos (2008) shows this matter with respect to pre-earthquake strengthening of buildings, i.e. retrofit, in South Europe. In this paper, Kappos and Dimitrakopoulos stated that the purpose of a cost-benefit and life-cycle analysis is to find two objectives. First, the economic feasibility of a retrofit/rehabilitation option and second, the optimal retrofit level for a given seismic risk.

As for rehabilitations, a Japanese paper by Fukuyama and Sugano (2000) shows the techniques for seismic rehabilitation of existing reinforced concrete buildings. The authors stressed the importance of seismic rehabilitation and discussed the aims of rehabilitation which are: i) to recover original structural performance; ii) to upgrade original structural performance; and iii) to reduce seismic response. The paper concludes that there are lots of rehabilitation options, and that selecting effective rehabilitation options may

differ on the required performance level, approach, type of building and occupancy as well as social demands for buildings to stay operational under the rehabilitation process. This is a "hard task and takes a long time to complete" as stated by Fukuyama and Sugano "However, it should be implemented to mitigate disaster due to future earthquakes".

Although selecting a seismic retrofit/rehabilitation technique through a cost-benefit and life-cycle cost analysis is well defined, there are still some uncertainties such as the location of the site which was discussed in Williams et al. (2009). As different locations poses a different annual probability of exceeding a certain performance level, hence also different effective retrofit/rehabilitation options.

Another issue in a cost-benefit and life-cycle cost analysis is the vulnerability of the building. As the building suffers from different earthquakes and undergoes retrofits/rehabilitations, the seismic performance of the building certainly changes. Hence, to simplify this matter, a full seismic performance repair is assumed, i.e. each repair or retrofit or rehabilitation will return the building to its previous state.

2.5. Aftershock Effects

An aftershock is broadly explained as an earthquake that occurs in a certain period of time as a result of previous large earthquake in the same area. Generally, an aftershock is of smaller intensity than the main shock. However, some aftershocks can still be damaging, or even more damaging than the main shock, to buildings.

One example of aftershocks being a main issue is the Canterbury Earthquake Series. The main shock that happened in September 2010 was of a moment magnitude of 7.1. It was followed by a major aftershock on the 22nd of February 2011 with a moment magnitude of 6.3. However, due to the location of the epicentre being closer to the central business district (CBD), this aftershock was more damaging towards Christchurch than the 2010 Darfield Earthquake.

2.5.1. Previous Studies on Aftershock Effects

Recently, improvement in seismic hazard analysis allows for the modelling of aftershocks. However, the addition of aftershocks in loss assessments is still a novel idea and not a lot of research has been focused on this topic. Based on Jalayer and Ebrahimian (2017), there are a few ways to incorporate aftershocks in seismic risk assessments, such as back-to-back method, real sequence and artificial sequence.

The Back-to-back method, as the name states, imposes a back-to-back main shock ground motion time history. This is done to estimate the residual capacity of the building as done by Luco et al. (2004). This approach unfortunately tends to over predict the damage to the building due to difference in frequency content between main shocks and aftershocks.

Real sequences uses historical records of main shocks and aftershocks as is. This eliminates the over prediction of damage from the back-to-back method. Such work on estimating demands via real sequences can be seen in Ruiz-García and Negrete-Manriquez (2011). This approach, however, still

poses a problem due to the fact that there is not enough data for a multi-stripe type of analysis with a suite of main shock – aftershock records of different intensities.

Hence, to overcome this problem, Goda and Taylor (2012) proposes the use of artificial sequences in order to obtain enough data. While the method does take into account the frequency of the aftershocks, the fact that 'creating' sequences introduces additional bias cannot be overlooked.

Besides the aftershock incorporation, the residual stiffness of the building post-earthquake or the new stiffness of the building post-retrofit/rehabilitation is also of an issue (Jalayer & Ebrahimian 2017). A number of studies on this matter are Iervolino (2017); Iervolino et al. (2014); Jeon et al. (2015); Li and Ellingwood (2007).

From the previous works, it can be summarized that the PBEE is an advanced method. Hence, it can be utilized as a framework for this research. However, the amount of work that focuses on retrofits with respect to the effect of aftershocks is still minimum. This is one of the key aspects of this research as explained in section 1.2.

3. Formulation of Research Questions

As explained in chapter 1, the objective of this research is to examine questions of cost-effective retrofit/rehabilitation of steel buildings. In this work, an important case study building, the Pacific Tower building, will be examined and used as a basis to test different possibilities. This is explained in detail in the next sections and chapters. It is also explained that the building was damaged in the 2010-2011 Canterbury earthquake series for which several ground motion recordings nearby the site were obtained.

3.1. General Performance of Steel Buildings in Canterbury Earthquakes

Over the decades, there have been a lot of earthquakes from small to large devastating magnitudes in New Zealand. In return, a variety of structural response were involved in those earthquakes. Some buildings suffered from minor damage, others may even collapsed. One of the earthquakes that is well documented is the 22 February 2011 Christchurch earthquake.

Note that, according to a report done by Clifton et al. (2011), the February 2011 earthquake in Christchurch was approximately 1.5 to 2 times the New Zealand ultimate limit state design spectrum over the period range of 0.5 to 4 seconds.

As expected, a lot of unreinforced masonry structures as well as a few of reinforced concrete structures collapsed. Almost all multi-storey structures suffered structural damage. Many parts of Christchurch also suffered from soil liquefaction.

The performance of steel structures was observed to be satisfactory. However, some structural damage still occurred. The Pacific Tower, a 22-storey-EBF steel structure, suffered from permanent deformations as well as a fractured link in the 6^{th} floor (Figure 3.1), some partition cracks and flaking of paint.

Figure 3.1. Fractured EBF Link (Clifton et al. 2011)

While the Club Tower, a 12-storey-EBF steel structure suffered from various yielding of braces as well as cracking of slabs, masonry infills and gypsum plaster boards. Besides the high-rise structures, the low-rise EBF structures, such as parking garages, also suffered from non-structural damage. The spandrel panels beside the epoxy mastic connection between panels fractured (Figure 3.2). Another low-rise building suffered from fractured links (Figure 3.3), paint flaking and excessive displacements at the top ramp expansion joint (Figure 3.4) (Clifton et al. 2011).

Figure 3.2. Fractured Spandrel Panels (Clifton et al. 2011)

Figure 3.3. Fractured Link of Parking Garage (Clifton et al. 2011)

Figure 3.4. Displacement of Expansion Joint (Clifton et al. 2011)

Overall, EBF steel structures performed quite well structurally in the Canterbury earthquake series due to the fact that most of them were quickly operational (Clifton et al. 2011). However, some links, such as the one on the 6th floor of the Pacific Tower, had to be replaced due to severe damage.

On the contrary, non-structural elements did not perform as well as the structural elements. Some ceilings were severely damaged, e.g. collapse of ceilings (Figure 3.5), others were moderately damaged, e.g. a few ceiling panels failed, and a few rare cases show little to no damage (Hogg et al. 2011). Besides ceilings, facades also suffered from damage (Figure 3.6). Although not as severe as ceilings, the damage is still significant to the loss due to downtime and repair costs (Baird et al. 2011).

Figure 3.5. Collapse of Ceiling (Hogg et al. 2011)

Figure 3.6. Disconnection of a Cladding (Baird et al. 2011)

The repairs/retrofits and/or rehabilitations done may not be the most cost-effective solution. Hence, this research is conducted in order to develop an identification for cost-effective retrofit/rehabilitation via suggested retrofit/ rehabilitation options through a PEER-PBEE assessment, explained in chapter 4. The cost-benefit analysis results of such structures will be useful for constructions and modifications in the future.

3.2. Description of Pacific Tower Building and Summary of Performance in Earthquakes

The Pacific Tower, a 22-storey EBF located at 166 Gloucester St. was one of the buildings that suffered from damage during the 2010-2011 earthquake series.

The building uses precast concrete cladding and lower levels are clad with stone tiles (EUROfox) on the north and west side. The south side is a reinforced concrete block wall parking building seismically separated from the tower. The floor construction is 150mm thick composite steel deck with comflor 80 supported on composite steel beams. The concrete slab uses H10-300 c/c reinforcements in both directions. The lateral supports of the structure consists of "tube-arranged" K and D shaped Eccentrically Braced Frames (EBFs) as well as Moment Resisting Frames (MRFs) for controlling torsional response. Due to the discontinuity of the lateral system, 3 transferring floor diaphragms (levels 2, 6 and 11) are designed to maintain the load path. The foundation consists of bored piles and steel screw piles (mostly for tension) connected by reinforced concrete foundation beams. For a more detailed explanation refer to section 4.1.

A report from the Christchurch City Council by CPG New Zealand Ltd. show that there were damage to exterior claddings mostly at the lower half of the building. Table 3-1 shows this damage summary accompanied with the drawings in Appendix C.

Table 3-1. Exterior Pacific Tower Damage Summary by CPG New Zealand, Ltd.

East Elevation	South Elevation	North Elevation	West Elevation
Level 15 Panel D-E	Repair Base of Antenna Mast	Level 10 Panel 2-4	Level 10 Panel B-C
Level 11 Panel D-E	Level 12 Panel 5-7	Level 9 Panel 2-4	Levels 1-6 Panel E-F
Level 9 Panel E-F	Level 9 Panel 5-7		
Level 6 Panel B-C	Level 8 Panel 3-5		
Level 5-6 Panel E-F	Level 7 Panel 5-7		
Level 5 Panel B-C			
Level 3 Panel B-C			
Level 2 Panel E-F			

From Table 3-1, it can be seen that most of the damage happened in the East-West direction and from levels 1 to 11/12 except for one panel at the East side. There is also a repair needed in the base of the antenna mast at the South side of the building.

A few other observed damages were also reported, such as ceilings, partitions and piping. These observed damage are summarized from the report and are as following,

- Stone claddings at the ground floor (podium) movement engaging the veneer ties, no damage was observed.

- Minor cracking in concrete panels as well as isolated spalling. Some of the concrete panels locked on to each other and needs to be separated.
- Some north-face balcony soffit linings fell off. Tiled junctions between balconies and precast cladding panels are also damaged due to pounding of the elements.
- Fire-rated GIB panels around the stairwell were damaged throughout the height of the structure.
- Cross-bracing of car stackers "unhooked" at mid-span and the columns of the car-stackers where not vertical due to residual displacement.
- Seismic flashings between the south reinforced masonry and the tower have been crushed most likely due to pounding. The exterior of the masonry block shell in the south podium also suffered from damage.
- Minor permanent displacement renders the lift un-operable at full speeds as well as minor damage at the lift landing areas.
- Cracked walls, ceilings, linings, tiles, glass doors and wardrobes in most rooms as well as the jamming of several doors.
- Base of antenna mast also suffered cracking.
- Moderate cracking of ground floor slab.
- North-east and North-west corner concrete panels suffered spalling.
- Residual deformation of less than 0.3% drift.
- Yielding and some minor permanent deformation of active links as well as one fractured link.
- Some top fixings of precast panels were damaged but not the lower fixings.
- Worst case permanent displacements are 66mm to the South relative to the base at around levels 11/12 returning to 38mm at level 18 and 50mm to the East relative to the base at around levels 11/12 returning to 25mm at level 19
- Two fly-brace connections (top panel fixings) at the east wall of level 2 were missing their anchors.

3.3. Scope of Research

In order to obtain the objectives of this research as mentioned in section 1.2, the scope of this research is limited to:

- Based on data collection and literature reviews, refer to section 2.2, a typical office steel structure in Japan is assumed to have steel Moment Resisting Frames (MRFs), while in New Zealand, Eccentrically Braced Frame (EBF) structures are mainly used as modern office buildings.
- The analyses used for loss assessment is a multi-stripe non-linear response history analyses (NLRHA) with 9 intensity measures, refer to section 4.2, and a scenario based analyses; using ground motions provided by others, either selected records using the GCIM approach (Bradley 2010) from the PEER Next Generation Attenuation (NGA) data, provided by Trevor Yeow, for the multi-stripe analyses and taken from strong-motion recordings close to the case study building for the scenario based analyses.

As for the aftershocks loss assessment mentioned in section 1.2, the second phase is done by,

- Using real recognizable sequences of previous earthquakes, such as Darfield 2010, Kaikoura 2016 and Kumamoto 2016.
- Using Strong Motion Stations (SMSs) around the earthquake epicentre that have approximately similar distance and soil conditions as well as being opposite of each other (e.g. North – South) as sites for the model building.
- The ground motions recorded in the SMSs, a loss assessment of the model building is done and the results are averaged. This is done to incorporate the uncertainty of the direction of the earthquake series into the loss assessment process.

- Using different main earthquake magnitudes and distances of SMSs, the losses for different intensities can be simulated, as shown in Figure 3.7, note that this is an example, and that neither the intensities nor losses are necessarily correct.
- The losses, both for MS only or MS + AS, for different intensities from phase two are plotted with a certain IM (e.g. PGA).
- The difference between the MS and the MS + AS losses is used to modify the loss curve obtained in phase one to compare the effects of aftershocks, as shown in Figure 3.8, note that this is an example, and that neither the intensities nor losses are necessarily correct.
- Note that when the retrofit/rehabilitation is applied as well as the duration for the retrofit/rehabilitation inherently a variable. Hence, the most efficient retrofit/rehabilitation can be obtained as a result of this "time" variable.

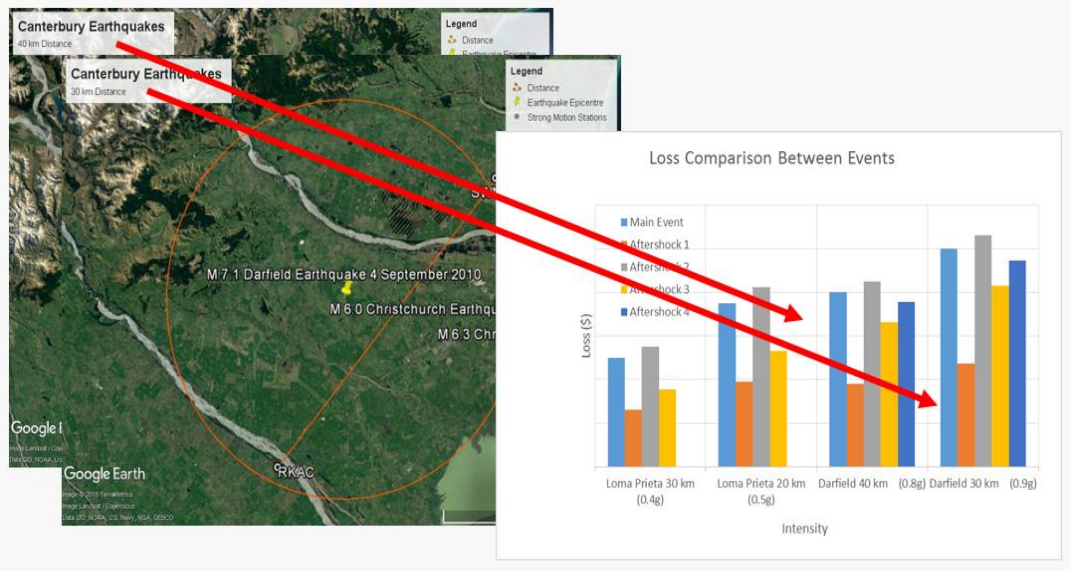

Figure 3.7. Losses for different intensities; example: 30km and 40km radius from Darfield event epicentre

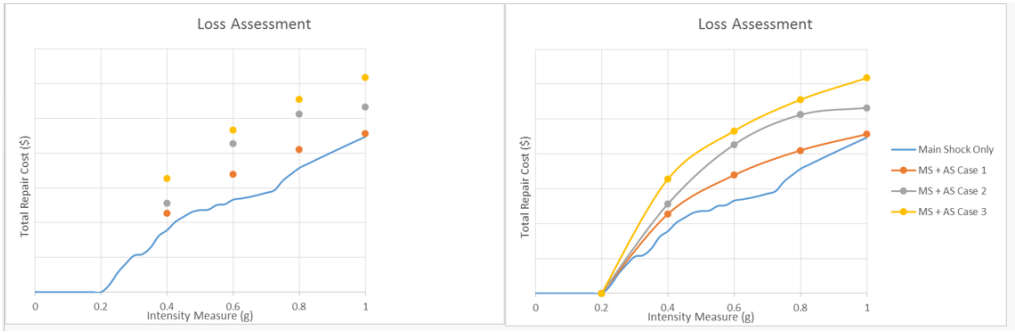

Figure 3.8. Modification of Expected Loss Example

There are certainly many options for retrofitting and/or rehabilitating structures. However, some options may not be suitable for steel structures or for the site location (i.e. Japan or New Zealand). Nevertheless, a list of retrofit/rehabilitation techniques for examination in this work are as follows:

1. Retrofitting/Rehabilitation of Non-Structural Elements
    a. Novel Sliding/Frictional Gypsum Partitions (Araya-Letelier & Miranda 2012);
    b. Exterior Cladding Connections.
2. Retrofitting/Rehabilitation of Structural Elements
    a. Viscous Fluid Dampers

3.4. Research Questions

With these objectives, scopes and limitations, this research attempts to answer the following questions

1. Can the loss on a specific New Zealand building for one specific earthquake be modelled?

* It is complicated to assess a building's earthquake performance due to the fact that there are many significant factors that influence the performance of a building, as evident by the discussion provided in section 2.3

2. What is the most sensitive component of loss?

* As discussed in section 3.1, the structural components are not expected to contribute largely to losses. Hence, the elements that contribute to the loss are mainly non-structural. Different non-structural elements are sensitive to different engineering demand parameters, and so it is expected that the most sensitive component of loss can depend on the type of ground motion that strikes the structure.

3. What is the most cost-efficient retrofit and rehabilitation option?

* As non-structural elements are likely to dominate losses, their retrofit or rehabilitation may be most cost-effective. Especially retrofit or rehabilitation to the elements that contribute the most to losses.

4. How do aftershocks impact the answers to the above?

* As discussed in sections 2.4 and 2.5. There are two main things aftershocks affects in terms of seismic assessments. First, the economic value of a retrofit/rehabilitation option, and second, the vulnerability of a building. The latter, however, is not considered in this research as an assumption of repair to full capacity after each event is taken. Hence, it is expected that the non-structural elements will still dominate losses. The interesting point will be 'when' the retrofit/rehabilitation should be applied.

4. PEER-PBEE of Pacific Tower Building

The structure, the Pacific Tower building, is modelled using the lateral systems only with lumped plasticity and is run through a multi-stripe NLRHA with selected ground motions. The obtained data, such as maximum inter-storey drifts and peak transient floor accelerations is run through damage measure-fragility curve analyses with PACT (FEMA P-58.3). This process is done in line with the PEER-PBEE process and, with given damage states, produces a decision variable of expected annual loss.

Prior to calculating the expected annual loss, this research seeks some level of verification of the tools available to obtain the Loss Estimation data. In order to obtain confidence that the structural models, analyses, damage and loss assessments of the PEER-PBEE approach are reasonable, a model of an existing structure with available damage and loss assessments data is built and analysed through a set of scenario earthquakes, i.e. the 2010-2011 Canterbury Earthquake Series. The loss information obtained is compared with the available reports on damage and repairs from the Christchurch City Council, refer to section 4.4.2.

4.1. Case Study Building Assessment

During the 22 February 2011 Earthquake in Christchurch, a lot of structures were damaged. Reports stated that this was due to the fact that the earthquake was 1.5 to 2 times the Ultimate Limit State (ULS) design spectrum (Clifton et al. 2011). One of the structures that suffered damage was the Pacific Tower, presented in Figure 4.1. This 22-storey EBF structure suffered from both structural and non-structural damage. The tower was designed according to the NZS1170.5:2004 with a design ductility of three as well as according to the NZS3404:1997 before the second amendment. (Gardiner et al. 2013). The data on damage due to both the 2010 and the 2011 series earthquakes in Christchurch of the Pacific Tower is available through other reports and researches such as

The Canterbury Earthquakes Royal Commission Report on The Performance of Christchurch CBD Buildings (Canterbury Earthquakes Royal Commission 2012), NZSEE Bulletin Volume 43 (Bruneau et al. 2010) and the Christchurch City Council, which was summarized as presented previously in section 3.2.

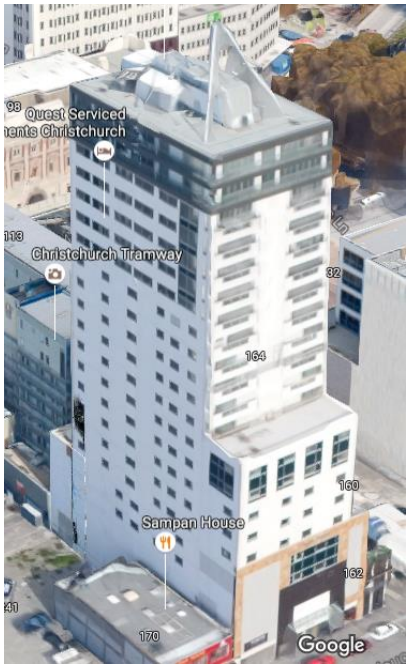

Figure 4.1. Pacific Tower (Google Street View 2016)

4.2. Hazard Analysis

The hazard analysis done for this research, as explained in section 2.1.1, is based on a probabilistic seismic hazard analysis (PSHA) for the Christchurch Central Business District area. The ground motion selection utilized the Generalized Conditional Intensity Measure (GCIM) proposed by Bradley (2010) for the Christchurch area (Vs of 200m/s). The hazard level used is hazard spectrums with probabilities of exceedance of 80%, 50%, 20%, 10%, 5%, 2%, 1%, 0.5% and 0.2% in 50 years. Each probability of exceedance is represented by 20 ground motions that are selected from the NGA database and scaled to fit the demand of a 4s structural period, the hazard levels for the specific case study building can be seen in Figure 4.2 and Table 4-1.

This process however, is not in the scope of this research and the hazard levels and selected ground motions are provided Yeow et al. (2017)

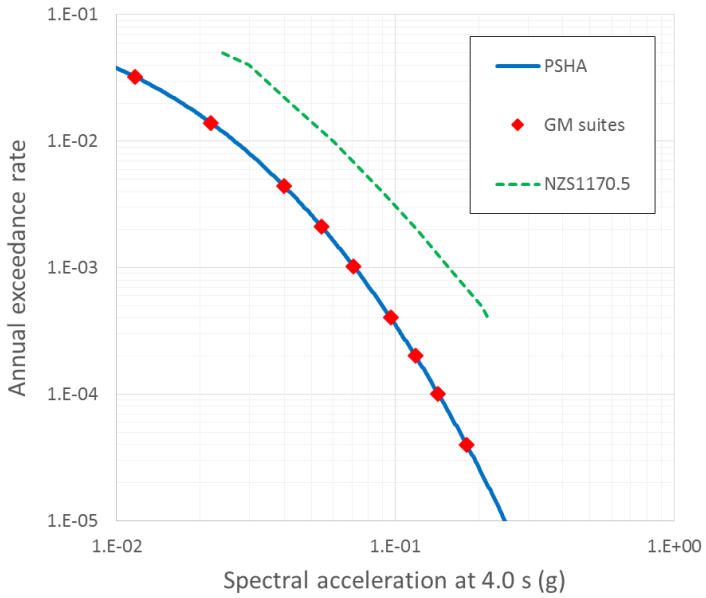

Figure 4.2. Hazard Levels for Structures with T = 4.0s on Soil Class D in Christchurch CBD (Yeow et al. 2017)

Table 4-1. Spectral Accelerations and Annual Exceedance Rate of Intensity Measures for Structures with T = 4.0s on Soil Class D in Christchurch CBD (Yeow et al. 2017)

Probability of Exceedance in 50 years	Sa(4.0s) (g)	Annual exceedance rate
80	0.012	0.0322
50	0.022	0.0139
20	0.04	0.0045
10	0.054	0.0021
5	0.071	0.0010
2	0.096	0.0004
1	0.118	0.0002
0.5	0.143	0.0001
0.2	0.180	0.00004

These ground motions' response spectra are presented in Figure 4.3 to Figure 4.11.

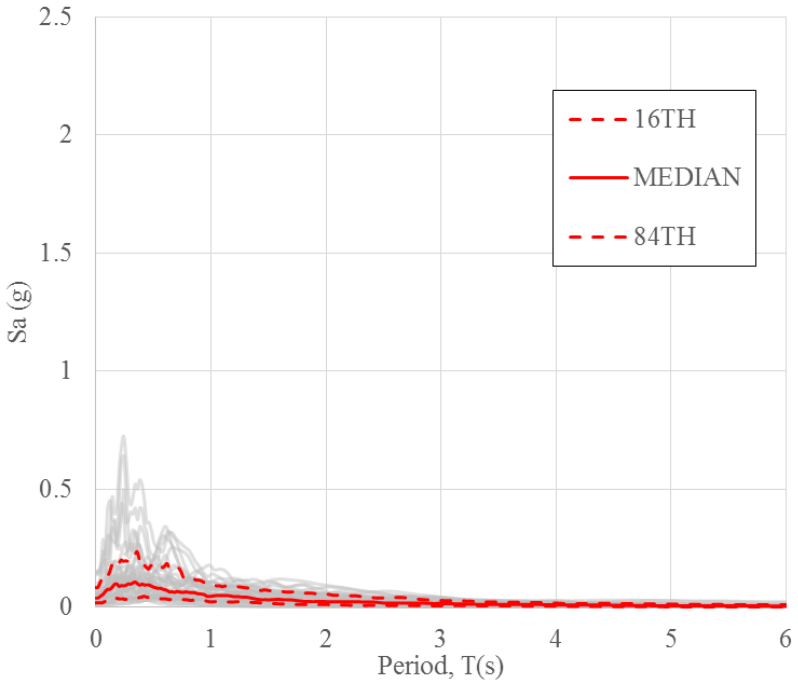

Figure 4.3. Response spectra for 80% in 50 years; Sa(4.0s) = 0.012g

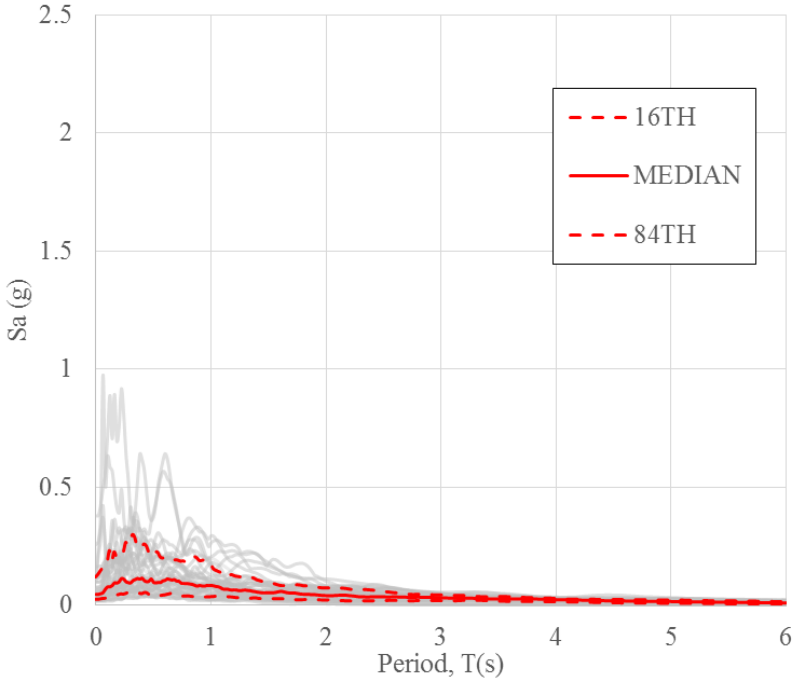

Figure 4.4. Response spectra for 50% in 50 years; Sa(4.0s) = 0.022g

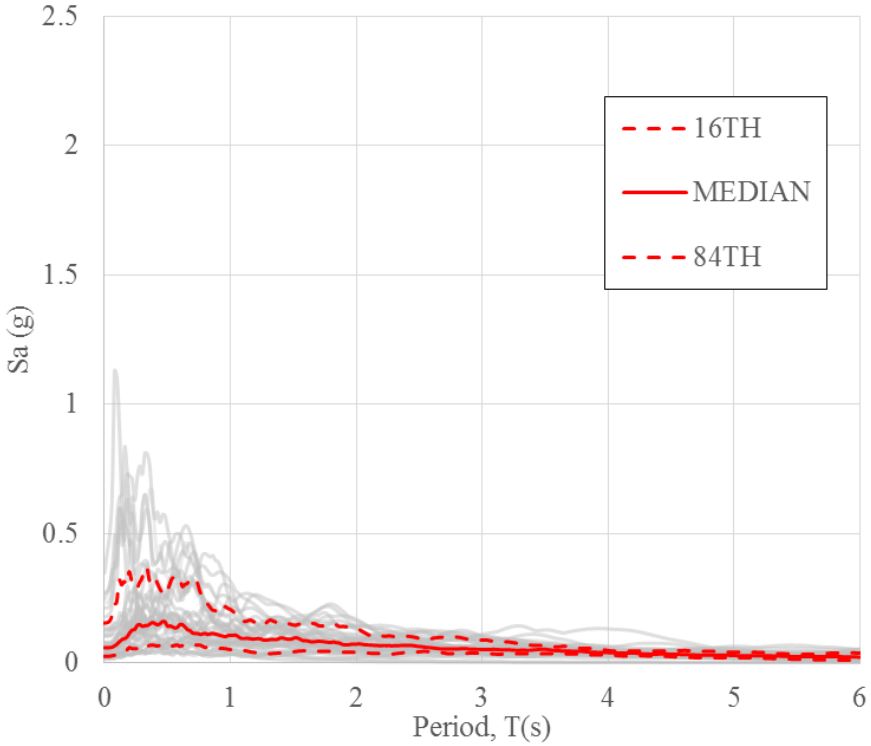

Figure 4.5. Response spectra for 20% in 50 years; Sa(4.0s) = 0.04g

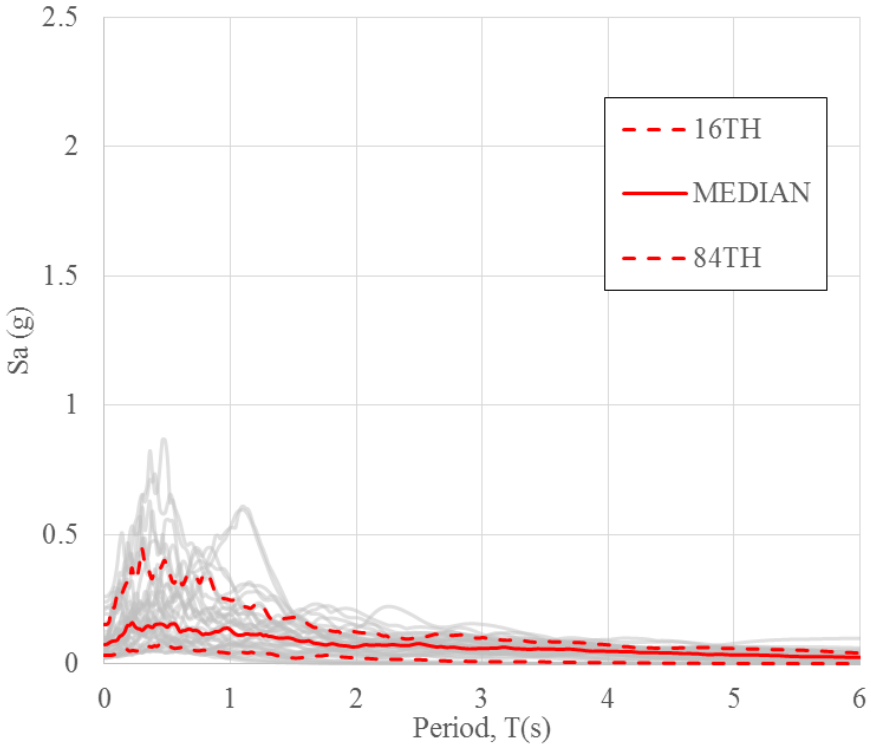

Figure 4.6. Response spectra for 10% in 50 years; Sa(4.0s) = 0.054g

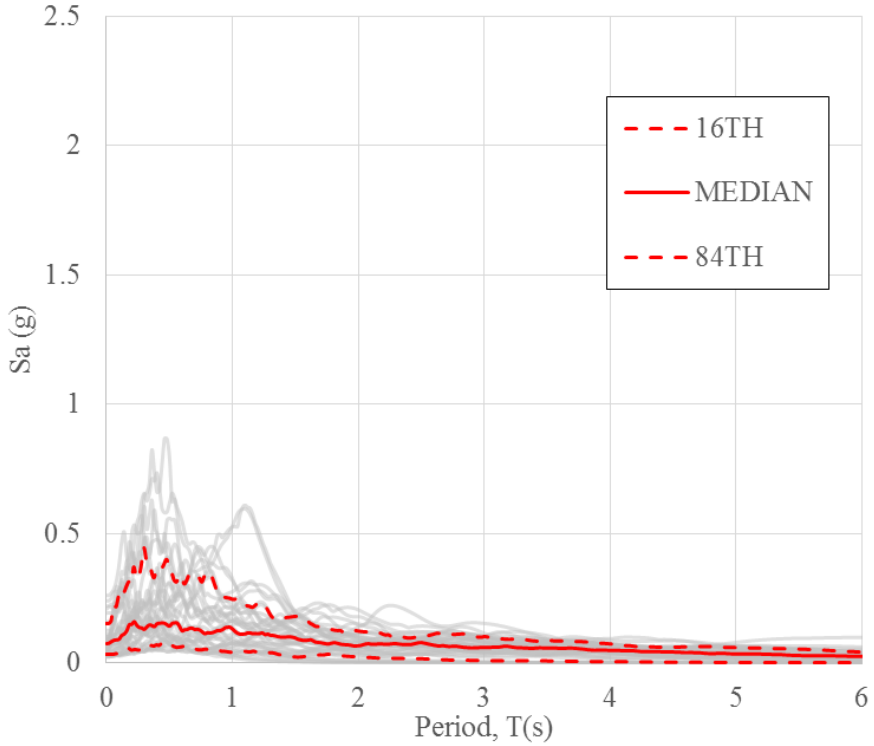

Figure 4.7. Response spectra for 5% in 50 years; Sa(4.0s) = 0.071g

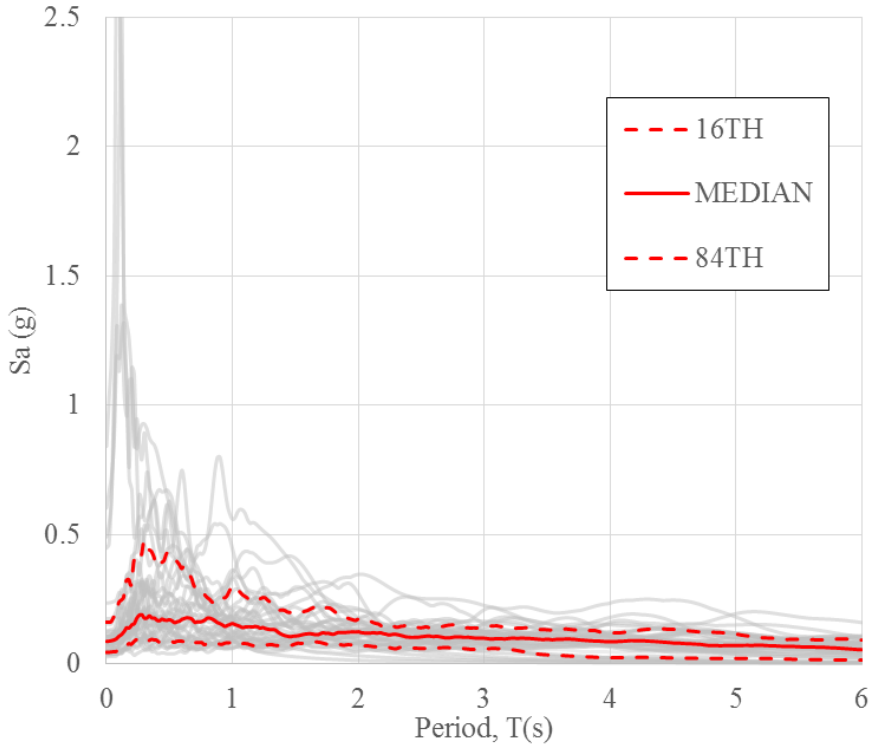

Figure 4.8. Response spectra for 2% in 50 years; Sa(4.0s) = 0.096g

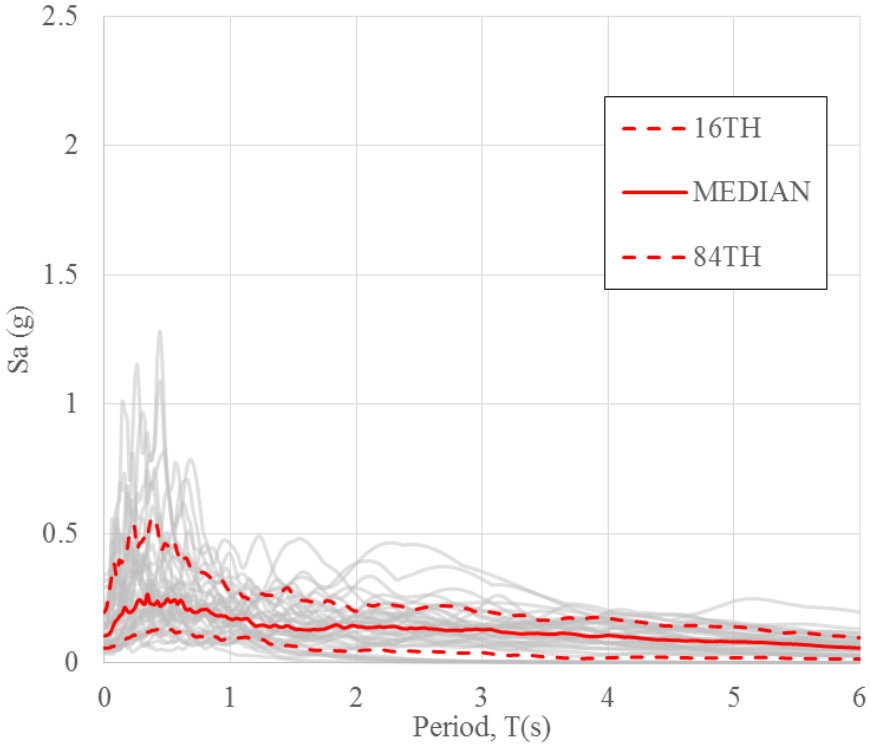

Figure 4.9. Response spectra for 1% in 50 years; Sa(4.0s) = 0.118g

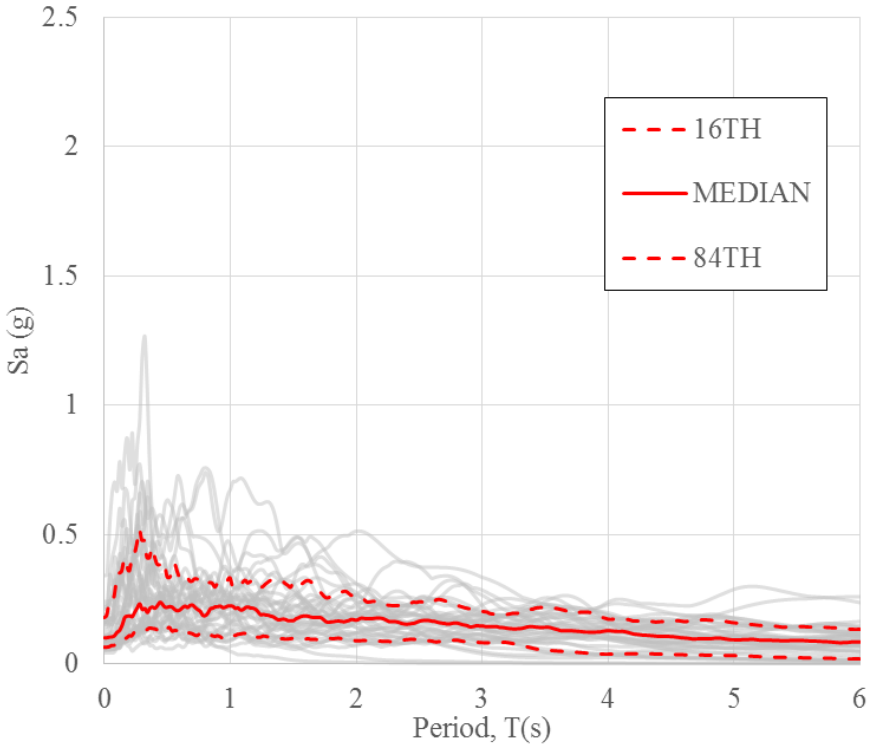

Figure 4.10. Response spectra for 0.5% in 50 years; Sa(4.0s) = 0.143g

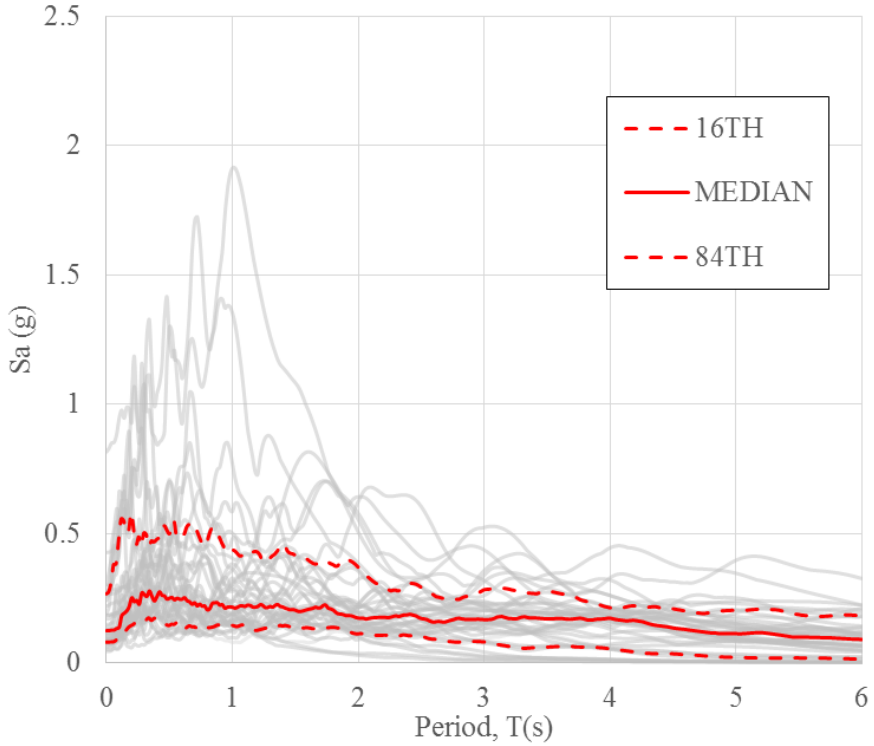

Figure 4.11. Response spectra for 0.2% in 50 years; Sa(4.0s) = 0.18g

4.3. Structural Analysis

The structure, Pacific Tower Building, is modelled only with the lateral structural system elements (EBFs). This data is obtained from the structural drawings provided by the Christchurch City Council. From the structural plans, the Pacific Tower is modelled accordingly with drawn element sizes and lengths noting that the data obtained is not necessarily the as-built data. For the data on the structural drawings, refer to Appendix G

4.3.1. Structural Modelling

As an overview, refer to Figure 4.12, Figure 4.13 and Figure 4.14, the model in Ruaumoko 3D (Carr 2017) is shown.

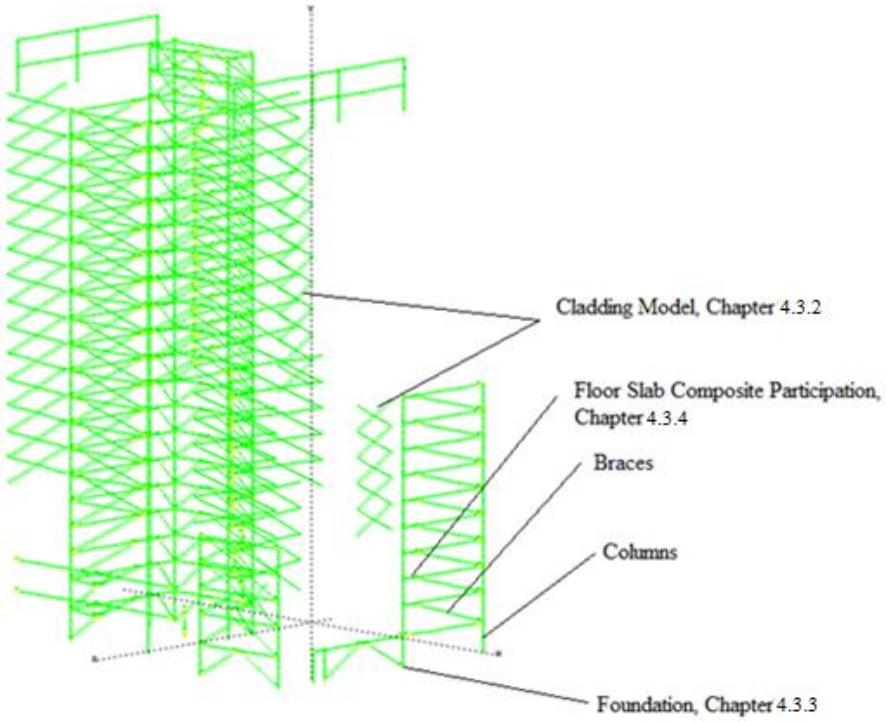

Figure 4.12. 3D View of Ruaumoko3D Model

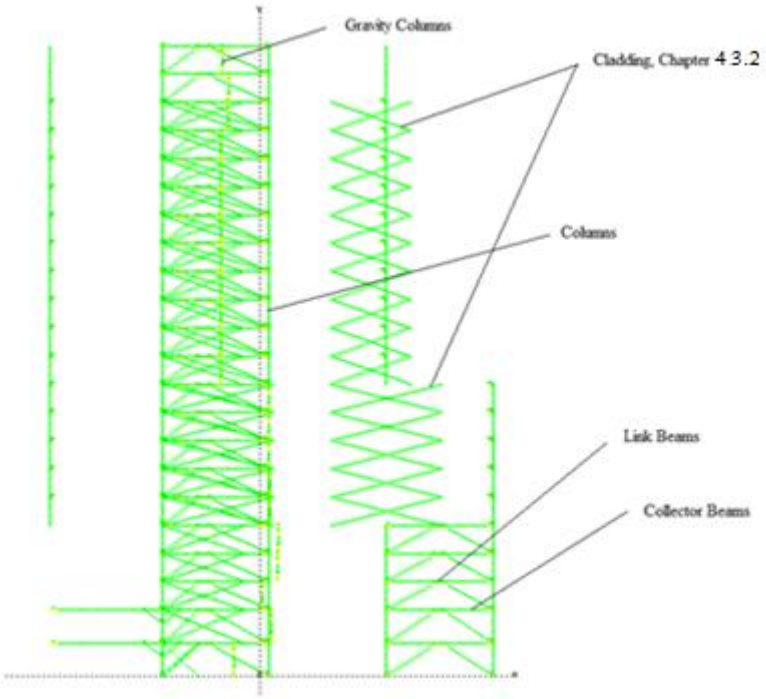

Figure 4.13. Z-Direction Elevation of Ruaumoko3D Model

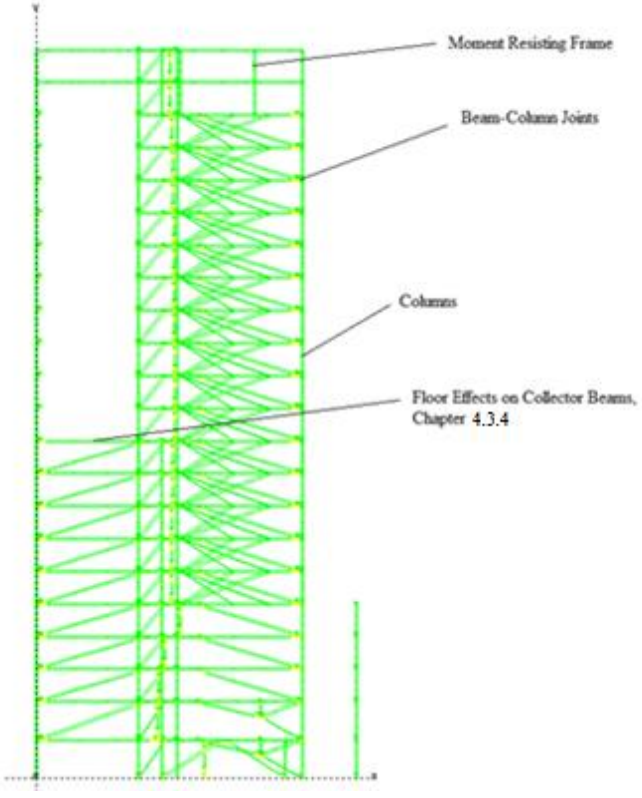

Figure 4.14. X- Direction Elevation of Ruaumoko3D Model

In order to generate an efficient numerical model, a number of assumptions and approximations were made.

The list of these assumptions follows:

- Steel expected yield strength (fye) is taken as 1.1 times nominal yield strength (fy) as suggested by FEMA-356 (FEMA 2000).
- An initial stiffness proportional damping with 3% damping in every mode (i.e. Caughy Damping) is used as suggested in the Ruaumoko3D Manual (Carr 2004). This is an ICTYPE of 2 with 3% damping specified in modes 1 and 3 (1st and 2nd X-Translation modes) in Ruaumoko 3D (Carr 2017).
- Foundations are modelled as vertical axial springs only, refer to section 4.3.3, and are assumed to be rigid while the column base supports are pinned.
- Overstrength is not fully considered, therefore some member demands may be underestimated.
- Beam, column and brace joints are assumed as pinned based on the detailing given in the drawings, as shown in Figure 4.15. However, there are MRFs on levels 21-22, refer to Figure 4.16 and Figure 4.17, that are assumed to be fixed.

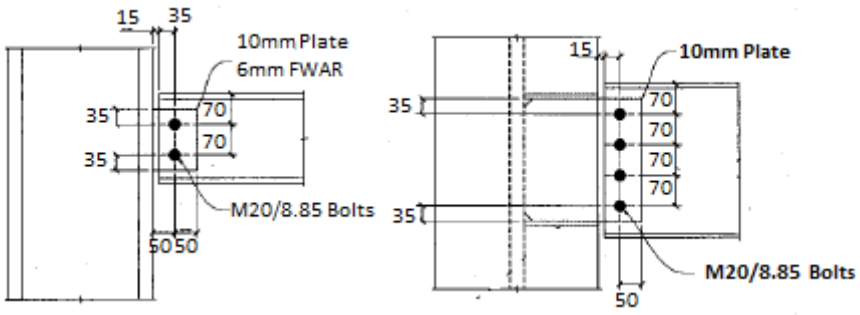

(a) (b)

Figure 4.15. Typical beam-column (a) flange and (b) web joint (Christchurch City Council 2016c)

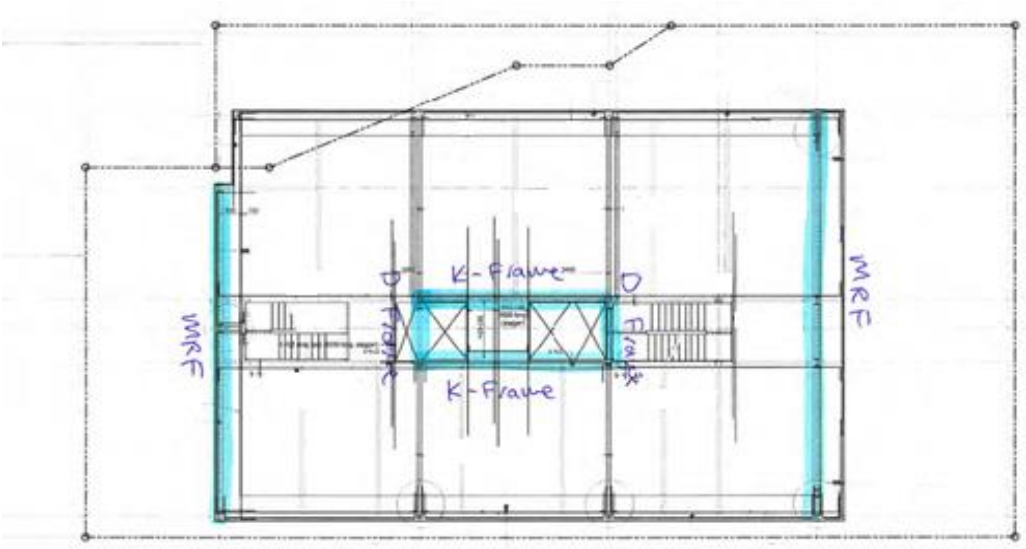

Figure 4.16. Plan of Moment Resisting Frames on Levels 21-22 (Christchurch City Council 2016c)

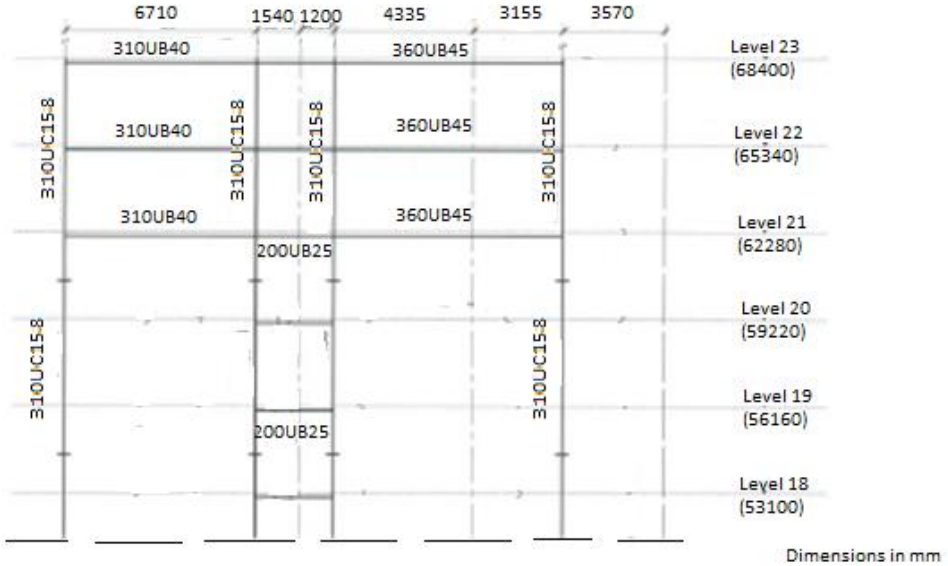

Figure 4.17. Elevation of Moment Resisting Frame on Grid E (Christchurch City Council 2016c)

- Beams outside the link area are modelled as elastic as they are not expected to yield. Due to details of studs in the drawings, composite action between these beams and the slab above it is evident. Hence,

the stiffness of the beams are increased by 20%, both shear and flexural, as suggested in the appendix N of NZS3404:Part 1:1997 (NZS 2007), refer to section 4.3.4.

- Columns are modelled as inelastic elements as it is possible to yield in axial or flexural loads. The axial yield capacity is obtained by section area multiplied by the expected steel yield strength (i.e. 330 MPa) while the flexural yield capacity is obtained by section plastic modulus multiplied by the expected steel yield strength. The P-M interaction was not considered due to the fact that even though possible, the columns are not likely to yield.
- Braces are modelled as inelastic elements as it is possible for the braces to yield in axial load. Similar to the columns, the axial yield capacity is obtained by section area multiplied by the expected steel yield strength.
- Link beams are modelled as inelastic elements as it is possible for the link beams to yield in flexural or shear load. Similar to the columns, the flexural yield capacity is obtained by the smaller of section plastic modulus multiplied by the steel yield strength or the shear capacity multiplied by the link length (e) divided by two,

$$\boldsymbol{Mp = \frac{Vp \times e}{2}} \qquad \textbf{(4-1)}$$

  Similar to the beams, the stiffness of the beams are increased by 20%, both shear and flexural, as suggested in the appendix N of NZS3404:Part 1:1997 (NZS 2007), refer to section4.3.4, and the strength of the links are increased by assuming an effective width according to the NZS3404:Part 1:1997 (NZS 2007)
- Hysteresis models for the inelastic elements are assumed bi-linear (Ruaumoko type IHYST=2) with a bi-linear factor r of 0.03, as suggested in Ibarra et al. (2005).

- Stairs are not modelled as they have no effect on the storey stiffness. This is due to the detailing that allows the stairs to slide between levels during lateral loading.
- Precast Panels are modelled as diagonal struts with the connections modelled accordingly, refer to section 4.3.2**.**
- All in-plane loads are assumed to be able to be transferred through the concrete topping, which is around 60 mm thick, i.e. a rigid diaphragm.

And the approximations made were:

- The applied gravity loads are taken from NZS1170.1 (NZS 2002) and ComFlor Product Brochures (Corus New Zealand 2005). These are listed in Table 4-2.

Table 4-2. Model Mass Considerations

Component	Weight	Units
ComFlor 80	2.5	kN/m^2
Pre-cast Cladding Panels	24	kN/m^3
Ceiling	0.24	kN/m^2
Services	0.25	kN/m^2
Finishing	0.57	kN/m^2
Partitions	1	kN/m^2
Live loads	1	kN/m^2

- Centre of mass is calculated using floor mass, main lateral columns and main beams, ignoring secondary beams and gravity columns. This approximation is assumed to be sufficient as the floor mass is the most significant factor in determining the location of a floor's centre of mass. While secondary beams and columns do not significantly affect the location of the floor mass due to the mass proportions in comparison to the floor mass, approximately 5-10% of the total floor mass, and symmetry of the beam and column locations. The centre of masses is listed in Table 4-3.

Table 4-3. Centre of Mass

Storey	X Direction Centre of Mass (m)	Z Direction Centre of Mass (m)	Storey	X Direction Centre of Mass (m)	Z Direction Centre of Mass (m)
Level 2	19.49	11.07	Level 13	18.48	9.11
Level 3	22.32	7.98	Level 14	18.48	9.11
Level 4	21.65	8.07	Level 15	18.5	9.07
Level 5	22.81	8.45	Level 16	18.49	9.05
Level 6	22.85	9.48	Level 17	18.49	9.04
Level 7	22.18	8.95	Level 18	18.5	9.04
Level 8	22.18	8.95	Level 19	18.5	9.01
Level 9	22.14	8.95	Level 20	18.5	9.01
Level 10	22.14	8.96	Level 21	19.07	8.91
Level 11	22.12	9	Level 22	19.09	8.81
Level 12	18.48	9.11	Level 23	18.61	8.8

- Gravity masses (i.e. dead loads, superimposed dead loads and live loads) is lumped at centre of mass for each floor for x, y and z direction masses. The total masses are shown in Table 4-4.

Table 4-4. Gravity Masses

Storey	Gravity Mass (kN)	Storey	Gravity Mass (kN)
Level 2	5361	Level 13	3479
Level 3	2474	Level 14	3479
Level 4	2571	Level 15	3479
Level 5	2329	Level 16	3290
Level 6	4865	Level 17	3290
Level 7	4510	Level 18	3290
Level 8	4510	Level 19	3290
Level 9	4440	Level 20	3290
Level 10	4440	Level 21	2850
Level 11	4401	Level 22	2850
Level 12	3479	Level 23	2878

- A rotational inertia is specified at the centre of mass by approximating the radius of gyration for each floor (e.g. calculating for the location of each precast panel, partition, floor mass, etc.),

which was obtained from ETABS (Wilson et al. 1979). And the resulting rotational inertia is shown in Table 4-5.

Table 4-5. Radius of Gyration and Rotational Inertia

Storey	Radius of Gyration (m)	Rotational Inertia (kNm^2)	Storey	Radius of Gyration (m)	Rotational Inertia (kNm^2)
Level 2	13.0	904774	Level 13	9.2	297217
Level 3	9.9	244840	Level 14	9.2	297458
Level 4	10.1	261965	Level 15	9.3	299053
Level 5	9.7	221001	Level 16	9.3	283751
Level 6	11.5	646804	Level 17	9.3	284297
Level 7	11.2	566451	Level 18	9.3	284428
Level 8	11.2	566313	Level 19	9.3	285626
Level 9	11.2	556538	Level 20	9.3	286099
Level 10	11.2	556731	Level 21	9.3	247336
Level 11	11.1	546356	Level 22	9.3	248157
Level 12	9.2	297217	Level 23	9.4	253084

- Floor levels are taken as beam centrelines.
- Gravity "dummy" columns to continue the gravity masses and model structural response due to masses (both torsional and translational) are modelled as axially rigid pinned columns. This is achieved by using a modulus of elasticity 10 times that of steel for the element. The element connects the floor mass node of one floor to level below it at its particular location. Both column nodes in one floor (one for the mass of the floor above and one for the current floor) are constrained vertically to ensure the vertical load transfer from each floor to the ground as seen in Figure 4.18.

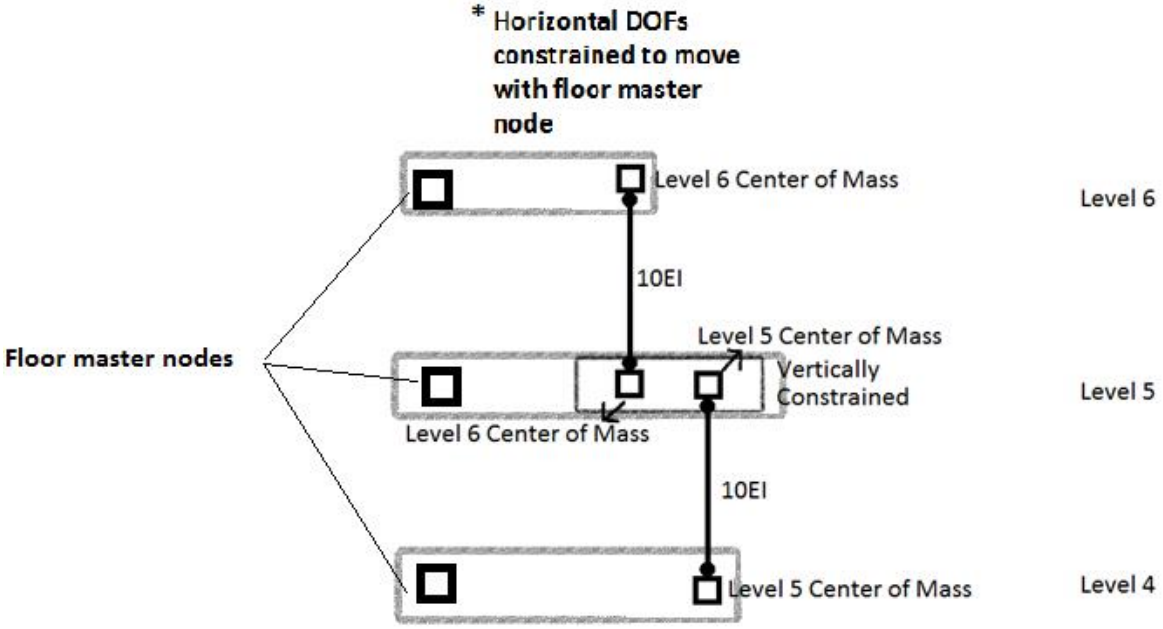

Figure 4.18. Elevation of Levels 4 to 6 "Dummy" Columns

- The characteristic steel yield stress, according to the drawings, was 300MPa for all members. Hence, a yield stress of 330 MPa is used as an expected yield stress value.
- Plastic hinge lengths are approximated by assuming that the plastic curvature is the same as the plastic hinge rotation (i.e. a Giberson beam member with two springs as hinges on the end).
- A node, approximately in the middle, is selected for each floor, refer to Figure 4.19, as a reference point for data (i.e. drifts and acceleration) observation. All the other nodes in that node's floor is constrained as a rigid diaphragm to that node (i.e. the centre node is the master node of that floor). With this approximation, it is expected that the master node represents the floor response.

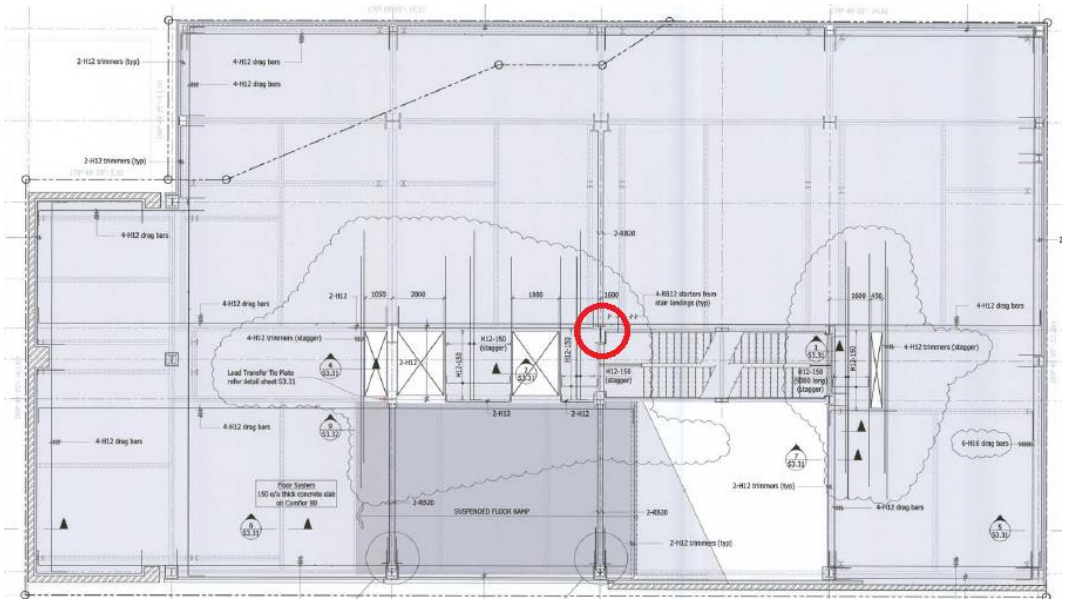

Figure 4.19. Master Node Location (Christchurch City Council 2016c)

- The concrete block wall on the south side of the building (Grids A-B) is seismically separated from the main structure via a seismic joint shown in Figure 4.20. Hence, this part of the building is not considered in the model.

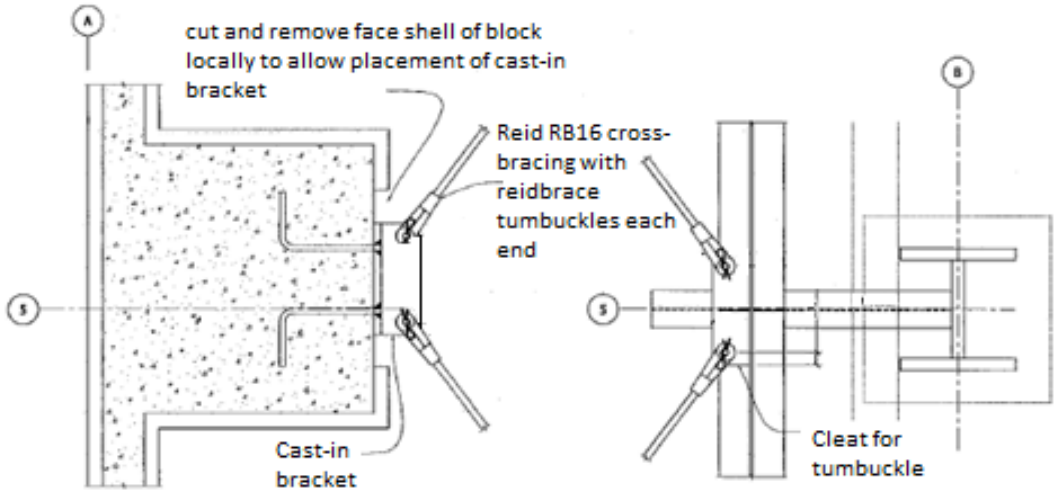

Figure 4.20. Seismic Joint on Level 6 Grid B (Christchurch City Council 2016c)

- There are some architectural exterior claddings on the lower levels (one through six), seen in Figure 4.21, which from the detail drawings, presented in Figure 4.22, do not provide additional stiffness due to the flexible joints that allow for horizontal and vertical movement of the panels (EuroFOX panels). Hence, these panels are not considered in the model.

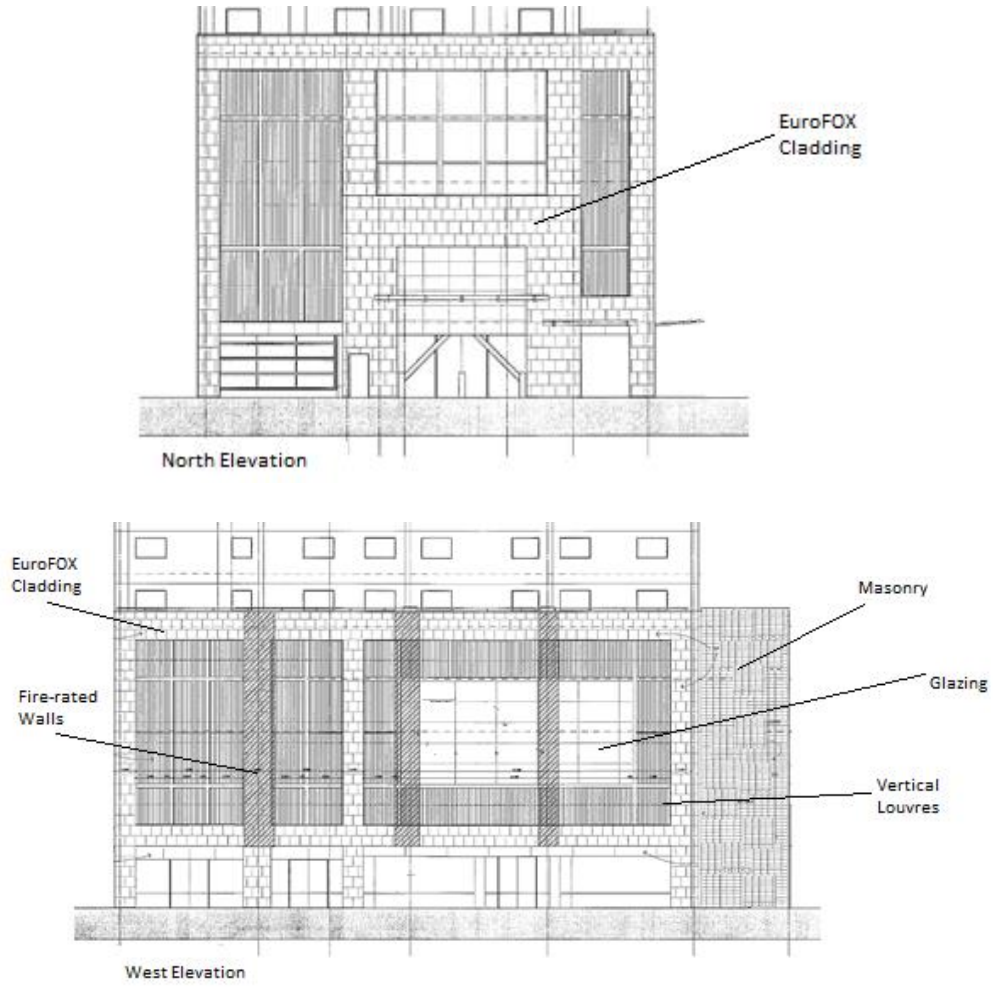

Figure 4.21. North and West Elevation of the Pacific Tower (Christchurch City Council 2016a)

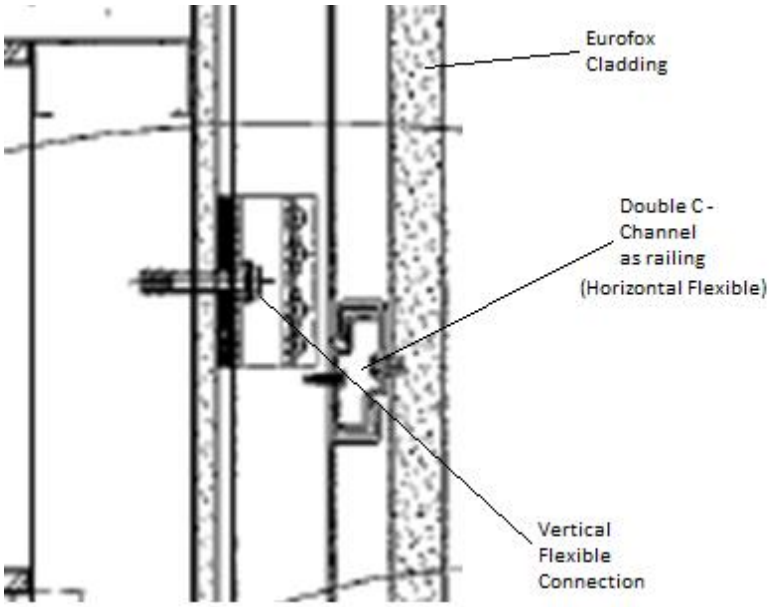

Figure 4.22. Exterior Cladding Connection (Christchurch City Council 2016a)

In order to obtain a level of confidence that the produced model represents the structural performance of the building, a displacement based assessment (DBA) based on Sullivan (2013) was done. The DBA approximation calculates the yield drift of each floor for a given EBF bay, for example presented in Figure 4.23 and Figure 4.24. Using the yield drifts approximated, the building yield drift can be determined as the average of drifts during first-yield. Due to the fact that this is not the main focus of this research, the process is explained in detail in Appendix A.

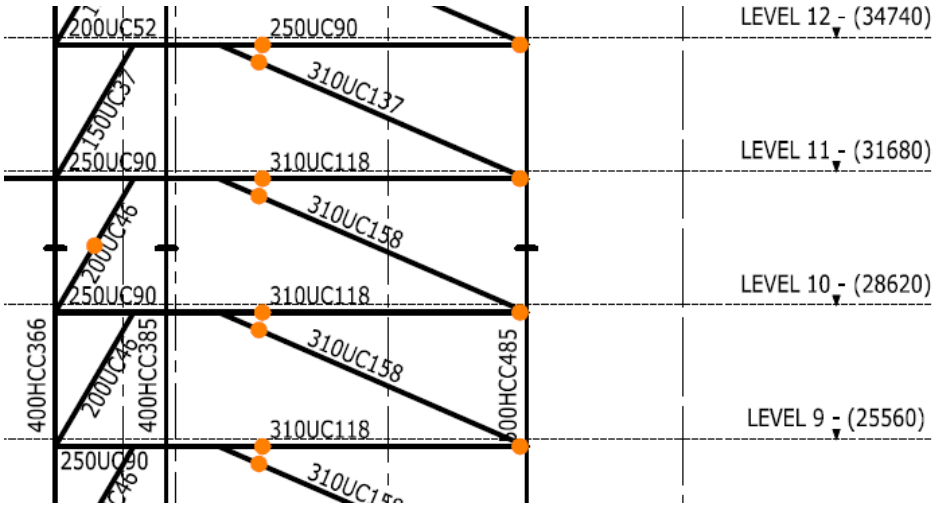

Figure 4.23. Frame Grid C Floors 9-12 (Christchurch City Council 2016c)

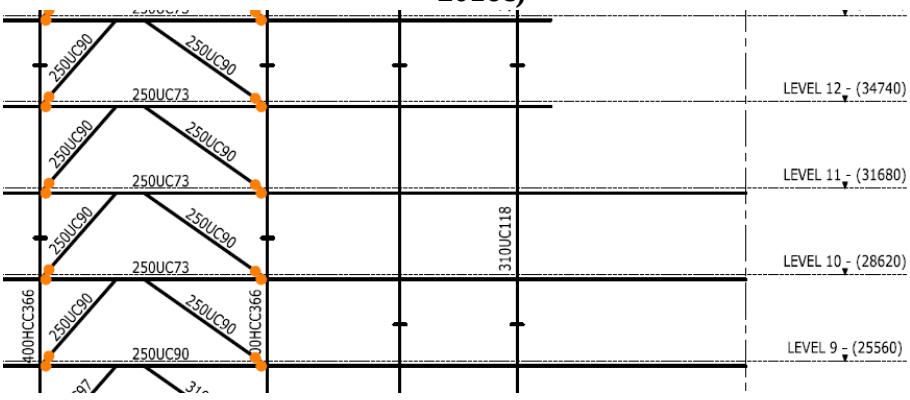

Figure 4.24. Frame Grid 6 Floors 9-12 (Christchurch City Council 2016c)

In order to calculate the story yield drift, an approximation of the strain ratios of the braces, approximated $k_{br} = 0.3\ \varepsilon_y$, and the columns, approximated $k_{cols} = 0.2\ \varepsilon_y$ is made. The resulting structural period is compared in Table 4-6 while the calculation process is listed in Appendix A.

Table 4-6. Displacement Based Assessment and Model Structural Period Comparison

Direction	DBA Simplified Approach	Ruaumoko 3D	Difference
X	3.53s	3.56s	0.81%
Z	4.72	4.64s	1.68%

The difference of period in both the X-direction and Z-direction from the displacement based approximation and the model is acceptable. Hence, it is concluded that the model is representative enough of the building in terms of yield drifts and structural period.

4.3.2. Cladding Modelling

The Pacific Tower uses pre-cast concrete panels as claddings. Depending on the connection details, these pre-cast panels can either increase the floor stiffness by a lot or not at all. For the Pacific Tower, the provided connection details show that the panels are connected rigidly, as seen in Figure 4.25, to the structure. Besides, since not all floors have these exterior claddings, refer Figure 4.26 and drawings in Appendix C, the influence of the panels are quite influential towards the structural response.

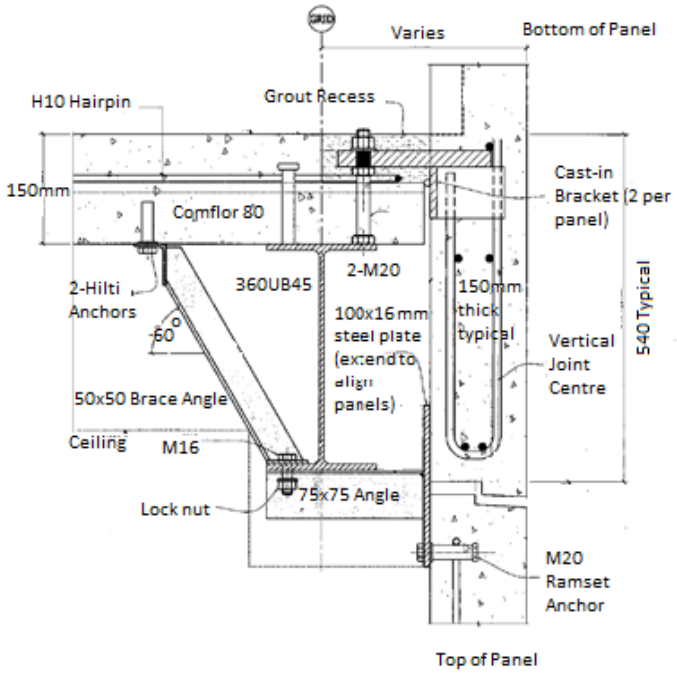

Figure 4.25. Pre-cast Concrete Panel Connection (Christchurch City Council 2016c)

Information was provided that during construction, the cladding panels were temporarily packed in position with steel plates. However, these steel plates were not removed, which may have caused the panels to lock up with one another during the earthquakes. The possibility of such locking is not considered in this model further suggesting that the model developed here is not an exact

representation of reality. The impacts of this could be examined as part of future research.


Floors 1 to 23
CHRISTCHURCH CITY COUNCIL
12 OCT 2007
Philip Hector
Building Consent Officer
WALL ELEVATION GRID 2 (WEST WALL)

Figure 4.26. West Wall Panel Elevation (Christchurch City Council 2016c)

In order to model this increase of stiffness, the panels are modelled as struts, as seen in Figure 4.27. This strut-based model is based on the suggestion by Crisafulli (1997). As there are more than one panel in a given level, to reduce the amount of DOFs in the model, the struts are only modelled as one per face of the structure (i.e. one north, one south, one west and one east for each floor). The length of the strut is taken as the average length of the diagonals of the panels in a given face of a floor. While the thickness is taken as the thickness of the concrete panels. As for the width, based on Priestley and Paulay (1992), is taken as 0.25 times the strut length while its properties (Inertia, Shear and Area) is multiplied by the number of panels in the given face of the floor. The strength of the panel is assumed to be similar to concrete. Hence, the modulus of elasticity of concrete is used for the panels. For example, on the 6th floor, there are four concrete panels each with a length of 8520mm, 8050mm, 8850mm and 8105mm respectively. With a floor height of 3.06m, the average diagonal length can be calculated as 8923mm. The strut width can also be calculated as 0.25 X average length (0.25 X 8923mm = 2.23075m).

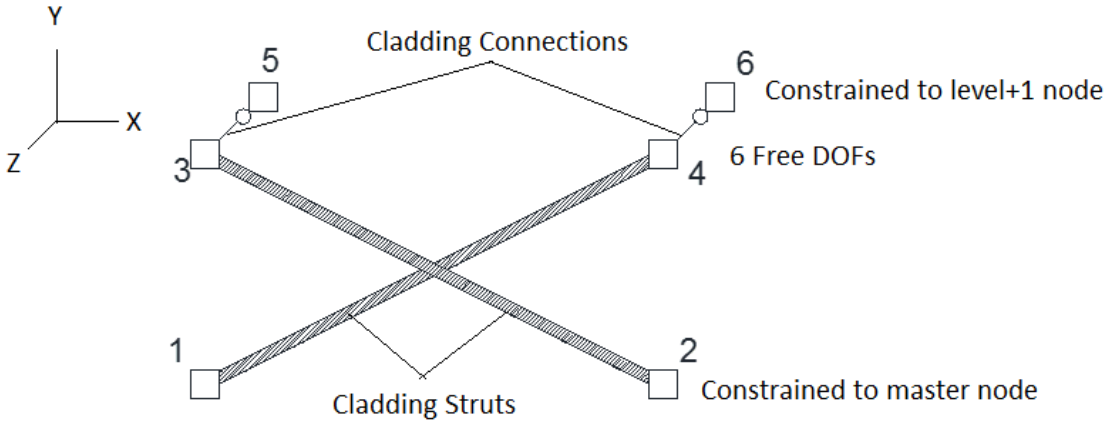

Figure 4.27. Strut Model of the Pre-cast Panels

In Ruaumoko3D (Carr 2017), the nodes and connectivity are modelled according to the connection details. From Figure 4.25, it can be seen that the bottom part of the cladding is fixed to the floor diaphragm. Hence, nodes 1 and 2, refer to Figure 4.27, are constrained to the corresponding floor's diaphragm (i.e. N1 = N3 = N5 = 2) as well as constrained vertically to the mass node of the corresponding floor (i.e. N2 = 3). In addition, to ensure that the struts represent the claddings, nodes 1 and 2 are restrained rotationally in-plane (i.e. depends on the orientation of the cladding, N4 or 6 = 1) of the panel thus not allowing the struts to rotate in-plane but still allows movement out-of-plane. Nodes 3 and 4 are modelled as fully free since they are only connected to the floor diaphragm through the steel angle connection. Finally, nodes 5 and 6 are representing the connection point of the cladding top part to the floor diaphragm. These nodes are constrained to the corresponding floor's diaphragm, restrained in rotation and also vertically to the mass node of the corresponding floor, refer to Table 4-7.

Table 4-7. Cladding Node Properties Example in Ruaumoko3D

No.	X	Y	Z	N1	N2	N3	N4	N5	N6	KUP1	IOUT	KUP2
1	5.56	0	9.45	2	3	2	1	2	0	7	0	9
2	5.56	0	15.3755	2	3	2	1	2	0	7	0	9
3	5.56	3.06	9.45	0	0	0	0	0	0	0	0	0
4	5.56	3.06	15.3755	0	0	0	0	0	0	0	0	0
5	5.86	3.06	9.45	2	3	2	1	2	1	8	0	10
6	5.86	3.06	15.3755	2	3	2	1	2	1	8	0	10

*Where, Nodes 7-8 are the master nodes of floors 1 and 2 while nodes 9-10 are the mass nodes of floors 1 and 2 respectively.
** In Ruaumoko, 0 is a free DOF, 1 is fixed, 2 is a slaved node to KUP 1 and 3 is a slaved node to KUP 2
*** N1, N2 and N3 is the global X, Y and Z direction respectively. While N4, N5 and N6 is the rotation about the global X, Y and Z axis respectively.

The elements that model the cladding is divided to the panel itself and the connection to the floor diaphragm, the steel angles (refer to Figure 4.25). The panels, as explained earlier, are modelled as struts. These struts are modelled as fully fixed into the joints (nodes), elements 1-4 and 2-3 in Figure 4.27 are fixed on both ends. These elements are modelled as inelastic elements with a bilinear hysteresis assumption as they are expected to yield. While the steel angle connections, elements 3-5 and 4-6 in Figure 4.27, are modelled to have an end-flexibility in the cladding connection end (explained in the next paragraph) and pinned in the other, the floor diaphragm side, to approximate the conditions from Figure 4.25. These elements are also modelled as inelastic elements as they are also expected to yield. Unfortunately, the length and size of the angle used for each panel was not clear from the structural drawings. Hence, a length of 0.3m and a size of 75X75X8EA was assumed for all panels. Since for each floor face there is only one cladding model, the steel angles' properties are also multiplied accordingly.

The end flexibility, mentioned previously, is included due to the fact that the connection between the steel angle and the cladding itself is not a fully rigid connection. There are a few parts that need to be accounted for towards the modelling of the steel angle connection, such as the additional source of deformations and yield drift as well as reduced yield moments.

- Angle Yield

From Figure 4.25, it can be seen that the steel plate suffers from restrained torsion. A simple 3D model of this connection is created in SAP2000 (Wilson & Habibullah 2002), seen in Figure 4.28.

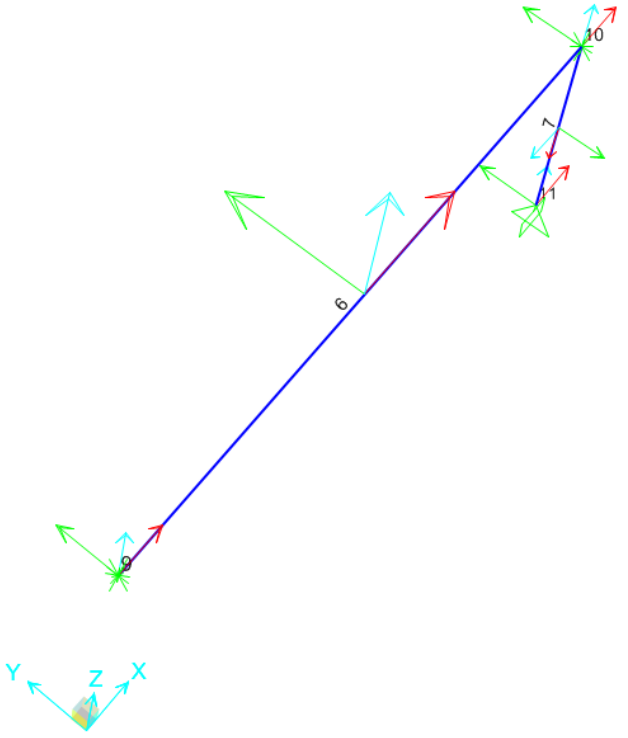

(a)

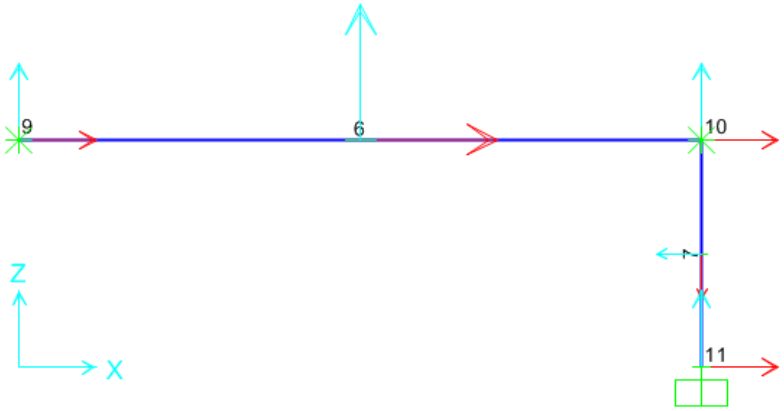

(b)

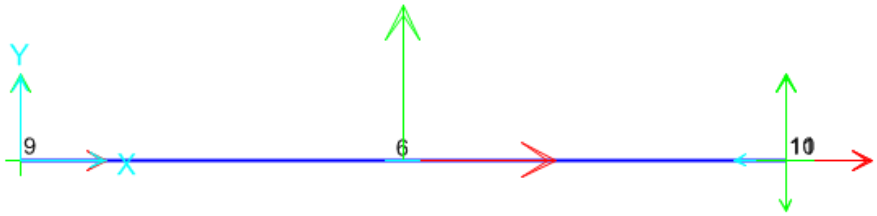

(c)

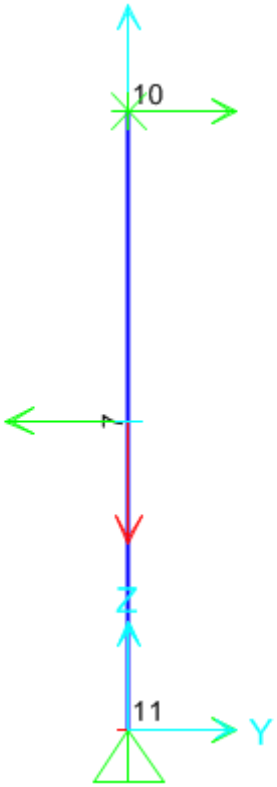

(d)

Figure 4.28. SAP2000 Model (a) 3D perspective (b) X-Z plane (c) Y-X plane (d) Z-Y plane

Table 4-8. Local Axes Colours

Colour	Local Axes
Red	1
Green	2
Blue	3

Table 4-9. SAP2000 Model Constraints

Node	Translation	Rotation
9	1, 3	1, 2
10	-	3
11	1, 2, 3	2, 3

The model in Figure 4.28 is run through a static non-linear analysis with deformation controlled load imposed in node 9 in the Y direction. Using element properties as specified in the Ruaumoko3D model, including element properties such as torsion and flexural as well as a hinge property is developed in the SAP2000 model as well. The results from this model is listed in Appendix B and summarized as following,

Table 4-10. SAP2000 Model Results

Item	Angle	Plate
Yield Drift (U2/UY)	12.2 mm	0 mm (Reference Point)
Yield Moment (M3/MZ)	2.97 kNm	-
Yield Moment (M2/MY)	0.7 kNm	0.16 kNm
Yield Torsion (M1/MX)	0.84 kNm	2.97 kNm (Top of Plate)
Yield Force (F1/FX)	5.23 kN	5.23 kN
Yield Force (F2/FY)	9.92 kN	9.92 kN
Yield Force (F3/FZ)	1.12 kN	1.12 kN

- Steel Plate Yield

Assuming yield lines as seen in Figure 4.29, the 16mm thick steel plate capacity can be calculated as,

$$\sigma_z = \frac{M_z y}{I} \qquad \sigma_y = \frac{M_y y}{I} \qquad \textbf{(4-2)}$$

$$330 = \frac{M_z\, 8}{\frac{1}{12} bh^3} \qquad 330 = \frac{M_y\, 8}{\frac{1}{12} bh^3}$$

$$M_z = \frac{\left(330 \times \frac{1}{12} 100\ 16^3\right)}{8} \qquad M_y = \frac{\left(330 \times \frac{1}{12} 100\ 16^3\right)}{8}$$

$$M_z = 1.408\ kNm \qquad M_y = 1.408\ kNm$$

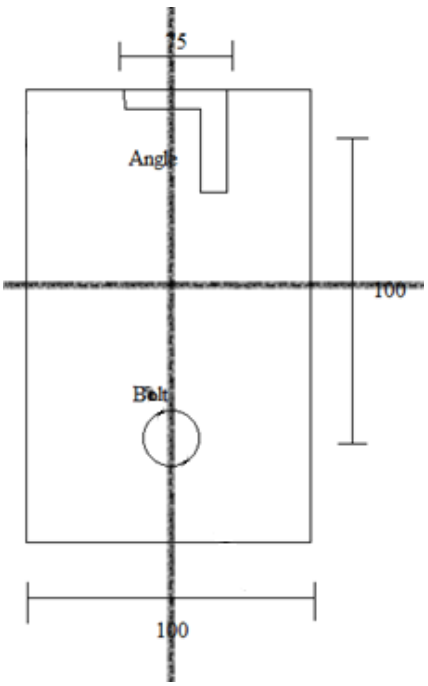

Figure 4.29. Steel Plate Yield Line Assumption

- Bolt Yield

The bolt used in Figure 4.25 is a 20mm Ramset Anchor (Ramset 2017). As such, a table from the product brochure is obtained and the maximum tensile and shear load can be compared with the results from the SAP2000 model in Table 4-11, note that the torsion-shear interaction is not considered in this calculation.

TruBolt™ Stud Anchors - Indicative Working Loads in 32MPa Concrete

Thread Size	Embedment Depth (mm)	Tightening Torque (Nm)	Min Edge Distance (mm)	Min Anchor Spacing (mm)	Max Tensile Load, N_s (kN)*	Max Shear Load, V_s (kN)*
M6	32	10	50	100	3.4	2.8
M8	54	20	80	160	7.2	4.9
M10	72	35	110	220	9.9	6.8
M12	86	50	130	260	12.7	8.6
M16	115	155	170	340	20.9	14.4
M20	145	355	220	440	32.5	27.3

*The design engineer should ensure the structural element is capable of supporting these loads.
Refer to Ramset™ Specifiers Resource Book for more information or explanation of technical data.

Figure 4.30. Ramset Anchor Product Specifications (Ramset 2017).

Table 4-11. Bolt Forces Comparison

Item	SAP2000 Results	Product Specifications	Calculations
Max Tensile	5.23 kN	32.5 kN	-
Max Shear	9.92 kN	27.3 kN	-
Max Concrete Pull-out	5.23 kN	-	55 kN

Other than the product brochure, the concrete pull-out is also considered based on the concrete breakout strength in tension by Oakley (2008),

$$N_b = k_c\sqrt{f'_c}h_{ef}^{1.5} \qquad \textbf{(4-3)}$$

$$N_b = 55\ kN$$

Where,

$N_b = Maximum\ concrete\ pull - out\ (lb)$

$k_c = 24\ for\ cast - in;\ 17\ for\ post - installed$

$f_c' = Concrete\ Strength\ (psi), taken\ as\ 4351\ psi\ (30MPa)$

$h_{ef} = Anchor\ effective\ length\ (inch), taken\ as\ 3.94"\ (100mm)$

Comparing the limits of the three elements (i.e. angle, plate and bolt), the plate yield is the weakest link. Hence, the connection behaviour is governed by the plate yield. With this consideration, the end flexibility can be calculated as the difference between flexibility of the element modelled in Ruaumoko3D (Carr 2017) and the flexibility of the element modelled in SAP2000 (Wilson & Habibullah 2002),

$$f_{Ruaumoko3D} = 0.0001\ m/kN$$

$$f_{SAP2000} = 0.0011\ m/kN$$

$$f_{additional} = 0.001\ m/kN \rightarrow\ 0.011\ rad/kNm$$

The yield moment, governed by the yield of the plate, is taken as 1.41 kNm which is the moment in the Z-direction of the angle when the plate yield occurs. This yielding occurs at a displacement of 5.7 mm, refer to Appendix B. Due to the fact that in the model, each face is only modelled by one set of claddings, the flexibility is divided according to the number of claddings.

4.3.3. Foundation Modelling

While the scope of this research does not reach to the details of foundation modelling, to incorporate the effects of the foundation towards the seismic demands, a very simple model that only accounts for the vertical axial (push and pull) stiffness for the foundations is utilized.

The foundations of the Pacific Tower uses two types of foundations, screw piles and bored piles. From the foundation plans in Figure 4.31, six groups of piles as well as a few other bored piles can be seen as a support for the columns.

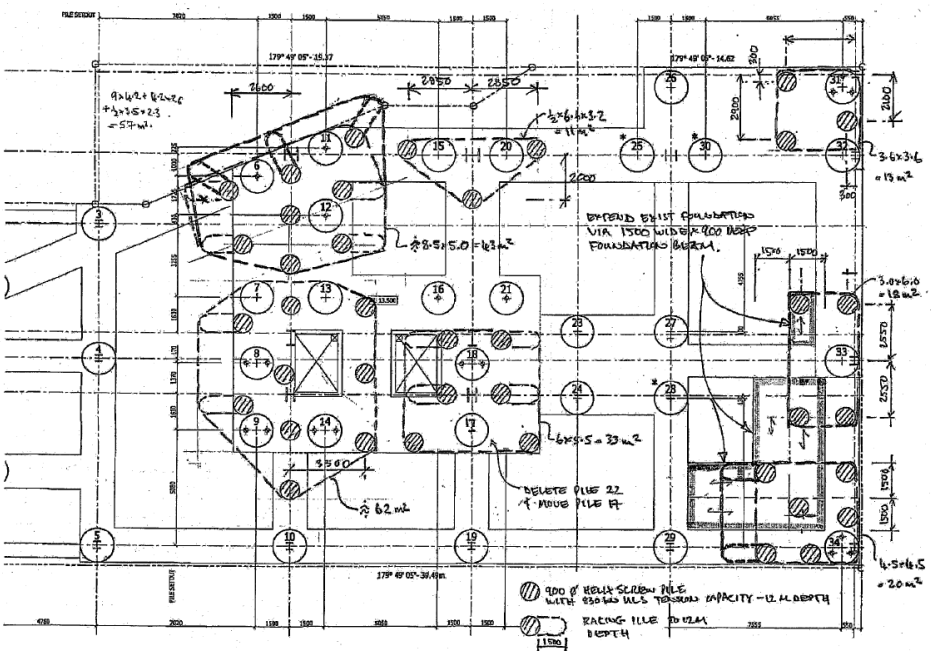

Figure 4.31. Foundation Plan (Christchurch City Council 2016b)

The model of the Pacific Tower created in Ruaumoko3D (Carr 2017), only includes columns that are part of the structure's lateral resisting system. Hence, only the foundation in those areas are considered. A report obtained from the Christchurch City Council, refer to Figure 4.32, Figure 4.33 and Figure 4.34, shows the compression and uplift design for both the screw piles and bored piles as well as a design settlement of less than ±25mm.

Depth to pile tip (m)	Compression Design	Test June	Test April	Uplift design	Test June	Test April
6	4,800			250		
7	6,000			620		
8	8,000	8340	1570	880	5870	560
9	8,000			1,450		
10	8,600			2,000		
11	9,400			2,450		
12	10,000	9620	5100	2,950	6040	2730

Figure 4.32. Bored Piles Design Load (Christchurch City Council 2016b)

Pile group	ULS Uplift (kN)	group perimeter	group area	shear = 133xP	weight = 84xA	Total	T x 0.7	> ULS?	Actual capacity reduction factor
C2	6397	26	43	3458	3612	7070	4949	no	0.90
D2	2070	16	11	2128	924	3052	2136.4	yes	0.68
F1	2061	14.5	13	1928.5	1092	3020.5	2114.35	yes	0.68
F5	2658	18	18	2394	1512	3906	2734.2	yes	0.68
F7	3614	18	20	2394	1680	4074	2851.8	no	0.89
C6	7039	29.5	62	3923.5	5208	9131.5	6392.05	no	0.77
D6	4602	23	33	3059	2772	5831	4081.7	no	0.79
C2	6397	26.1	57	3737	4788	8525	5968		0.75
F7	3614	21	27	2793	2268	5061	3543		0.71

Figure 4.33. Screw Piles Uplift Design Load (Christchurch City Council 2016b)

Screw pile design & details

The Ultimate Limit State (ULS) design loads have been determined in accordance with AS/NZS1170.

The required minimum design capacities are:

Compression	1450 kN/pile
Tension	830 kN/pile

The screw piles shall be designed by a suitably experienced engineer to support the ultimate limit state loads stated above. Deflections/settlements at these loads shall not exceed +-25mm. This deflection criteria may dictate the minimum size and strength of the helix. The engineer shall provide a Producer Statement–Design before installation of the screw piles and a Producer Statement-Construction Review after installation stating that the piles comply with this specification.

The design of the piles shall be for a "design life" of 100 years. Details of the durability and/or corrosion protection design shall be submitted to the engineer for review.

The screw piles shall extend to a depth of 12mm below existing ground level, unless otherwise agreed with the structural engineer and geotechnical engineer.

The screw pile designer/manufacturer shall submit the following information to the engineer and contractor for review prior to commencement of fabrication and installation:

Figure 4.34. Screw Piles Design Load and Design Settlement (Christchurch City Council 2016b)

Based on the data obtained and assuming the foundation has a uniform settlement, a simple vertical axial spring, Figure 4.35(a) on the ground-side of each column is used to model the foundations. The stiffness of these springs are calculated as the total design load of the bored piles and screw piles for each column divided by the settlement. Due to the fact that the foundations have different compression and tension properties and the assumption that the foundations stay elastic, an elastic hysteresis with different positive and negative stiffness as seen in Figure 4.35(b) was chosen. The settlement chosen was 20mm at first, assumed reasonable compared to the limit of 25mm. For comparison, a model with 10mm settlement was also created. However, the difference between both models were quite significant (larger than 2.5%), refer to Table 4-12. In order to obtain an average result that still represents the structure, it was decided for a settlement of 15mm as the details of the foundation is outside of the scope of this research.

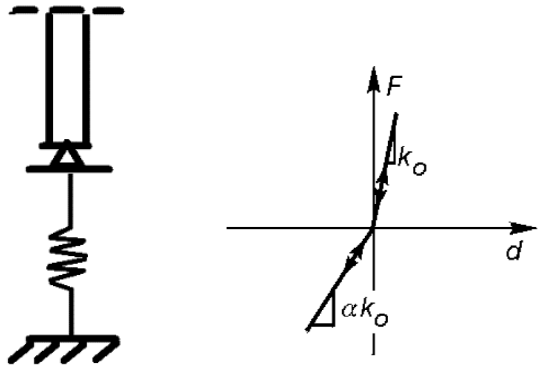

Figure 4.35. Foundation (a) Spring Model and (b) Stiffness Model (Carr 2004)

Table 4-12. Foundation Elastic Deformation Effects on Building Fundamental Periods

Settlement	10mm	% Diff	15mm	20mm	% Diff
Translation Z Mode 1	4.45	4.1	4.64	4.81	3.6
Translation X Mode 1	3.42	4.0	3.56	3.67	3.3
Torsional Y Mode 1	2.76	4.3	2.89	2.93	1.5
Translation Z Mode 2	1.59	1.1	1.60	1.62	0.8
Translation X Mode 2	1.24	1.6	1.26	1.27	1.1

4.3.4. Floor Composite Action

The details from the structural drawings, shown in Figure 4.36, show that the floor slabs are connected with shear studs. This results in a composite action between the beams and the floor slabs.

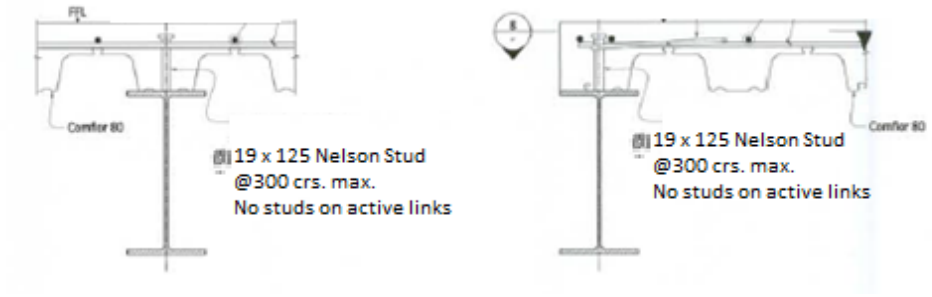

Figure 4.36. Floor Slab – Beam Connection Details (Christchurch City Council 2016c)

In order to incorporate this effect, the elastic stiffness of the beams, both flexural (i.e. I) and shear (i.e. Av), is increased by 20% as suggested in Appendix N of NZS3404:Part 1:1997 (NZS 2007). While for the links, the strength of the element was increased by taking an effective width of 0.25 and 0.1 times the beam length for internal beams and external beams respectively as suggested in section 13.4.2 of NZS3404:Part 1:1997 (NZS 2007). This effective

length is used to calculate the moment capacity of the floor slab, obtained from ComFlor 80 Brochure (Corus New Zealand 2005), in addition to the moment of the beam. This is done, instead of a full composite action, due to the fact that the floor slabs detach from the link during plastic loading thus making it an independent element. The section properties of ComFlor80 can be seen in Figure 4.37 while an example of a moment calculation is as following,

Section Properties (per metre width)					
Nominal thickness (mm)	Profile weight (kN/m^2)	Area of steel (mm^2)	Moment of inertia (cm^4/m)	Ultimate Moment capacity (kNm/m)	
				Sagging	Hogging
0.90	0.11	1387	185	15.4	12.5
1.2	0.15	1871	245	22.2	18.5

Figure 4.37. ComFlor 80 Properties (Corus New Zealand 2005)

$$\boldsymbol{b_{eff} = 0.25 \times L = 0.25 \times 8.1m \approx 2m} \quad \textbf{(4-4)}$$

$$\boldsymbol{M^{+}_{Slab} = M_c \times b_{eff} = 22.2 \times 2 = 44.4\ kNm} \quad \textbf{(4-5)}$$

$$M^{-}_{Slab} = 18.5 \times 2 = 37\ kNm$$

Hence, the additional moment capacity of the internal link beams is increased by 44.4kNm in positive bending and 37kNm in negative bending.

4.3.5. Sensitivity Analyses

Due to the fact that the model used to represent the Pacific Tower incorporates a few assumptions and approximations, a sensitivity analyses is of importance. This is to highlight the differences due to these assumptions and approximations to the results of the structural analyses, i.e. the engineering demand parameters.

There are 7 parameters of interest, which may influence big discrepancies in the results, in the assumptions and approximations taken, refer to section 4.3.1. The parameters of interest are,

- Damping Type

The main model, henceforth named Control, uses a Caughy Damping as suggested by Carr (2004). However, there are a variety of damping types available, such as the Rayleigh Damping which is also commonly used. Hence, a model using Rayleigh Tangent Secant Damping (Ruaumoko3D ICTYPE 6) is also analysed.

- Damping Value

Based on the Ruaumoko3D manual (Carr 2004), a damping value of 3% was used for Control. A model using two values, 2% and 4%, were also analysed to highlight the significance of the damping value chosen.

- Foundation Stiffness

As mentioned in section 4.3.3, the foundations are modelled as axial springs only with a stiffness determined by the design loads and expected settlement obtained from documents on the Pacific Tower, refer to section 4.3.3. The settlement used to determine the Control model stiffness was 15mm. Due to the fact that the settlement has a large uncertainty, two models with different foundation stiffness, derived from settlements of 10mm and 20mm, was analysed.

- Beam-Column Joints

In section 0, the beam-column joints were assumed as pinned due to the details from the drawings. Another model with the assumption that the beam-column joints are fixed is analysed to show the extremes of this parameter. It is important to note that the drawings obtained show tendencies towards a pinned beam-column connection, refer to section 0.

- Hysteresis Model

A bilinear model with a post-yield stiffness of 3% was used for Control. Due to the certainty of this parameter (Bosco & Rossi 2009; Ibarra et al. 2005; Ricles & Popov 1994), only a slight parameter change was applied. A model with a post-yield stiffness of 2% was analysed.

- Panel Width

The exterior claddings in the Pacific Tower were modelled as struts based on the work by Crisafulli (1997) applying a strut width suggested by Priestley and Paulay (1992) of,

$$\boldsymbol{w = 0.25\, d_m} \qquad \textbf{(4-6)}$$

Other strut widths were also suggested in the thesis by Crisafulli (1997) such as the one by Holmes (1961) which takes the width as,

$$\boldsymbol{w = \frac{d_m}{3}} \qquad \textbf{(4-7)}$$

Due to the large uncertainty in the strut width, two more models, an upper lower bound that is $w = 0.2\, d_m$ and a lower bound that is $w = \frac{d_m}{3}$, were taken to show the effects of the change in stiffness.

- Floor-Slab Interactions

The work by Ricles and Popov (1989) highlights the increased stiffness and strength of EBFs in composite action with the floor. The increase of stiffness of the EBF depends on the location of the link, whether it is an interior or exterior link. An interior and exterior link, based on experimental data in

Ricles and Popov (1987) has an increased stiffness of about 2.57 times and 1.28 times, respectively. The increase in strength based on the effective width of the slab was suggested similarly to the NZS3404:Part 1:1997 (NZS 2007). To show the effects of the composite action, a model with neither an increase in stiffness nor strength and a model applying the increased stiffness suggested by Ricles and Popov (1989) was analysed.

The sensitivity analyses in done by running the model with modifications in the 7 parameters discussed earlier through four sets of ground motion records of the Canterbury 2010-2011 series. Each set contains three strong motion site records, CBGS, CCCC and CHHC (except for the June 2011 event which one of the three sites, CCCC, did not record the ground motion), presented in Figure 4.38. The acceleration demands from each station is then averaged for each event, which its response spectra (based on maximum horizontal acceleration to comply with the New Zealand Code (McVerry et al. 2006)) is shown in Figure 4.39 (for the complete records, refer to Appendix D), in which the structural analysis resulting peak transient floor accelerations and drift demands are averaged. This is done to highlight the effects of the parameters in different earthquake intensities and demands.

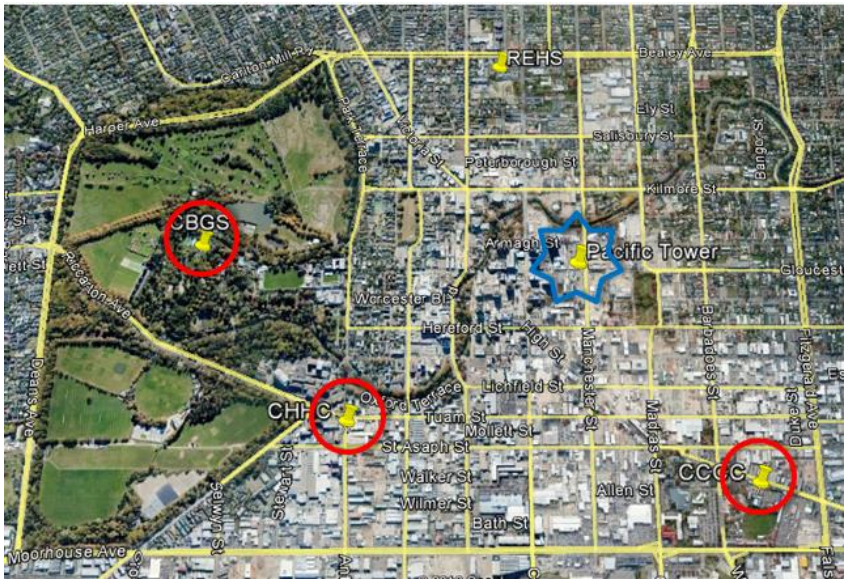

Figure 4.38. Strong Motion Sites in the Christchurch CBD considered

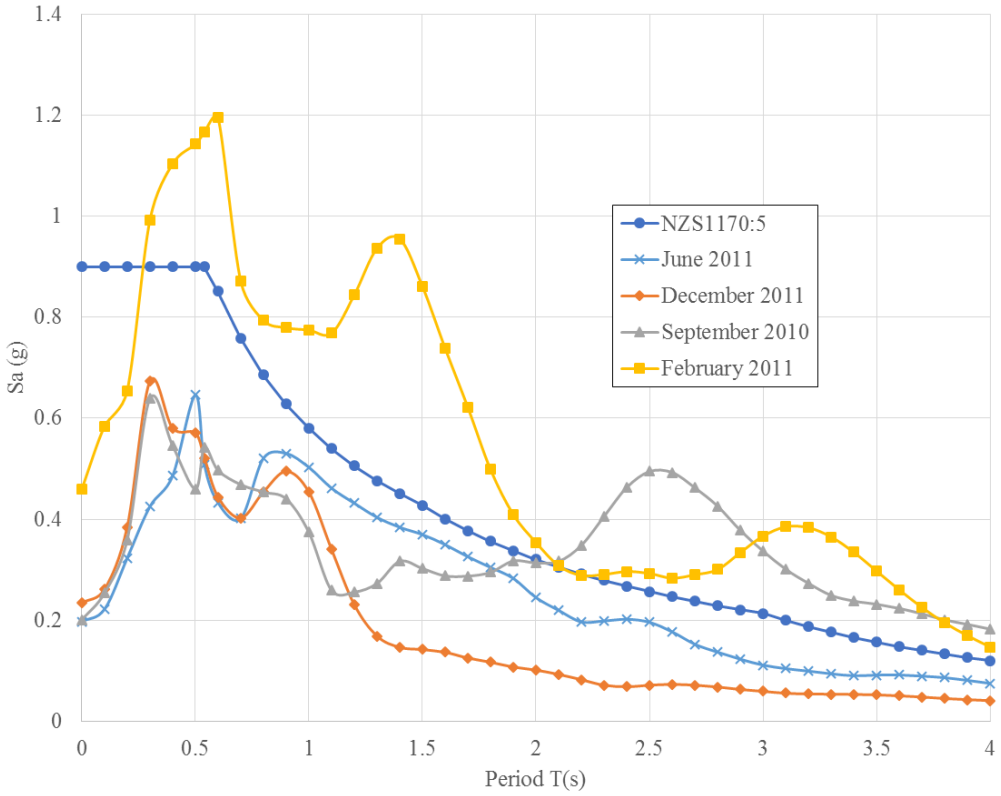

Figure 4.39. Acceleration Response Spectra of Earthquake Records for the Canterbury 2010-2011 Earthquake Series

In conclusion, the sensitivity tests are summarized in Table 4-13.

Table 4-13. Sensitivity Analyses

Model	Damping Model	Damping Value	Foundation Stiffness	Beam-Column Joint	Hysteresis Model	Precast Panel	Floor Effects
Control	Linear Damping (ICTYPE 2)	3%	15mm	Pinned	Bilinear 0.03	0.25 X Length	1.2 X Stiffness + Strength from Slab
Damping Type	Rayleigh Tangent Secant Damping (ICTYPE 6)	3%	15mm	Pinned	Bilinear 0.03	0.25 X Length	1.2 X Stiffness + Strength from Slab
Damping Value 2%	Linear Damping (ICTYPE 2)	2%	15mm	Pinned	Bilinear 0.03	0.25 X Length	1.2 X Stiffness + Strength from Slab
Damping Value 4%	Linear Damping (ICTYPE 2)	4%	15mm	Pinned	Bilinear 0.03	0.25 X Length	1.2 X Stiffness + Strength from Slab
Foundation 10	Linear Damping (ICTYPE 2)	3%	10mm	Pinned	Bilinear 0.03	0.25 X Length	1.2 X Stiffness + Strength from Slab
Foundation 20	Linear Damping (ICTYPE 2)	3%	20mm	Pinned	Bilinear 0.03	0.25 X Length	1.2 X Stiffness + Strength from Slab
Beam-Column Joint	Linear Damping (ICTYPE 2)	3%	15mm	Fixed	Bilinear 0.03	0.25 X Length	1.2 X Stiffness + Strength from Slab
Hysteresis	Linear Damping (ICTYPE 2)	3%	15mm	Pinned	Bilinear 0.02	0.25 X Length	1.2 X Stiffness + Strength from Slab
Panel Low	Linear Damping (ICTYPE 2)	3%	15mm	Pinned	Bilinear 0.03	0.2 X Length	1.2 X Stiffness + Strength from Slab

Table 4-14. Sensitivity Analyses (cont.)

Model	Damping Model	Damping Value	Foundation Stiffness	Beam-Column Joint	Hysteresis Model	Precast Panel	Floor Effects
Panel High	Linear Damping (ICTYPE 2)	3%	15mm	Pinned	Bilinear 0.03	0.33 X Length	1.2 X Stiffness + Strength from Slab
Floor Low	Linear Damping (ICTYPE 2)	3%	15mm	Pinned	Bilinear 0.03	0.25 X Length	1 X Stiffness and No Additional Strength
Floor High	Linear Damping (ICTYPE 2)	3%	15mm	Pinned	Bilinear 0.03	0.25 X Length	1.28 X Stiffness (+) and 2.57 X Stiffness (-) + Strength from Slab

The results of the sensitivity analyses are shown in Table 4-13 and Table 4-14 comparing the Fundamental Periods of the case study building and Figure 4.40 to Figure 4.67 comparing the EDPs of different parameters to the Control Model in different intensities of earthquakes.

Table 4-15. Fundamental Period of Building Comparison

	Fundamental Periods (s)				
Model	Z Translation Mode 1	X Translation Mode 1	Torsional Mode 1	Z Translation Mode 2	X Translation Mode 2
Control	4.64	3.56	2.86	1.60	1.26
Damping Type	4.64	3.56	2.86	1.60	1.26
Damping Value 2%	4.64	3.56	2.86	1.60	1.26
Damping Value 4%	4.64	3.56	2.86	1.60	1.26
Foundation 10	4.45	3.42	2.76	1.59	1.24
Foundation 20	4.81	3.67	2.93	1.62	1.27
Beam-Column Joint	3.85	3.38	2.38	1.23	1.08
Hysteresis	4.64	3.56	2.86	1.60	1.26
Panel Low	4.67	3.60	2.89	1.61	1.27
Panel High	4.60	3.51	2.82	1.59	1.25
Floor Low	4.79	3.61	2.92	1.67	1.31
Floor High	4.56	3.44	2.78	1.51	1.15

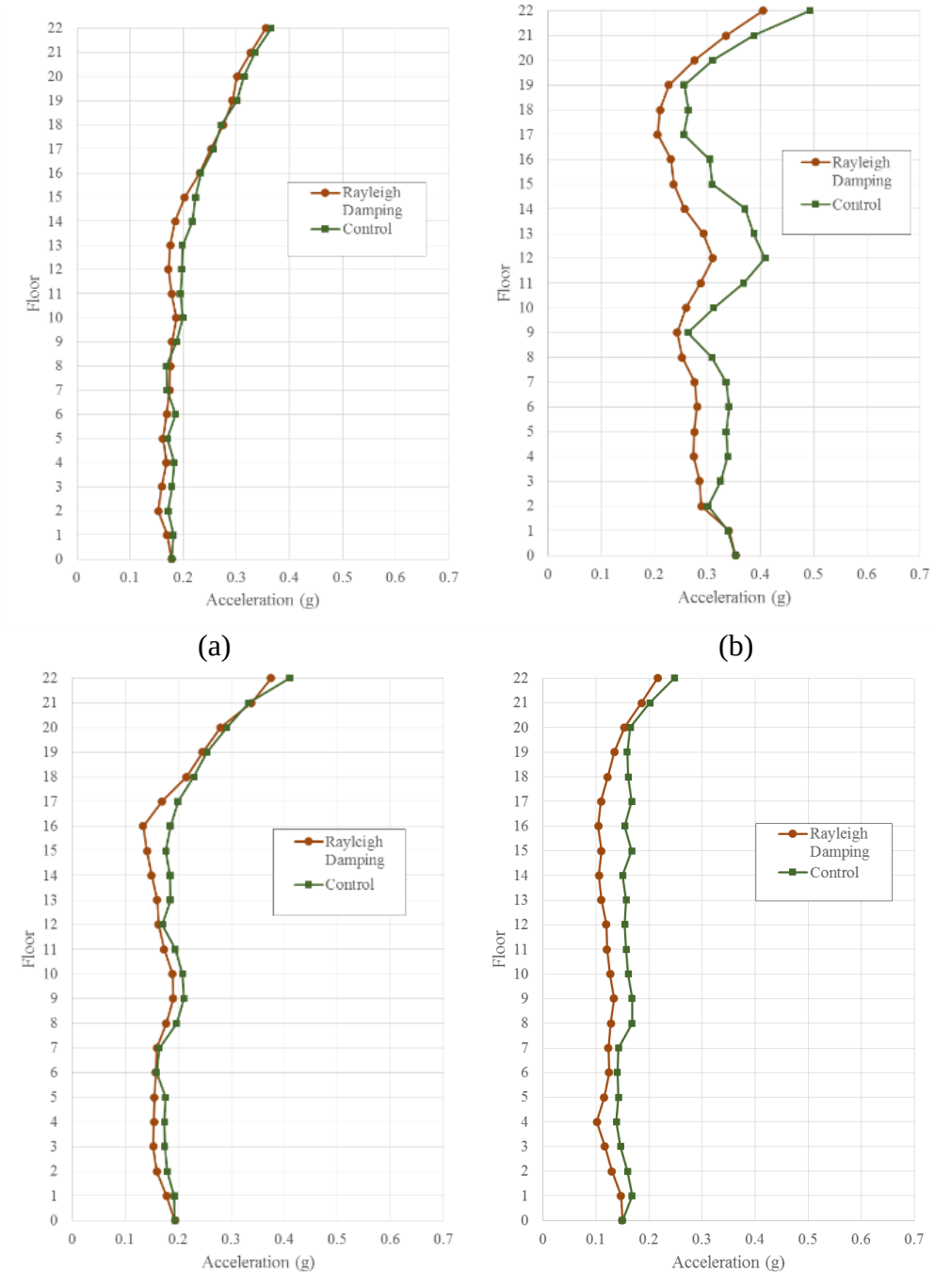

Figure 4.40. Damping Type - Peak Floor Acceleration Demands in the X-Direction (average of all stations for each event) for (a) September 2010 (b) February 2011 (c) June 2011 and (d) December 2011

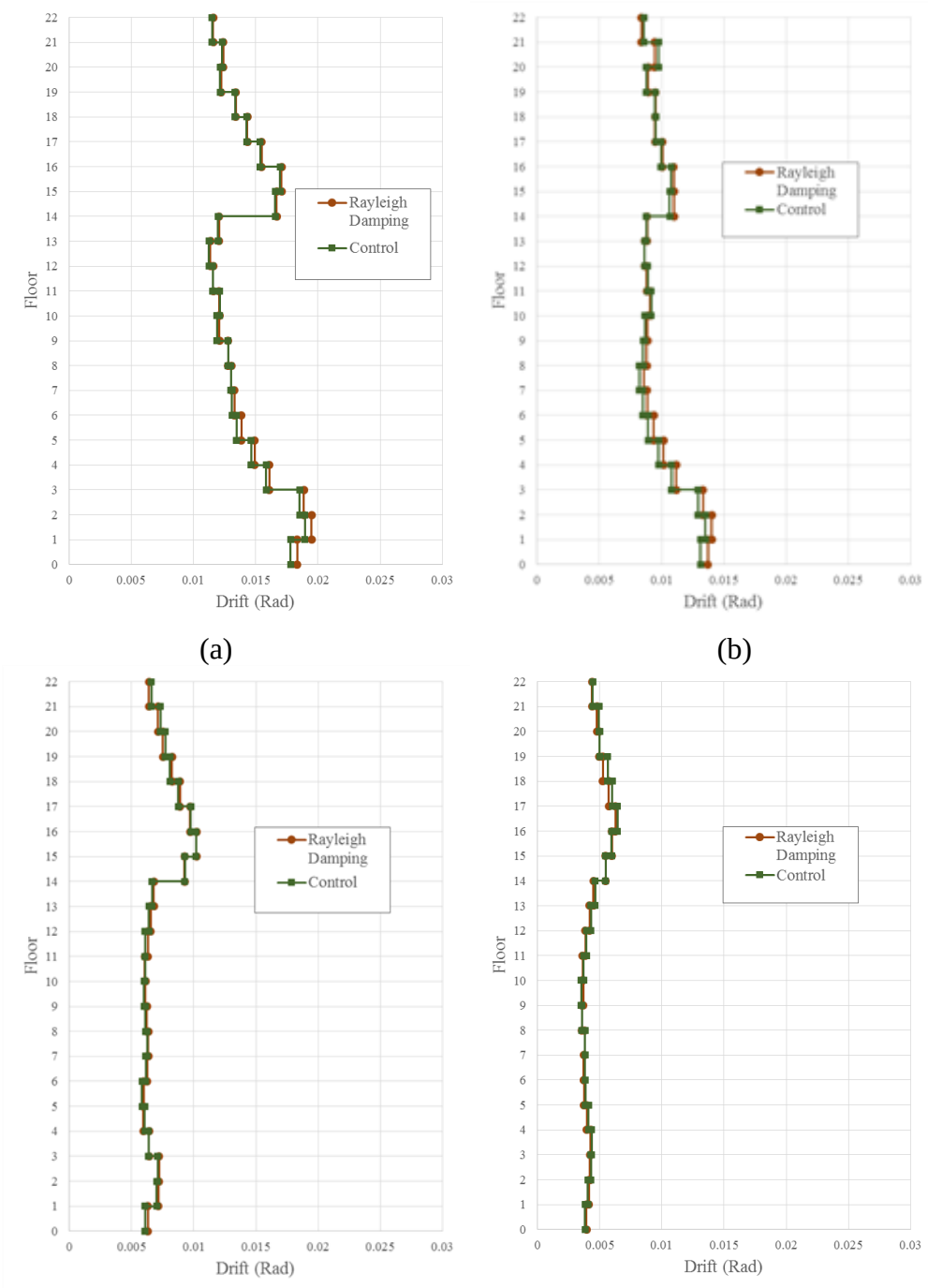

Figure 4.41. Damping Type - Peak Drift Demands in the X-Direction (average of all stations for each event) (a) September 2010 (b) February 2011 (c) June 2011 and (d) December 2011

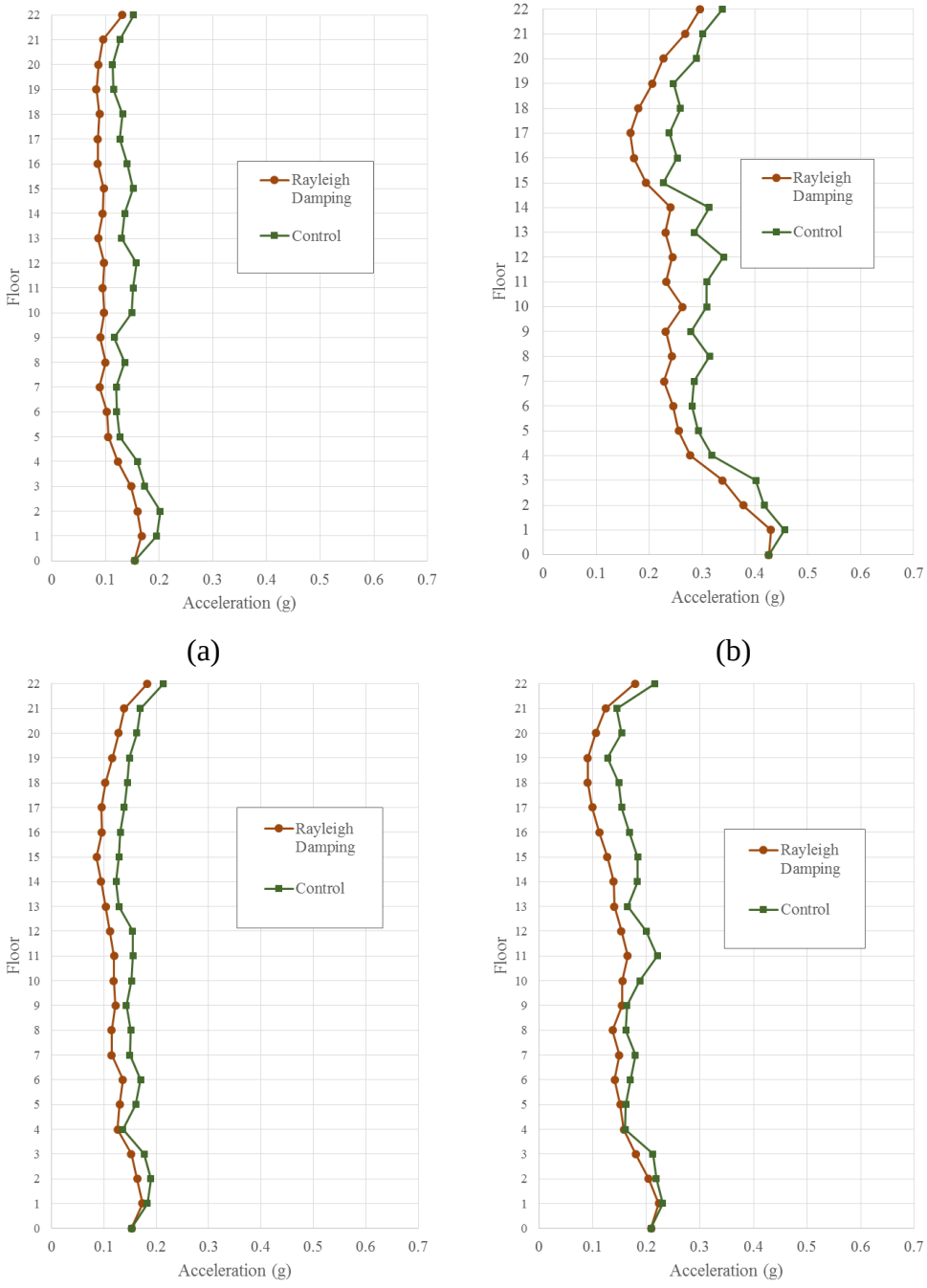

Figure 4.42. Damping Type - Peak Floor Acceleration Demands in the Z-Direction (average of all stations for each event) (a) September 2010 (b) February 2011 (c) June 2011 and (d) December 2011

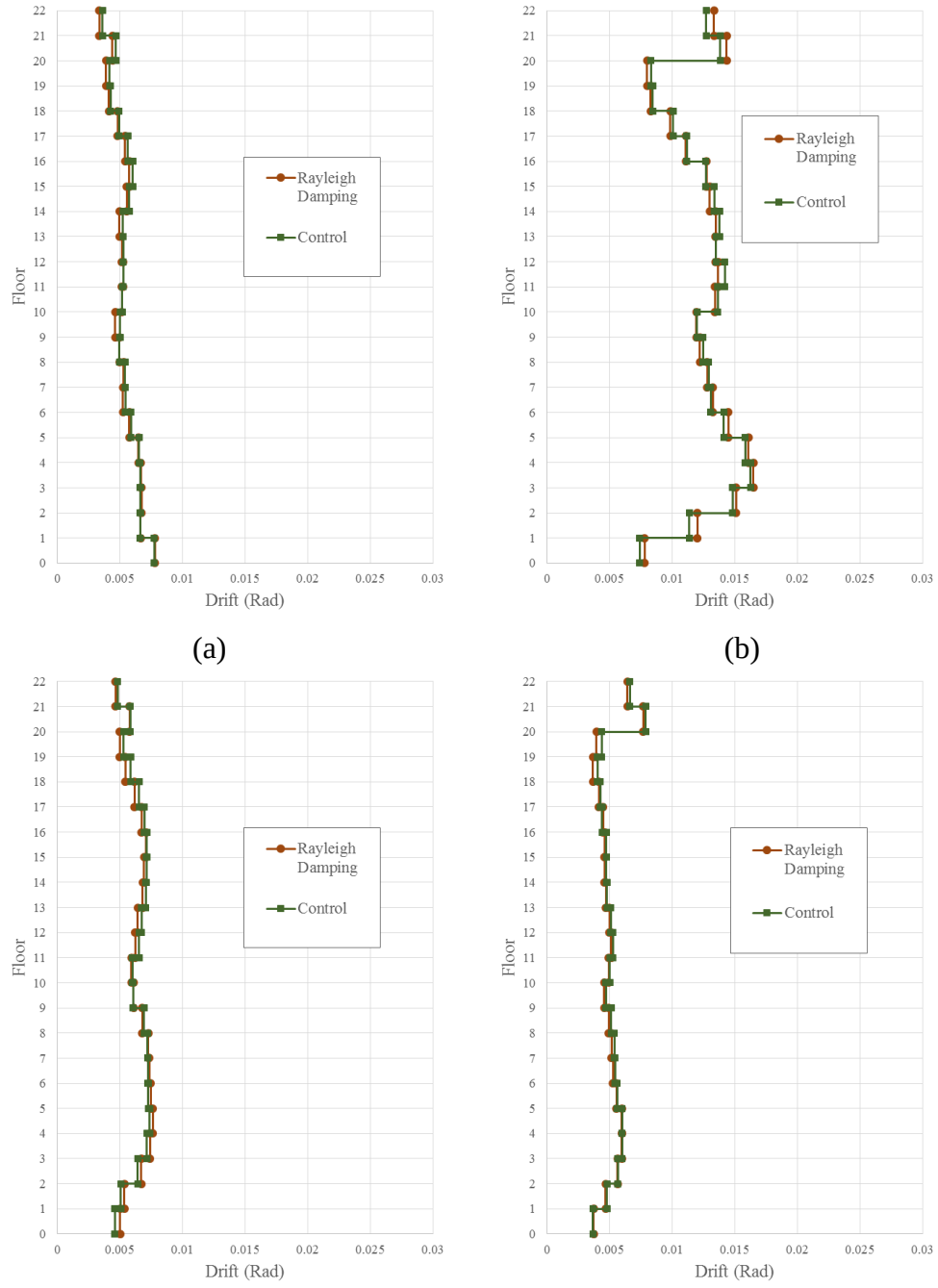

(a) (b)

(c) (d)

Figure 4.43. Damping Type - Peak Drift Demands in the Z-Direction (average of all stations for each event) (a) September 2010 (b) February 2011 (c) June 2011 and (d) December 2011

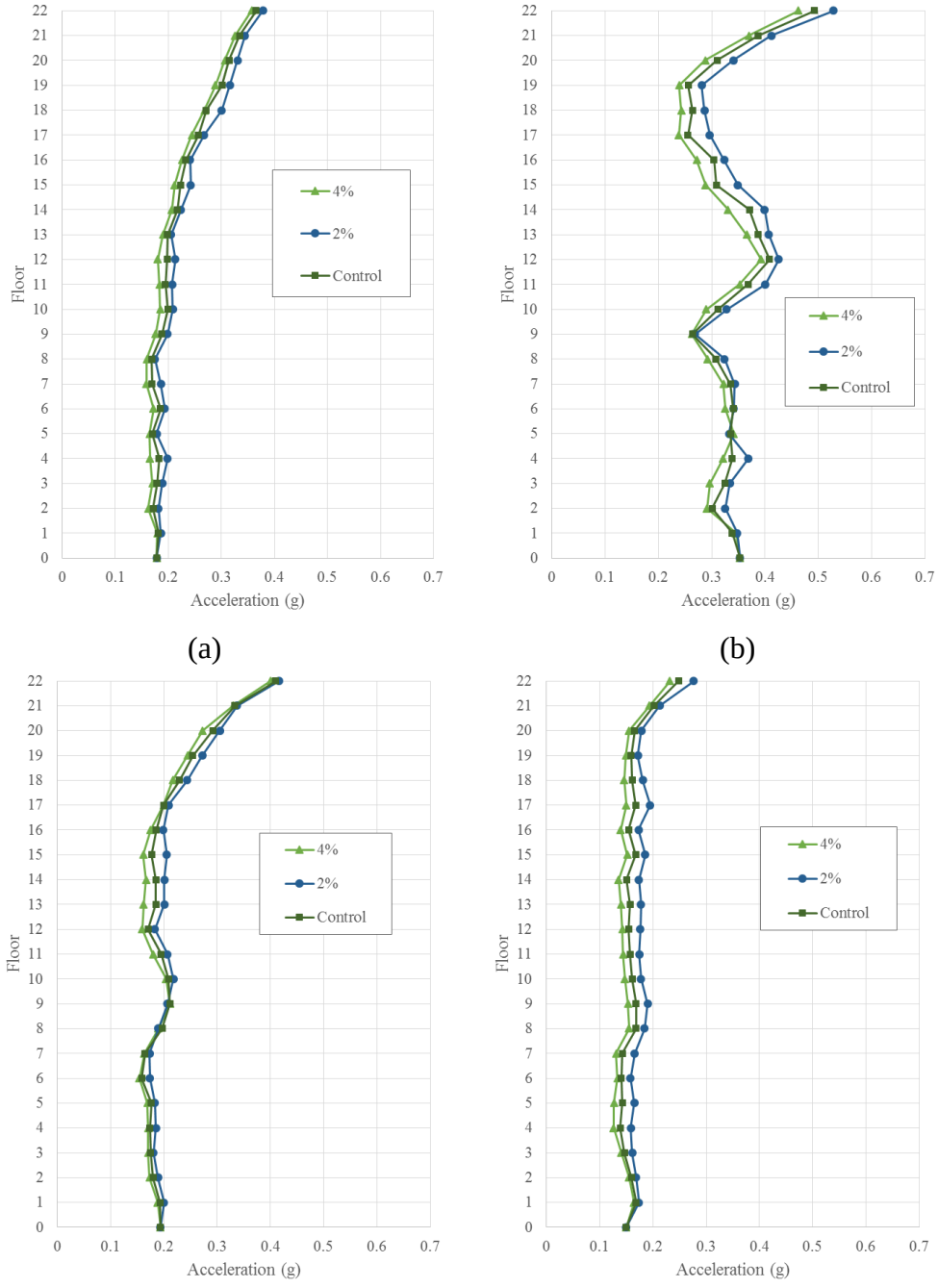

Figure 4.44. Damping Value - Peak Floor Acceleration Demands in the X-Direction (average of all stations for each event) (a) September 2010 (b) February 2011 (c) June 2011 and (d) December 2011

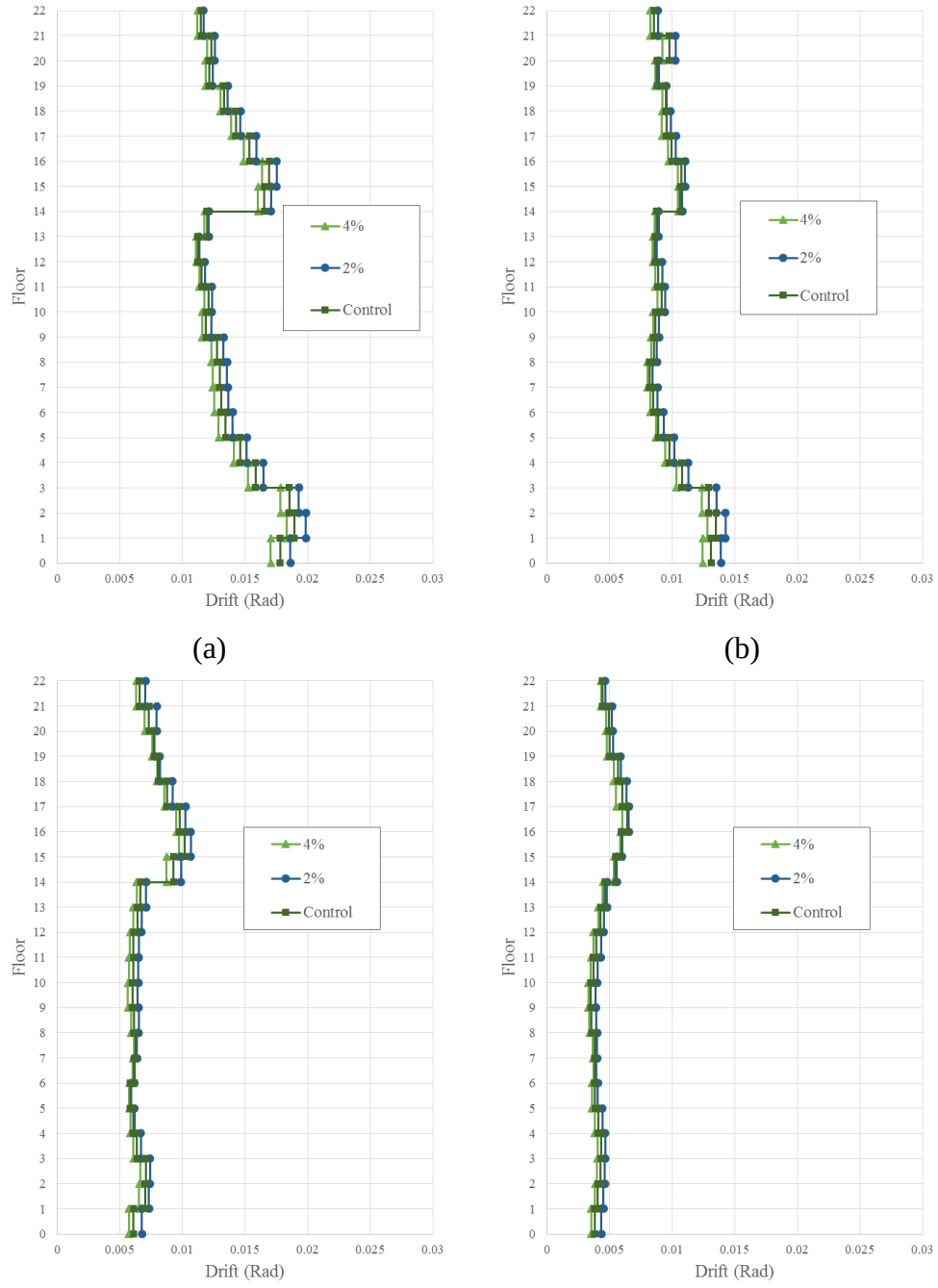

Figure 4.45. Damping Value - Peak Drift Demands in the X-Direction (average of all stations for each event) (a) September 2010 (b) February 2011 (c) June 2011 and (d) December 2011

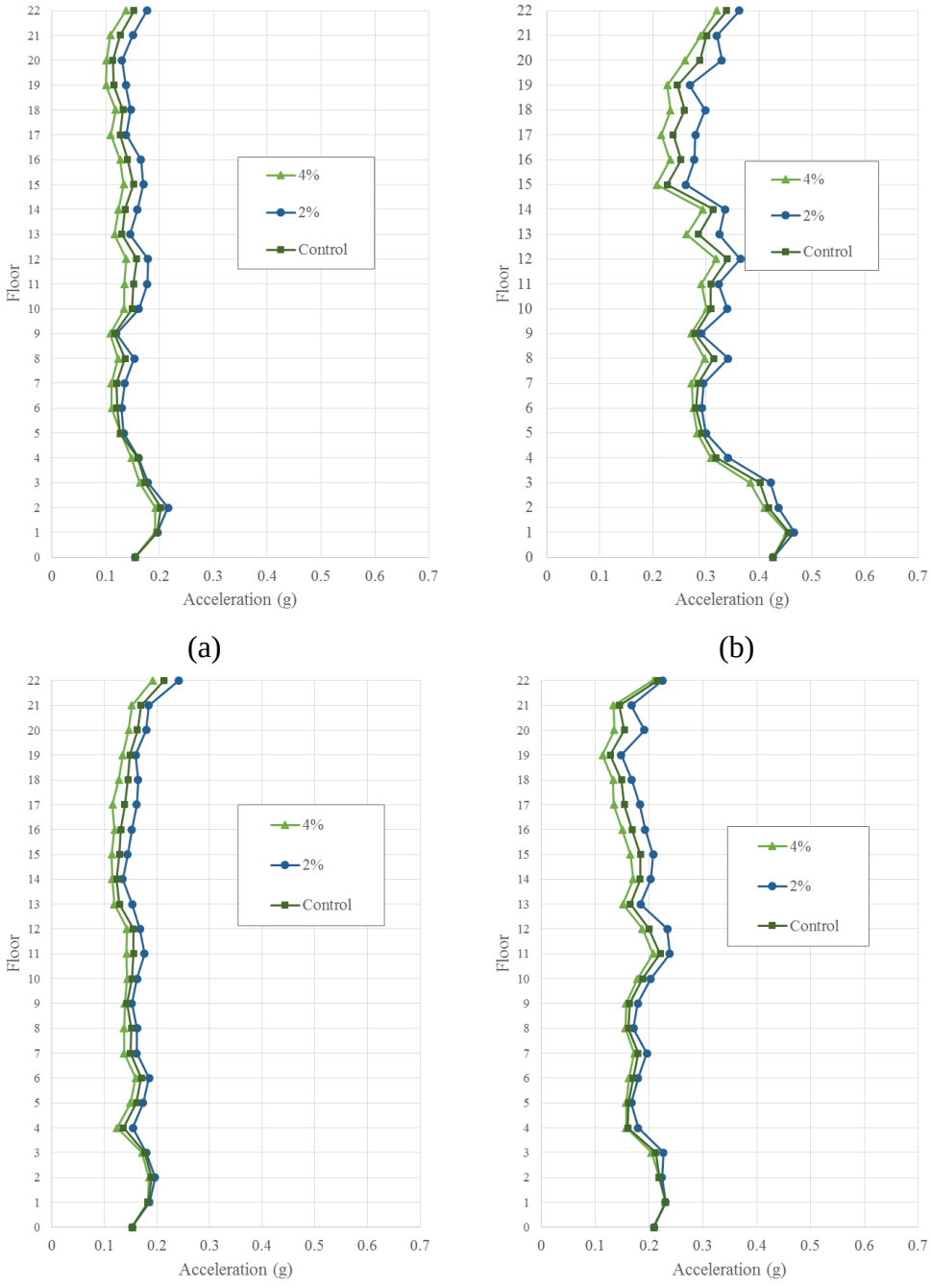

Figure 4.46. Damping Value - Peak Floor Acceleration Demands in the Z-Direction (average of all stations for each event) (a) September 2010 (b) February 2011 (c) June 2011 and (d) December 2011

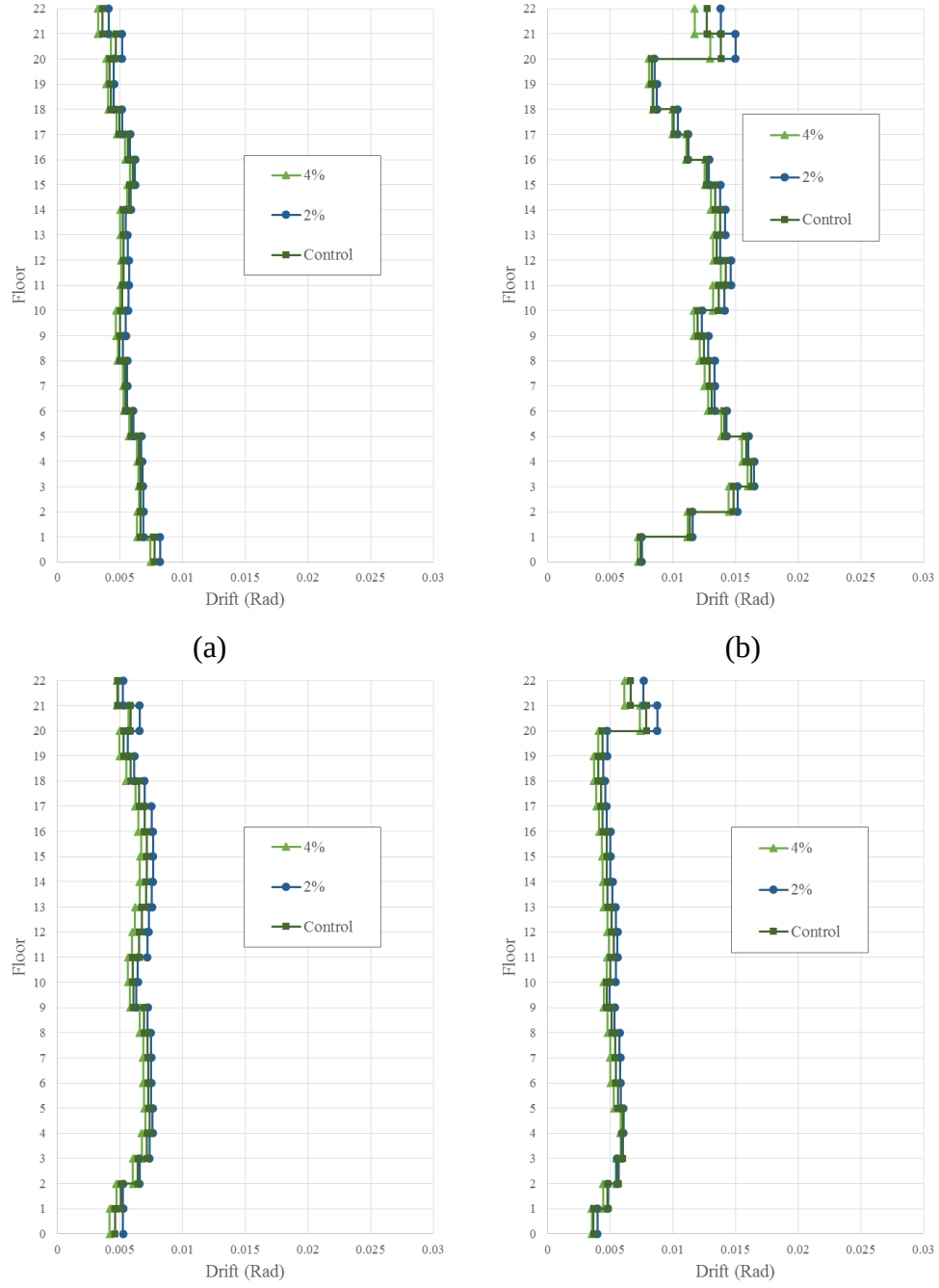

Figure 4.47. Damping Value - Peak Drift Demands in the Z-Direction (average of all stations for each event) (a) September 2010 (b) February 2011 (c) June 2011 and (d) December 2011

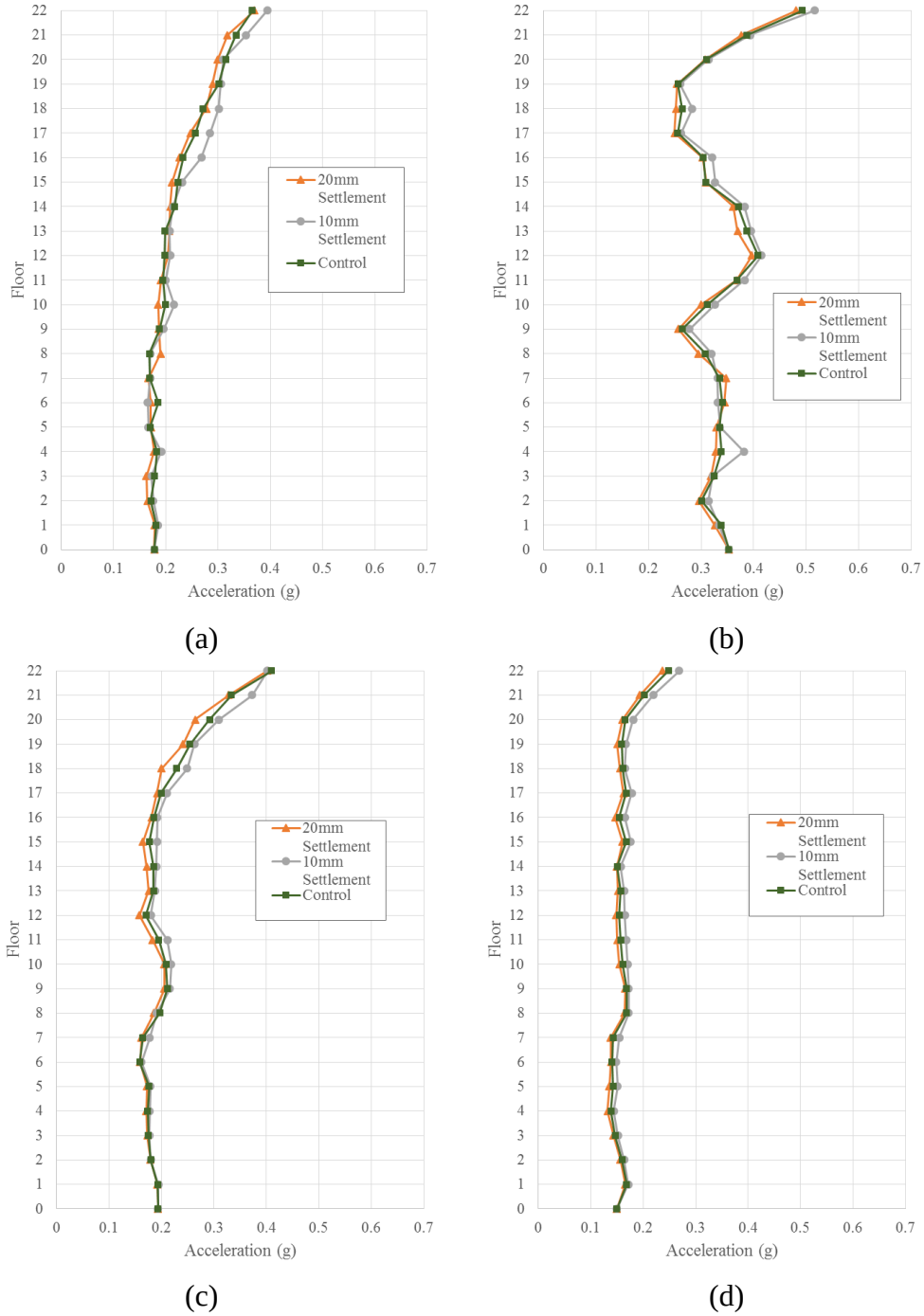

Figure 4.48. Foundation Settlement - Peak Floor Acceleration Demands in the X-Direction (average of all stations for each event) (a) September 2010 (b) February 2011 (c) June 2011 and (d) December 2011

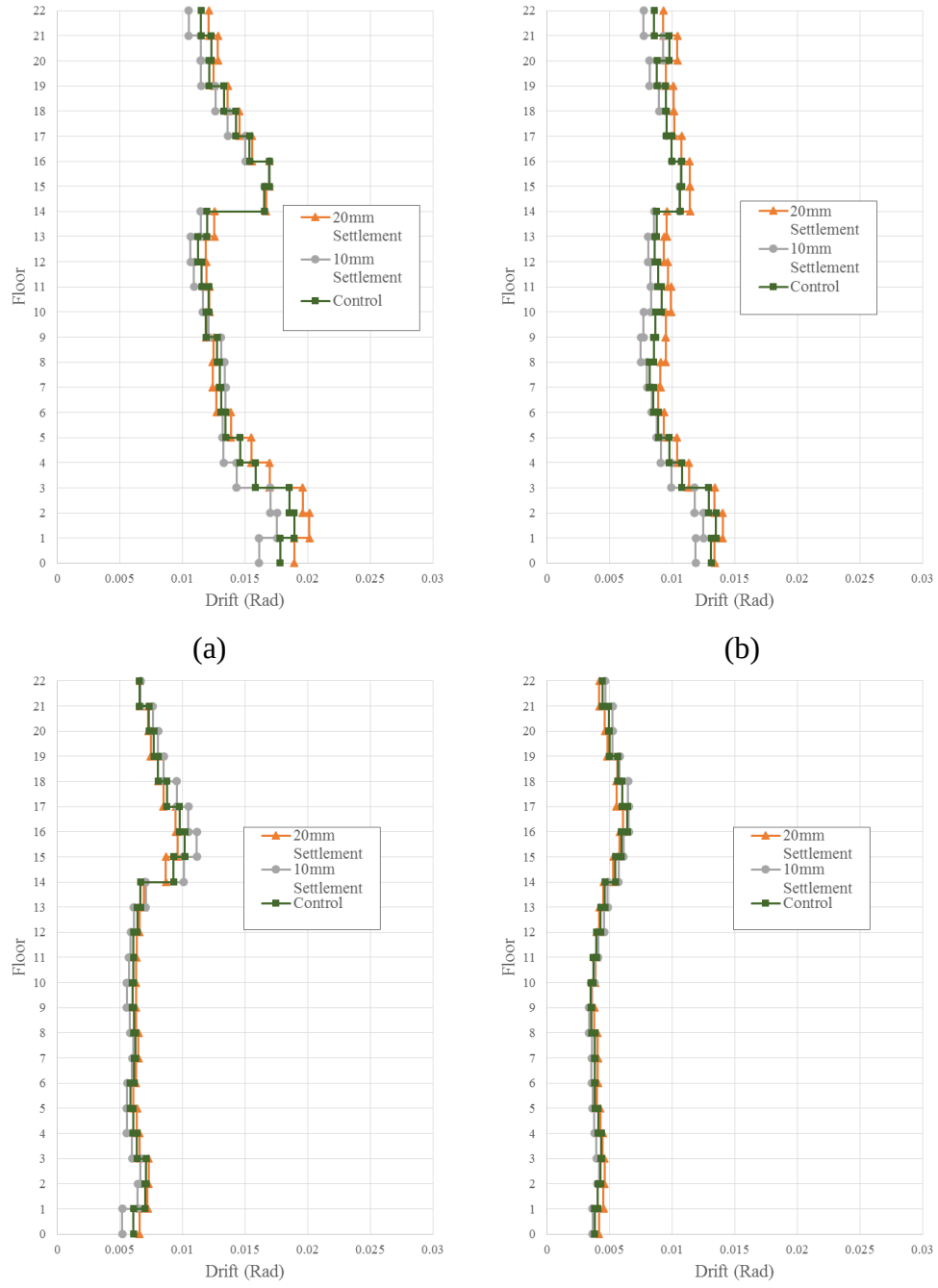

Figure 4.49. Foundation Settlement - Peak Drift Demands in the X-Direction (average of all stations for each event) (a) September 2010 (b) February 2011 (c) June 2011 and (d) December 2011

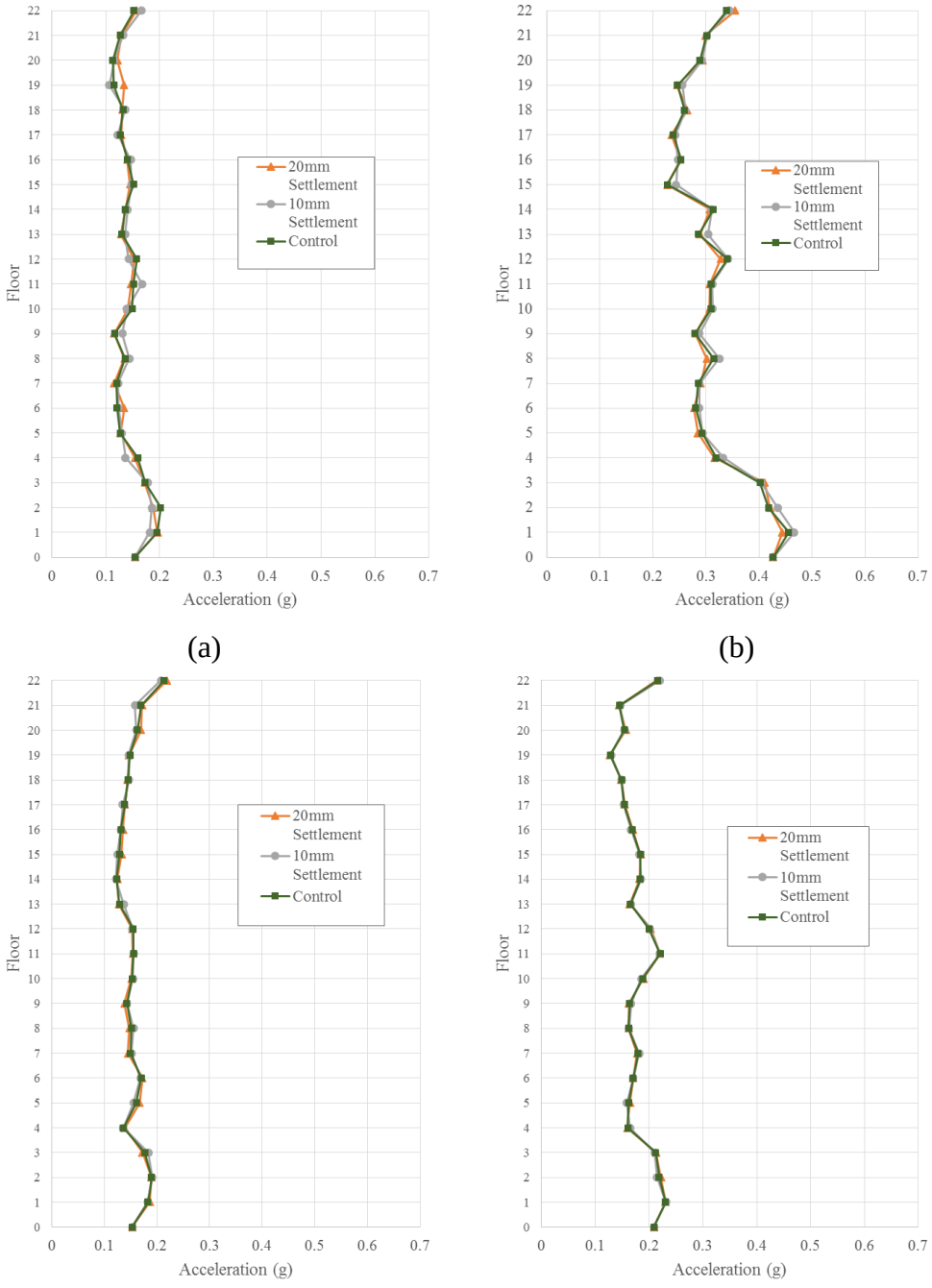

Figure 4.50. Foundation Settlement - Peak Floor Acceleration Demands in the Z-Direction (average of all stations for each event) (a) September 2010 (b) February 2011 (c) June 2011 and (d) December 2011

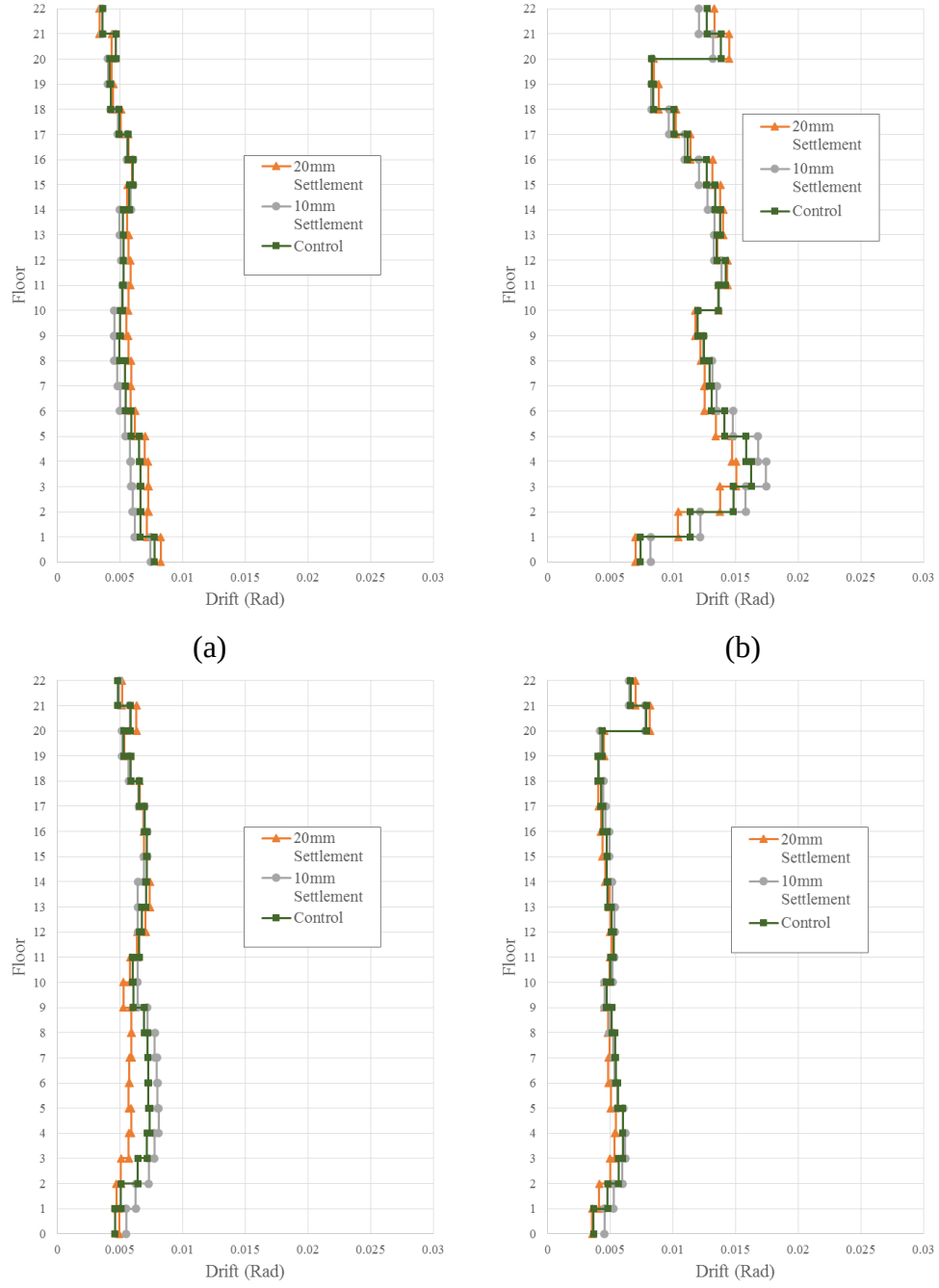

Figure 4.51. Foundation Settlement - Peak Drift Demands in the Z-Direction (average of all stations for each event) (a) September 2010 (b) February 2011 (c) June 2011 and (d) December 2011

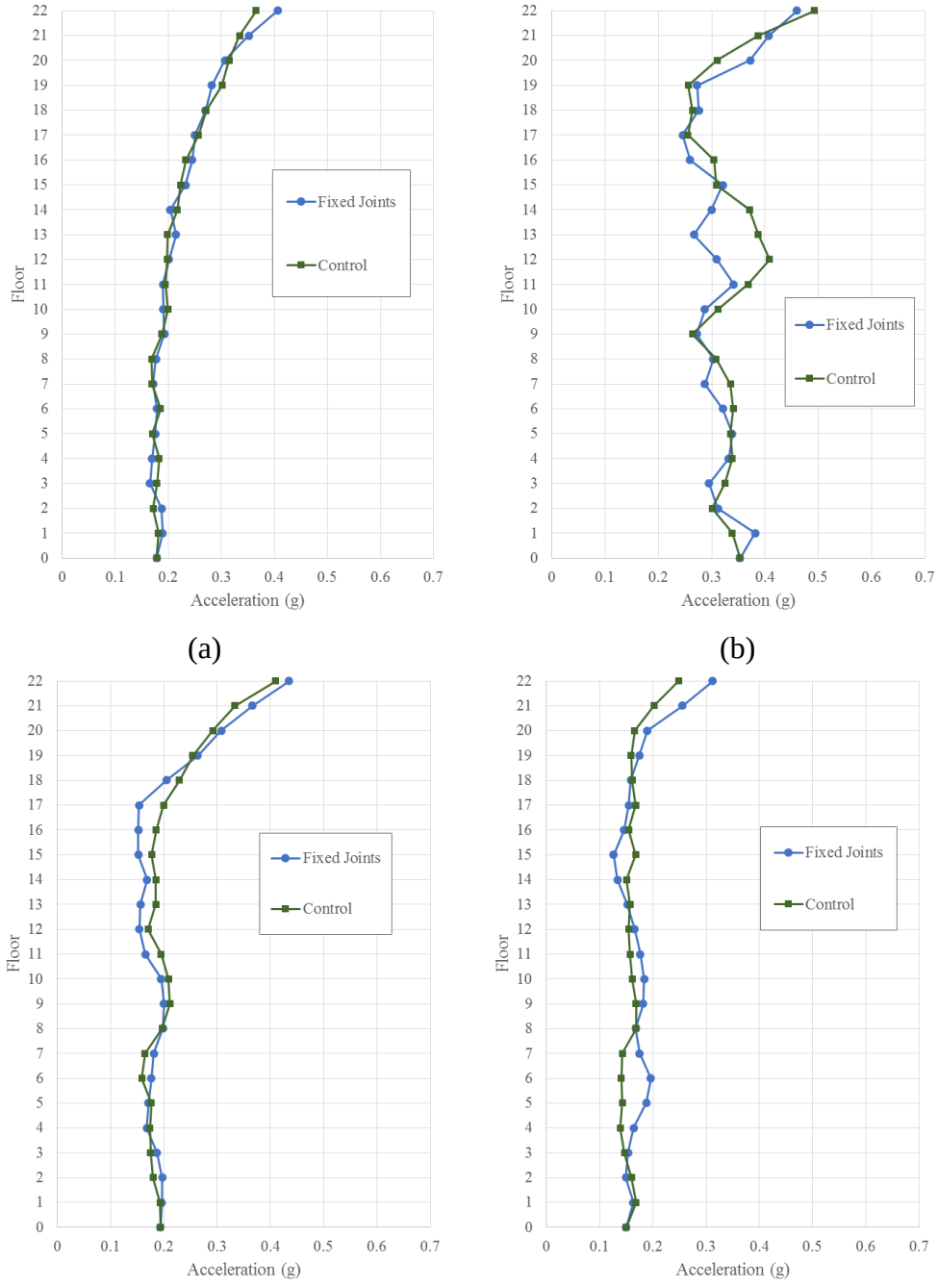

Figure 4.52. Beam-Column Joints - Peak Floor Acceleration Demands in the X-Direction (average of all stations for each event) (a) September 2010 (b) February 2011 (c) June 2011 and (d) December 2011

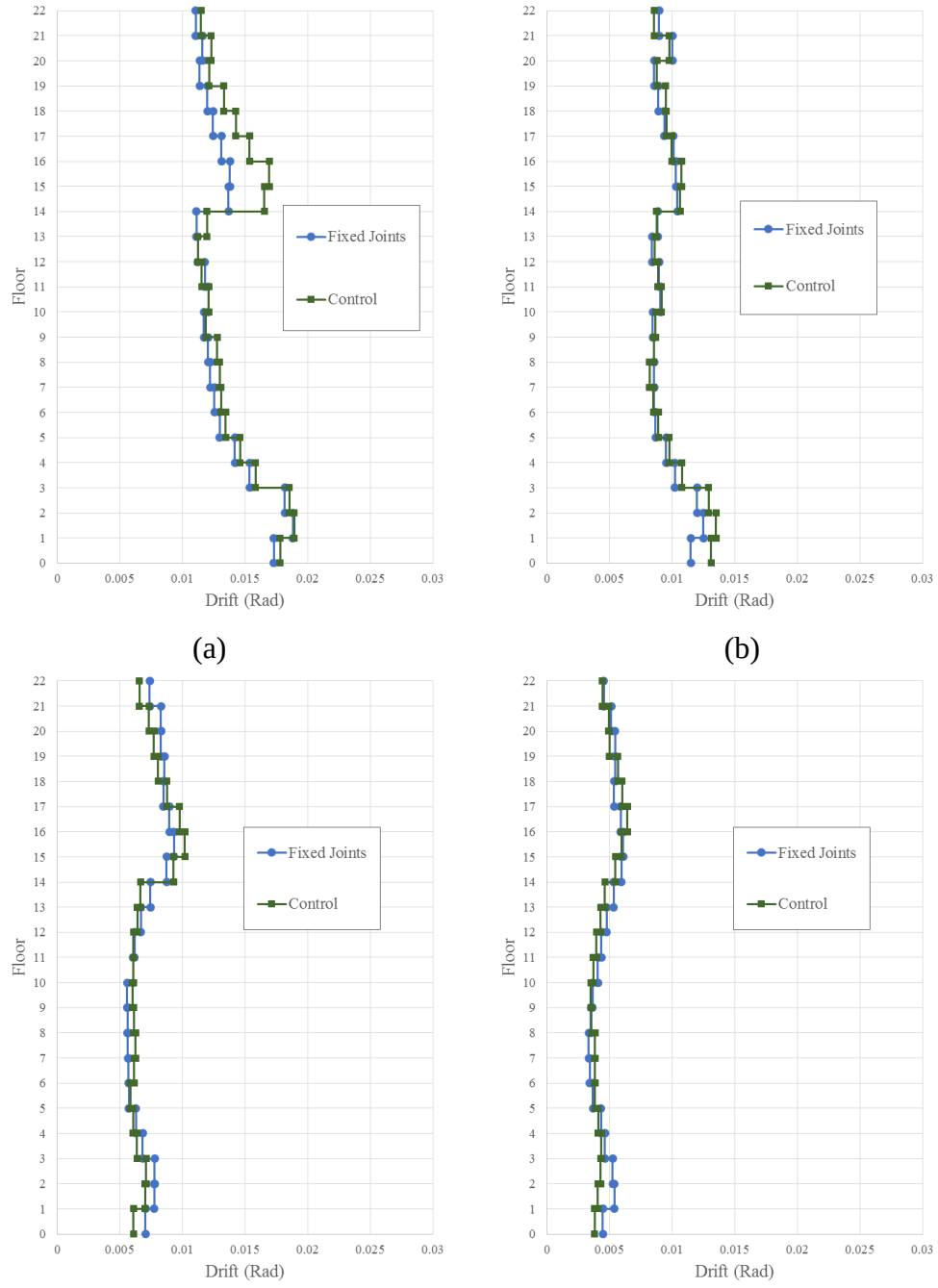

Figure 4.53. Beam-Column Joints - Peak Drift Demands in the X-Direction (average of all stations for each event) (a) September 2010 (b) February 2011 (c) June 2011 and (d) December 2011

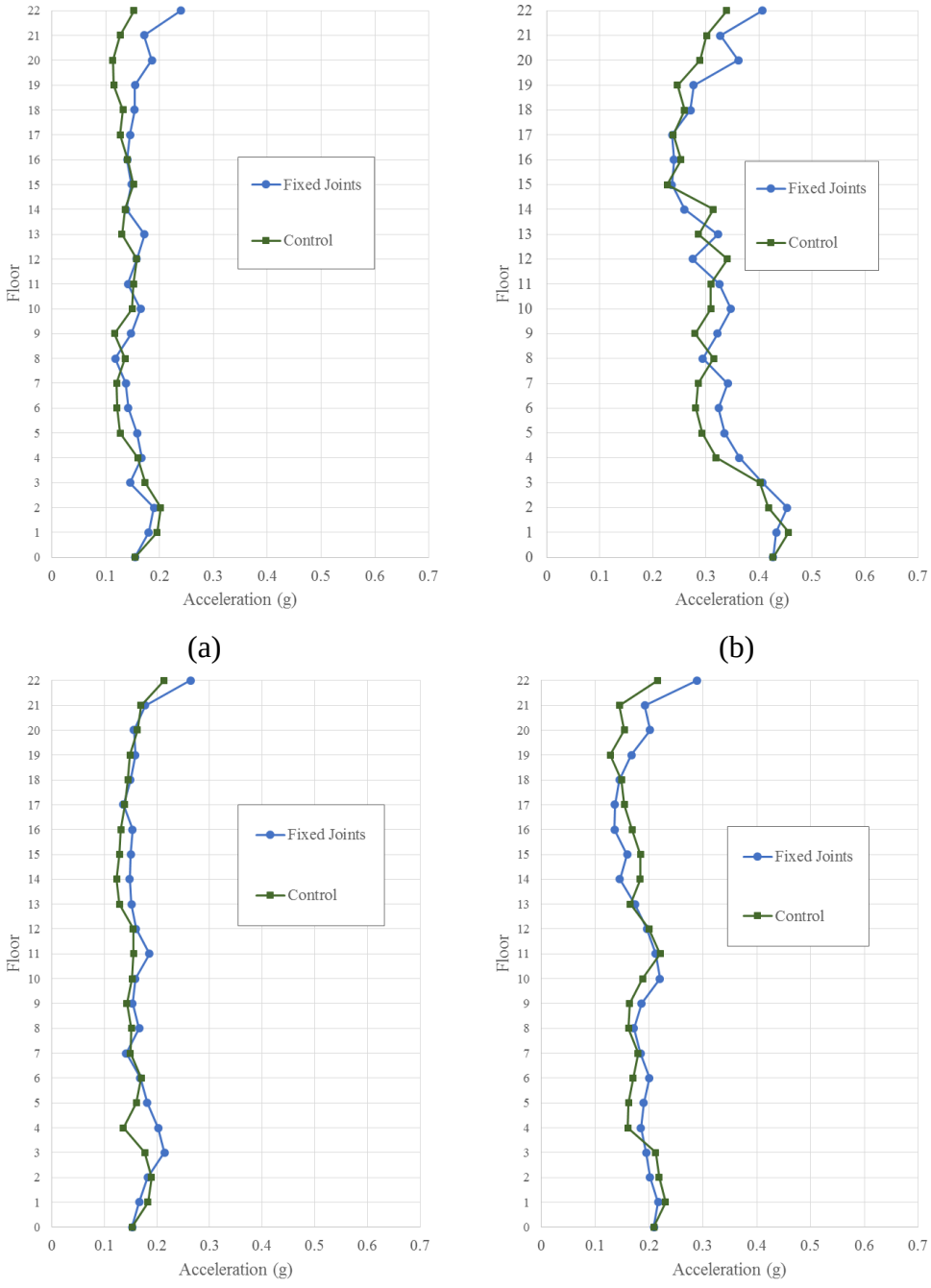

Figure 4.54. Beam-Column Joints - Peak Floor Acceleration Demands in the Z-Direction (average of all stations for each event) (a) September 2010 (b) February 2011 (c) June 2011 and (d) December 2011

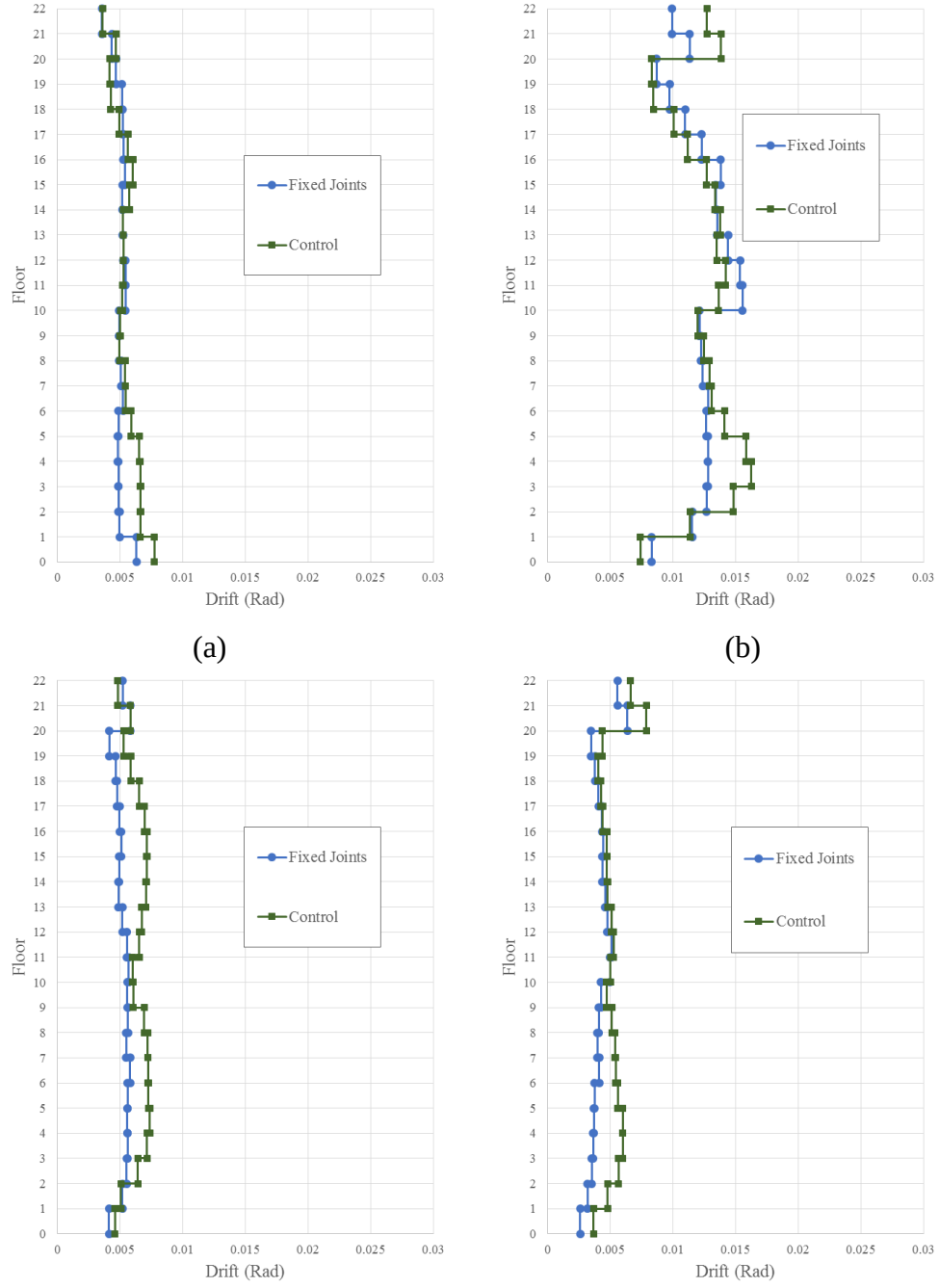

Figure 4.55. Beam-Column Joints - Peak Drift Demands in the Z-Direction (average of all stations for each event) (a) September 2010 (b) February 2011 (c) June 2011 and (d) December 2011

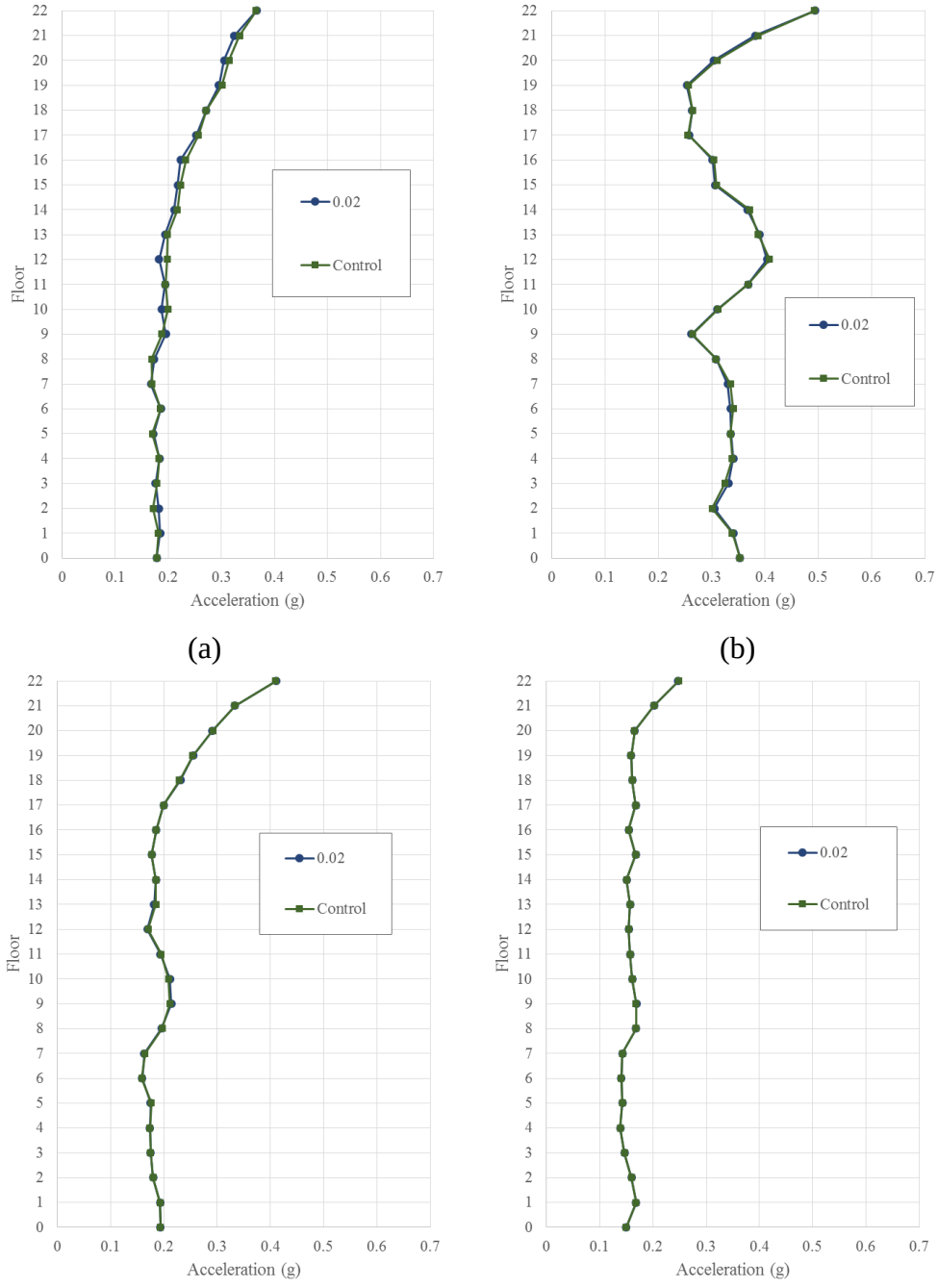

Figure 4.56. Hysteresis Model Factor - Peak Floor Acceleration Demands in the X-Direction (average of all stations for each event) (a) September 2010 (b) February 2011 (c) June 2011 and (d) December 2011

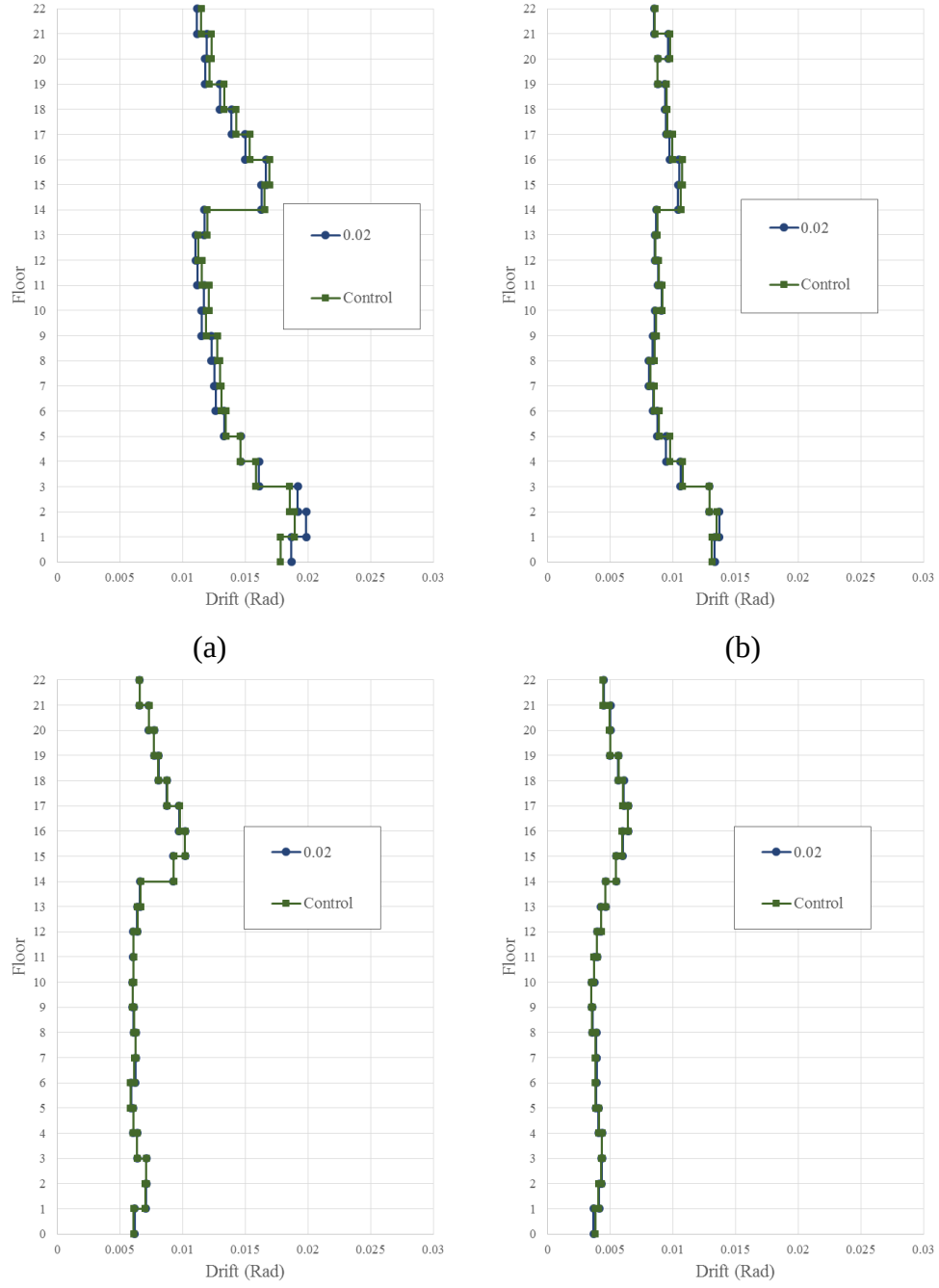

Figure 4.57. Hysteresis Model Factor - Peak Drift Demands in the X-Direction (average of all stations for each event) (a) September 2010 (b) February 2011 (c) June 2011 and (d) December 2011

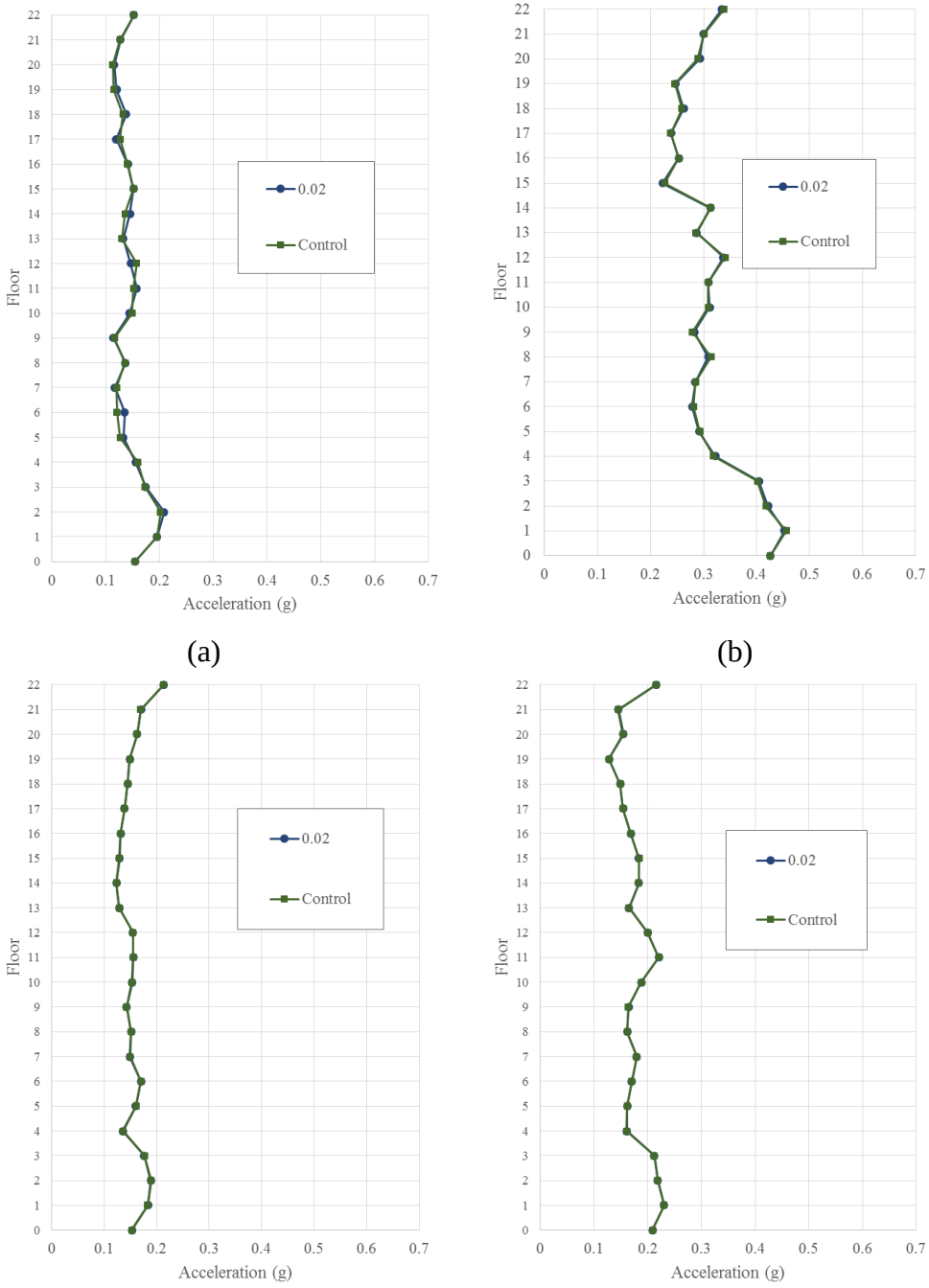

Figure 4.58. Hysteresis Model Factor - Peak Floor Acceleration Demands in the Z-Direction (average of all stations for each event) (a) September 2010 (b) February 2011 (c) June 2011 and (d) December 2011

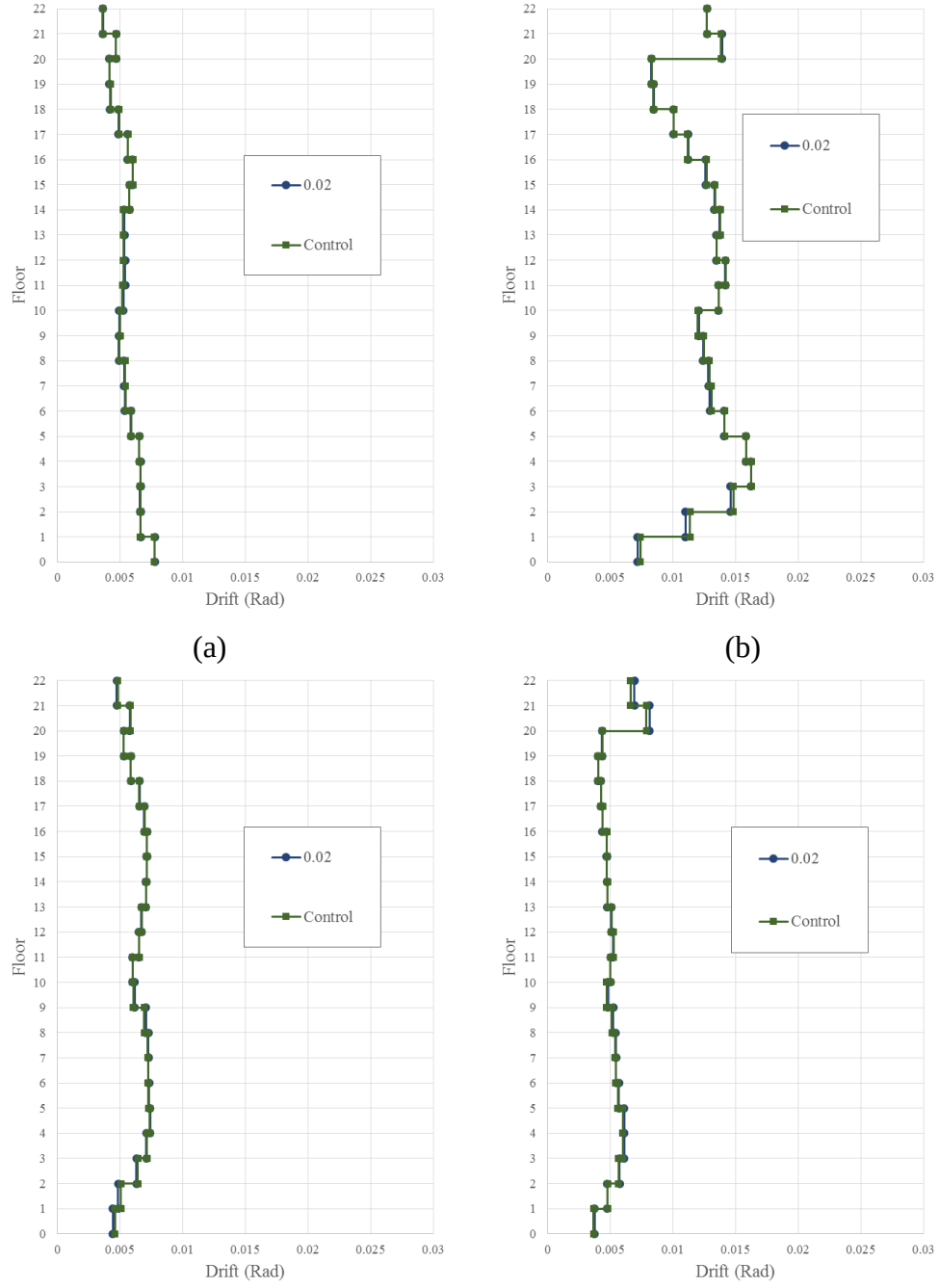

Figure 4.59. Hysteresis Model Factor - Peak Drift Demands in the Z-Direction (average of all stations for each event) (a) September 2010 (b) February 2011 (c) June 2011 and (d) December 2011

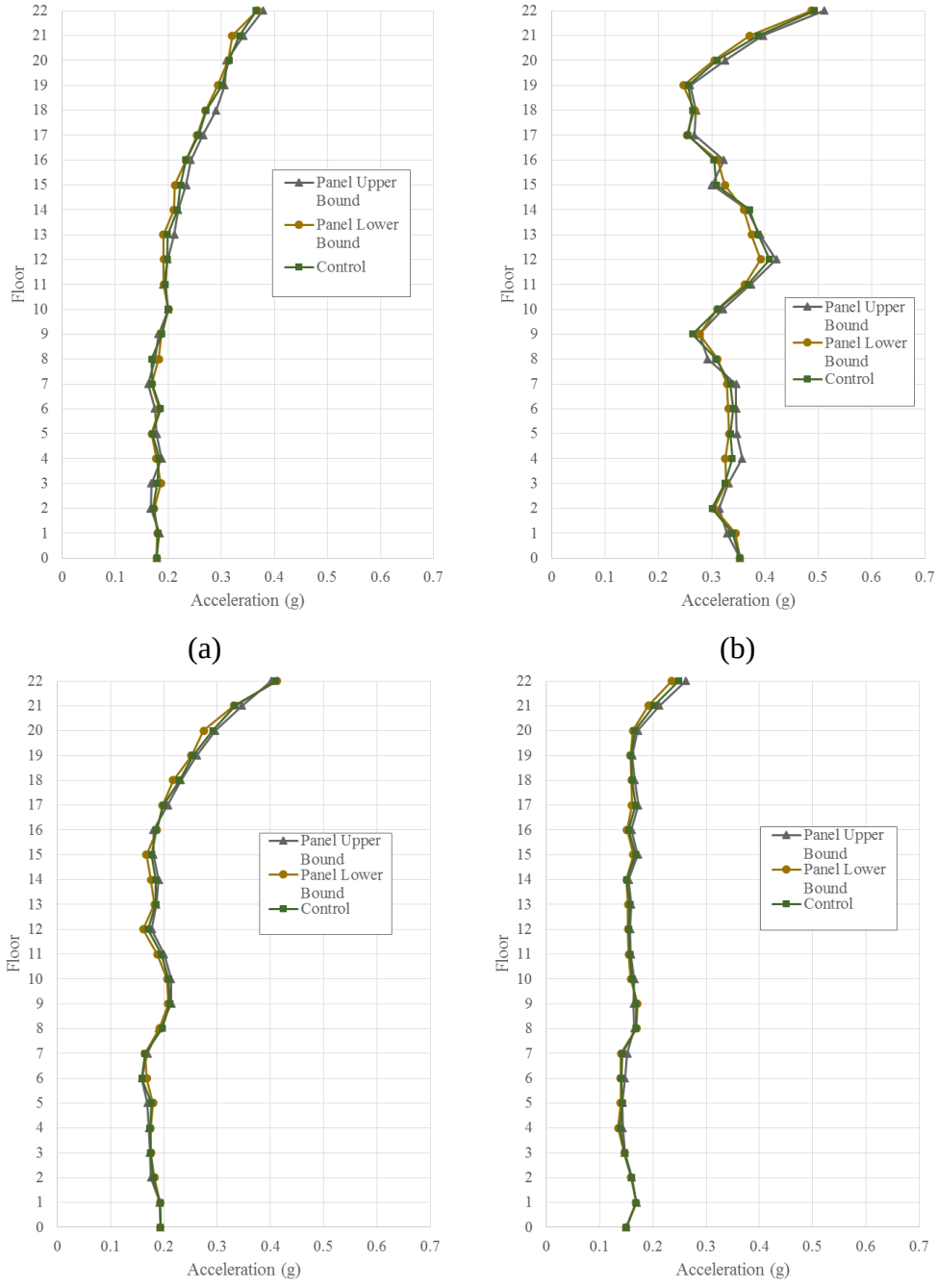

Figure 4.60. Panel Width - Peak Floor Acceleration Demands in the X-Direction (average of all stations for each event) (a) September 2010 (b) February 2011 (c) June 2011 and (d) December 2011

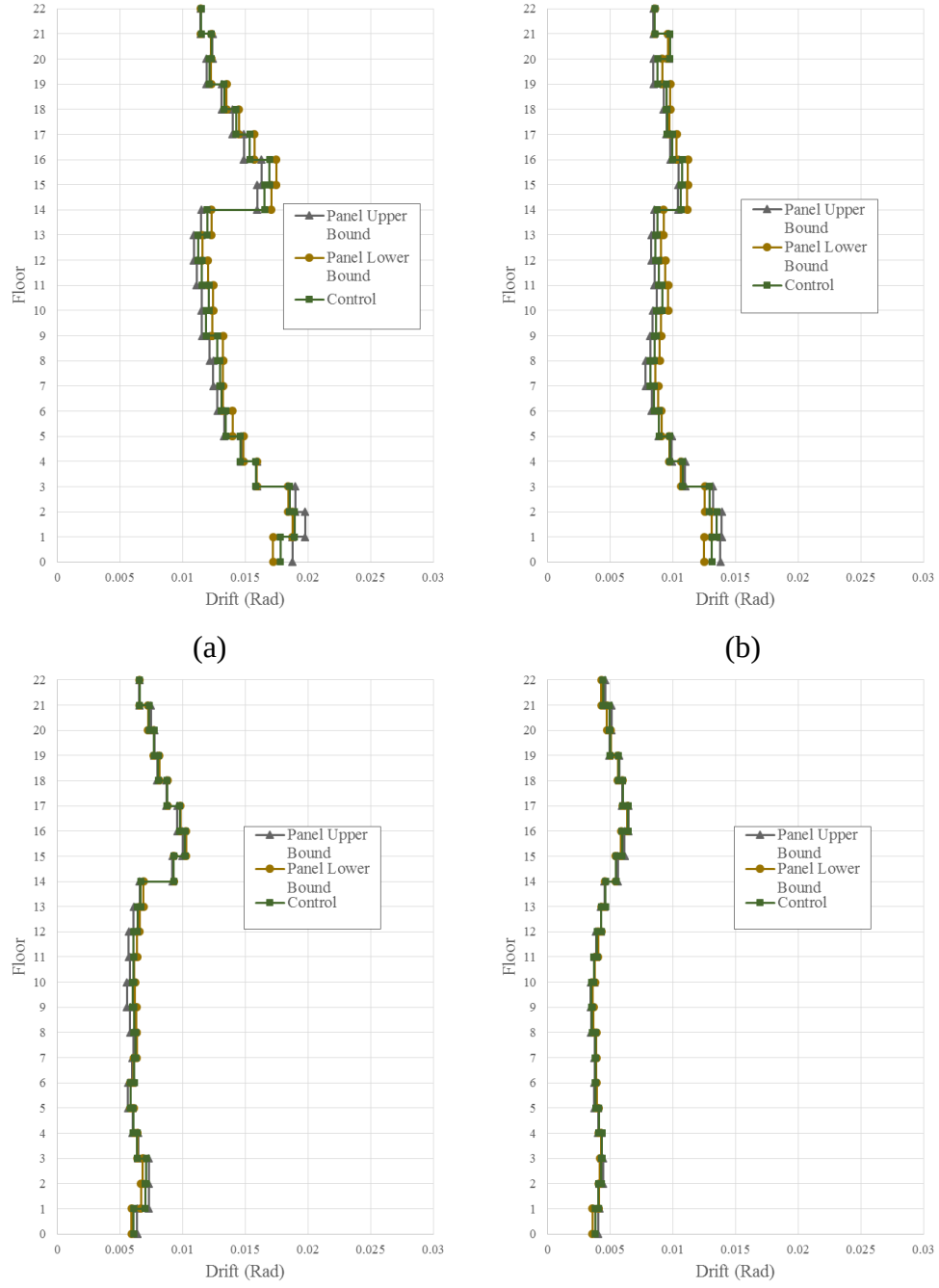

Figure 4.61. Panel Width - Peak Drift Demands in the X-Direction (average of all stations for each event) (a) September 2010 (b) February 2011 (c) June 2011 and (d) December 2011

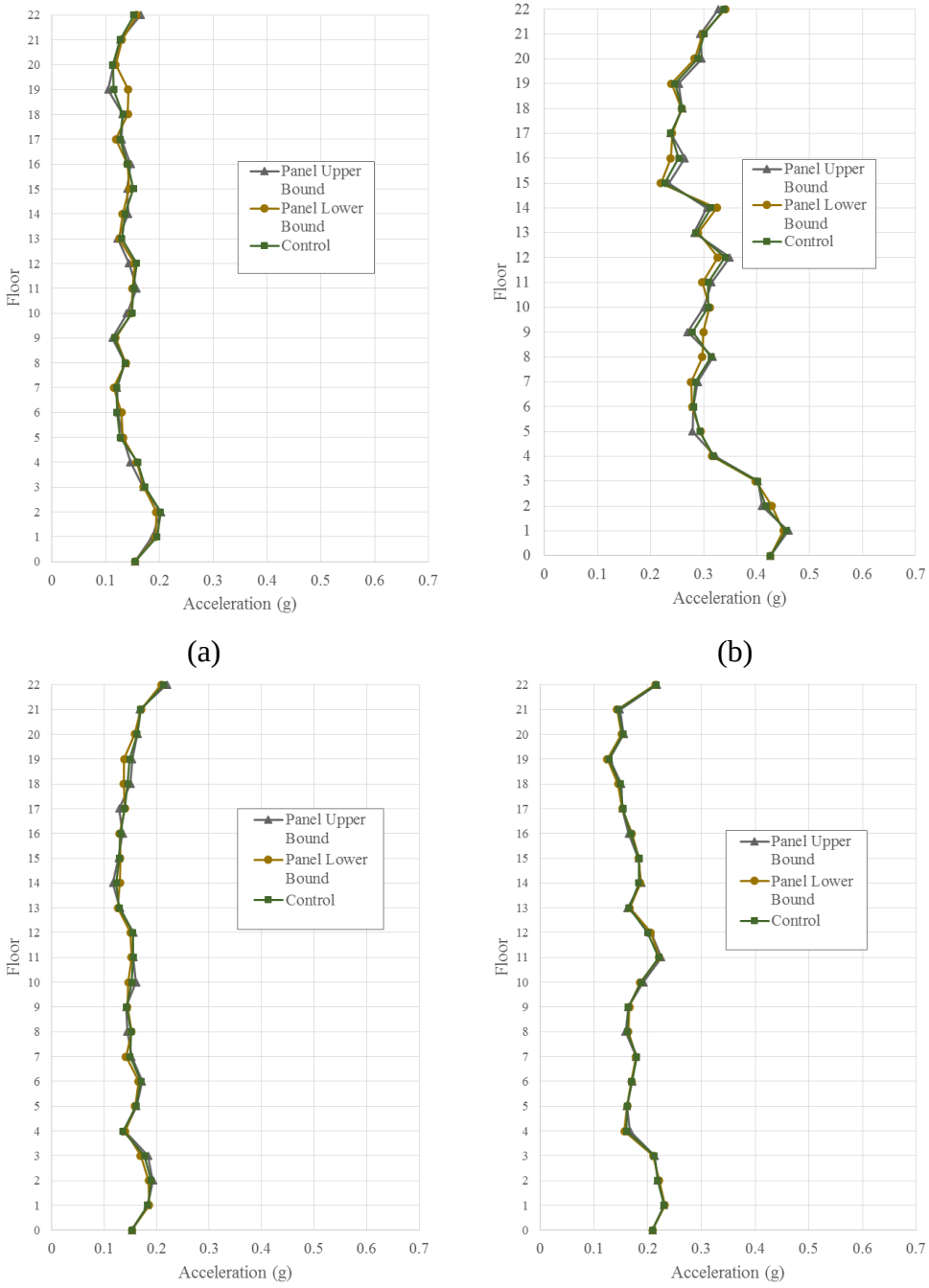

Figure 4.62. Panel Width - Peak Floor Acceleration Demands in the Z-Direction (average of all stations for each event) (a) September 2010 (b) February 2011 (c) June 2011 and (d) December 2011

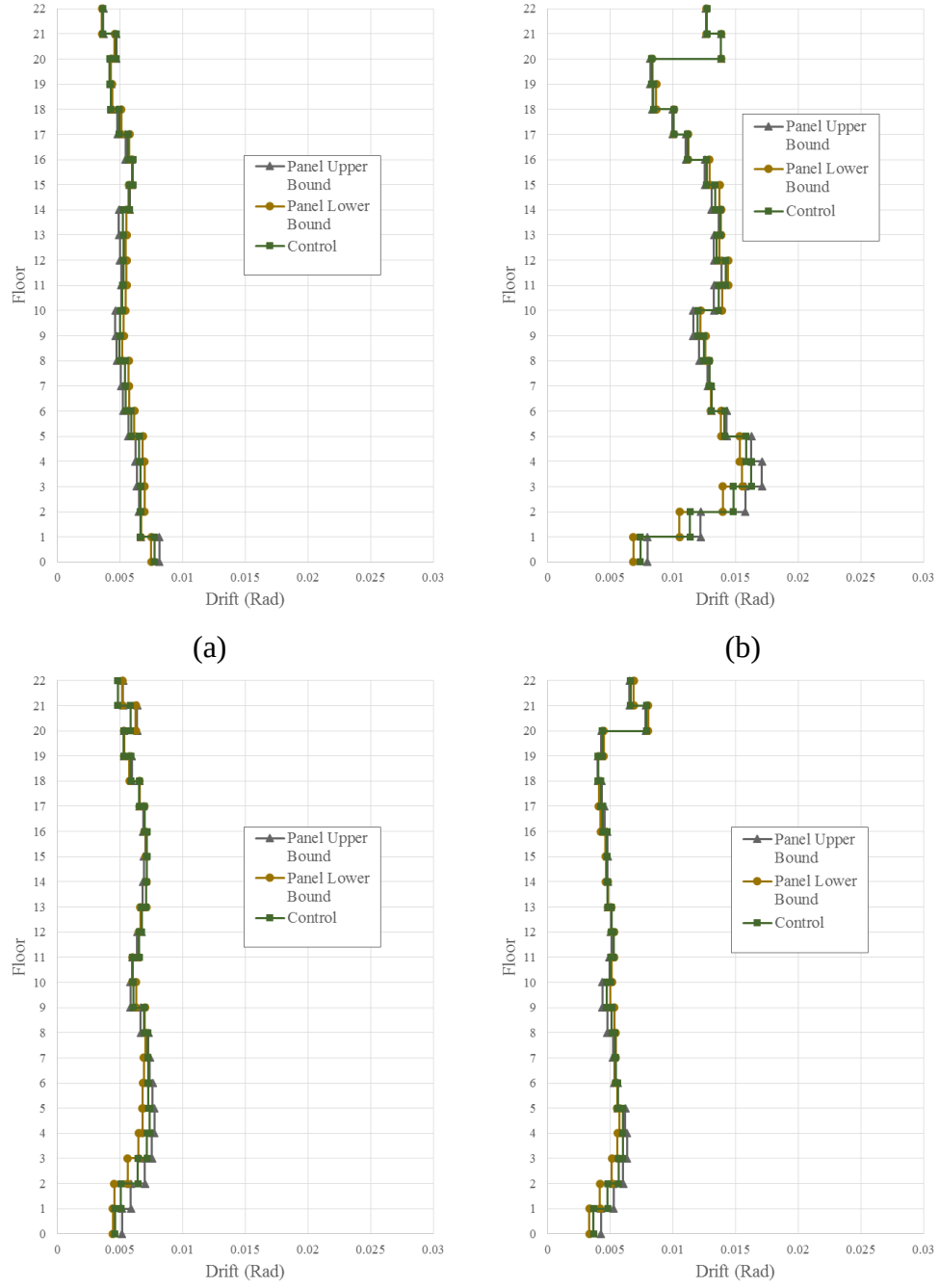

Figure 4.63. Panel Width - Peak Drift Demands in the Z-Direction (average of all stations for each event) (a) September 2010 (b) February 2011 (c) June 2011 and (d) December 2011

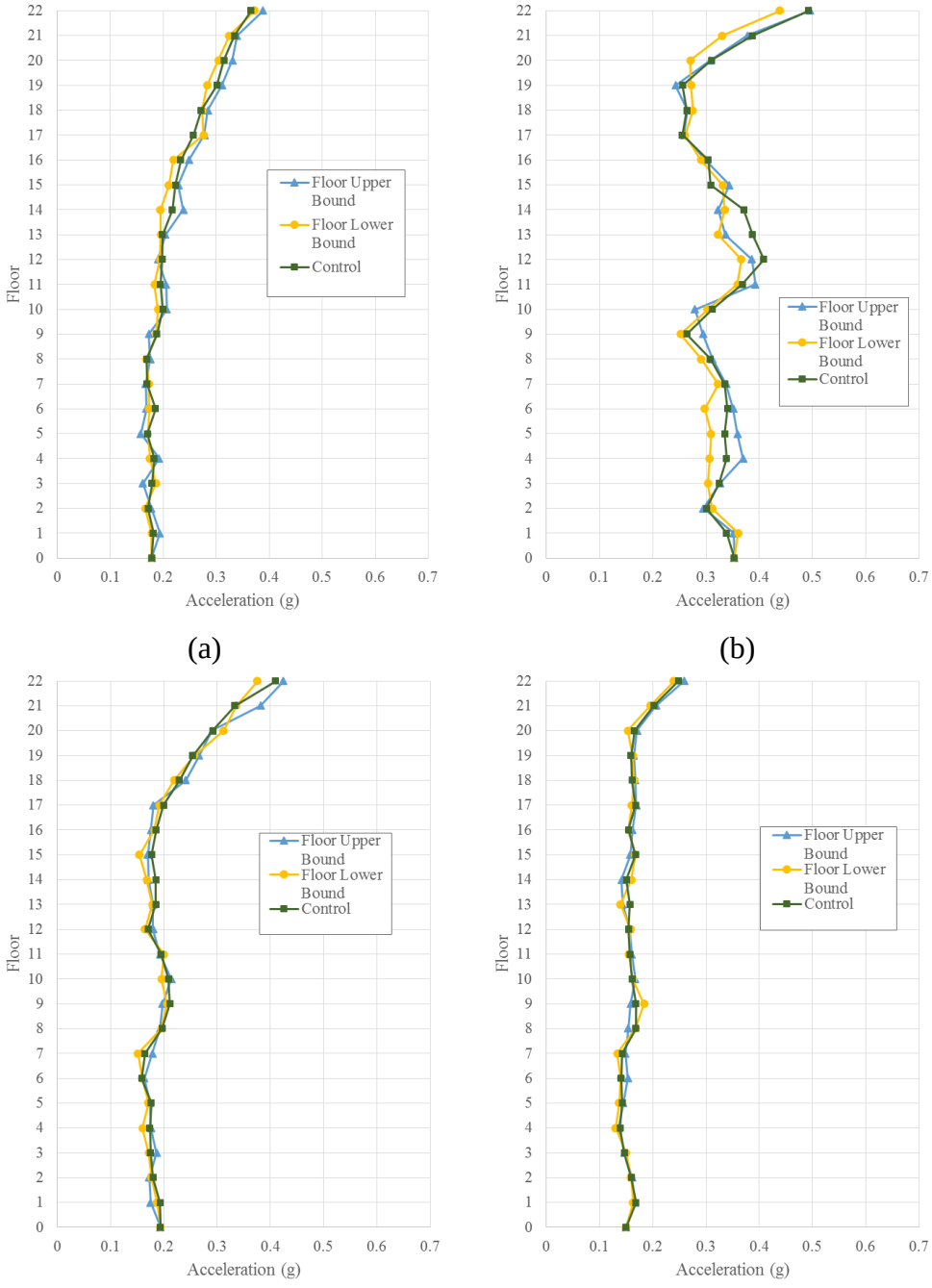

Figure 4.64. Floor-Slab Interaction - Peak Floor Acceleration Demands in the X-Direction (average of all stations for each event) (a) September 2010 (b) February 2011 (c) June 2011 and (d) December 2011

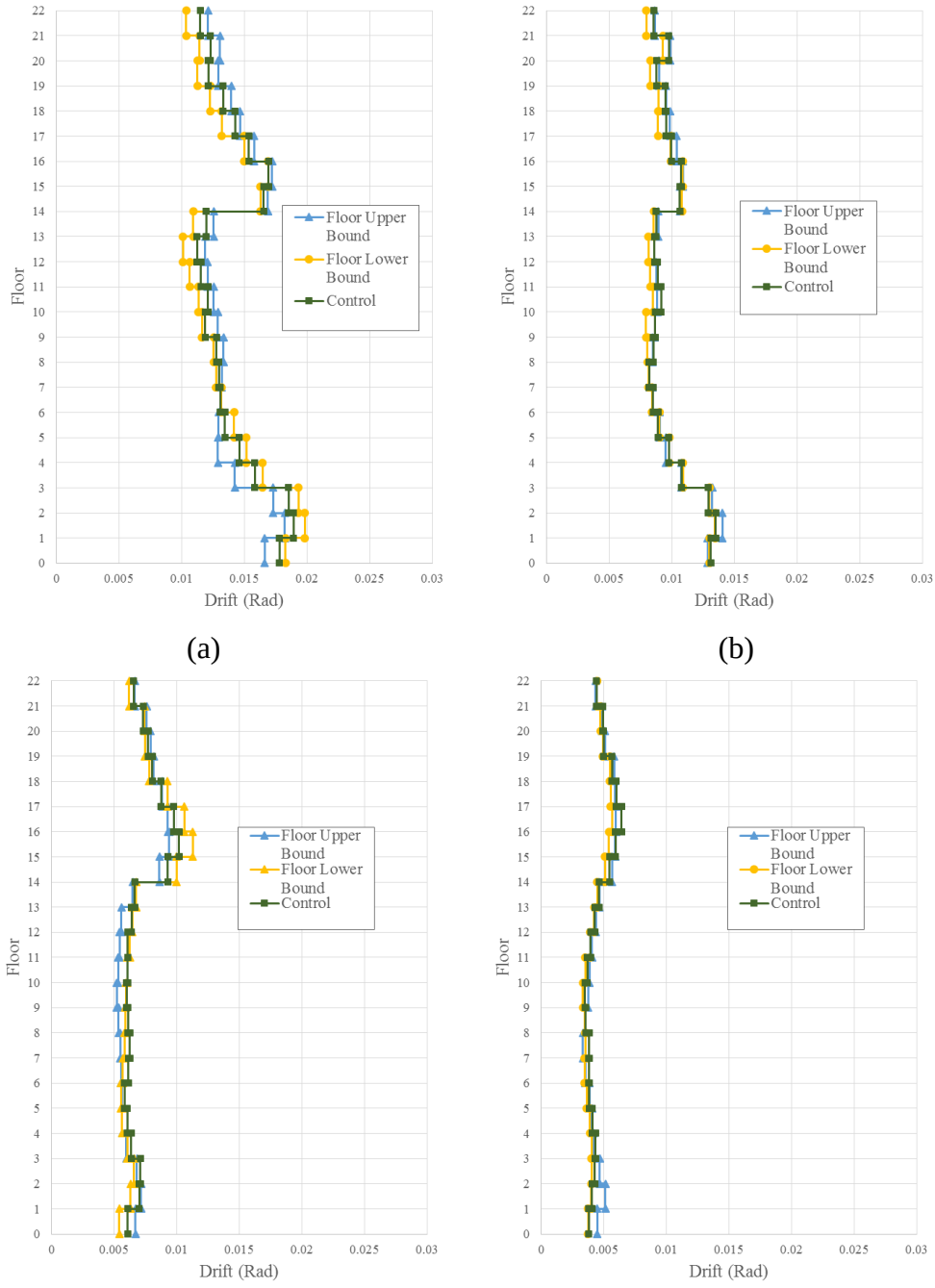

Figure 4.65. Floor-Slab Interaction - Peak Drift Demands in the X-Direction (average of all stations for each event) (a) September 2010 (b) February 2011 (c) June 2011 and (d) December 2011

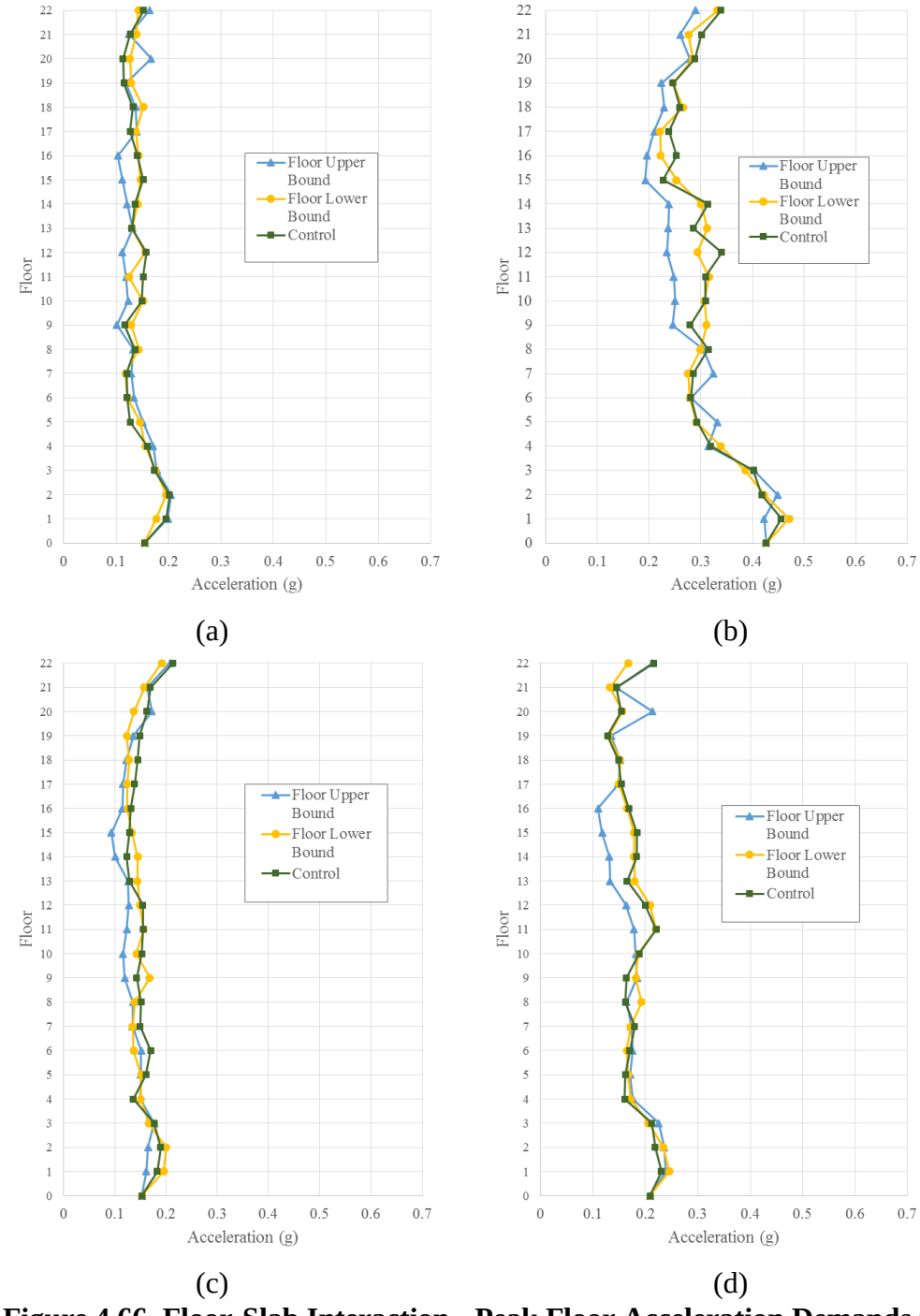

Figure 4.66. Floor-Slab Interaction - Peak Floor Acceleration Demands in the Z-Direction (average of all stations for each event) (a) September 2010 (b) February 2011 (c) June 2011 and (d) December 2011

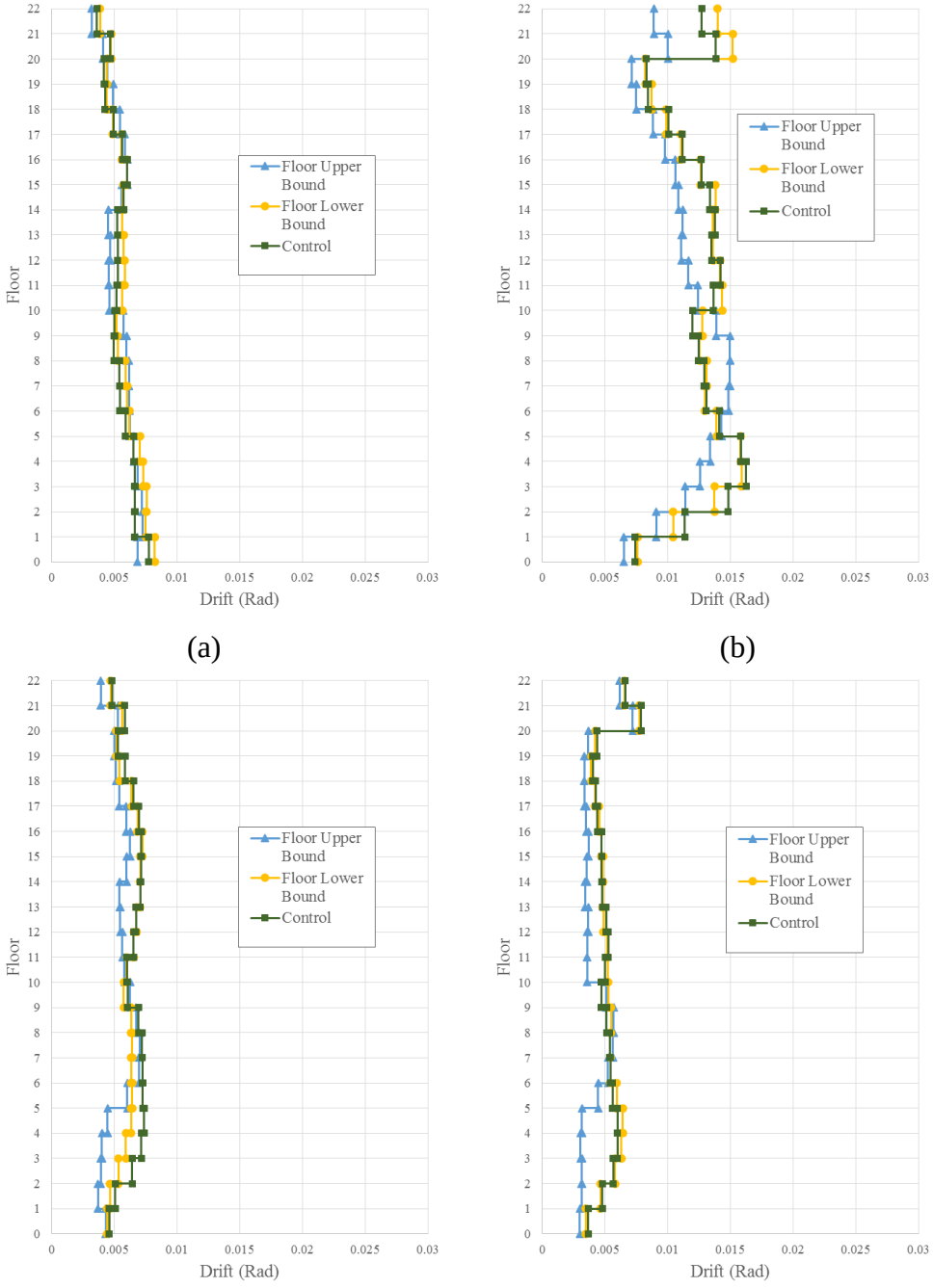

Figure 4.67. Floor-Slab Interaction - Peak Drift Demands in the Z-Direction (average of all stations for each event) (a) September 2010 (b) February 2011 (c) June 2011 and (d) December 2011

From Figure 4.40 to Figure 4.67, the following observations are made:

The effects of changing the damping type is more evident in acceleration than drift. The acceleration of the tangent damping model is lower while the drifts are higher in lower levels, but not necessarily in higher levels. This is due to the fact that Rayleigh Tangent Secant Damping reduces the damping of lower modes compared to Linear Damping but it increases the damping significantly in higher modes. The effect of the earthquake intensity is also evident for both acceleration drifts, increased intensity increases the discrepancy in both acceleration and drifts. These changes, however, are not significant.

Similar to damping type, changing the damping value also has more effects on the acceleration compared to drifts. However, since the damping type of all three models are the same (i.e. Caughy Damping), a clearer trend of reduced/increased acceleration/damping can be observed. Similarly, the changes are not significant.

Changing the foundation stiffness by the assumption of a settlement does not have a significant effect on both drifts and accelerations. Although, it is evident that a higher intensity increases the discrepancy between the models. Especially in high drift demands, e.g. the September 2010 X-Direction drift demand.

Modifying the assumptions of the beam-column joints into a fixed connection changes the response of both the acceleration and the drifts especially in large demands. However, this is an upper bound sensitivity as the real details of the drawings show connections that are in the intermediate to pinned region.

The bilinear factor of the hysteretic properties has little to no effect on the structural response. However, in large intensities, the difference can be spotted, especially in drift demands.

The panel width affects the response both in drift and acceleration insignificantly, especially in lower intensities. This, however, is increased in large intensities, albeit not by a large margin.

Increasing or decreasing the stiffness and strength of the beams due to the composite action of the slab has insignificant effects in smaller intensities in both acceleration and drifts. In larger intensities this change does show some difference, but is still of small significance. With exception, the Z direction acceleration and drift demands of the February 2011 event shows significant difference which might be due to certain modes being excited.

The fact that the sensitivity studies highlight the discrepancies that are arguably insignificant provides a level of confidence that the assumptions and approximations chosen do not affect largely the engineering demand parameters. Hence, the modelling assumptions and approximation is considered adequate.

4.3.6. Scenario Structural Analysis Results

As stated earlier, in the beginning of chapter 4, a scenario analysis, Canterbury 2010-2011 Earthquake Series, is run to obtain a level of confidence that the modelling approach represents the building. Hence, the using the results from the control model in Ruaumoko3D (Carr 2017) of the sensitivity analyses, the following EDPs, presented in Figure 4.68, are obtained.

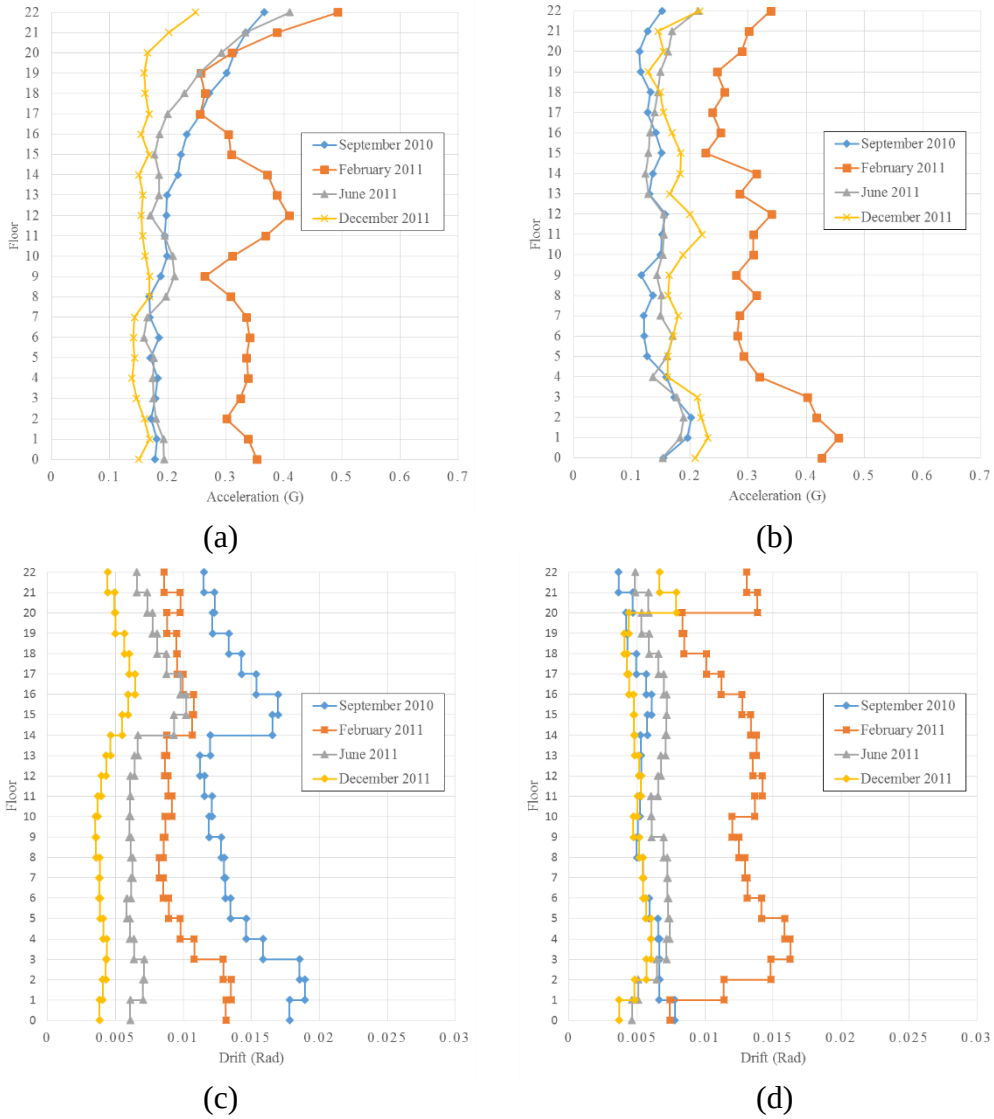

Figure 4.68. Scenario Analysis Average (a) X-Direction Peak Transient Floor Acceleration Demand (b) X-Direction Peak Drift Demand (c)Z-Direction Peak Transient Floor Acceleration Demand (d) Z-Direction Peak Drift Demand

4.3.7. Time-based Structural Analysis Results

The structural analysis for the interest of time-based analysis uses the same model used in section 4.3.6. Ruaumoko 3D (Carr 2017) returns the following EDPs for each intensity measure aforementioned in section 4.2, presented in Figure 4.69 to Figure 4.86,

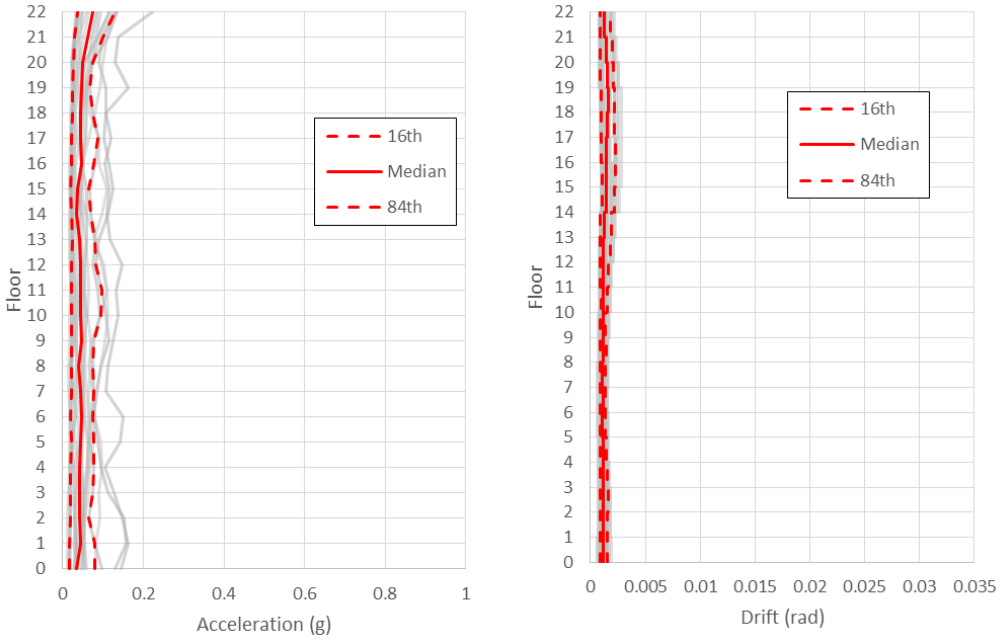

(a) (b)

Figure 4.69. NS EDP for 80% in 50 years; Sa(4.0s) = 0.012g; (a) peak transient floor acceleration and (b) peak inter-storey drift

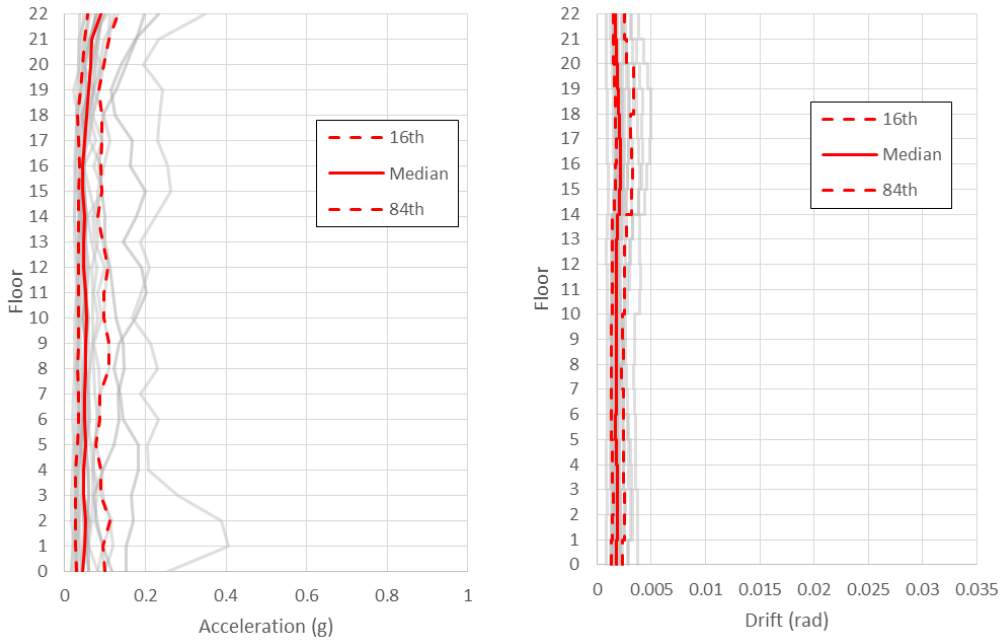

(a) (b)

Figure 4.70. NS EDP for 50% in 50 years; Sa(4.0s) = 0.022g; (a) peak transient floor acceleration and (b) peak inter-storey drift

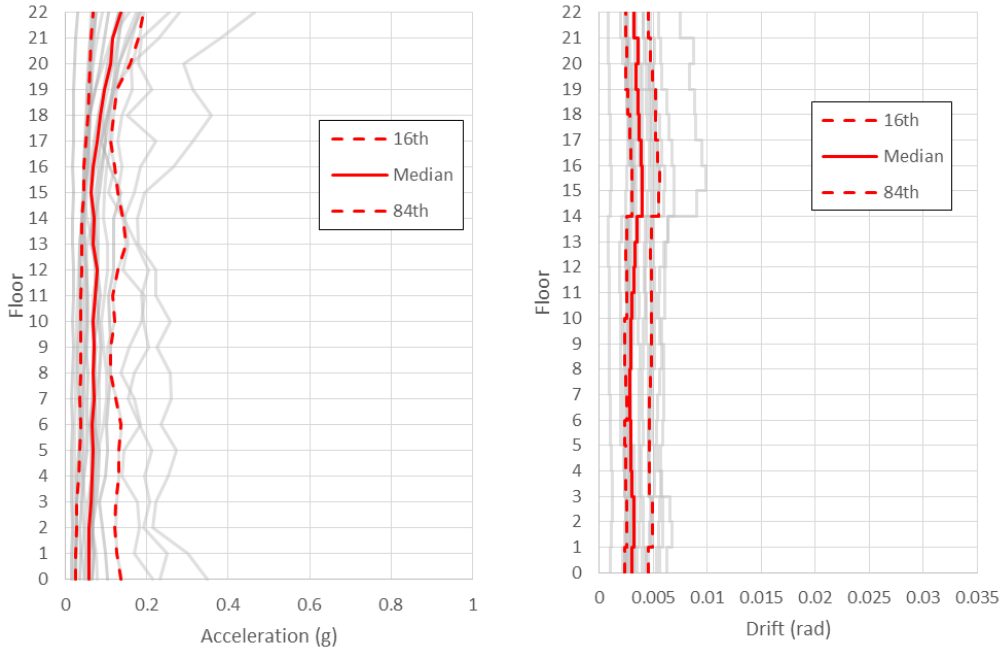

(a) (b)

Figure 4.71. NS EDP for 20% in 50 years; Sa(4.0s) = 0.04g; (a) peak transient floor acceleration and (b) peak inter-storey drift

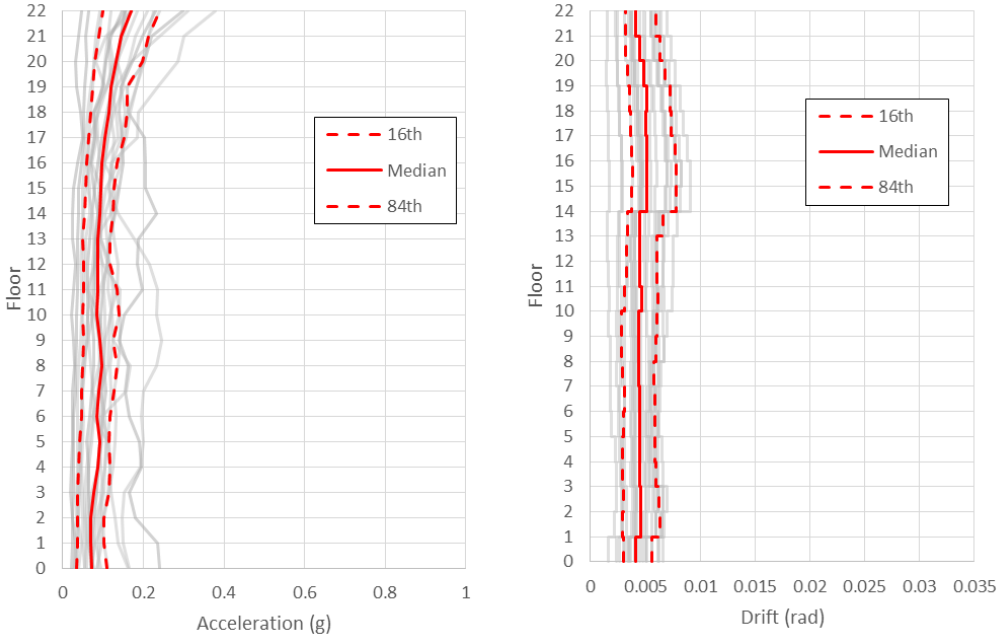

(a) (b)

Figure 4.72. NS EDP for 10% in 50 years; Sa(4.0s) = 0.054g; (a) peak transient floor acceleration and (b) peak inter-storey drift

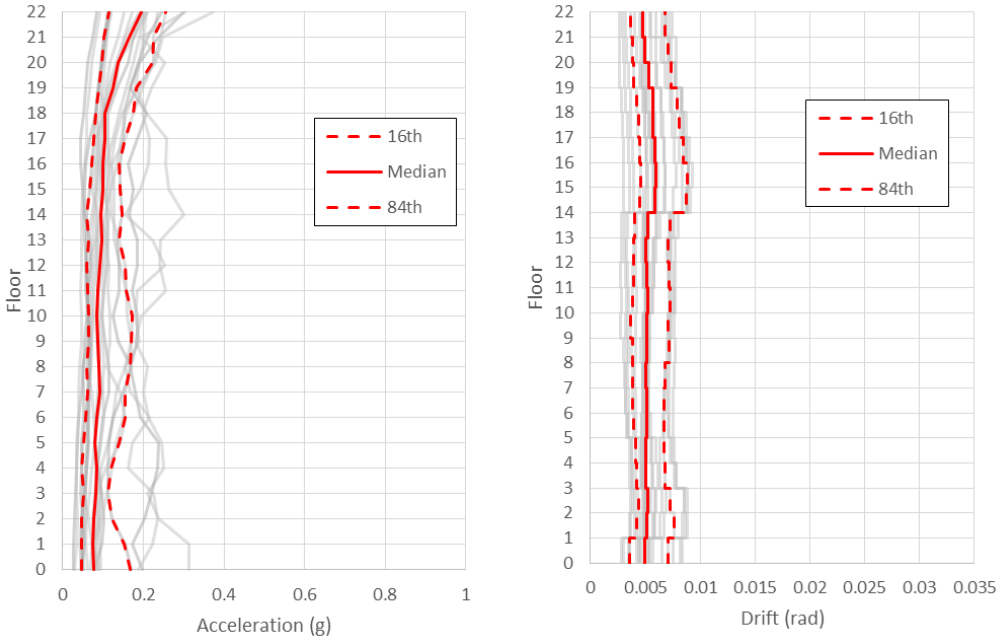

(a) (b)

Figure 4.73. NS EDP for 5% in 50 years; Sa(4.0s) = 0.071g; (a) peak transient floor acceleration and (b) peak inter-storey drift

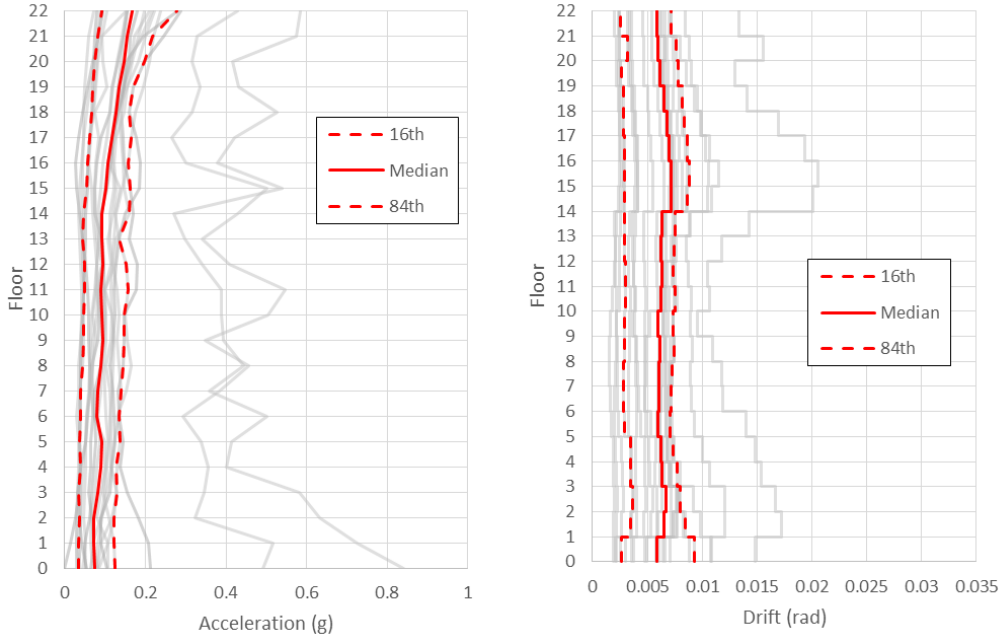

(a) (b)

Figure 4.74. NS EDP for 2% in 50 years; Sa(4.0s) = 0.096g; (a) peak transient floor acceleration and (b) peak inter-storey drift

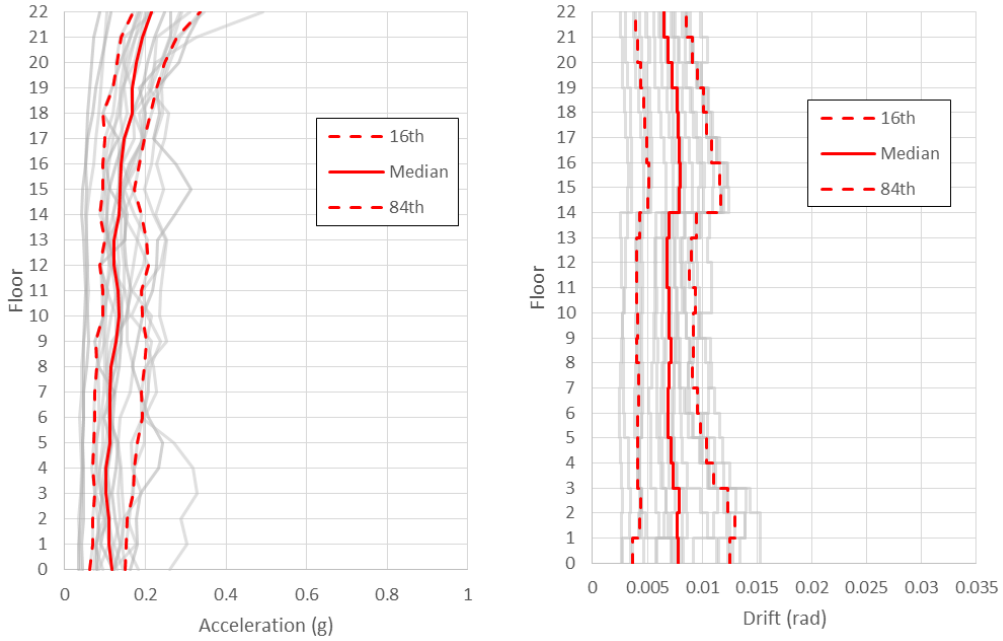

(a) (b)

Figure 4.75. NS EDP for 1% in 50 years; Sa(4.0s) = 0.118g; (a) peak transient floor acceleration and (b) peak inter-storey drift

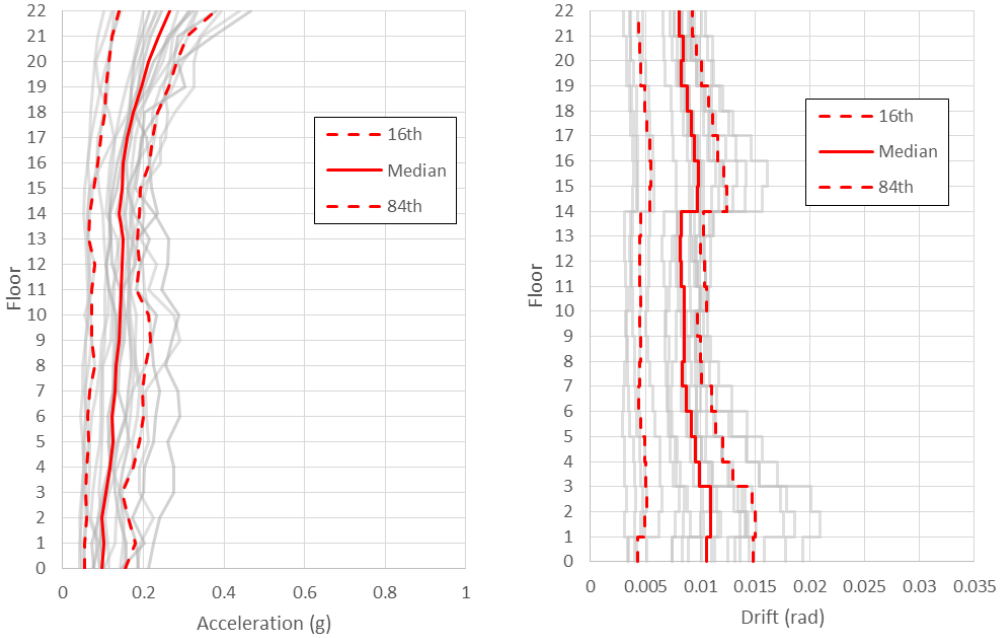

(a) (b)

Figure 4.76. NS EDP for 0.5% in 50 years; Sa(4.0s) = 0.143g; (a) peak transient floor acceleration and (b) peak inter-storey drift

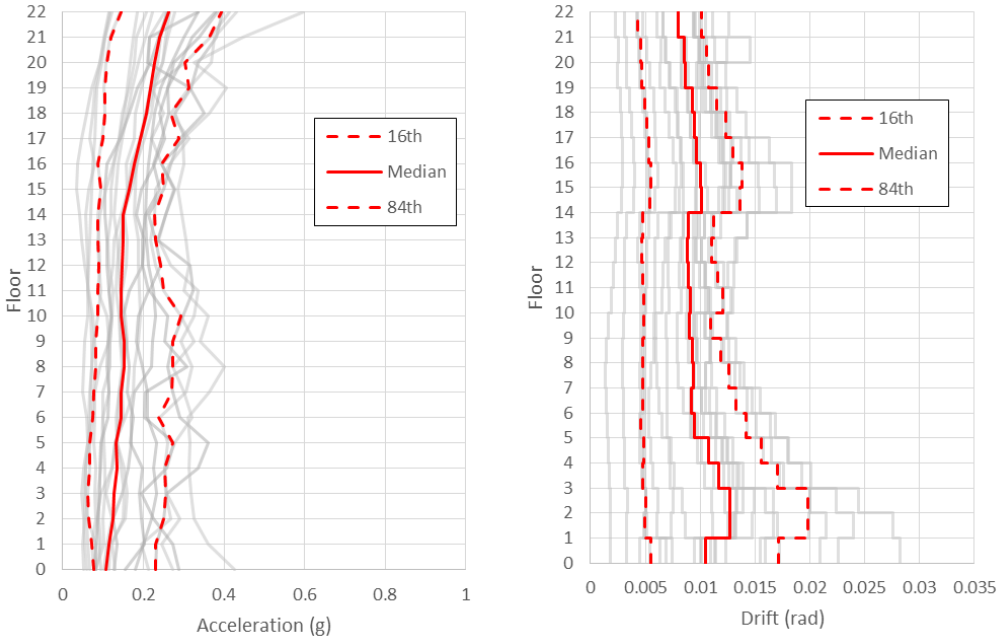

(a) (b)

Figure 4.77. NS EDP for 0.2% in 50 years; Sa(4.0s) = 0.18g; (a) peak transient floor acceleration and (b) peak inter-storey drift

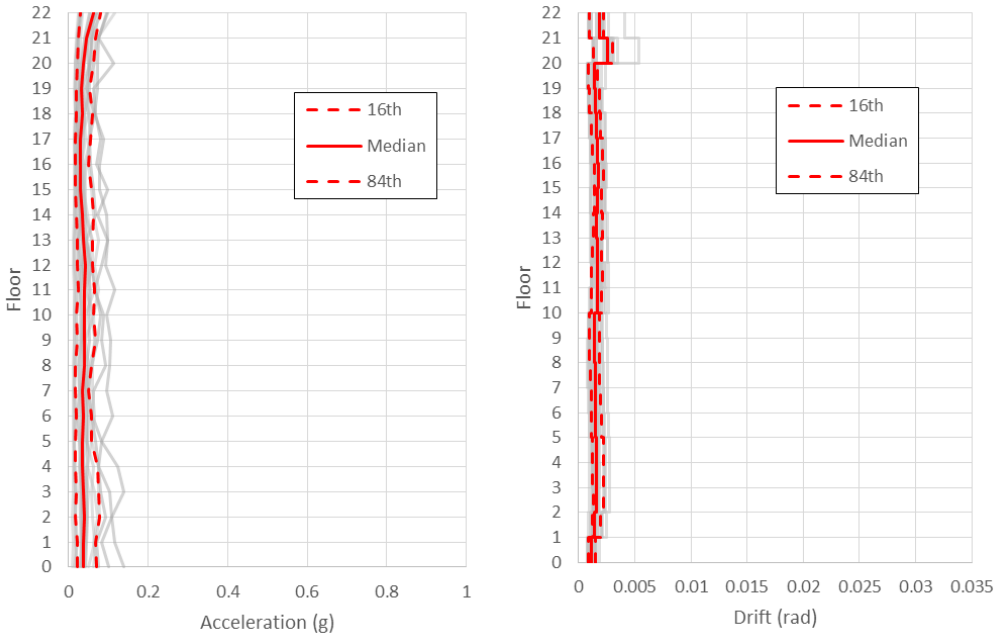

(a) (b)

Figure 4.78. EW EDP for 80% in 50 years; Sa(4.0s) = 0.012g; (a) peak transient floor acceleration and (b) peak inter-storey drift

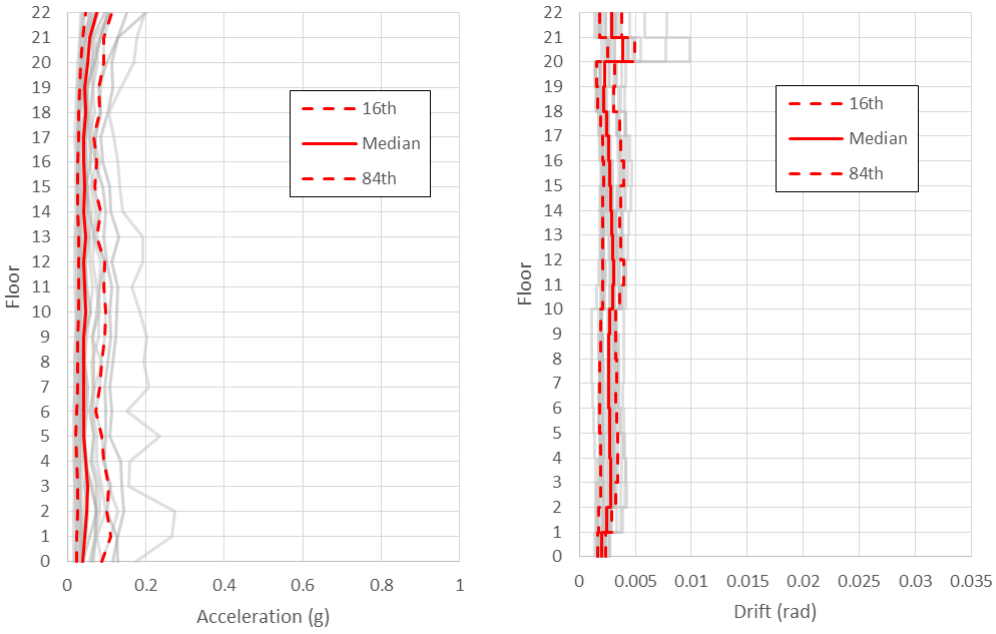

(a) (b)

Figure 4.79. EW EDP for 50% in 50 years; Sa(4.0s) = 0.022g; (a) peak transient floor acceleration and (b) peak inter-storey drift

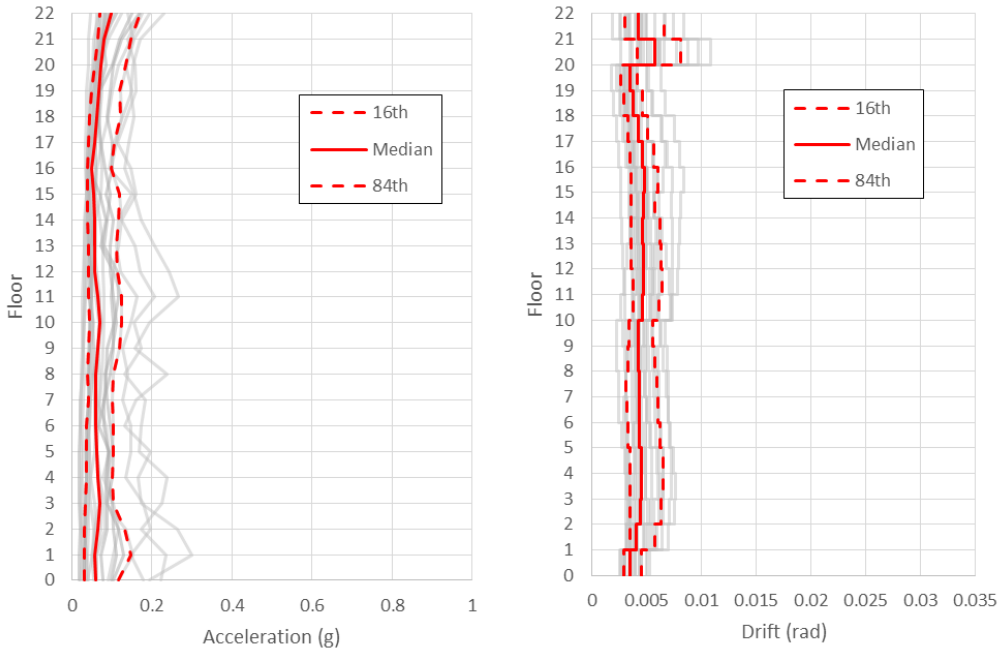

(a) (b)

Figure 4.80. EW EDP for 20% in 50 years; Sa(4.0s) = 0.04g; (a) peak transient floor acceleration and (b) peak inter-storey drift

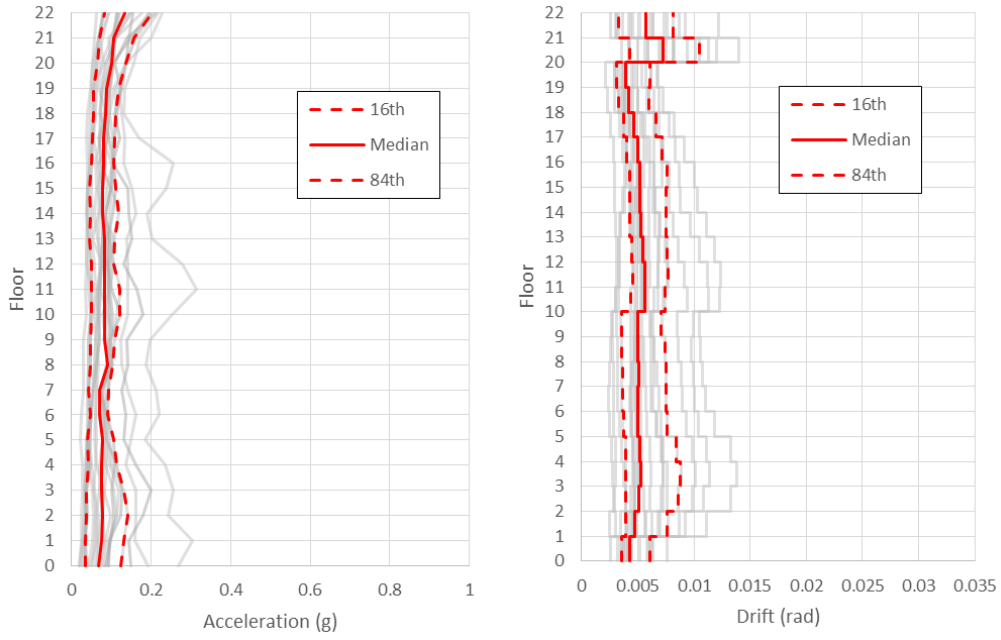

(a) (b)

Figure 4.81. EW EDP for 10% in 50 years; Sa(4.0s) = 0.054g; (a) peak transient floor acceleration and (b) peak inter-storey drift

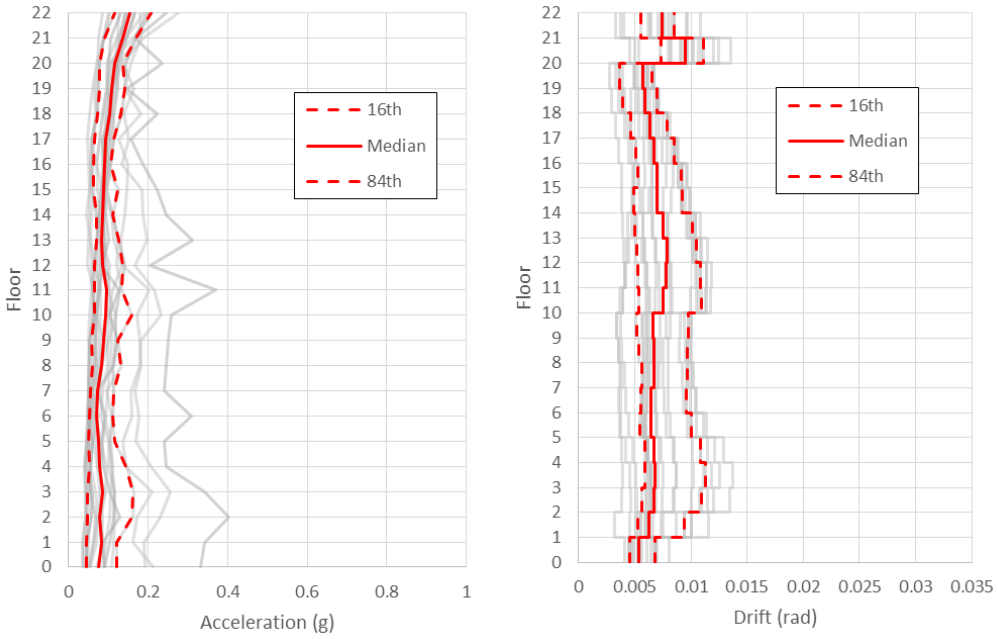

(a) (b)

Figure 4.82. EW EDP for 5% in 50 years; Sa(4.0s) = 0.071g; (a) peak transient floor acceleration and (b) peak inter-storey drift

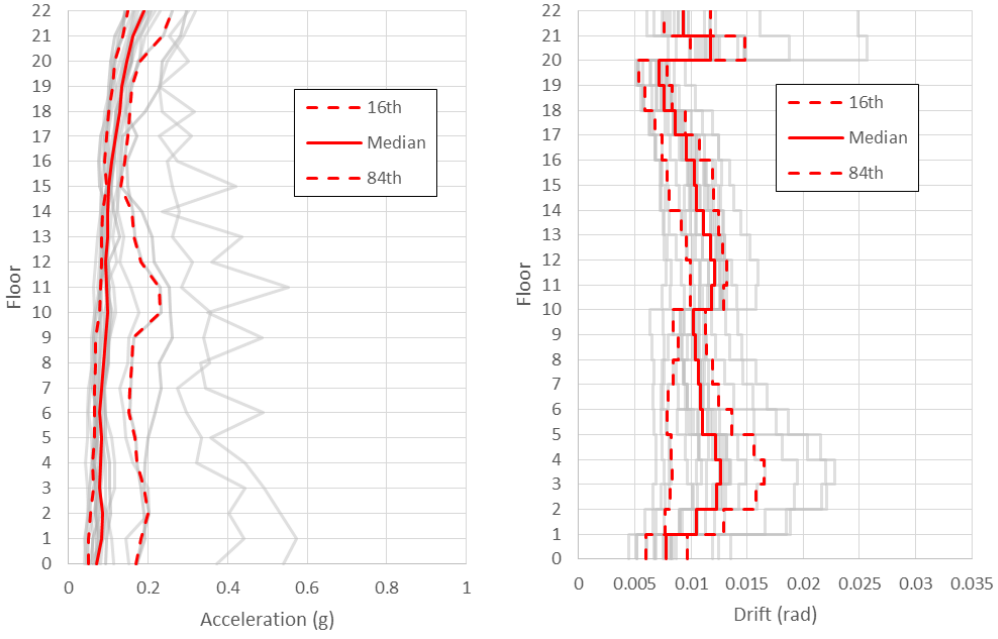

(a) (b)

Figure 4.83. EW EDP for 2% in 50 years; Sa(4.0s) = 0.096g; (a) peak transient floor acceleration and (b) peak inter-storey drift

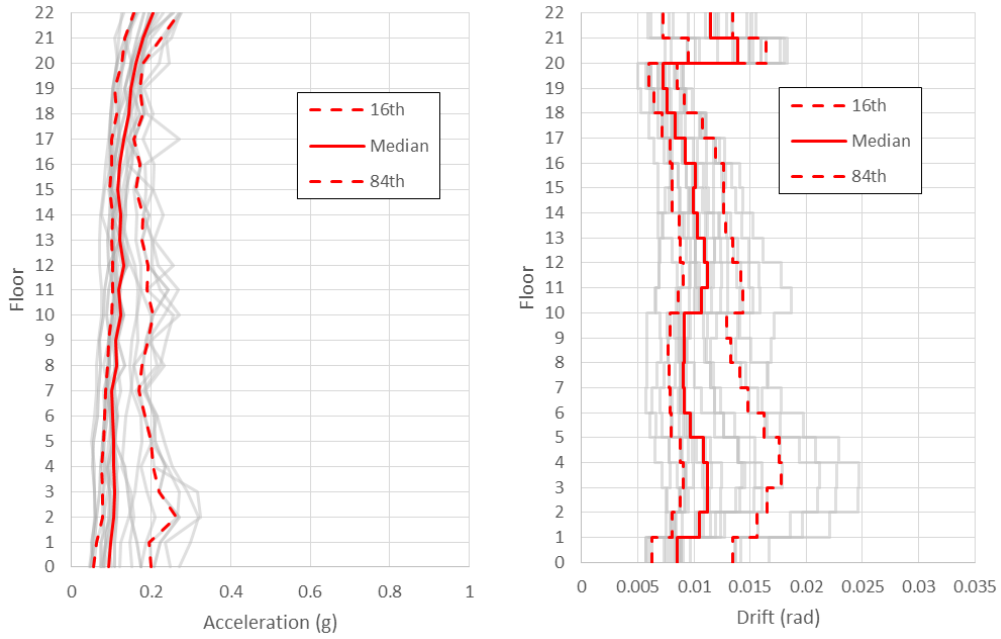

(a) (b)

Figure 4.84. EW EDP for 1% in 50 years; Sa(4.0s) = 0.118g; (a) peak transient floor acceleration and (b) peak inter-storey drift

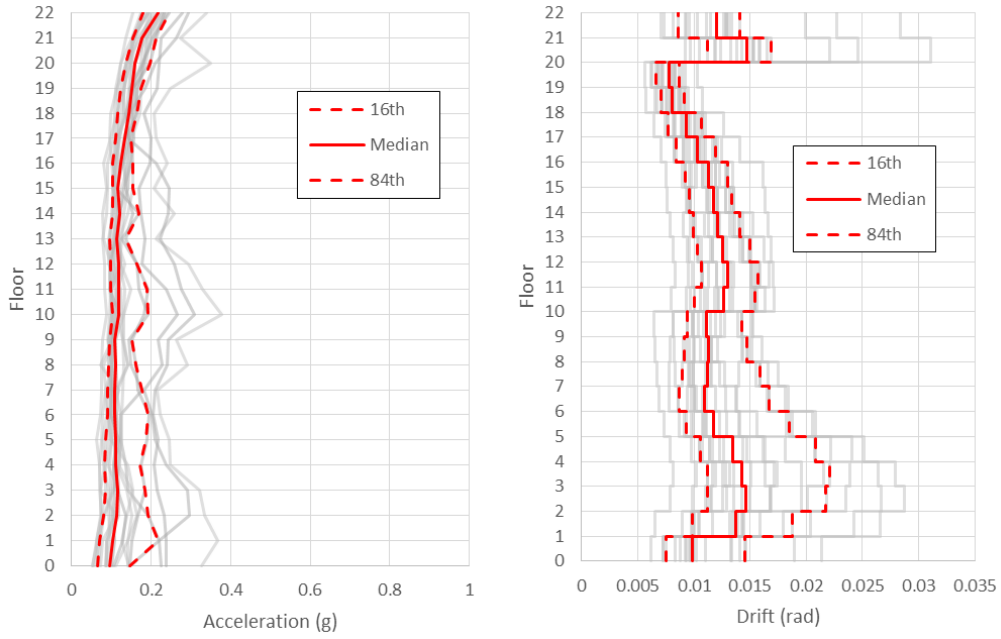

(a) (b)

Figure 4.85. EW EDP for 0.5% in 50 years; Sa(4.0s) = 0.143g; (a) peak transient floor acceleration and (b) peak inter-storey drift

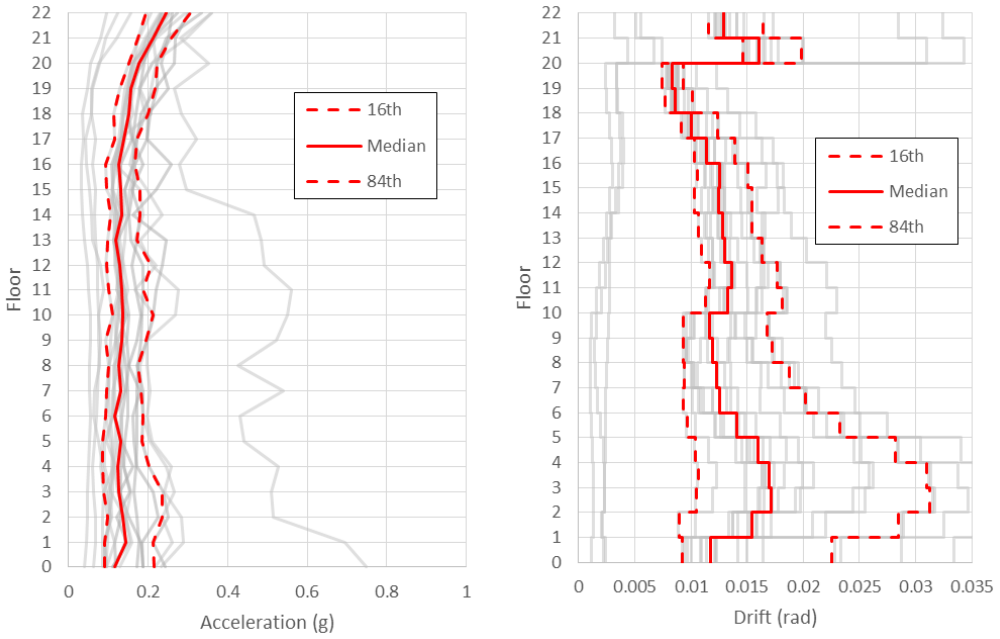

(a) (b)

Figure 4.86. EW EDP for 0.2% in 50 years; Sa(4.0s) = 0.18g; (a) peak transient floor acceleration and (b) peak inter-storey drift

4.4. Damage and Loss Analysis

In order to run the damage and loss analysis, a software, PACT (FEMA P-58.3), is used. The inputs used are the EDPs obtained from 4.3.6 and fragility and loss curves. There are fragility and loss curves are available inside PACT itself and other fragilities can be added manually. In the interest of this research, a few fragility curves and loss functions that are deemed representative, explained previously in section 2.1.5, are added to the PACT database. The following is the summary of fragility and loss functions. Note that all values of costs have been modified to 2011 US$, via foreign exchange conversion rates to and/or during 2011, to match inputs from PACT itself.

- Eccentrically Braced Frames

The EBF fragilities used are based of the recent work on EBF fragilities from O'Reilly and Sullivan (2016). While the loss function is

modified from PACT itself to match with values from local engineers in New Zealand. Note that in Table 4-16, the EBF value is just an example value due to the large number of EBF fragilities, due to the fact that each different EBF has its own fragility. For the complete list of EBF fragilities, refer to Appendix E.

- Panels (Exterior Claddings)

The panel fragilities and losses are based of the work of Baird (2014) which is one of the recent works on claddings based in New Zealand.

- Panel Connections

The panel connections fragility is created via mechanics and a SAP2000 model, as explained in section 4.3.2. The yield drift, of 0.19%, is multiplied by three to assume a certain ductility before failure of the connection and a large dispersion of 0.5 is used due to the uncertainty in this approach. The costs is some modifications on the work by Baird (2014). This is possible due to the fact that in the referenced work, material costs are far smaller compared to labour costs.

- Partitions

Partition fragility functions are taken from the paper by Yeow and Sullivan (2017) which is an adoption of the work of Davies et al. (2011). While the loss functions from Dhakal et al. (2016) is applied. This is possible due to the fact that the damage states used in both papers are the same.

- Ceilings

Both ceiling fragility and loss functions follows the suggested values by Dhakal et al. (2016), a recent work on ceiling fragilities based in New Zealand.

- Elevators

Fragility and loss functions for elevators are taken directly from PACT's library. This includes 1 Damage State which incorporates 4 simultaneous Damage Groups each with its own probability of happening.

- Piping Systems

Piping systems' fragility and loss functions, which include Cold Water Piping and Bracing; Hot Water Piping and Bracing; Sanitary Waste Piping and Sprinklers, are also based directly from PACT's library. Due to lack of data on the amount of piping and braces, this value is estimated via the Normative Quantity Estimator available within FEMA P-58 (FEMA P-58.3).

Table 4-16, Table 4-17 and Table 4-18 summarizes the fragility and loss functions in the model.

Table 4-16. Drift Sensitive Fragility and Loss Functions

Item	Damage State	Median Drift (rad)	Disp.	Upper Cost (2011 US$)	Disp.	Unit of Cost	Description
EBF	DS1	0.0148	0.238	20552	0.3	Link	Damage to concrete slab above the link beam
	DS2	0.0195	0.26	26820	0.3	Link	Web local buckling, flange local buckling
	DS3	0.025	0.304	45662	0.3	Link	Initiation of fracture in the link beam and link flange
Panel	DS1	0.0023	0.4	10.2	0.365	m^2 of Cladding	First visible cracking of the panel
	DS2	0.0041	0.4	104.27	0.49	m^2 of Cladding	Maximum crack width for serviceability exceeded
Angle	DS	0.006	0.4	510	0.5	# of Connections	Plate Failure
Partitions	DS1	0.0029	0.53	20.19	0.263	m^2 of Floor	Cracking of the paint and/or drywall
	DS2	0.007	0.45	46.9	0.101	m^2 of Floor	Broken drywall panel
	DS3	0.0123	0.59	87.95	0.182	m^2 of Floor	Damage to the panels and frame

Table 4-17. Acceleration Sensitive Fragility and Loss Functions

Item	Damage State	Acc. (g)	Disp.	Upper Cost (2011 US$)	Lower Cost (2011 US$)	Disp.	Upper Quantity	Lower Quantity	Unit of Cost	Descriptio
Ceilings	DS	1.63	0.25	70.95	70.95	0.06			m^2 of Floor	Collapse
Cold Piping	DS1	2.25	0.5	700	210	0.6488	250	500	1000ft	Minor leakage at flange connections
	DS2	4.1	0.5	6700	2010	0.4038	250	500	1000ft	Pipe Break
Cold Pipe Bracing	DS1	1.5	0.5	700	210	0.6488	250	500	1000ft	Lateral Brac Failure
	DS2	2.25	0.5	1000	300	0.4695	250	500	1000ft	Vertical Bra Failure
Hot Piping	DS1	2.25	0.5	700	210	0.6488	250	500	1000ft	Minor leakage at flange connections
	DS2	4.1	0.5	6700	2010	0.4038	250	500	1000ft	Pipe Break
Hot Pipe Bracing	DS1	1.5	0.5	700	210	0.6488	250	500	1000ft	Lateral Brac Failure
	DS2	2.25	0.5	1000	300	0.4695	250	500	1000ft	Vertical Bra Failure
Sanitary Pipes	DS	2.25	0.5	800	240	0.5758	250	500	1000ft	Isolated support failure w/o leakage
Fire Sprinkler Pipes	DS1	1.9	0.4	700	210	0.6488	250	500	1000ft	Spraying & Dripping Leakage at joints
	DS2	3.4	0.4	760	228	0.603	100	500	1000ft	Joints Break Major Leakage
Fire Sprinkler Drop	DS	0.95	0.4	550	450	0.3665	10	50	100 Units	Spraying & Dripping Leakage at drop joints

Table 4-18. Elevator Fragility and Loss Functions

Item	Damage State/ Group	Median Drift (rad)/ Probability	Disp.	Average Cost (2011 US$)	Disp.	Unit of Cost	Description
Elevator	DS1	0.39	0.45				
	DG1	0.26		1333	0.92	# of Elevators	Controller anchorage failed, and or machine anchorage failed, and or motor generator anchorage failed, and or governor anchorage failed, and or rope guard failures.
	DG2	0.79		4630	0.27	# of Elevators	Rail distortion, and or intermediate bracket separate and spread, and or counterweight bracket break or bend, and or car bracket break or bend, and or car guide shoes damaged, and or counterweight guide shoes damaged, and or counterweight frame distortion, and or tail sheave dislodged and/or twisted
	DG3	0.68		4450	0.35	# of Elevators	Cab stabilizers bent, or cab walls damaged, or cab doors damaged
	DG4	0.17		2000	0.49	# of Elevators	Cab ceiling damaged

4.4.1. Scenario Damage and Loss Analysis

As mentioned earlier, for the loss assessments, 11 ground motion records, which are three station records for the September 2010, February and December 2011 event and two station records for the June 2011 event, are considered for comparison with data obtained from the Christchurch City Council. Using the updated library for PACT and the resulting EDPs from all 11 analysis of different ground motions, loss models are built in PACT 2011. Note that downtime and deaths are not considered in this research. Hence, only direct losses are considered in PACT.

In summary, the model is built using a known inventory of damageable elements. In some cases, the quantity of a certain damageable element was uncertain (e.g. sprinkle pipe length) and is such cases, the Normative Quantity Estimator available within FEMA P-58.3 is used to estimate the likely quantity. Besides the quantity for each considered element, another value is the total cost replacement and repair threshold for the building. The final inventory of damageable components is included in Appendix F. Based on a report from the Christchurch City Council, the Pacific Tower Building is valued at approximately NZ$21,600,000 (approximately US$ 17,142,857.14). Assuming a demolition cost of 25%, as recommended in FEMA P-58, the total replacement cost of the Pacific Tower is expected to be around NZ$27,000,000 (approximately US$ 21,428,571.43), while the core and shell replacement is approximated to be NZ$13,000,000 (approximately US$ 10,317,460.32), which is 60% of the building value. The total replacement threshold, also recommended by FEMA P-58, is assumed to be at 50% of total replacement cost. These values, along with the building area and height are input into PACT as seen in Figure 4.87. Note that the two input values of Replacement Time and Max Workers per sq. ft. are arbitrary as these are not considered in this research. The same applies for the Population Tab, as this is also not considered in this research and the values have no impact on the results of this research.

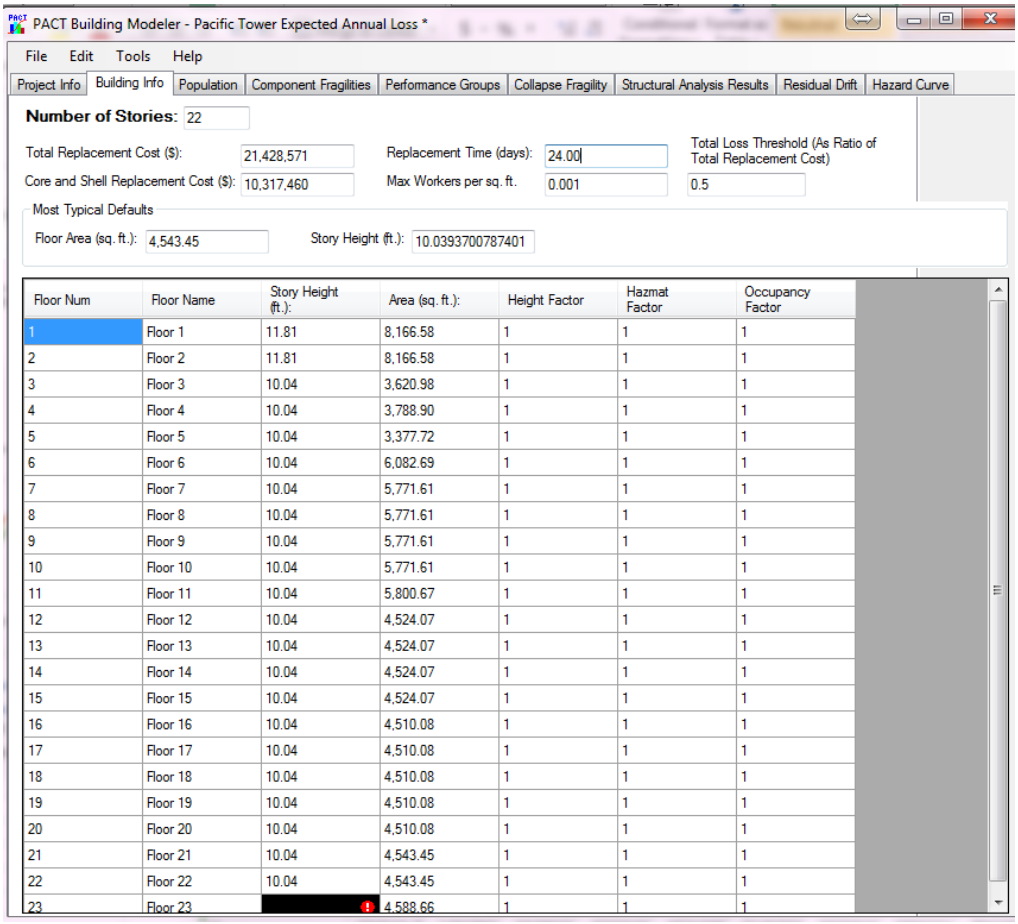

Floor Num	Floor Name	Story Height (ft.):	Area (sq. ft.):	Height Factor	Hazmat Factor	Occupancy Factor
1	Floor 1	11.81	8,166.58	1	1	1
2	Floor 2	11.81	8,166.58	1	1	1
3	Floor 3	10.04	3,620.98	1	1	1
4	Floor 4	10.04	3,788.90	1	1	1
5	Floor 5	10.04	3,377.72	1	1	1
6	Floor 6	10.04	6,082.69	1	1	1
7	Floor 7	10.04	5,771.61	1	1	1
8	Floor 8	10.04	5,771.61	1	1	1
9	Floor 9	10.04	5,771.61	1	1	1
10	Floor 10	10.04	5,771.61	1	1	1
11	Floor 11	10.04	5,800.67	1	1	1
12	Floor 12	10.04	4,524.07	1	1	1
13	Floor 13	10.04	4,524.07	1	1	1
14	Floor 14	10.04	4,524.07	1	1	1
15	Floor 15	10.04	4,524.07	1	1	1
16	Floor 16	10.04	4,510.08	1	1	1
17	Floor 17	10.04	4,510.08	1	1	1
18	Floor 18	10.04	4,510.08	1	1	1
19	Floor 19	10.04	4,510.08	1	1	1
20	Floor 20	10.04	4,510.08	1	1	1
21	Floor 21	10.04	4,543.45	1	1	1
22	Floor 22	10.04	4,543.45	1	1	1
23	Floor 23		4,588.66	1	1	1

Figure 4.87. PACT Building Information Input.

The next input tab is the Component Fragilities tab, which tells PACT which fragilities are used for the building and in which direction of the building are those components sensitive to, an example presented in Figure 4.88. As explained earlier, there are 7 categories of elements considered, EBFs, Panels, Panel Connections, Partitions, Ceilings, Elevators and Piping Systems.

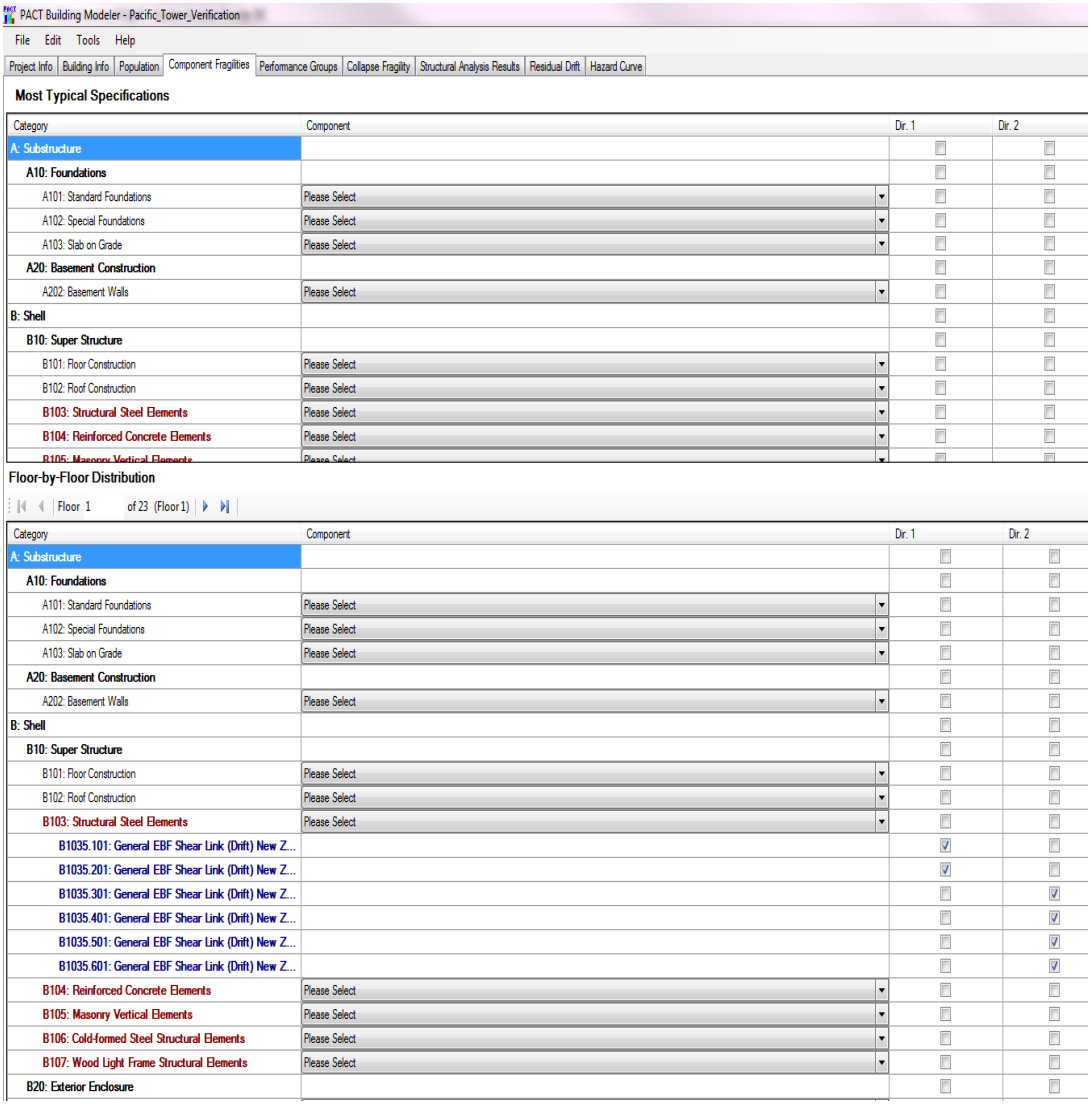

Figure 4.88. PACT Component Fragilities Input

Following the component fragility input is the Performance Groups, in which the number of units for each component is specified for each floor, as shown in Figure 4.89. For the complete values for each floor (i.e. inventory), refer to Appendix F.

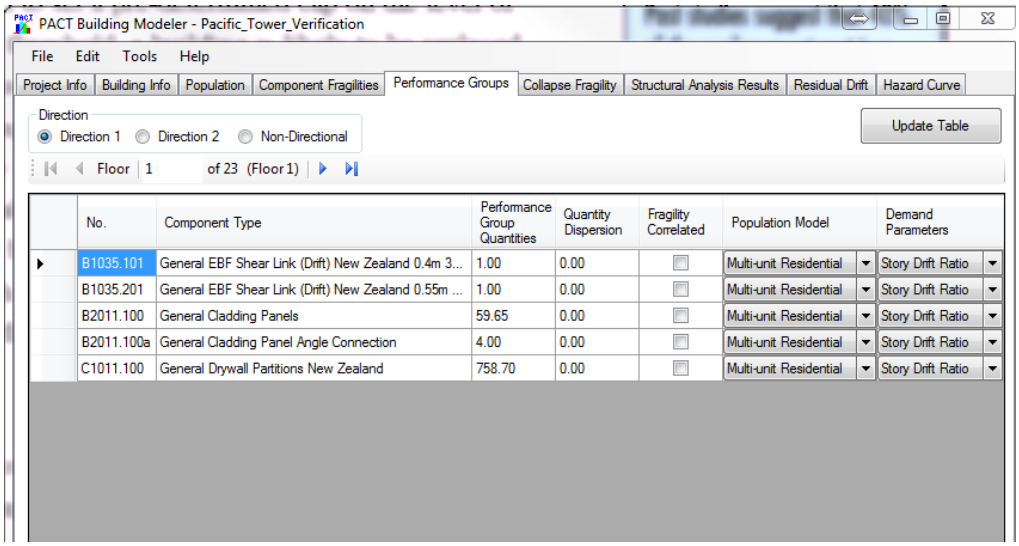

Figure 4.89. PACT Performance Groups Input (Directional)

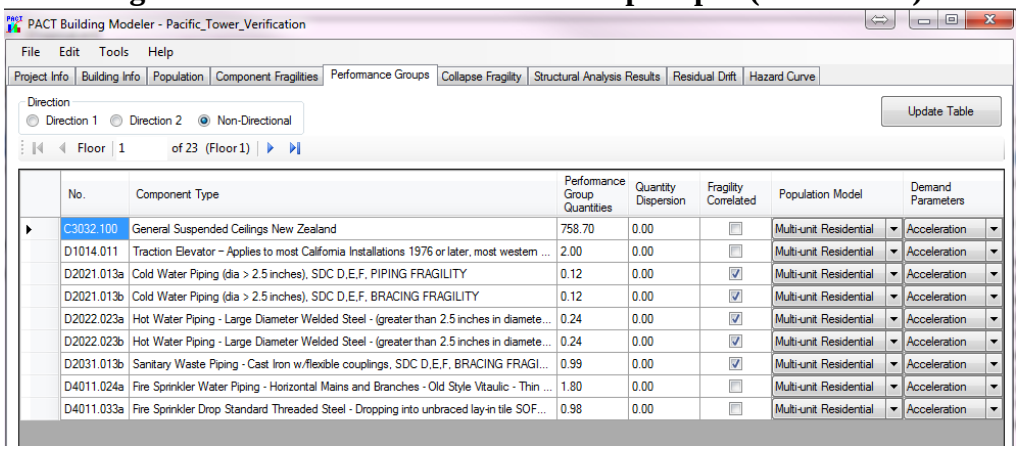

Figure 4.90. PACT Performance Groups Input (Non-Directional)

Due to the fact that this research focuses on retrofitting and rehabilitation as means of repair, i.e. direct losses and that before a collapse the structure would undergo a total replacement due to the 50% total replacement cost repair threshold. The collapse assessment is not considered. Hence, the next input is straight to the structural analysis results which is the analysis results of inter-storey drifts and peak transient accelerations from Ruaumoko3D, an example presented in Figure 4.91. Note that a non-directional conversion factor of 1.2 and a response demand dispersion of 0.6 is taken as suggested by FEMA P-58. The analysis is set to run for 200 Monte Carlo Simulations (MCS)/realizations,

which its average is assumed to be enough to represent the losses of the Pacific Tower.

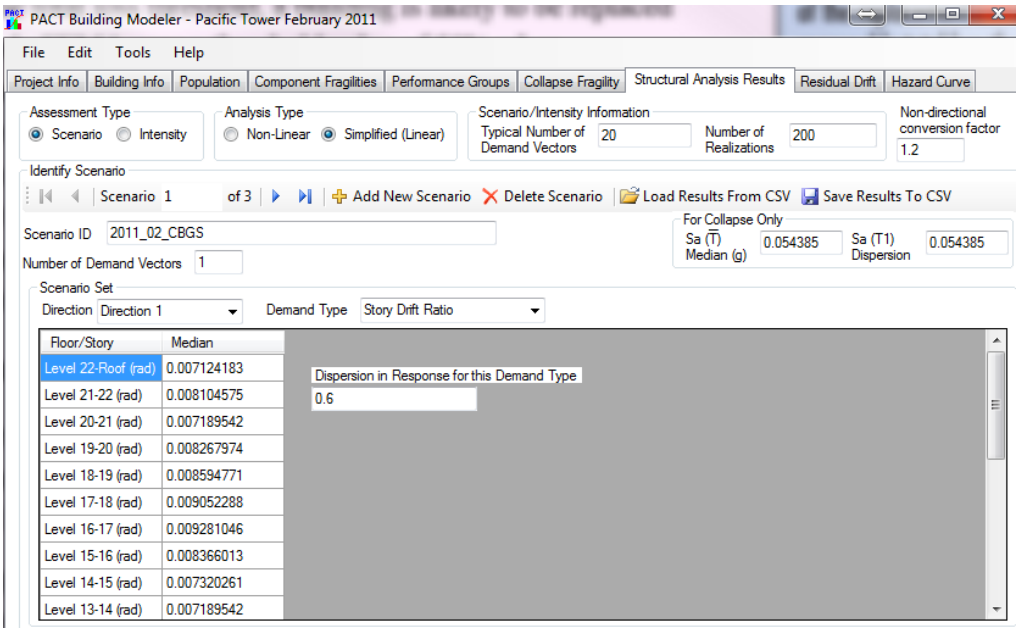

Figure 4.91. PACT Structural Analysis Result Input

Similarly, results from Ruaumoko3D on Residual Drifts are also input into the Residual Drift Tab assuming a Median Irreparable Residual Storey Drift Ratio of 1% and a dispersion of 0.3 as recommended by FEMA P-58, this is shown in Figure 4.92.

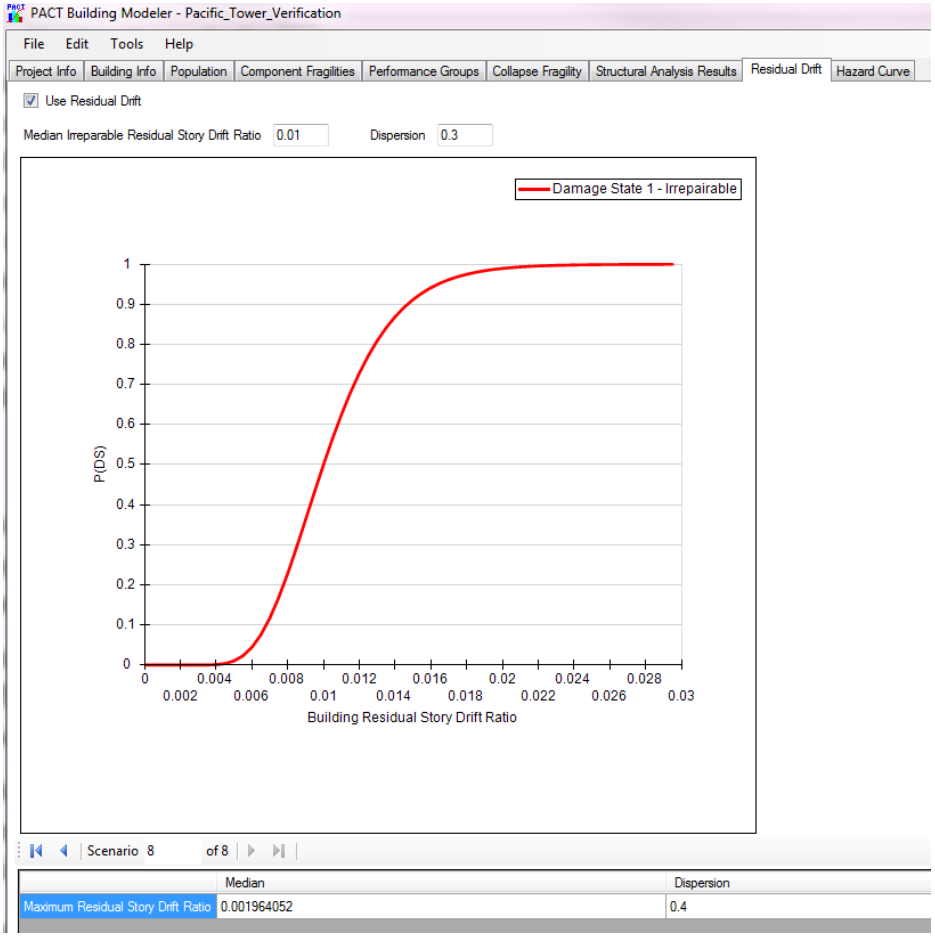

Figure 4.92. PACT Residual Drift Input

As for the Hazard Curve, it is not of interest in the scenario based analysis at this point, due to the fact that the average loss of all the realizations for each earthquake is the point of interest in this section. It will, however, be used in the multi-stripe analysis for calculating the expected annual loss (EAL) in section 4.4.3.

Prior to executing the loss analysis in PACT, a few modifications to the PACT model needs to be done in order to simulate the actual repairs made in the Pacific Tower. A report by Gardiner (2012), CPG New Zealand Ltd. explains that a complete Earthquake Damage Report by Structex was done after the February 2011 event. In the report, it is stated that the EBFs needed repair

and that during the following events, June and December 2011, no significant structural damage was observed.

This raises a question of the effects of the repair after the February 2011 event towards the losses of future events. Hence, further research on losses of running the analyses in a sequential ground motion, i.e. back-to-back sequence, as compared to running each ground motion individually is needed. In order to run this sequential model, the recorded earthquakes on each station is plotted after each other chronologically with a 100 second break in between as presented in Figure 4.93.

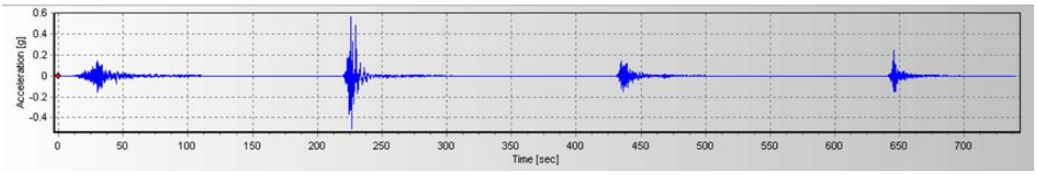

Figure 4.93. Sequential Ground Motion Record

Due to the difference in the way that repairs of EBFs are considered between sequential and individual records, that a sequential model does not permit repairs of EBFs mid-analysis, to show a fair comparison between the sequential model and non-sequential model, the EBF repairs are assumed to be only done once after the last aftershock, i.e. the December 2011 event, for both scenarios. This is done by running the EBF loss assessment separately from the other non-structural components. The EDPs for the EBFs are taken from the maximum inter-storey drift from all four events. With these assumptions, the losses obtained by running the records back-to-back and individually are compared as shown in Figure 4.94 and Figure 4.95.

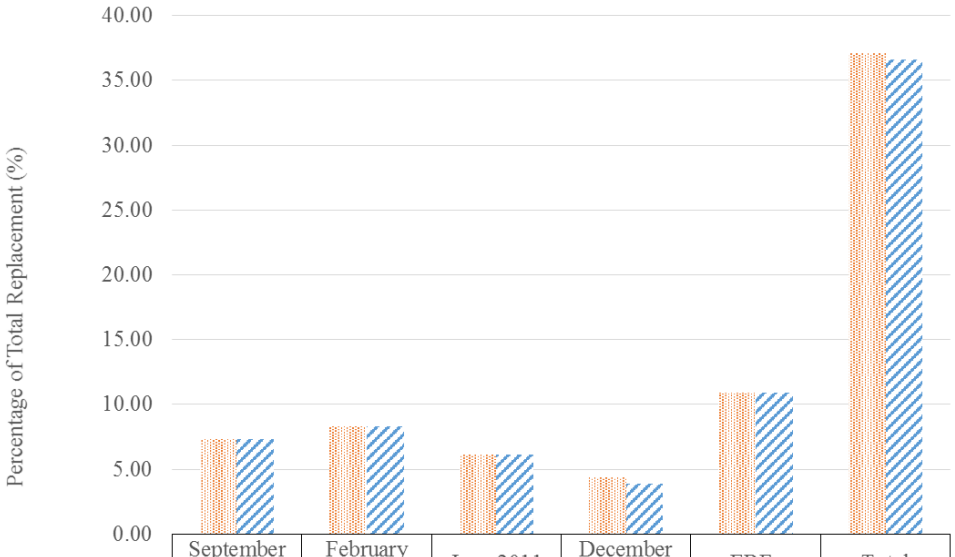

	September 2010	February 2011	June 2011	December 2011	EBFs	Total
Back-to-back	7.34	8.30	6.15	4.41	10.91	37.10
Individual	7.339120497	8.298670131	6.145747546	3.889655944	10.90562549	36.57881961

Figure 4.94. Comparing event loss prediction: Back-to-back and Individual records

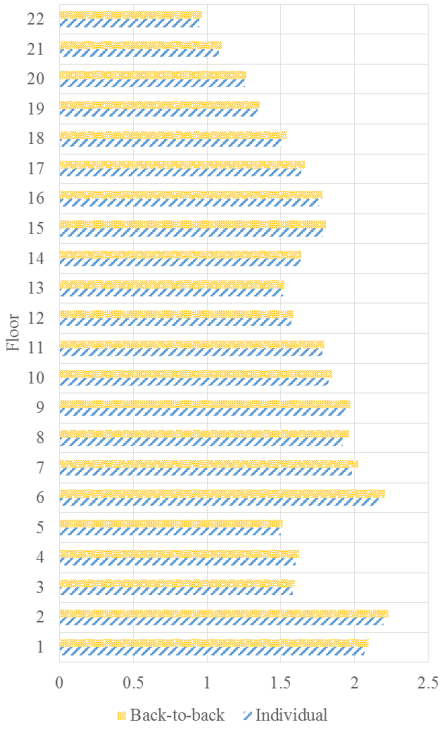

Figure 4.95. Comparing total floor loss prediction: Back-to-back and Individual records

While there is some difference in terms of losses, the total difference is within a small margin, 36.58 % and 37.1% of total building replacement for individual and sequential records, respectively. This is only a 2% difference which may be negligible. Hence, either using back-to-back or individual records is acceptable. However, note that this difference may be more significant at higher intensities. For the purposes of this research, the back-to-back records are used.

As such, with regard to the report from the Christchurch City Council, the EBFs are only included as a component in the February 2011 model as only during that event the EBFs got inspected. The analysis is then executed and the resulting average losses from PACT are averaged for each event, i.e. September 2010, February 2011, June 2011 and December 2011. The results of losses for each earthquake are as shown in Figure 4.96.

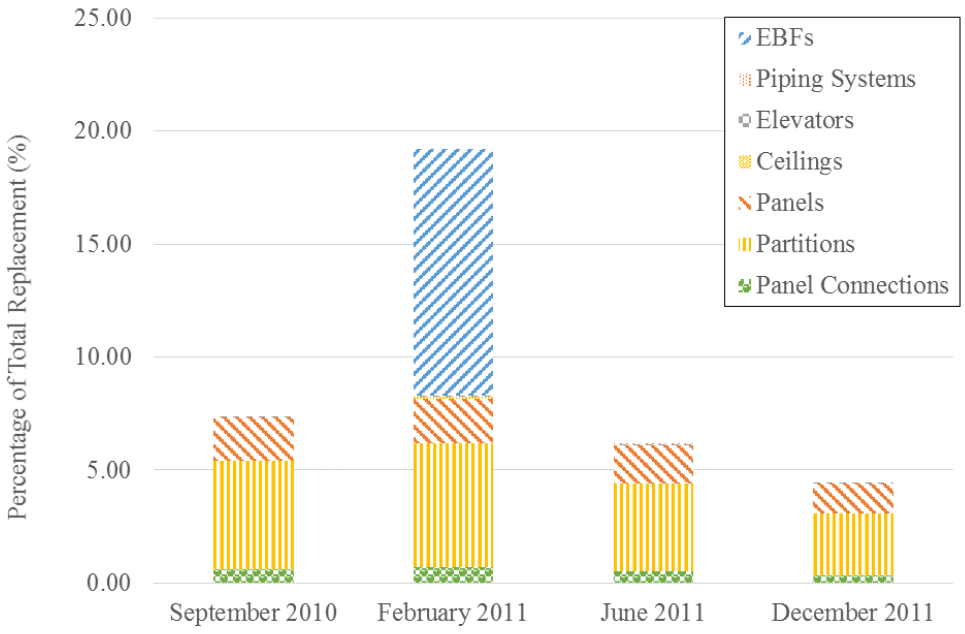

Figure 4.96. Average Losses Predicted for Each Earthquake

This result is obtained from PACT using the average loss of 200 Monte Carlo simulations. An example of the outputs from PACT are as seen in Figure 4.97, Figure 4.98 and Figure 4.99.

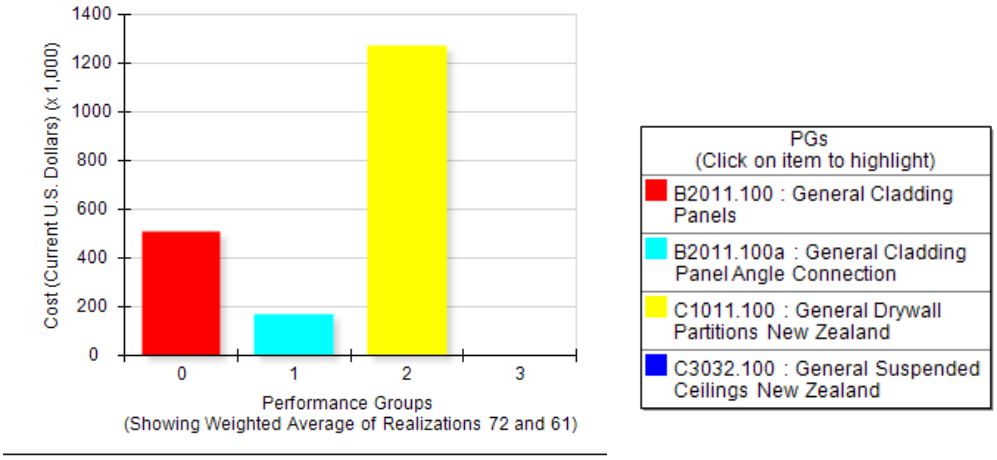

Figure 4.97. Item Loss Prediction for Weighted Averages of 2 Monte Carlo simulation for The September 2010 Event

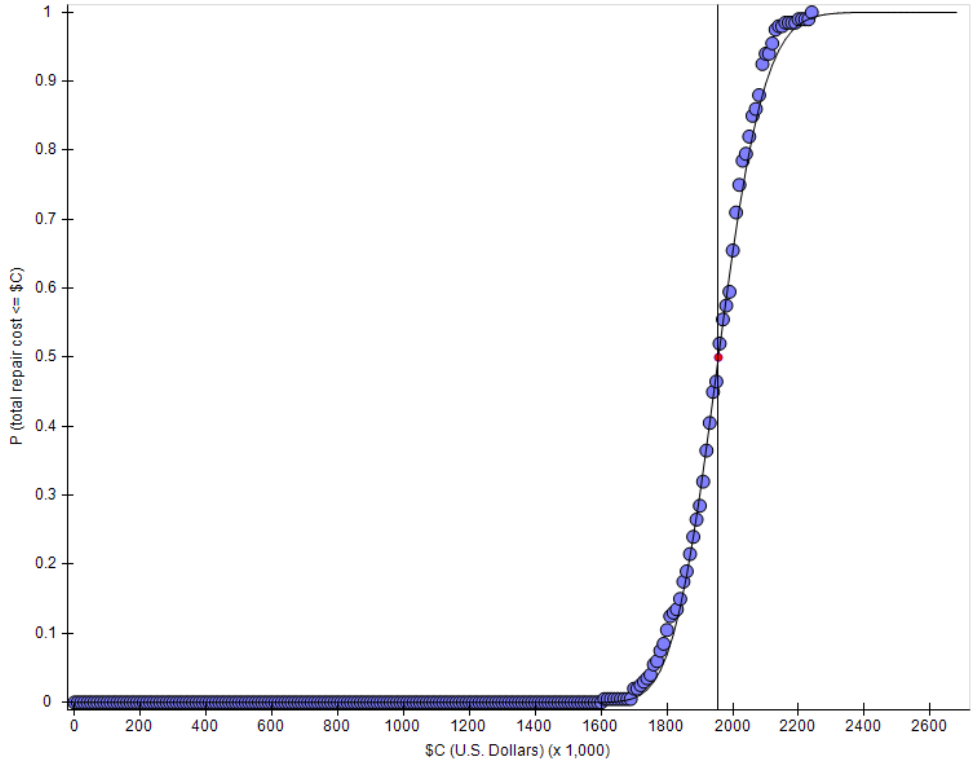

Figure 4.98. Monte Carlo Simulation Total Losses Prediction for The September 2010 Event

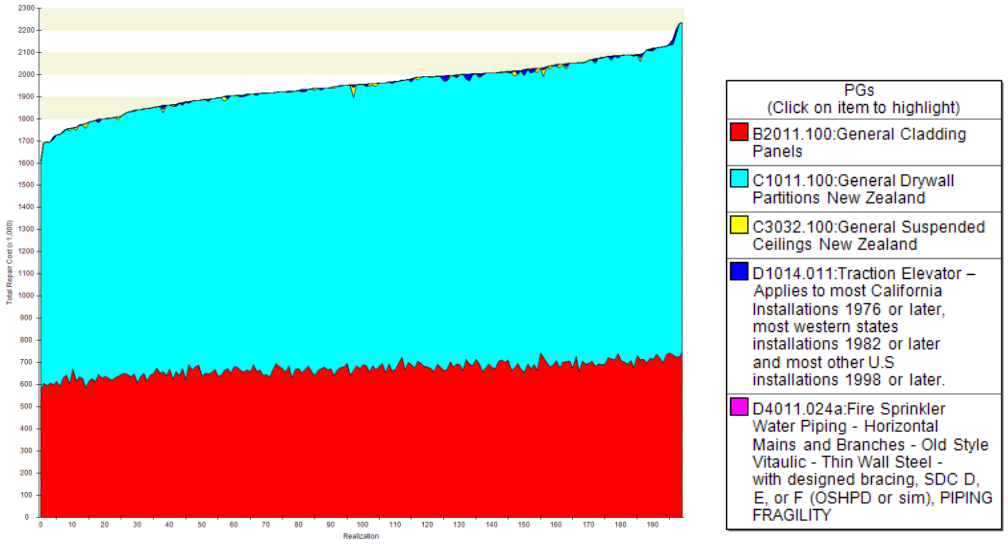

Figure 4.99. Monte Carlo Simulation Item Losses Prediction for The September 2010 Event

4.4.2. Comparing with Loss Prediction with Observed Data

In order to obtain a level of confidence that the model represents the actual building, a comparison between actual data and predicted data is done. Note that, as explained in section 2.3, it is difficult to obtain exact results. Hence, a general comparison in structural behaviour and predicted results is mainly considered.

According to reports obtained from the CCC, residual drifts of less than 0.3% were recorded in the building. The model predicts similar residual drifts, with the largest residual drift recorded as 0.28% (fourth floor after the February 2011 earthquake in the EW direction). This model prediction is shown in Figure 4.100.

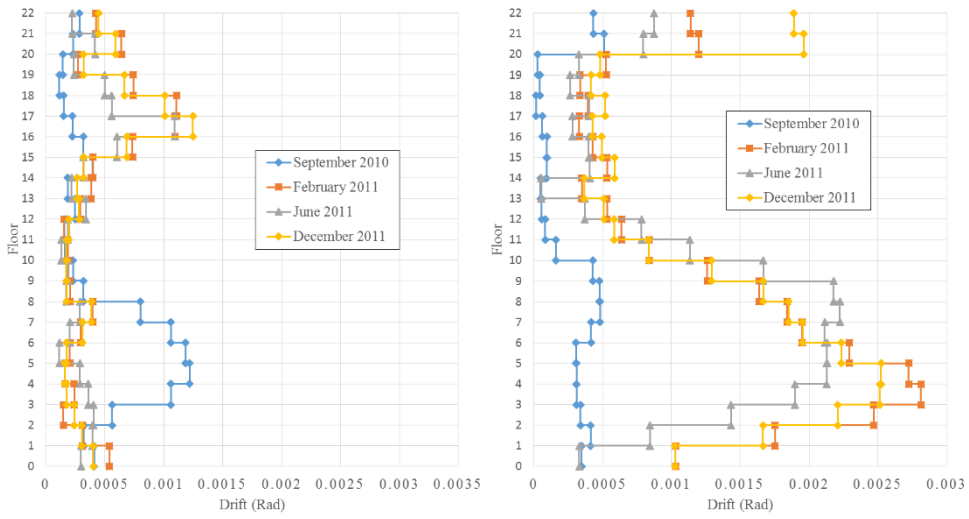

(a) (b)

Figure 4.100. Residual Drifts in the (a) NS and (b) EW Direction

The second item of comparison is the magnitude of total loss between the four events. As presented previously in Figure 4.96, the model predicted that the February 2011 was the most severe. This is as expected owing to the intensity of the February 2011 in the Christchurch CBD.

The third item of comparison is floor loss. Reports from CPG, shown earlier in Table 3-1, summarize that the damage is more evident in the lower floors of the buildings up to level 12, with a few increase on the 15th floor. The models also predicts similar floor losses, in the order of magnitude, in comparison to each floor, as presented in Figure 4.101.

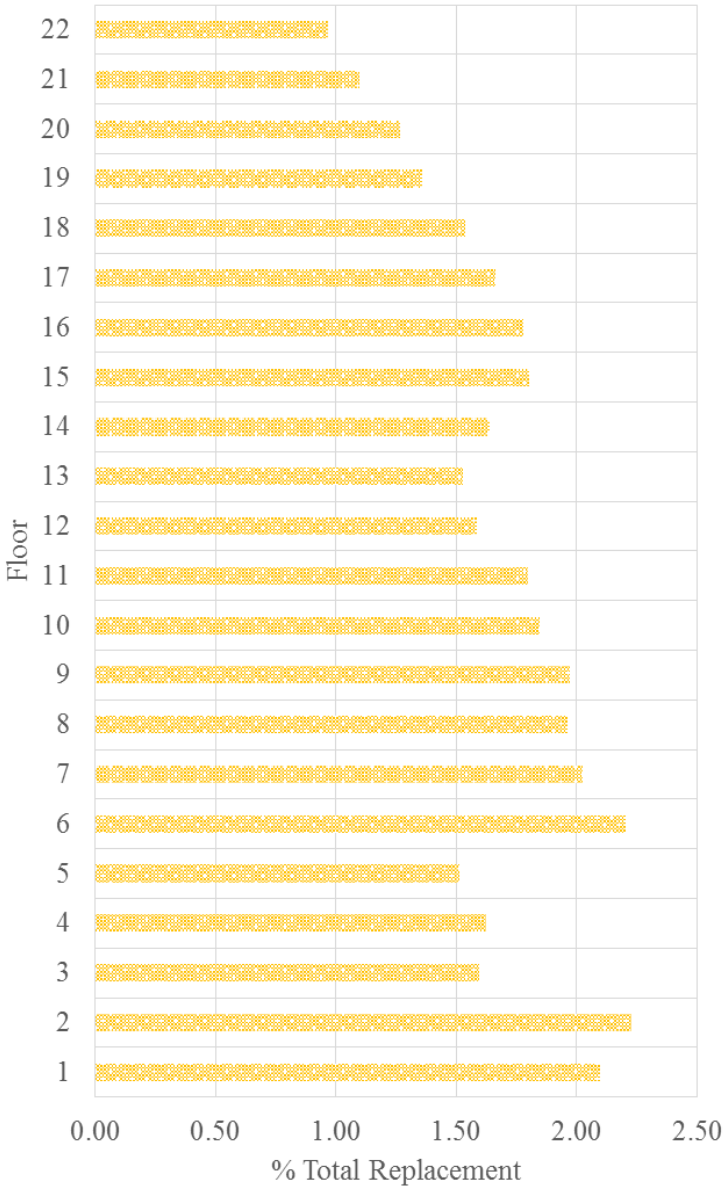

Figure 4.101. Total floor losses predicted from four events

Another item that increases the level of confidence is the comparison of losses due to each different component. Reports from the CCC indicate that the largest contributor towards losses was the drywall partitions. "Fire-rated GIB panels around the stairwell were damaged throughout the height of the structure" and "Cracked walls, ceilings, linings, tiles, glass doors and wardrobes in most rooms as well as the jamming of several doors" were statements taken from the report. The model predicts similar results as the drywall partitions and panels were mostly damaged, while there is some ceiling damage as presented in Figure 4.102.

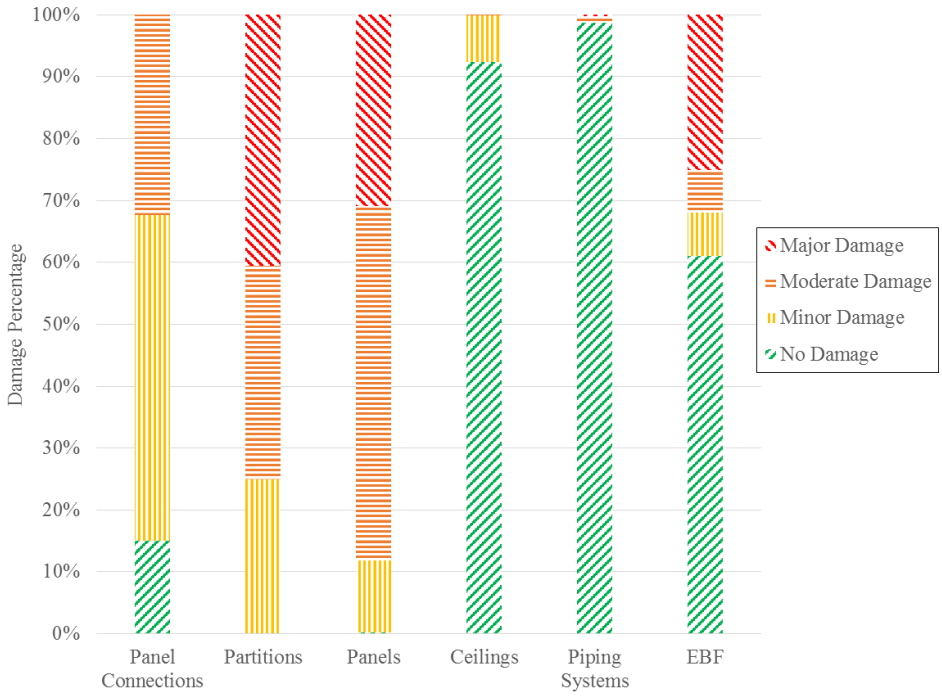

Figure 4.102. Percentage of damage predicted for each item

This is also in-line with information from Sean Gardiner, an engineer of the earthquake assessment of the Pacific Tower which stated that the partitions were damaged and repaired more than 3 times during the 2010 Canterbury Earthquake Series.

With these comparisons, it may be safe to assume that the model represents the general behaviour of the building and hence is plausible to be used in more advanced analysis such as the expected annual loss (EAL) and aftershock assessments.

4.4.3. Time-based Loss Analysis (Expected Annual Loss)

The expected annual loss is calculated for Christchurch CBD hazard levels as explained in section 4.2. The damage and loss model as well as PACT (FEMA P-58.3) inputs for time-based analysis is similar to that of scenario based. The EDP input, however, for the time-based results is different as the EDPs from section 4.3.7 are used. In addition to the inputs of scenario based analysis, time-based analysis also requires the hazard curve, aforementioned in section 4.2, to be input as well, presented in Figure 4.103.

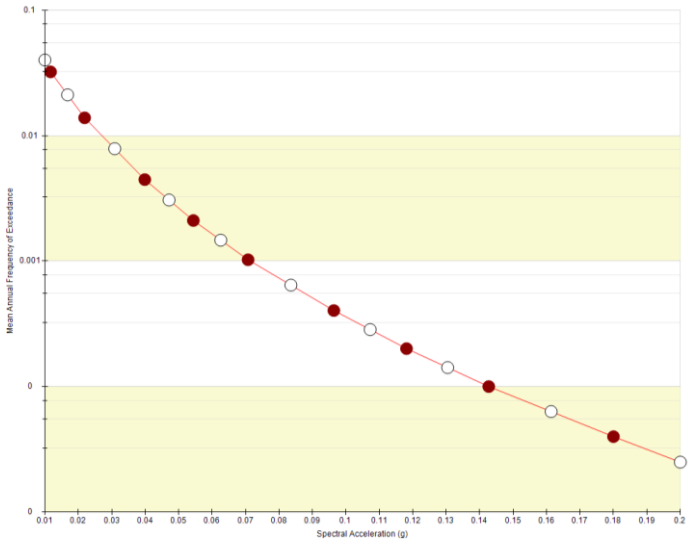

Figure 4.103. Hazard curve input in PACT (FEMA P-58.3)

As explained earlier in section 4.4.2, PACT process results in damage states and losses of each Monte Carlo simulation for each item for each intensity, losses presented in Figure 4.104. This information is used to calculate

the expected annual loss. Which, described previously in section 2.1.4, is a sum (by integration) of each case of loss for each intensity measure for a certain mean annual frequency of exceedance (MAFE), presented in Figure 4.105 and Table 4-19.

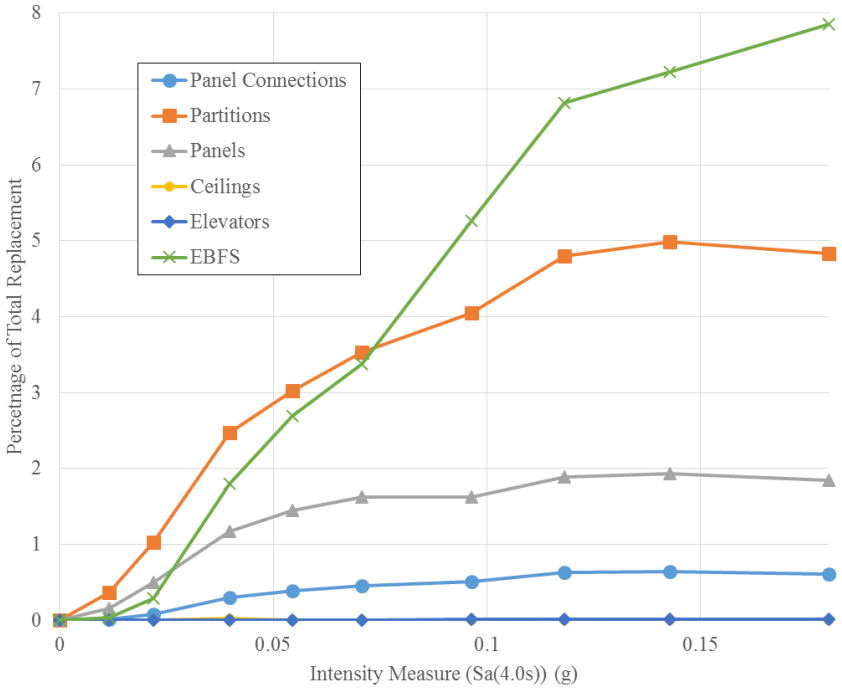

Figure 4.104. Loss Prediction by item for each IM

Table 4-19. Loss Prediction by item for each IM

	Percentage of Total Replacement (%)						
Sa (4.0s) (g)	Panel Connections	Partitions	Panels	Ceilings	Elevators	EBFS	Total
0.01	0.02	0.37	0.16	0.00	0.00	0.03	0.58
0.02	0.07	1.02	0.49	0.00	0.00	0.29	1.89
0.04	0.30	2.47	1.17	0.03	0.01	1.80	5.78
0.05	0.39	3.03	1.44	0.00	0.01	2.69	7.55
0.07	0.45	3.53	1.62	0.00	0.00	3.38	8.98
0.10	0.51	4.05	1.62	0.00	0.01	5.26	11.44
0.12	0.63	4.80	1.89	0.00	0.01	6.81	14.14
0.14	0.64	4.98	1.93	0.00	0.01	7.23	14.79
0.18	0.60	4.83	1.84	0.00	0.01	7.85	15.14

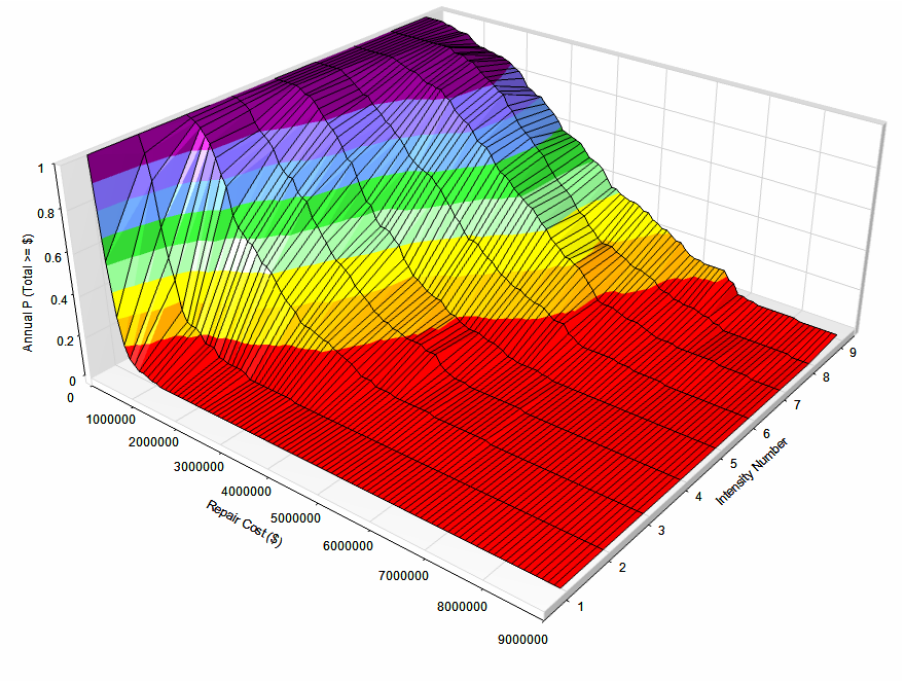
Annual P (Total >= $)
1
0.8
0.6
0.4
0.2
0
0
1000000
2000000
3000000
4000000
5000000
6000000
7000000
8000000
9000000
Repair Cost ($)
1
2
3
4
5
6
7
8
9
Intensity Number

(a)

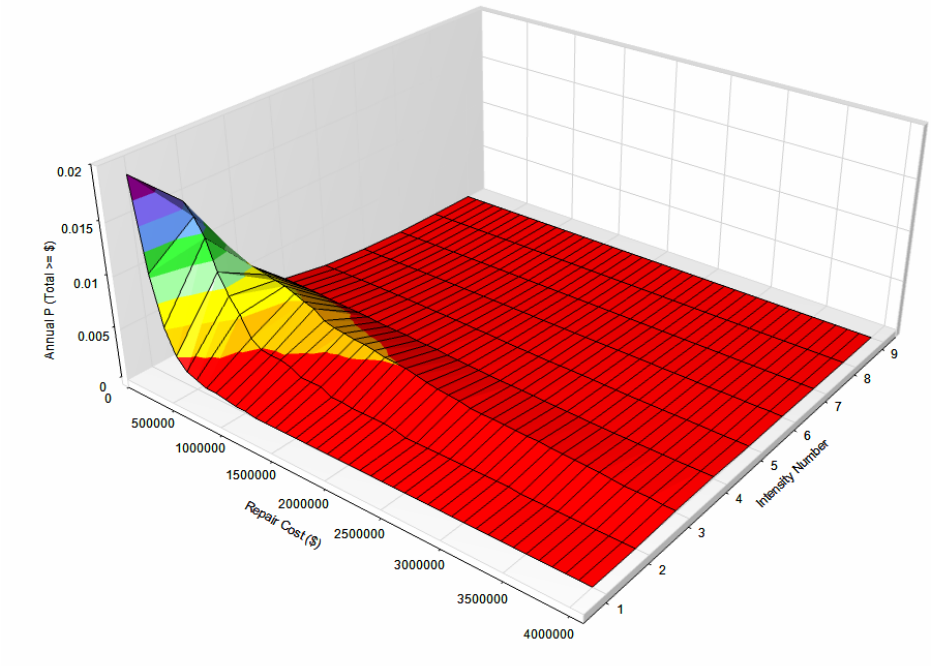
Annual P (Total >= $)
0.02
0.015
0.01
0.005
0
0
500000
1000000
1500000
2000000
2500000
3000000
3500000
4000000
Repair Cost ($)
1
2
3
4
5
6
7
8
9
Intensity Number

(b)

Figure 4.105. Surface plot of losses predicted (a) un-adjusted and (b) adjusted by MAFE

As such, the expected annual loss can be calculated as the integration of Repair Costs/Annual Probability and Intensity/Annual Probability (i.e. the volume under the surface in Figure 4.105b) using equation 4-8.

$$\boldsymbol{C = \int_{c=0}^{c=\infty} \left(\int_{\lambda im=a}^{\lambda im=b} P(C = c|\lambda im) d\lambda im \right) \times c \; dc} \qquad \textbf{(4-8)}$$

Where,

a = Mean annual frequency for lowest considered IM;

b = Mean annual frequency for highest considered IM;

C = Expected annual loss ($);

c = Average cost of repair ($);

λim = Mean annual frequency for a given IM;

Applying equation 4-8 to the intensity based loss assessment result returns a value of NZ$26,231.25. This is the expected annual loss (EAL) of the 'base' model.

In order to communicate seismic risk, explaining in terms of expected losses may be a better option to help the general public understand. Kappos and Dimitrakopoulos (2008) suggests using Equation 4-9 to calculate expected loss.

$$\boldsymbol{E[C(t, R_L)] = C_0 + \overline{C} \cdot \frac{1 - e^{-\lambda t}}{\lambda} \cdot \sum_{J=VI}^{IX} N_j \cdot D_{mv,j}} \qquad \textbf{(4-9)}$$

Where,

$E[C(t, R_L)]$ = Expected loss for a given time (t (Years)) for a given retrofit level (R_L)

C_0 = Initial Costs ($)

λ = Discount Rate (%)

$\bar{C} \cdot \sum_{J=VI}^{IX} N_j \cdot D_{mv,j}$ = Expected Annual Losses

Data from the CCC show that the building cost was NZ$21,600,000. This is the initial costs, assuming no retrofit (for retrofits, refer to chapter 5). A practical discount rate between 1 and 7% was suggested by Beck et al. (2002), presented in Figure 4.106. A high discount rate (i.e. 7%) will reduce the loss over time compared to a low discount rate which returns increased losses. The determination of the discount rate is done based on the expected utility of the building. Due to the fact that the case study building is a multi-residential building, it is neither first priority (e.g. hospitals) nor least priority (e.g. single-residential), it is assumed that a discount rate of 4% is adequate.

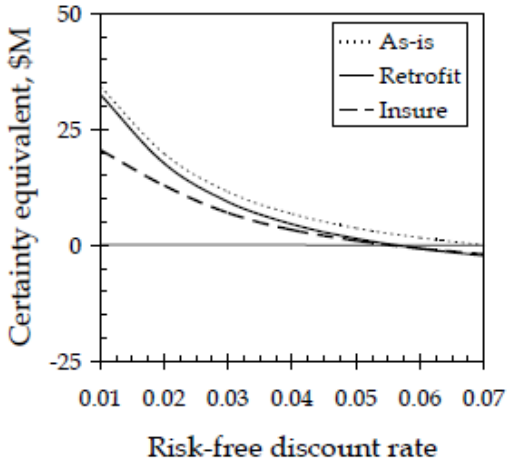

Figure 4.106. Discount rate for a given certainty equivalent (Beck et al. 2002)

As such, it is possible to calculate the expected losses over time of the case study building by applying the variables to Equation 4-9, which results in an expected loss graph as presented in Figure 4.107.

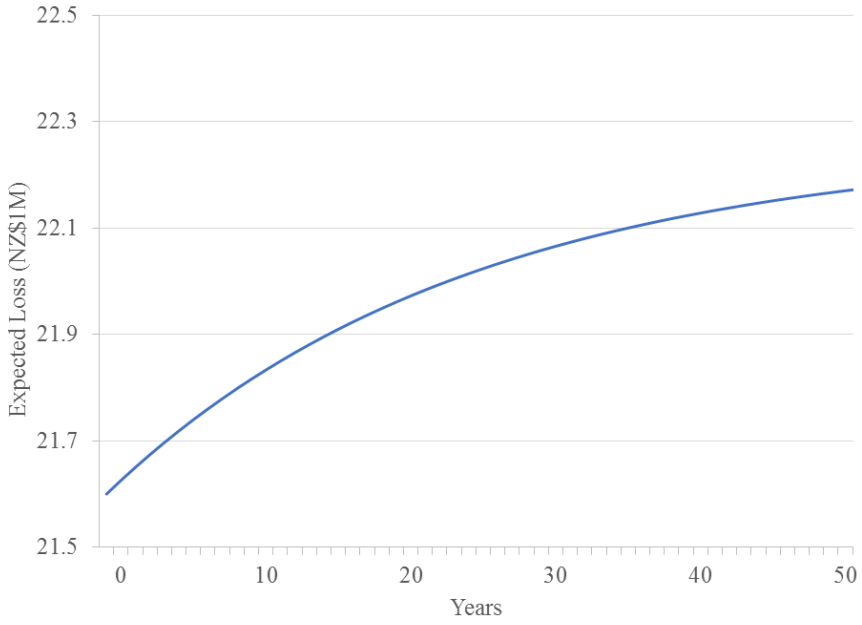

Figure 4.107. Expected loss of case study building for 50 years

Owing to the uncertainties in calculating the expected losses (costs and discount rate), a lower and upper bound is created to highlight this uncertainty. While it is difficult to predict the inflation and future economic conditions, assuming a risk-free discount rate, practical values of 1 to 7% may be enough to show aleatory uncertainties (e.g. future inflation, future economy, or building expected utility) in expected losses.

In addition to the discount rate, another uncertainty is the expected annual loss itself. In order to sum up all cases, a certain random probability is selected as a means of obtaining damage states and losses. It is true that by using enough simulations (MCS) to generate these random probabilities, the uncertainty due to this random selection may be reduced. However, this does not remove the fact that the damage and cost itself is uncertain. For example, an EBF designed using the same requirements may have different strengths due to the material even if it was erected by the same company. Hence, to address this matter, an uncertainty in the expected annual loss is taken. A lower bound and upper bound of two standard deviations, assuming a normal distribution, are

taken from the average repair cost, as presented in Figure 4.108. These lower and upper bounds are then used to calculate an expected loss using Equation 4-8, resulting in a lower and higher expected annual loss, of NZ$10,131.4 and NZ$81,462.7 respectively. Note that due to the unlikelihood of a negative EAL, which occurs on low intensities, the normal distributions are truncated at $0.

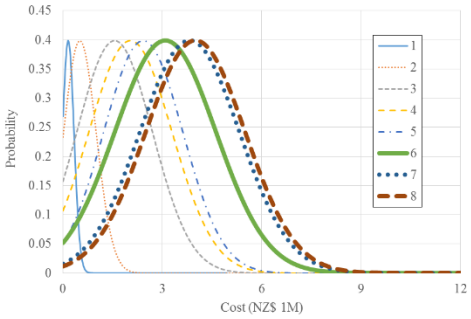

(a)

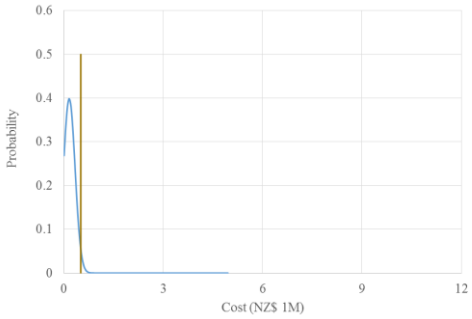

(b)

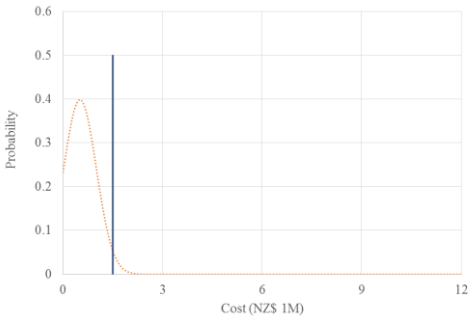

(c)

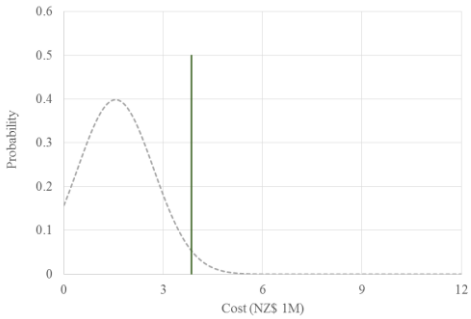

(d)

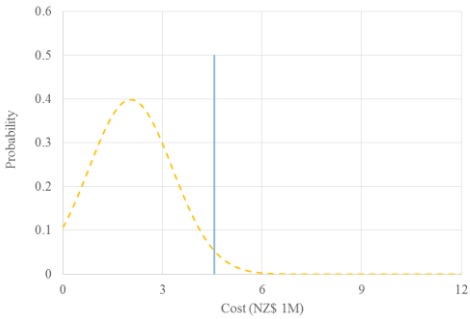

(e)

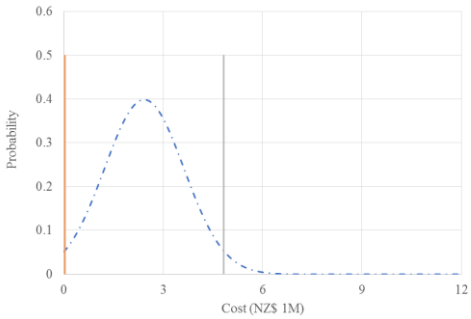

(f)

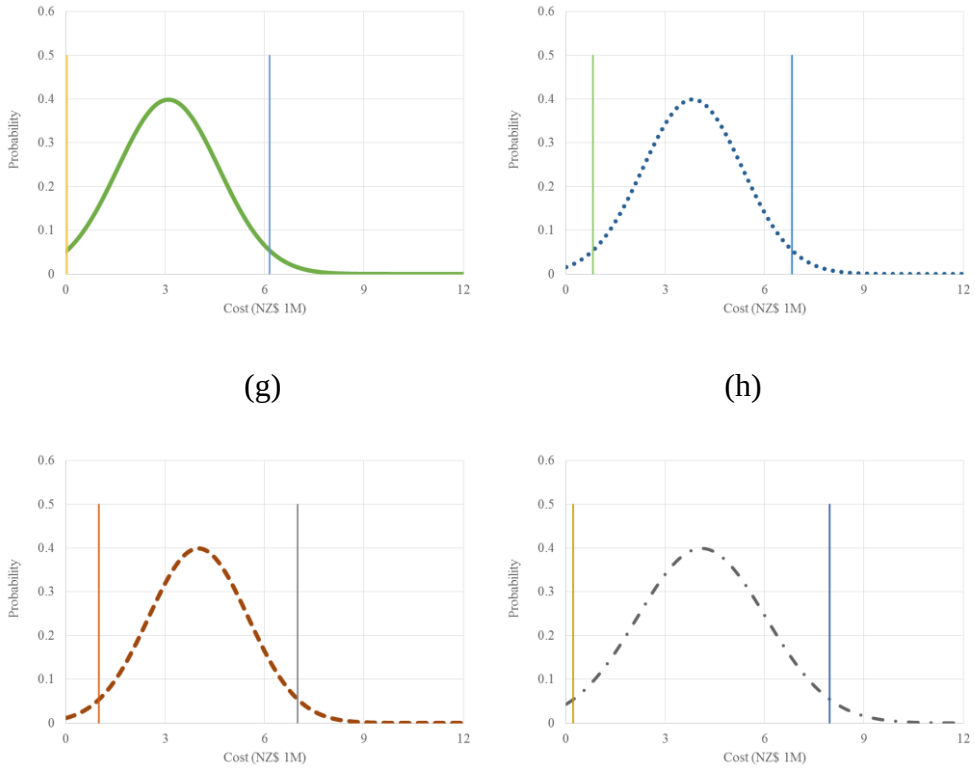

Figure 4.108. Truncated normal distribution for (a) all intensities, (b) 1, (c) 2, (d) 3, (e) 4, (f) 5, (g) 6, (g) 7, (i) 8, (j) 9

With respect to these uncertainties (discount rate and average costs), the expected losses are re-calculated and the difference in the expected loss in 50 years is shown in Figure 4.109. Effects of uncertainty in (a) discount rate and (b) repair costs. Note that the probability of the upper and lower bounds are lower (approximately 25%) than the average expected losses presented earlier.

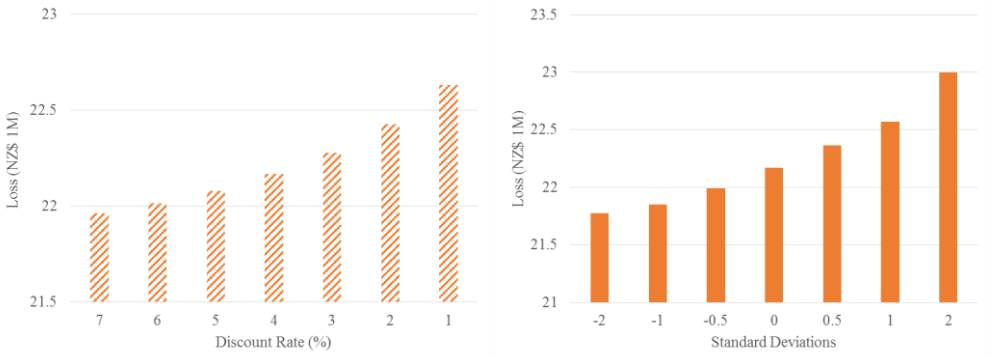

(a) (b)

Figure 4.109. Effects of uncertainty in (a) discount rate and (b) repair costs over a 50 year period

This is done to highlight the uncertainty in the process of assessing losses. While it is true that with these uncertainties the losses may be presented as Figure 4.110, the fact that probability of the worst case exceeded is rare should not be overlooked.

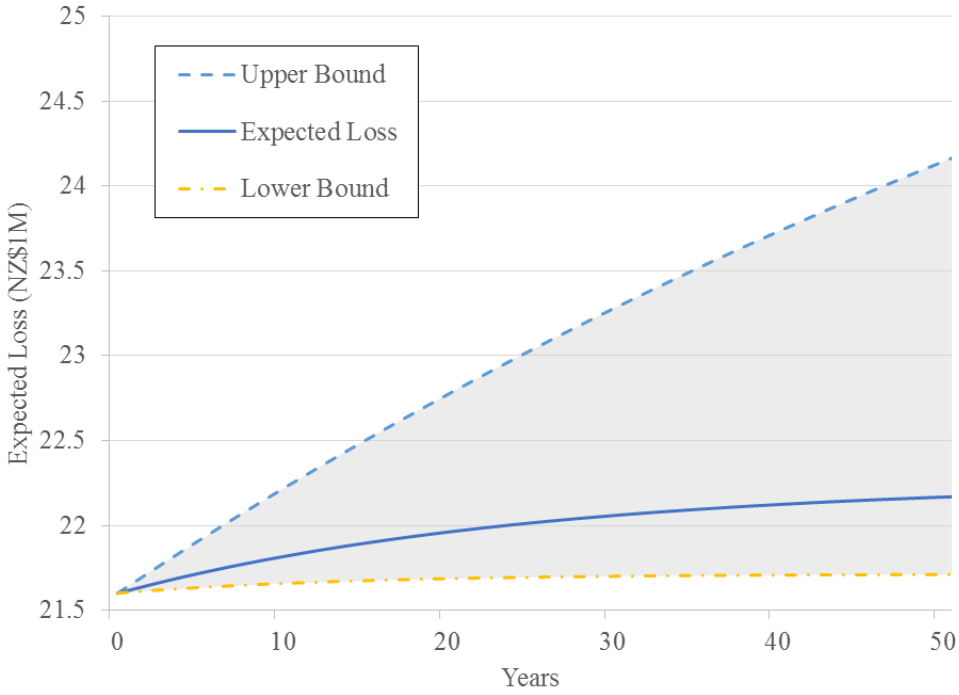

Figure 4.110. Expected loss uncertainty

4.5. Conclusions

The expected loss graph shows an increase of expected loss to up to 10% the building value over a 50 year period. This underlines the importance of planning the losses as with better planning (i.e. design or retrofit) this unnecessary loss can be reduced, discussed further in the next chapter. Although there is an increasing dispersion with time owing to the epistemic and aleatory variables, it still represents the expected loss due to seismic hazard of the case study building. It might even be a better tool for communicating seismic risk due to the general terms used (dollars over time). Which results in a better risk communication towards the general public.

Another interesting find is the fact that at lower intensity seismic events (i.e. more frequent) the non-structural elements (e.g. partitions) are the most significant contributor towards losses. Hence, the fact that attention should be given to these non-structural elements is true.

5. Identification of Retrofit/Rehabilitation Options

5.1. Introduction

The identification of effective retrofit/rehabilitation options is done by modifying parts of the process of calculating the building loss, (i.e. PEER-PBEE process). This is accomplished by alterations according to the needs of each retrofit option considered below.

5.2. Consideration of Retrofit/Rehabilitation Options

In order to explain the process, this section is divided into three parts; the concepts of the retrofit/rehabilitation options considered; the application of the options to the Pacific Tower; the cost-benefit analyses of applying the retrofit/rehabilitation to the Pacific Tower.

5.2.1. Concepts of Retrofit/Rehabilitation Options

There are two retrofit/rehabilitation options considered in this research, Improving Drywall Partitions and Re-detailing Cladding Connections.

5.2.1.1. Improving Drywall Partitions

One retrofit/rehabilitation option is to use the "Novel Sliding/Frictional Connection for Improved Seismic Performance of Gypsum Wallboard Partitions" following the work of Araya-Letelier and Miranda (2012). In the paper, a new sliding/frictional connection was suggested as an improvement towards partitions' seismic performance.

This connection involves adding thin steel plates between a beam/slab of the upper floor and the upper cold-formed steel track of the partition. These cold-formed steel tracks are horizontally slotted (approximately 90mm in length) such that the partitions can move horizontally and are "clamped" with

steel square tubing. This surface between the steel plate, cold-formed upper track and steel tubing is the sliding/frictional surface. In order to allow for horizontal movement, i.e. allow for deformation under life load without increasing the normal force on the friction surface, the sides of the cold-formed upper track is also slotted vertically, as presented in Figure 5.1.

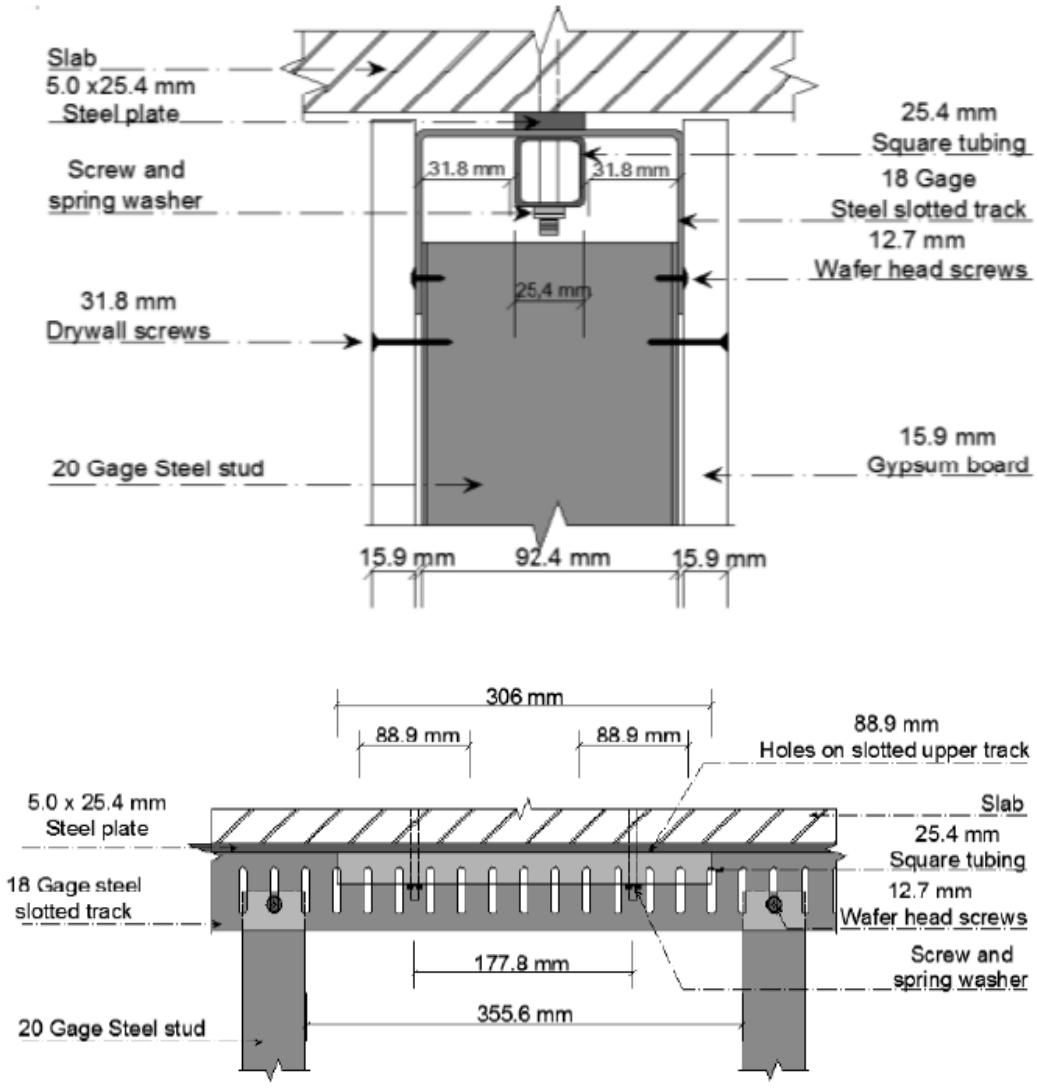

Figure 5.1. Sliding/Frictional Connection (Araya-Letelier & Miranda 2012)

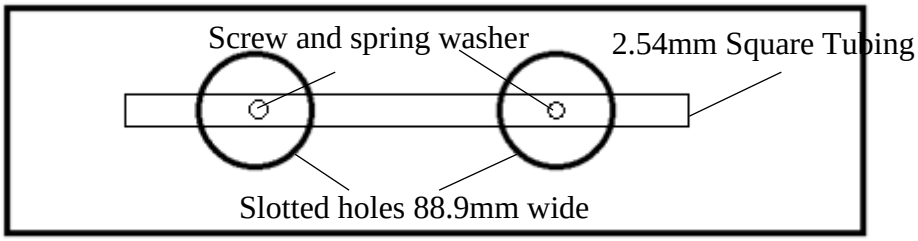

Figure 5.2. Top view of cold formed upper track

Using cyclic reversal tests, Araya-Letelier and Miranda conducted two full-scale specimen tests. One was conventional and the other used sliding/frictional connections shown in Figure 5.1. The conventional partitions were damaged at 0.1% storey drift while the improvement was damage free at 1.52% story drift. Unfortunately, since the improved partitions were only tested once, a fragility curve cannot be established. Instead, the maximum additional deformation of 31.8mm via sliding and gaps, refer to Araya-Letelier and Miranda (2012), is used to 'shift' the conventional fragility curves by the 'additional' storey drift, which is the maximum displacement divided by the storey height, as seen in Figure 5.3.

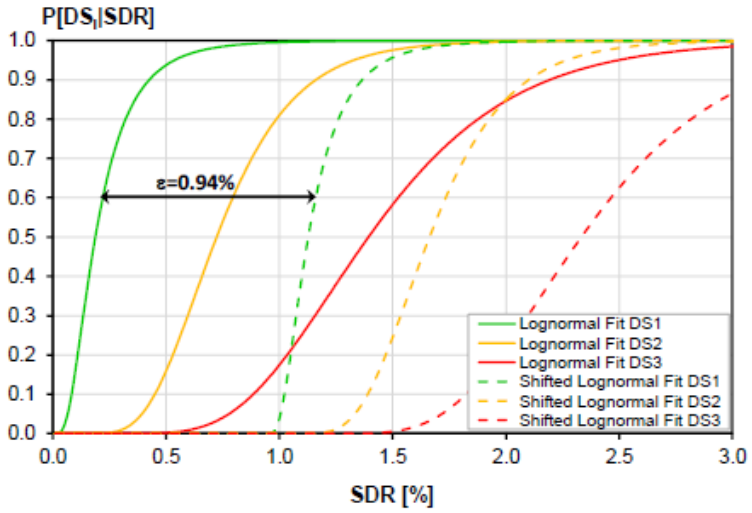

Figure 5.3. Conventional Partition and Improved Partition Fragility Curves (Araya-Letelier & Miranda 2012)

The damage states defined in this paper were similar to that defined by Davies et al. (2011) and Dhakal et al. (2016). The first damage state (DS1) is minor damage that can be repaired by patching, re-taping, sanding and/or painting. The second damage state (DS2) is severe cracking which will need replacement of the gypsum boards. And finally, damage state 3 (DS3) is defined as severe damage to studs, tracks and/or frames which requires a total replacement of the partitions. As such, the costs to repair such partition is assumed to be similar to that of conventional partitions with additional costs to replace tracks (i.e. DS3).

5.2.1.2. Alternative Cladding Connections

Another interesting point from the Pacific Tower model was the effects of the exterior cladding connections towards the seismic loss of the building. Hence, another considered retrofit option is the details on the cladding connections. Due to inflexible connections, explain in section 4.3.2, the exterior claddings provide an additional stiffness towards the structure. This certainly affects the seismic performance of the building. In order to examine the effects of this connection, a flexible one, such as one explained in 4.3.1, is assumed to remove this additional stiffness, and hence alter the seismic performance of the building. This, however, allows for the assumption that the cladding itself is free to move. As such, it may also be assumed that the claddings do not suffer damage.

5.2.2. Application of Suggested Retrofit/Rehabilitation Options

Both options in 5.2.1 (i.e. improving partitions and re-detailing cladding connections) endeavor to reduce losses by increasing the deformation capacity of vulnerable components which are the drywall partitions and cladding panels.

The improved partitions are not expected to alter the global structural performance. Hence, the EDPs from the first set of analyses may be used as EDPs for the improved partitions. This, however, is not the case for damage and loss analysis as the improved partitions are expected to increase the deformation, thus reducing damage in the expense of increased cost. By shifting the fragility curves and increasing the cost of replacement due to additional implementation costs, a new damage-loss-decision value is obtained for the first retrofit option. Finally, the expected annual loss for an improved partition retrofit can be calculated, using equation 4-8 as NZ$16,387.2. Similar to the 'base' model, a lower bound and upper bound using two standard deviations from the average loss is used to calculate a lower and upper bound to the EAL, which are calculated as NZ$6,048 and NZ$45,180, respectively.

Although the exterior cladding are not structural, the effects of the claddings on the structural response is evident as explained in chapter 4. Hence, "removing" the cladding via a flexible connection is expected to change the global performance of the structure. In order to account for this change, a new set of models were created in Ruaumoko3D similarly but without the cladding modelled. Using these models, the whole analysis process from structural up to loss analysis is re-run. The resulting EDPs, a part of it (IM 6) presented in Figure 5.4 and Figure 5.5, show that the claddings in fact do effect the structural performance, while the other results are included in Appendix F.

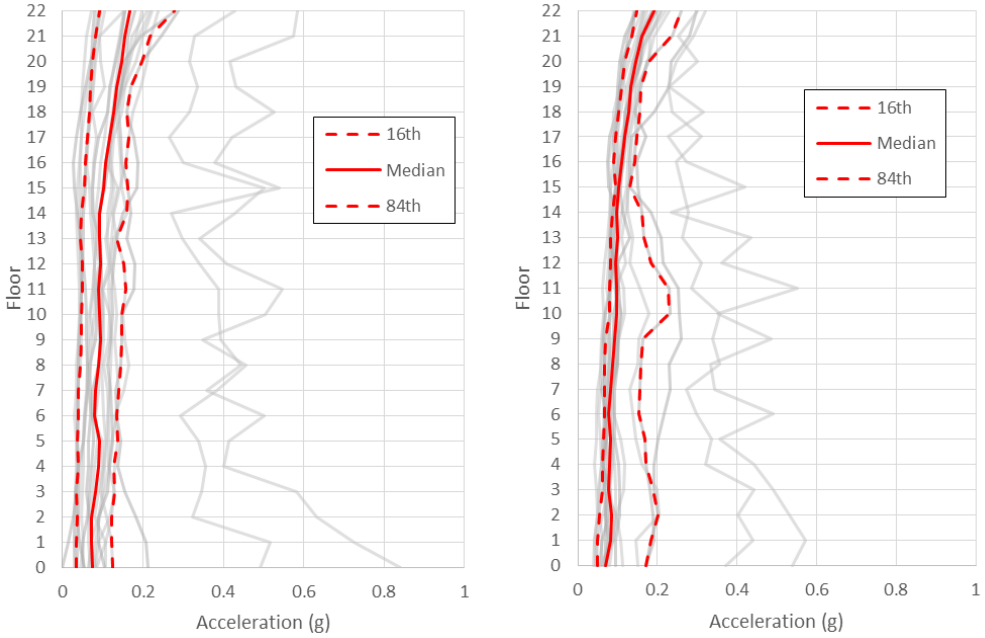

(a)

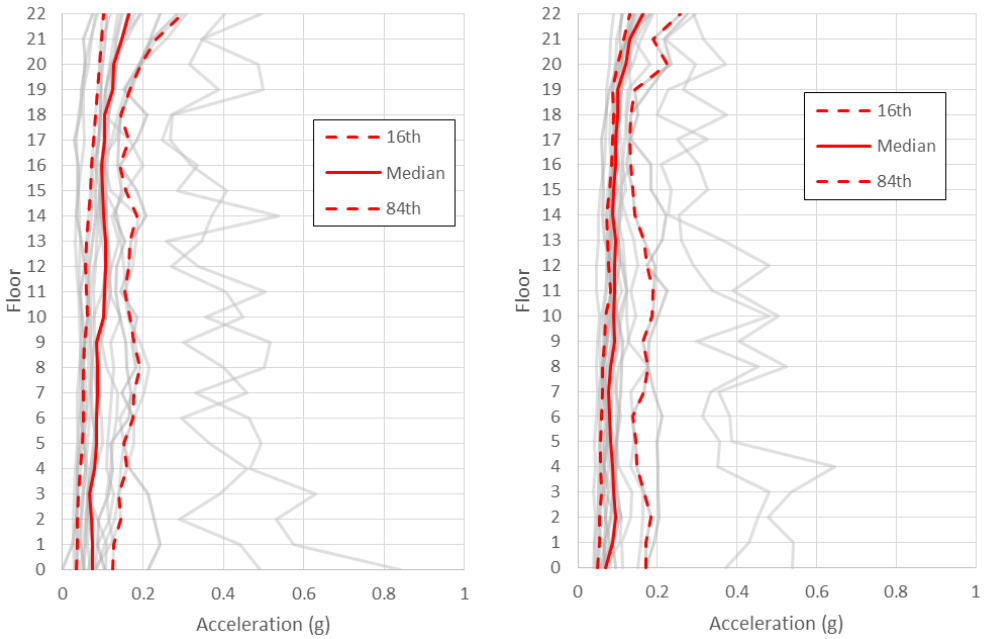

(b)

Figure 5.4. Peak transient floor acceleration for (a) As-Is Model with Claddings NS; EW and (b) Model without Cladding Contribution NS; EW

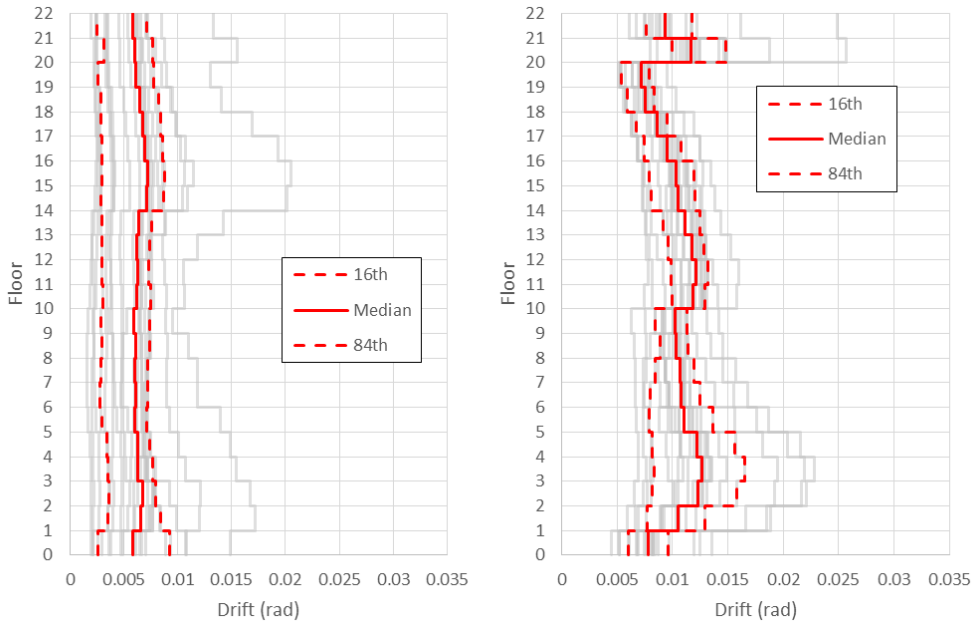

(a)

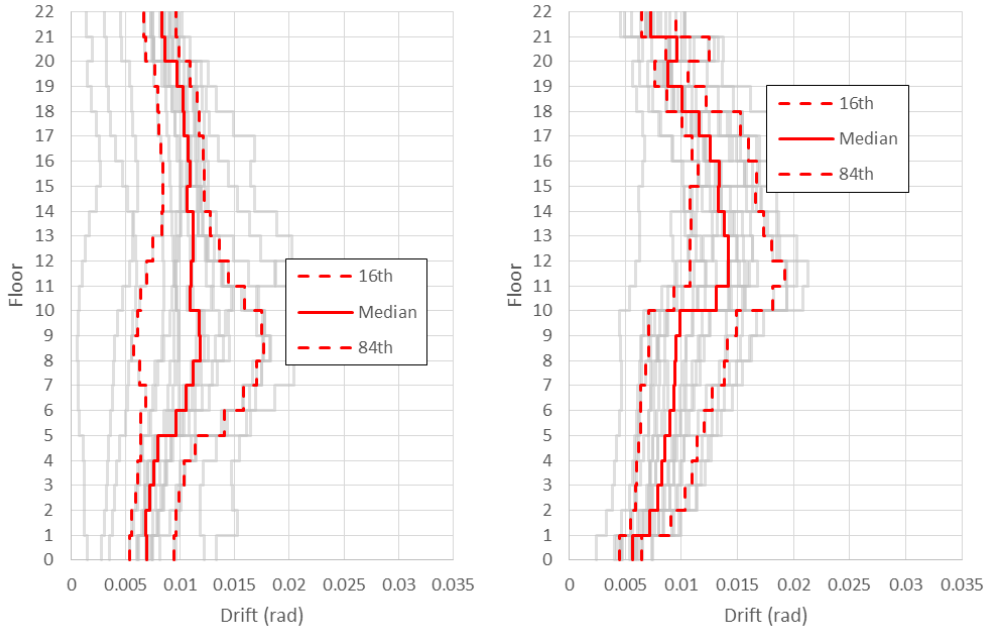

(b)

Figure 5.5. Peak inter-storey drifts for (a) As-Is Model with Claddings NS; EW and (b) Model without Cladding Contribution NS; EW

5.2.3. Cost-Benefit Analysis

As such, using the EDPs from the modified model, a damage and loss analysis is run with the same fragility curves and loss functions as the standard model. However, the claddings are removed from the PACT model as they are assumed to have enough deformation capacity due to the flexible connections. By doing so, the expected annual loss can be calculated as NZ$25,845.3

The last parameter that needs to be added to the retrofit/rehabilitation options is the implementation cost. This, however, is also an uncertainty as different contractors and engineers suggest different values. A suggested initial cost from structural engineers in Christchurch for implementing the railings in the improved partitions was 5 NZD/m^2 of drywall partition. This value however, is uncertain. Hence, a lower and upper bound of 7.5 NZD/m^2 and 2.5 NZD/m^2 is assumed. Similarly, re-detailing the claddings is assumed to cost 5 NZD/m2 with a lower bound of 2.5 NZD/m^2 and an upper bound of 7.5 NZD/m^2.

Similar to calculating the "standard" EAL, the improved partitions and re-detailed cladding connections EAL will also need to incorporate the uncertainties due to epistemic and aleatory variables such as the discount rate and the expected annual loss. As such, a discount rate of 1% to 7% and a lower and upper bound of two standard deviations from the mean is used to account for these uncertainties.

With the assumptions made, the expected losses for each retrofit/rehabilitation option can be calculated using Equation 4-9 and the result is presented in Figure 5.6 and .Figure 5.7.

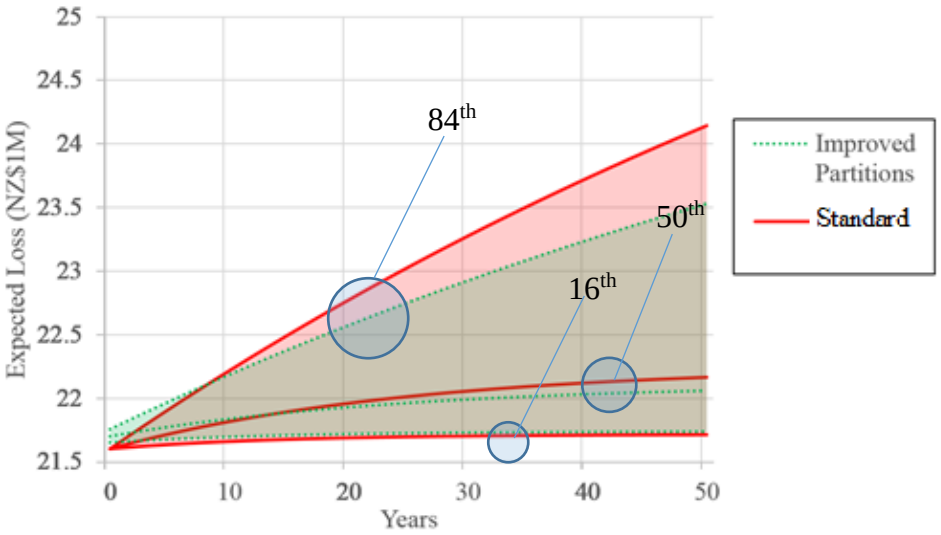

Figure 5.6. Cost-benefit of improving the partitions

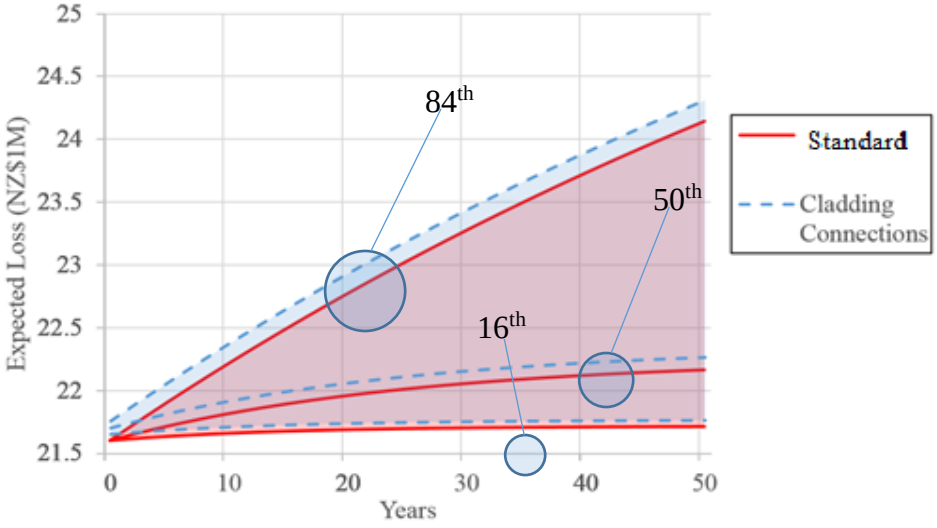

Figure 5.7. Cost-benefit of re-detailing the cladding connections

5.3. Conclusions

In conclusion, with the assumptions made, retrofitting the most critical component, in this case the drywall partitions, is worthwhile in the long run as, despite uncertainties, over time, the improved partitions show a trend towards reducing expected loss (for this particular case study, it is expected to be beneficial after approximately 15 years). However, there is a level of uncertainty in the analysis. As such, stakeholders should assess the 'believability' of this variations due to assumptions as part of their decision making process.

While it is true that taking into account the uncertainties, it becomes difficult to determine the most optimal solution. As the "areas" between bounds for each option overlap. Hence providing a probability of exceeding one another at different points. However, improving only the non-structural components (i.e. partitions) most likely will not change the global response of the structure therefore not altering the EDPs. With the same location and assuming the same structural response, the fact that increasing initial costs to improve critical elements will more often than not be worthwhile. However, note that in reality, changing the performance of the non-structural components, i.e. improving, will slightly change the global response of the structure.

Re-detailing the claddings and changing the global performance of the building, on the other hand, (i.e. increasing the drift whilst reducing losses due to claddings) is not worthwhile. As over time, the expected loss remains higher than that of the 'standard' expected loss While the EAL does reduce, overtime the option still does not show benefit up to 50 years. This due to the un-even trade-off between the cost to implement repair claddings and the increased damage due to increased drift.

Finally, highlighting the importance of considering the "improvement" of critical elements, it is important to consider the option of retrofitting towards leaving the building as is due to the fact that it is most likely to be beneficial to retrofit.

6. Consideration of Aftershocks

6.1. Methodology

Performance based earthquake engineering allows the analyses and assessments of losses in structures considering a given hazard level for a given location. PBEE, however, has not accounted for the possibility of additional losses due to aftershocks. It is a fact that most earthquakes are preceded, foreshocks, or followed, aftershocks, by smaller earthquakes. While these 'smaller' earthquakes may not be as severe as the main earthquake, they still pose a level of threat towards losses in a building. Hence, in order to bring into light this matter, a suggested "aftershock assessment" is proposed. Note that foreshocks are treated as aftershocks in this research and henceforth will be denoted as aftershocks. The aftershock assessment proposed utilizes real sequences of previous earthquakes, as explained in section 3.3. These real sequence earthquakes records are used to run nonlinear time history analyses using the case study building as a baseline for losses.

During an earthquake series, a building may suffer from a higher increase in losses if the building is unfortunate to be in the 'path' of the earthquake series. For example, the Christchurch Business District suffered a larger loss due to the February 2011 event owing to the aftershocks, as presented in Figure 6.1.

Figure 6.1. 2010 Canterbury Earthquake Series

The same building, however, may not suffer as much increased damage if the location of aftershocks were further away than the main shock. As such, in order to account for this uncertainty in the location of the aftershocks, records from strong motion stations that are approximately the same distance from the epicentre and have similar soil conditions (resulting in similar spectral accelerations) are assumed to be possible sites of the building, an example is presented in Figure 6.2. A loss assessment is run for each location through each earthquake (main shocks and aftershocks). Due to the fact that in reality it takes a lot of time to undergo structural repairs, in the loss assessment process, the losses due to structural damage are assume to only occur once, at the end of the earthquake series, by taking the largest EDP during the series. Nevertheless, the effects of residual drifts and cumulative stiffness effects are ignored throughout the process

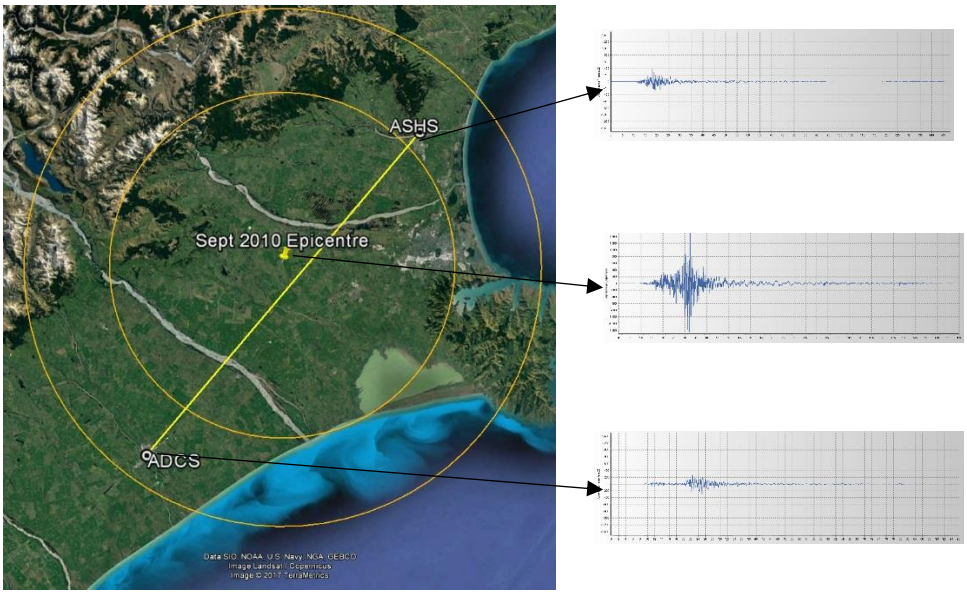

Figure 6.2. Location of building (strong motion sites) example

After the loss assessment for each event and location is complete, a graph comparing the losses due to main shocks only and main shocks with aftershocks against an intensity measure is presented and the increase in losses may show the effects of considering aftershocks in loss assessments.

6.2. Earthquakes Considered and Intensity Measures

To obtain a larger database for the aftershock assessment, three real sequences of earthquakes were used for the analyses. The 2010 Canterbury Earthquakes (EERI 2012), 2016 Kumamoto Earthquakes (EERI 2016) and 2016 Kaikoura Earthquakes (Wotherspoon et al. 2017). For each earthquake series, a few aftershocks with moment magnitudes larger than 5 (5.5 for 2010 Canterbury Series due to data availability) are considered for the assessment as smaller magnitudes are assumed to not induce loss towards the building. The considered earthquakes station together with the date and time of occurrence are presented in Table 6-1.

Table 6-1. Earthquakes considered

Earthquake Series	Earthquake Type	Time	Magnitude
2010 Canterbury	Main Event	09/03/2010 16:35:41	7.1
2010 Canterbury	Aftershock	02/21/2011 23:51:42	6.2
2010 Canterbury	Aftershock	02/22/2011 01:50:29	5.6
2010 Canterbury	Aftershock	06/13/2011 02:20:49	6
2010 Canterbury	Aftershock	12/23/2011 00:58:38	5.8
2010 Canterbury	Aftershock	12/23/2011 02:18:03	5.9
2016 Kumamoto	Foreshock	04/14/2016 21:26:00	6.5
2016 Kumamoto	Foreshock	04/14/2016 22:07:00	5.8
2016 Kumamoto	Foreshock	04/15/2016 00:03:00	6.4
2016 Kumamoto	Main Event	04/16/2016 01:25:00	7.3
2016 Kumamoto	Aftershock	04/16/2016 01:46:00	5.9
2016 Kumamoto	Aftershock	04/16/2016 03:03:00	5.9
2016 Kumamoto	Aftershock	04/16/2016 03:55:00	5.8
2016 Kumamoto	Aftershock	04/18/2016 20:42:00	5.8
2016 Kumamoto	Aftershock	04/19/2016 17:52:00	5.5
2016 Kumamoto	Aftershock	08/31/2016 19:46:00	5.2
2016 Kumamoto	Aftershock	03/02/2017 23:53:00	5.3
2016 Kumamoto	Aftershock	06/20/2017 23:27:00	5
2016 Kaikoura	Main Event	11/13/2016 11:02:56	7.8
2016 Kaikoura	Aftershock	11/14/2016 00:34:22	6
2016 Kaikoura	Aftershock	01/05/2017 11:17:34	5.4
2016 Kaikoura	Aftershock	02/01/2017 10:21:29	5.1
2016 Kaikoura	Aftershock	03/01/2017 19:01:02	5.2

For each earthquake, some distances of stations were considered as well to increase the data set for the assessment. The stations considered and the intensity measure (spectral acceleration) of each is presented in Table 6-2, Figure 6.4 and Figure 6.3.

Table 6-2. Strong motion stations for aftershock assessments

Earthquake Series	Station	Distance (km)	PGA (g)	SA(4.0s) (g)	Code	Source of Record
2010 Canterbury	OXZ	25	0.16	0.03	1a	GeoNet
2010 Canterbury	LINC	27	0.77	0.19	1b	GeoNet
2010 Canterbury	RKAC	28	0.21	0.03	1c	GeoNet
2010 Canterbury	ASHS	44	0.21	0.03	2a	GeoNet
2010 Canterbury	LPCC	46	0.37	0.05	3a	GeoNet
2010 Canterbury	CSHS	49	0.12	0.03	3b	GeoNet
2010 Canterbury	ADCS	54	0.11	0.03	2b	GeoNet
2010 Canterbury	MAYC	69	0.08	0.02	4a	GeoNet
2010 Canterbury	WAKC	76	0.16	0.03	4b	GeoNet
2010 Canterbury	CECS	120	0.04	0.02	5a	GeoNet
2010 Canterbury	TRCS	122	0.08	0.05	5b	GeoNet
2010 Canterbury	WTMC	124	0.04	0.02	6a	GeoNet
2010 Canterbury	FDCS	125	0.12	0.02	6b	GeoNet
2010 Canterbury	KIKS	174	0.01	0.01	7a	GeoNet
2010 Canterbury	LBZ	186	0.01	0.00	7b	GeoNet
2010 Canterbury	NNZ	275	0.00	0.00	8a	GeoNet
2010 Canterbury	DKHS	295	0.04	0.00	8b	GeoNet
2010 Canterbury	EAZ	296	0.01	0.00	9a	GeoNet
2010 Canterbury	WEL	328	0.01	0.00	9b	GeoNet
2016 Kumamoto	KMM006	5.04	0.39	0.16	10a	NIED - Japan[(1)]
2016 Kumamoto	KMMH14	12.81	0.22	0.06	10b	NIED - Japan[(1)]
2016 Kumamoto	KMM009	22.31	0.56	0.04	11a	NIED - Japan[(1)]
2016 Kumamoto	KMM003	28.48	0.08	0.02	11b	NIED - Japan[(1)]
2016 Kumamoto	KMM010	29.69	0.07	0.01	12a	NIED - Japan[(1)]
2016 Kumamoto	KMM002	30.72	0.16	0.03	13a	NIED - Japan[(1)]

[(1)] K-Net and KiK-net data, National Research Institute for Earth Science and Disaster Resilience (2017)

Table 6-2. Strong motion stations for aftershock assessment (cont.)

Earthquake Series	Station	Distance (km)	PGA (g)	SA(4.0s) (g)	Code	Source of Record
2016 Kumamoto	KMMH09	31.94	0.14	0.01	13b	NIED - Japan(1)
2016 Kumamoto	KMMH06	32.59	0.09	0.06	12b	NIED - Japan(1)
2016 Kumamoto	KMMH02	50.11	0.15	0.07	14a	NIED - Japan(1)
2016 Kumamoto	KMMH11	53.71	0.03	0.01	14b	NIED - Japan(1)
2016 Kumamoto	FKO013	55.98	0.06	0.01	15a	NIED - Japan(1)
2016 Kumamoto	KMM017	57.09	0.04	0.05	15b	NIED - Japan(1)
2016 Kumamoto	FKOH10	60.17	0.03	0.02	16a	NIED - Japan(1)
2016 Kumamoto	KMMH12	60.64	0.09	0.01	16b	NIED - Japan(1)
2016 Kumamoto	KMM016	61.51	0.04	0.02	17a	NIED - Japan(1)
2016 Kumamoto	FKO012	64.79	0.02	0.04	17b	NIED - Japan(1)
2016 Kumamoto	MYZ007	66.29	0.05	0.01	18a	NIED - Japan(1)
2016 Kumamoto	MYZ004	67.12	0.04	0.02	19a	NIED - Japan(1)
2016 Kumamoto	OIT012	67.15	0.02	0.05	20a	NIED - Japan(1)
2016 Kumamoto	KMMH10	72.70	0.07	0.00	20b	NIED - Japan(1)
2016 Kumamoto	SAGH04	75.97	0.03	0.01	18b	NIED - Japan(1)
2016 Kumamoto	SAGH05	77.66	0.01	0.01	19b	NIED - Japan(1)
2016 Kumamoto	KGS003	78.86	0.05	0.01	21a	NIED - Japan(1)
2016 Kumamoto	FKOH08	79.76	0.04	0.01	21b	NIED - Japan(1)
2016 Kumamoto	MYZH15	88.71	0.08	0.01	22a	NIED - Japan(1)
2016 Kumamoto	KGSH01	89.41	0.02	0.01	23a	NIED - Japan(1)
2016 Kumamoto	OIT006	91.05	0.02	0.01	23b	NIED - Japan(1)
2016 Kumamoto	KGS004	97.63	0.02	0.01	24a	NIED - Japan(1)
2016 Kumamoto	NGSH03	98.02	0.02	0.01	22b	NIED - Japan(1)
2016 Kumamoto	KGS005	98.77	0.03	0.01	25a	NIED - Japan(1)
2016 Kumamoto	FKOH06	100.02	0.02	0.01	25b	NIED - Japan(1)
2016 Kumamoto	OIT002	102.61	0.02	0.01	24b	NIED - Japan(1)
2016 Kumamoto	KGS008	111.30	0.02	0.01	26a	NIED - Japan(1)
2016 Kumamoto	FKO004	112.40	0.04	0.01	26b	NIED - Japan(1)
2016 Kumamoto	KGSH07	116.00	0.02	0.01	27a	NIED - Japan(1)
2016 Kumamoto	FKO003	121.02	0.02	0.01	27b	NIED - Japan(1)
2016 Kaikoura	WTMC	15.41	1.12	0.14	28a	GeoNet
2016 Kaikoura	CECS	17.33	0.29	0.11	28b	GeoNet
2016 Kaikoura	GVZ	23.64	0.15	0.04	28c	GeoNet
2016 Kaikoura	SCAC	23.83	0.31	0.05	2d	GeoNet
2016 Kaikoura	WAKC	37.99	0.15	0.03	29a	GeoNet
2016 Kaikoura	KIKS	61.73	0.26	0.21	29b	GeoNet
2016 Kaikoura	MOLS	75.85	0.36	0.04	30a	GeoNet
2016 Kaikoura	KPOC	76.63	0.08	0.04	30b	GeoNet

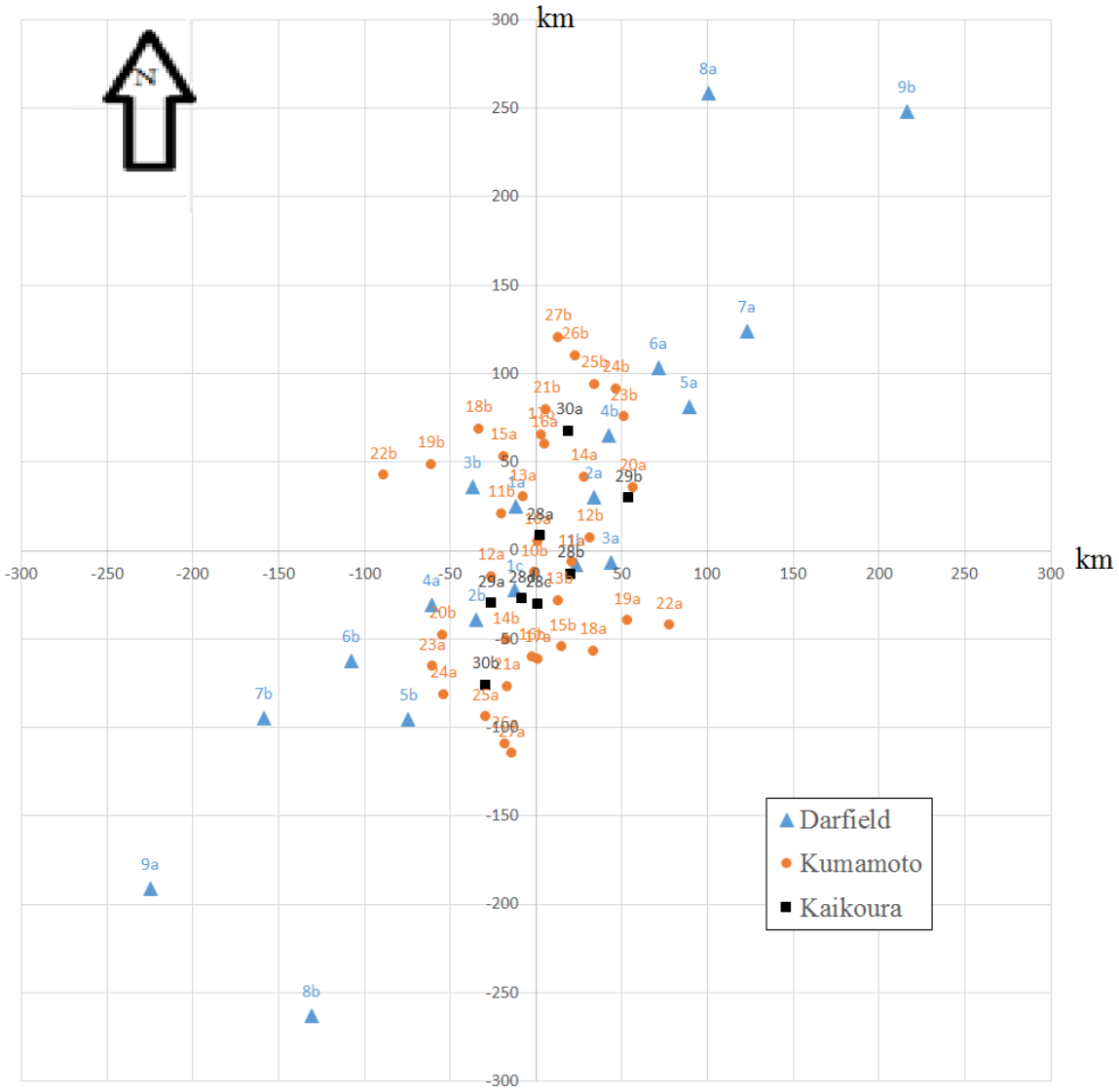

Figure 6.3. Station locations relative to the main shock.

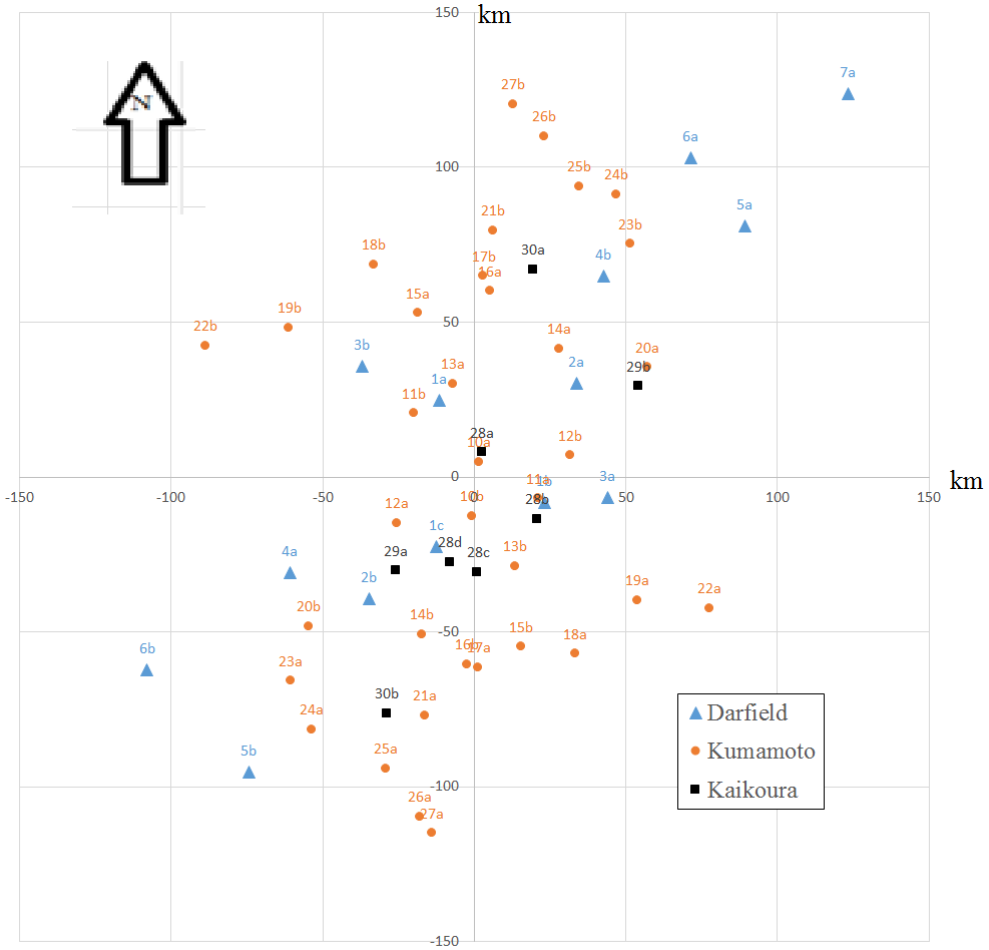

Figure 6.4. Station locations relative to the main shock (<150km distance)

Note: It is possible that a small magnitude event has a significant aftershock event at a specific station that may be more damaging than those considered if the epicentre of the aftershock are very close to the station. This effect, however, is not considered.

6.3. Aftershock Assessment

As aforementioned, for all the recordings for all the possible building sites, a PEER-PBEE process is done. Both structural analyses, which is the multi-stripe non-linear response history analyses and damage and loss analyses, which is done via PACT (FEMA P-58.3). Treating each ground motion as a separate event, due to the assumptions explained earlier, losses for both main shocks and aftershocks can be obtained. Ignoring the time required to repair non-structural elements and assuming only one structural repair at the end of the earthquake series (i.e. taking the largest EDP as an input for damage analysis), the losses can be plotted by its intensity, in this case, the spectral acceleration for 4.0s, which was obtained by the maximum horizontal acceleration. This is done to be in-line with the New Zealand code which uses the maximum horizontal component (Bradley & Baker 2015); McVerry et al. (2006), presented in Figure 6.5

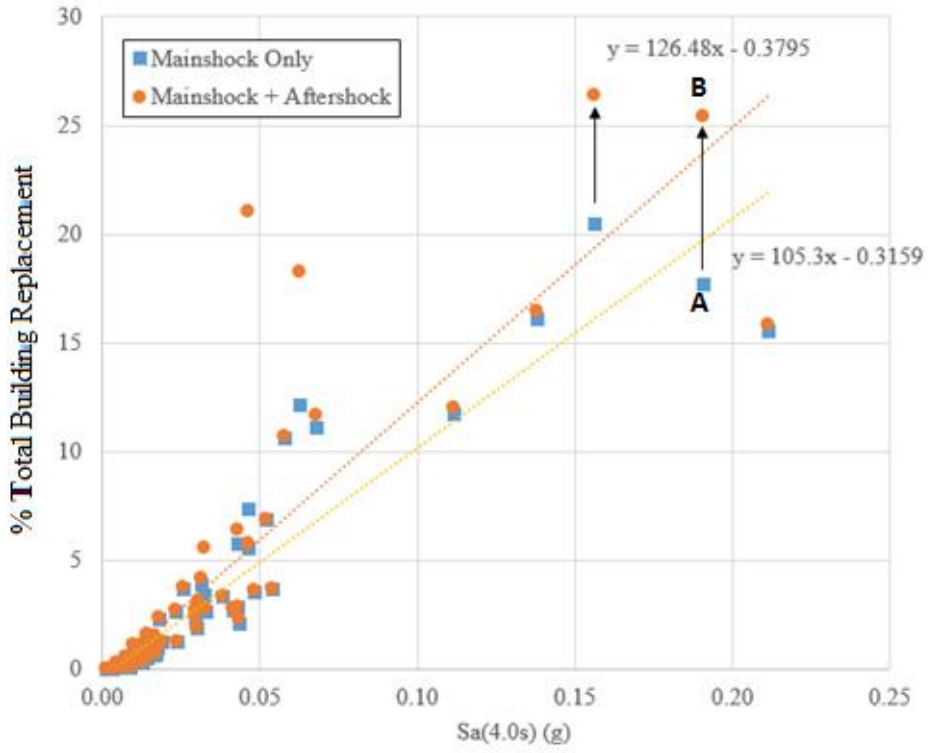

Figure 6.5. Main event and total loss for each station for all aftershocks

For example, in the main shock, site A suffered a loss of 17% total building replacement. If the aftershocks were considered, the loss of site A would increase (to B) to a total of 25% total building replacement value. As such, note that some events do not have significant aftershocks so the total losses (shown as orange dots) may be the same as the main event only loss (shown as blue squares).

The results show a trend in increase of losses due to aftershocks with increasing intensity. Trend lines for each case (Main shock only and main shock + aftershock) are derived by applying method of least squares and assuming an axes intersect at a spectral acceleration of 0.003g (as from the results, more often than not the losses are not present in intensities lower than 0.003g). However it is still important to note that even in lower intensities, damage is still present both due to main shock events and aftershocks, as presented in Figure 6.6.

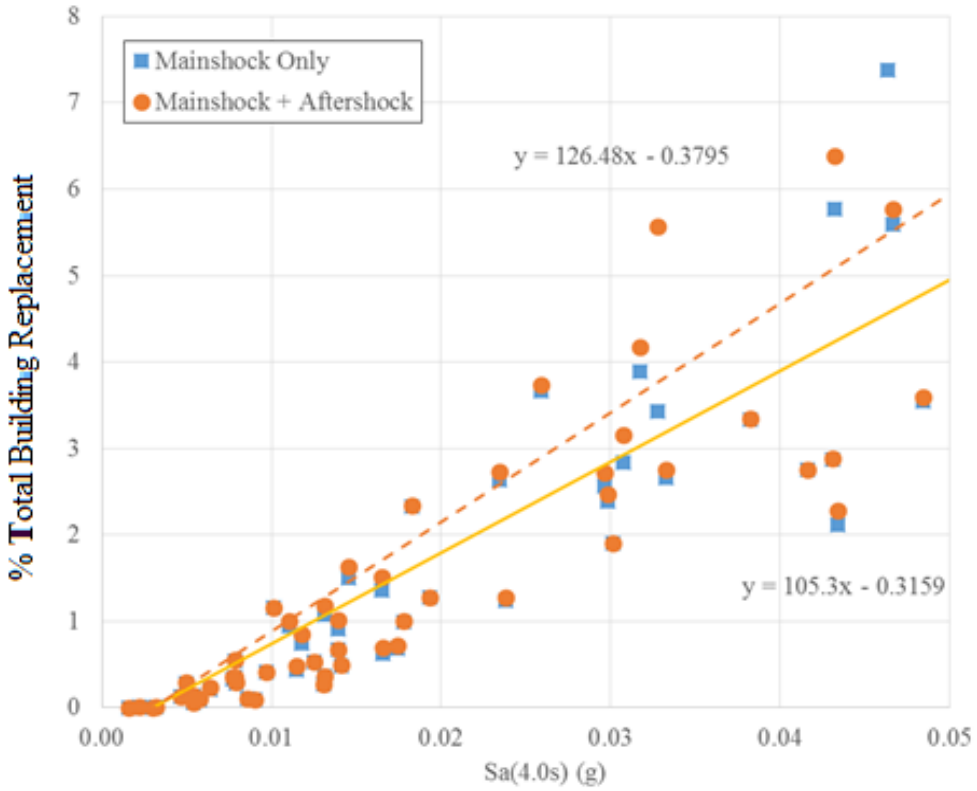

Figure 6.6. Main event and total loss for each station for all aftershocks for intensity Sa (4.0s) smaller than 0.05g

Another way of presenting the data is by using the maximum drift for each case's main event, seen in Figure 6.7, as by grouping it in drifts, the damage states may be easier to define. Hence, owing to the elements' damage states, the following groups were chosen. Little to no damage of non-structural element, (<0.1%), minimum damage of non-structural elements (0.1%-0.3%), moderate damage of non-structural elements (0.3%-0.5%), severe damage of non-structural elements (0.5%-1%), minimum damage of structural elements (1%-2%), moderate – severe damage of structural elements (>2%). As such, it is still evident that the aftershock losses increase with increased drift. This shows that in larger intensities (larger demands), the loss increase due to aftershocks is more significant. Note that the plot is of the 16th percentile, median and 84th percentile. However, due to lack of data, especially for larger intensities, the uncertainty increases.

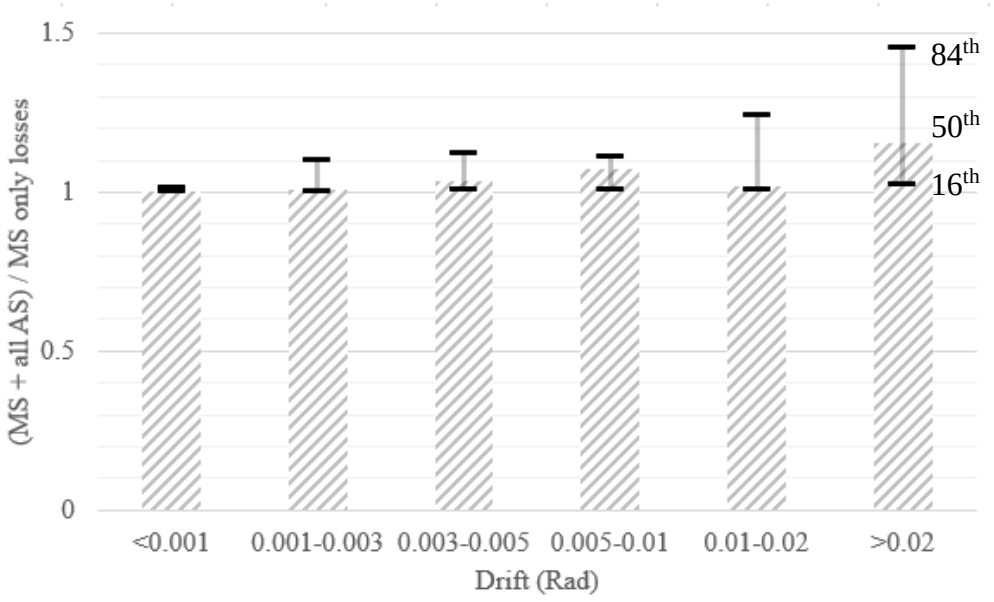

Figure 6.7. Ratio of losses between all aftershock + main shock and main shock only based on maximum drift recorded for the main event

Note that in Figure 6.7, for a few drift ranges (i.e. 0.001-0.003 and 0.01-0.02) the data available was not enough to provide a proper 16th and 84th percentile. Most of the data available tends towards the bottom while the others were near the top.

This increasing trend in loss ratio due to aftershocks is supported by the notion that larger magnitude earthquakes are more likely to result in higher magnitude aftershocks, i.e. the pyramid of magnitude. In addition, an aftershock is more likely to occur within a certain distance from the main shocks (i.e. not totally random distance-wise), as presented in Figure 6.9, Figure 6.10 and Figure 6.11. As such, larger magnitude main shocks are more likely to result in higher intensities of aftershocks, presented in Figure 6.8. Note that due to lack of data of earthquakes. The uncertainty (or spread) of this Main shock magnitude – aftershock intensity relationship is quite large.

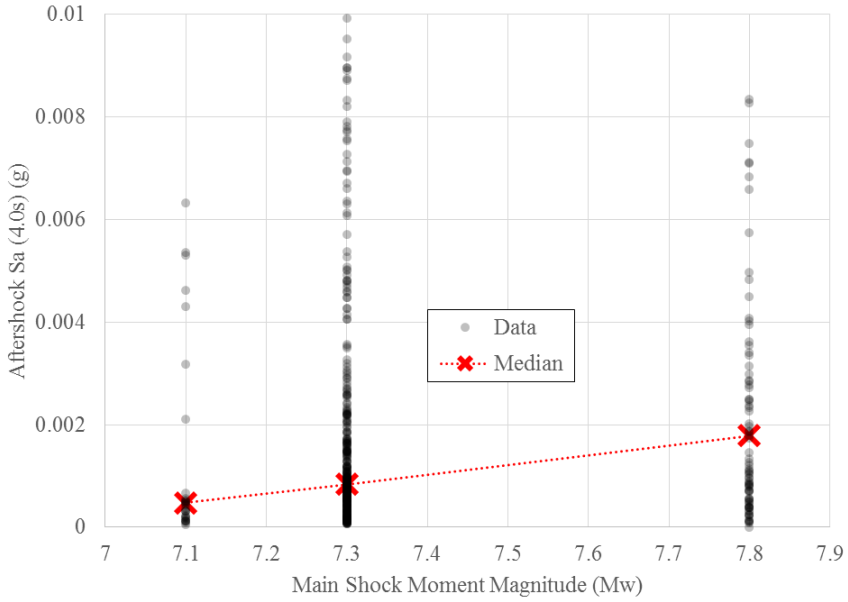

Figure 6.8. Aftershock intensity based on the main shock magnitude

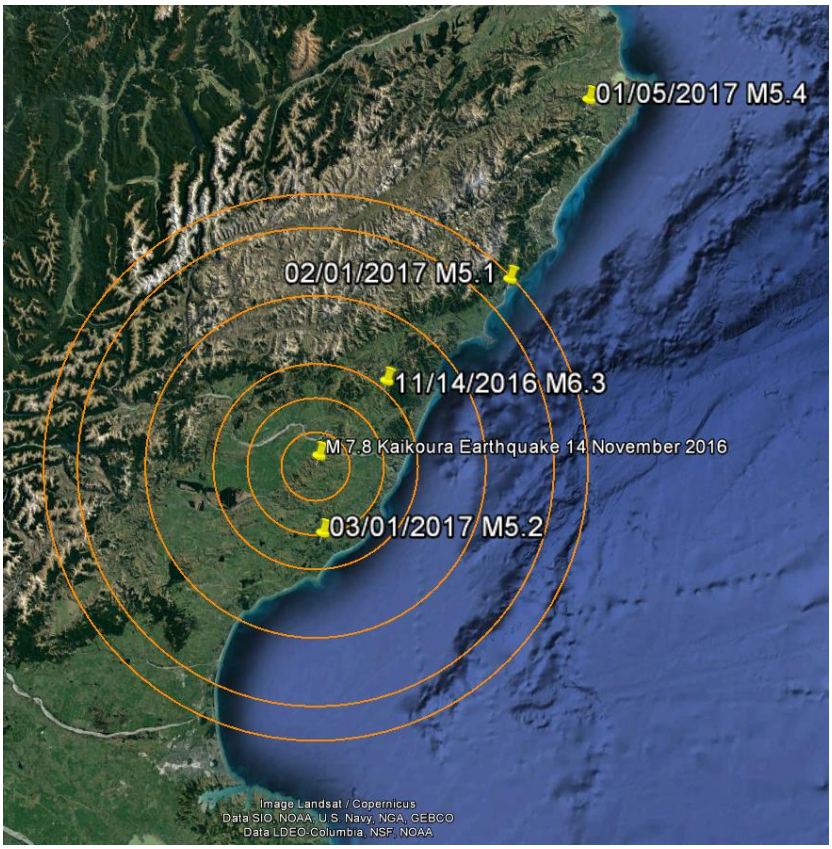

Figure 6.9. Kaikoura 2016 event and aftershocks

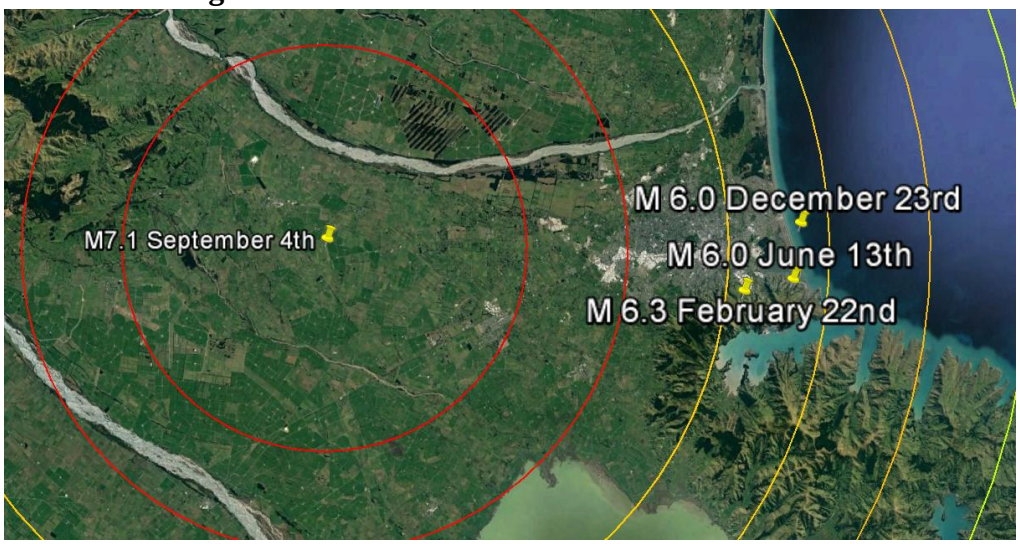

Figure 6.10. Canterbury 2010 event and aftershocks

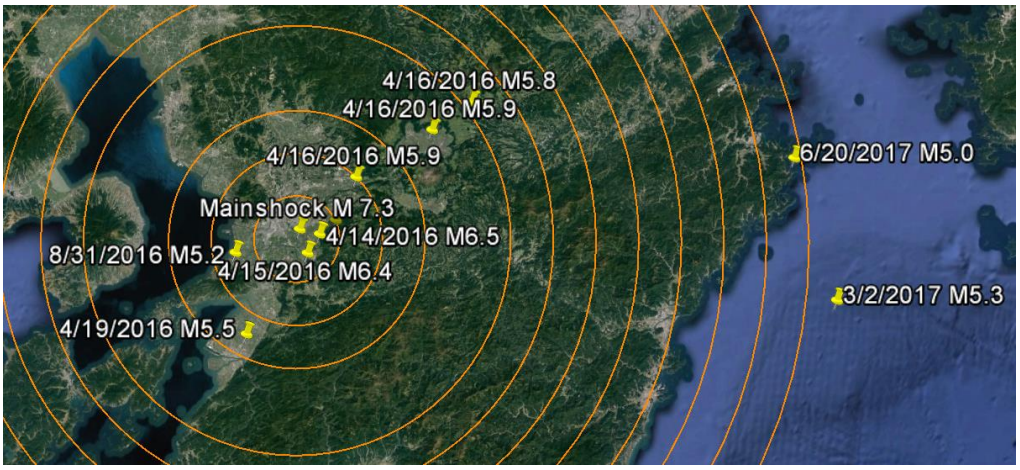

Figure 6.11. Kumamoto 2016 event and aftershocks

Note that, a few aftershocks, such as the 2nd of March Kumamoto event are considerably far from the main shock epicentre. And it may not be an aftershock of the 2016 Kumamoto event as it is an uncertainty. However, it was considered as an aftershock in this research.

6.4. Conclusions

It has been shown and it may be concluded that aftershocks will typically increase losses. This increase in losses tends to increase with increasing intensities. This, however, does not indicate that lower intensities are not a problem as non-structural elements may still be damaged and will need to be repaired in lower intensities. For this particular assessment of aftershocks, the total losses increase up to 10% on average from the losses due to main shocks only.

It was also found that earthquakes with larger magnitudes tend to increase total losses. This is due to the increase in aftershock intensity, which is a relation of magnitude and distance. As the magnitude of the main shock increases, the magnitude of the aftershocks also increase while the distance of the epicenter of an aftershock is more often than not, close to the main shock.

7. Summary and Conclusions

This study evaluated the losses of a particular New Zealand multi-storey steel building, the Pacific Tower, which was damaged in the 2010 Canterbury earthquakes, considered the benefit of different retrofit options and finally discussed the effects of aftershocks on the loss estimations. The findings which answer the four main questions are listed below.

1. Can the loss on a specific New Zealand building for one specific earthquake be modelled?

It was possible to model the loss of a case study building, The Pacific Tower, to a certain extent. Assumptions had to be made as well as the addition of aleatory and epistemic uncertainties. As such, losses for a specific event, the 2010 Canterbury Series, were predicted and by comparing with data from the Christchurch City Council a level of confidence that the model represents the building was achieved. Reported damage states of the elements also support the model in predicting the behaviour of the building as those elements that were reported to have been damaged were predicted to get damaged. Furthermore, the predicted residual drifts were also in-line with the reports from the Christchurch City Council. The model predicted losses for approximately 19% of the building value for the February 2011 event, in which the structural components were repaired following the earthquake. Hence, it is concluded that the losses for a specific New Zealand building for specific earthquake can be predicted with a reasonable level of confidence.

2. What is the most sensitive component of loss?

For the case study building, the drift sensitive elements, particularly the non-structural drywall partitions, were the most sensitive component of loss. The drywall was both the most damaged component, with over 40% predicted

to require replacement, and contributed the most to overall losses, contributing more than 11% of the total replacement costs during the 2010 Canterbury Earthquake Series.

While it is true that for the case study building in this research, note that the most sensitive component of loss was the partitions, each building has its own most sensitive component of loss. This is an uncertainty in the building design and earthquake loading.

3. What is the most cost-efficient retrofit and rehabilitation option?

Two retrofit options were considered in this research; improvement of partitions, by modifying the connections to allow for additional displacement to occur before damage is observed, and re-detailing of cladding connections, by assuming a flexible connection such that the claddings do not increase storey stiffness and are not damaged.

For the case study building, it was concluded that improving the partition connections using the sliding/frictional connections (Araya-Letelier & Miranda 2012) was the most beneficial as the partitions contributed the most towards losses. The cost-benefit analysis, Figure 5.6, showed that after approximately 15 years, improving the partitions should be beneficial. In contrast, altering the structural performance by re-detailing cladding connections was not worthwhile due to the un-even trade-off between "removing" cladding repair costs and the increased drift-related loss due to increased drift and implementation costs.

Notwithstanding the points made above, each building has its own most vulnerable component as explained previously in question 2. For most cases however, retrofitting/rehabilitating the most vulnerable component is expected to be the most cost-efficient solution. There is uncertainty in the cost of such

partition detailing. However, despite this, there appears to be a good motivation for improved partition detailing.

4. How do aftershocks impact the answers to the above?

A methodology to consider aftershocks in loss assessments was developed. It was shown that aftershocks, although hard to predict, tend to increase the losses above those from the main shocks. The magnitude of this increase was found to dependant the on main shock magnitude, with average increases of up to 10% observed. This is due to larger magnitude main shocks being likely followed by larger intensity aftershocks and that aftershocks most likely occur at a range of locations within a radius of the main shock, thus increasing the losses to nearby stations.

It was still possible to predict losses of a specific building while considering aftershocks. The uncertainty, however, is increased due to the nature of aftershock directionality. The most sensitive loss component was found to be the drywall partitions for the case study. As the intensities increase, some tendency for structural components to contribute more was seen. As such, it was concluded that aftershock considerations in loss assessments should not be overlooked, even for lower intensities, as the total loss is still increased and this may make retrofit efforts more worthwhile.

7.1. Limitations and Future Work

Although this research has covered the overall PEER – PBEE framework (Deierlein et al. 2003), with some extensions explained in chapter 4, there are some limitations in this study such as:

- Only one case study building was considered;
- Only three recorded earthquakes were used to evaluate aftershock loss assessments.

As such, as a suggestion for future research on the topic of this research, the following topics are highlighted:

- Implementing more retrofit options for comparison;
- Implementing retrofits as rehabilitation;
- Implementing retrofit/rehabilitation in aftershocks;
- Implementing study for different/broader types of buildings;
- Implementing more records of actual earthquakes and different types of buildings in the aftershock loss assessment.

Appendix A

Displacement Based Assessment of the Pacific Tower (Case Study Building)

Appendix A: Displacement Based Assessment of the Pacific Tower was included to support the statement that the structural model created in Ruaumoko3D (Carr 2017) represents the case study building used for the loss analysis in this research in terms of yield drifts and structural periods. The calculation of the yield drifts was based on Sullivan (2013), assuming a column yield factor (k_{cols}) of 0.2 and a brace yield factor (k_{br}) of 0.3,while the derivation of the fundamental structural period is based on Equation A-1.

$$\boldsymbol{T = 2\pi \sqrt{\frac{m}{k}}} \qquad \textbf{(A-1)}$$

Where,

T = Fundamental structural period (s);

m = First mode mass (kg);

k = Structural stiffness (N/m);

In order to obtain the yield drift of the building in both directions, the yield drift of each floor was calculated at first. Then, using the direct displacement based design (DDBD) (Priestley et al. 2007), the first floor's shear (i.e. base shear) was distributed throughout the height of the structure. This distributed shear (Vi_d) is then normalized to ensure that the floor shear does not exceed the floor's yielding shear force (both flexural and shear of the EBF links). The normalized shear (Vi) can be used to calculate the earthquake horizontal force acting on each floor (Fi). Using the scale factor of the normalized shear, the drift of each floor during first yield of the building for each floor can be calculated. Since an assumption of a single degree of freedom (SDOF) was used, the drifts of each floor was averaged and used as the SDOF yield drift.

Note that in the process of calculating the yield drifts of each floor, due to the fact that the EBFs in the Pacific Tower were not symmetrical, as presented

in Figure A.1, the bays were calculated as if they were separate EBF frames that are mirrored each with its own yield drift.

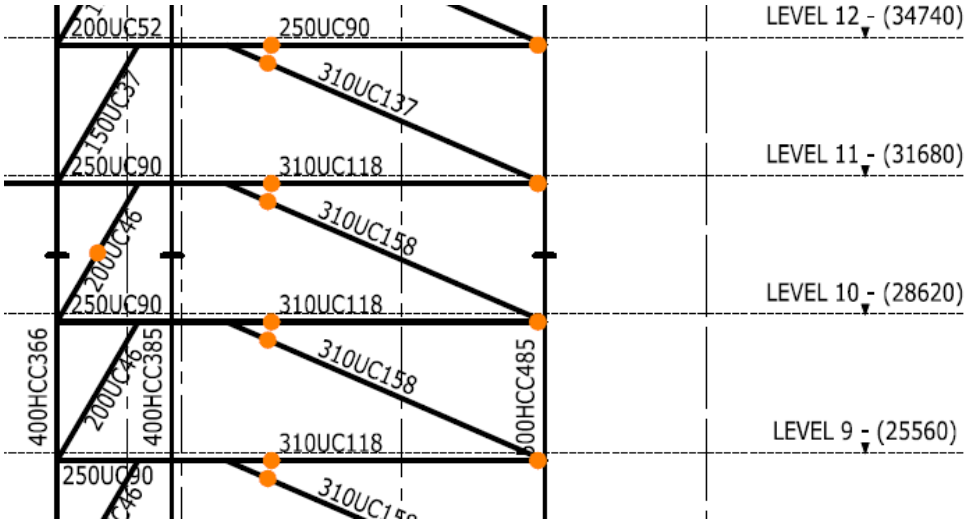

Figure A.1. EBF Frame Grid C, Floor 9

Example of floor yield drift calculation, Z-direction Grid C floor 9.

Left Bay:

EBF Classification: Intermediate with EBF factor e/(Mp/Vp) = 1.66

$$\delta_{v,i_{short}} = 0.577 F_y A_v \left(\frac{e^2(L_b - e)}{24EI} + \frac{e}{2GA_v}\right)$$

$$= 0.577 \times 330000 \times 0.00273 \left(\frac{(0.75 \times 2)^2(2 \times 2.54 - 2 \times 0.75)}{24 \times 205000000 \times 0.000143} + \frac{2 \times 0.75}{2 \times 81000000 \times 0.00273}\right)$$

$$= 0.0077$$

$$\delta_{v,i_{long}} = Mp \left(\frac{e(L_b - e)}{12EI} + \frac{1}{GA_v}\right)$$

$$= 405.9 \left(\frac{(0.75 \times 2)(2 \times 2.54 - 2 \times 0.75)}{12 \times 205000000 \times 0.000143} + \frac{1}{81000000 \times 0.00273}\right)$$

$$= 0.0077$$

$$\delta_{v,i} = 0.0078\ (by\ interpolation)$$

$$\theta_{y,i} = \theta_{link,i} + \theta_{br,i} + \theta_{cols,i}$$

$$\theta_{y,i} = \frac{2\delta_{v,i}}{L_b - e_i} + \frac{2k_{br,i}\varepsilon_y}{\sin(2\alpha_{br,i})} + \frac{2k_{cols,i-1}\varepsilon_y(h_i - h_s)}{L_b}$$

$$= \frac{2 \times 0.0078}{(2 \times 2.54) - (0.75 \times 2)} + \frac{0.6 \times 0.00165}{\sin(2 \times 59.68°)} + \frac{0.4 \times 0.00165 \times (40.86 - 3.06)}{2 \times 2.54}$$

$$= 0.0043 + 0.00111 + 0.00324$$

$$= 0.87\%$$

Right Bay:

EBF Classification: Intermediate with EBF factor e/(Mp/Vp) = 2.296

$$\delta_{v,i_{short}} = 0.577F_yA_v\left(\frac{e^2(L_b - e)}{24EI} + \frac{e}{2GA_v}\right)$$

$$= 0.577 \times 330000 \times 0.0075\left(\frac{(1.2 \times 2)^2(2 \times 8.24 - 2 \times 1.2)}{24 \times 205000000 \times 0.000277} + \frac{2 \times 1.2}{2 \times 81000000 \times 0.0075}\right)$$

$$= 0.0045$$

$$\delta_{v,i_{long}} = Mp\left(\frac{e(L_b - e)}{12EI} + \frac{1}{GA_v}\right)$$

$$= 646.8\left(\frac{(1.2 \times 2)(2 \times 8.24 - 2 \times 1.2)}{12 \times 205000000 \times 0.000277} + \frac{1}{81000000 \times 0.0075}\right)$$

$$= 0.0034$$

$$\delta_{v,i} = 0.00398\ (by\ interpolation)$$

$$\theta_{y,i} = \theta_{link,i} + \theta_{br,i} + \theta_{cols,i}$$

$$\theta_{y,i} = \frac{2\delta_{v,i}}{L_b - e_i} + \frac{2k_{br,i}\varepsilon_y}{\sin(2\alpha_{br,i})} + \frac{2k_{cols,i-1}\varepsilon_y(h_i - h_s)}{L_b}$$

$$= \frac{2 \times 0.00398}{(2 \times 8.24) - (1.2 \times 2)} + \frac{0.6 \times 0.00165}{\sin(2 \times 23.49°)} + \frac{0.4 \times 0.00165 \times (40.86 - 3.06)}{2 \times 8.24}$$

$$= 0.0057 + 0.0013 + 0.001$$

$$= 0.8\%$$

Example of calculating floor yield force and displacement, example: Grid C Floor 9 Left Bay

Yield force,

$$V_i = \frac{V_{link,i} \times Lb}{hs}$$

Hence,

$$V_{y,i} = \frac{V_{linky,i} \times Lb}{hs}$$

$$V_{y,9CL} = \frac{900.9 \times 2.54}{3.06} = 747.81\ kN$$

Yield displacement,

$$\Delta_{i,ls} = \theta_c h_i$$

$$\Delta_{9CL,ls} = 0.0053 \times 28.62 = 0.152m$$

$$\Delta_i = \omega_\theta \Delta_{i,ls}$$

$$\Delta_{9CL} = 0.6\ 0.152 = 0.091m$$

Using DDBD to distribute base shear, example: Grid C Left Bay,

Table A-1. DDBD of Grid C Left Bay for shear distribution

Level	Height (m)	Δ_i (m)	m_i (T)	$m_i\Delta_i$	$(m_i\Delta_i)^2$	$m_i\Delta_i h_i$	F_i (Vb)	V_i (Vb)
1	3.6	0.011	136.61	1.57	0.02	5.64	0.01	1.00
2	7.2	0.023	63.04	1.45	0.03	10.41	0.01	0.99
3	10.26	0.033	65.51	2.14	0.07	21.97	0.01	0.99
4	13.32	0.042	59.35	2.52	0.11	33.54	0.01	0.98
5	16.38	0.052	123.96	6.47	0.34	105.93	0.02	0.97
6	19.44	0.062	114.91	7.11	0.44	138.31	0.03	0.95
7	22.5	0.072	114.91	8.23	0.59	185.28	0.03	0.92
8	25.56	0.081	113.15	9.21	0.75	235.44	0.03	0.89
9	28.62	0.091	113.15	10.31	0.94	295.18	0.04	0.86
10	31.68	0.101	112.15	11.32	1.14	358.50	0.04	0.83
11	34.74	0.111	88.66	9.81	1.09	340.78	0.04	0.78
12	37.8	0.120	88.66	10.67	1.28	403.46	0.04	0.75
13	40.86	0.130	88.66	11.54	1.50	471.42	0.04	0.71
14	43.92	0.140	88.66	12.40	1.73	544.68	0.04	0.67
15	46.98	0.150	83.82	12.54	1.88	589.24	0.04	0.63
16	50.04	0.159	83.82	13.36	2.13	668.50	0.05	0.58
17	53.1	0.169	83.82	14.18	2.40	752.76	0.05	0.53
18	56.16	0.179	83.82	14.99	2.68	842.01	0.05	0.48
19	59.22	0.189	83.82	15.81	2.98	936.27	0.06	0.43
20	62.28	0.198	72.61	14.40	2.86	897.01	0.05	0.37
21	65.34	0.208	145.22	30.22	6.29	1974.64	0.11	0.32
22	68.4	0.218	146.67	31.95	6.96	2185.48	0.21	0.21
		Σ	2154.99	252.25	38.21	11996.44	1	

$$He = \frac{\sum m_i \Delta_i h_i}{\sum m_i \Delta_i} = \frac{11996.44}{252.21} = 47.6\ m$$

$$\Delta_y = \frac{\sum (m_i \Delta_i)^2}{\sum m_i \Delta_i} = \frac{38.21}{252.21} = 0.152\ m$$

$$M_e = \frac{\sum m_i \Delta_i}{\Delta_y} = \frac{252.21}{0.152} = 1665\ kg$$

Assuming first floor shear yield force as base shear,

$$V_b = V_{y,1CL} = 2435.44kN$$

Using this base shear, the floor shears can be obtained as,

Table A-2. Floor shear distribution and normalization

Level	Height (m)	V_iYield (kN)	V_iFloor (kN)		V_iScaled (kN)
1	3.6	2435.44	2435.44	1.00	575.97
2	7.2	2435.44	2421.82	0.99	572.75
3	10.26	1405.22	2409.26	1.71	569.78
4	13.32	1405.22	2390.65	1.70	565.38
5	16.38	1405.22	2368.77	1.69	560.20
6	19.44	1405.22	2312.57	1.65	546.91
7	22.5	1405.22	2250.73	1.60	532.28
8	25.56	747.81	2179.17	2.91	515.36
9	28.62	747.81	2099.11	2.81	496.43
10	31.68	747.81	2009.48	2.69	475.23
11	34.74	451.97	1911.13	4.23	451.97
12	37.8	451.97	1825.88	4.04	431.81
13	40.86	451.97	1733.12	3.83	409.87
14	43.92	451.97	1632.84	3.61	386.16
15	46.98	451.97	1525.06	3.37	360.67
16	50.04	405.40	1416.06	3.49	334.89
17	53.1	405.40	1299.96	3.21	307.43
18	56.16	405.40	1176.75	2.90	278.30
19	59.22	405.40	1046.45	2.58	247.48
20	62.28	405.40	909.05	2.24	214.98
21	65.34	405.40	783.88	1.93	185.38
22	68.4	405.40	521.23	1.29	123.27

This shear distribution, however, still needs to be checked for moment yield. Hence,

$$M_{link,y} = V_{link,y} \times e$$

Where,

$$V_{link,y} = \frac{V_{y,i} \times h_s}{L_b} = \frac{504.71 \times 3.06}{2.54} = 635.1kN$$

$$M_{link,y} = 635.1 \times 0.75 = 456.03\ kNm$$

$$M_{link,y}(456.03kNm) > M_{section,y}(405.9\ kNm)$$

The calculation shows that the yield moment of the section was exceeded. As such, the floor shear is scaled again to ensure that the moment does not exceed the allowed moment. This process is done for all link members and the resulting floor shear is listed in Table A-3.

Table A-3. Final floor shear for Grid C Left Bay

Level	Height (m)	V_iScale (kN)	F_i(kN)	F_i H_i(kN)
1	3.6	265.29	1.48	5.34
2	7.2	263.81	1.37	9.85
3	10.26	262.44	2.03	20.79
4	13.32	260.42	2.38	31.75
5	16.38	258.03	6.12	100.28
6	19.44	251.91	6.74	130.94
7	22.5	245.17	7.80	175.41
8	25.56	237.38	8.72	222.89
9	28.62	228.66	9.76	279.45
10	31.68	218.89	10.71	339.39
11	34.74	208.18	9.29	322.62
12	37.8	198.89	10.10	381.95
13	40.86	188.79	10.92	446.30
14	43.92	177.87	11.74	515.64
15	46.98	166.13	11.87	557.83
16	50.04	154.25	12.65	632.87
17	53.1	141.61	13.42	712.63
18	56.16	128.18	14.19	797.13
19	59.22	113.99	14.97	886.37
20	62.28	99.02	13.64	849.20
21	65.34	85.39	28.61	1869.39
22	68.4	56.78	56.78	3883.60
		Σ	265.29	13171.63

Using the scaled floor shear, assuming a linear elastic behaviour, the drift of each floor when the first yield occurs can be calculated. Owing to the assumption of first mode shape, the yield drift of the building can be approximated as the average of all the floors.

Table A-4. Floor yield drift

Level	Height (m)	V_iYield (kN)	V_iScale (kN)	Scale Factor	θ_y	θ_y Scaled
1	3.6	2435.44	265.29	0.11	0.0055	0.0006
2	7.2	2435.44	263.81	0.11	0.0059	0.0006
3	10.26	1405.22	262.44	0.19	0.0053	0.0010
4	13.32	1405.22	260.42	0.19	0.0057	0.0011
5	16.38	1405.22	258.03	0.18	0.0061	0.0011
6	19.44	1405.22	251.91	0.18	0.0065	0.0012
7	22.5	1405.22	245.17	0.17	0.0069	0.0012
8	25.56	747.81	237.38	0.32	0.0083	0.0026
9	28.62	747.81	228.66	0.31	0.0087	0.0026
10	31.68	747.81	218.89	0.29	0.0091	0.0027
11	34.74	451.97	208.18	0.46	0.0110	0.0051
12	37.8	451.97	198.89	0.44	0.0114	0.0050
13	40.86	451.97	188.79	0.42	0.0118	0.0049
14	43.92	451.97	177.87	0.39	0.0122	0.0048
15	46.98	451.97	166.13	0.37	0.0126	0.0046
16	50.04	405.40	154.25	0.38	0.0130	0.0050
17	53.1	405.40	141.61	0.35	0.0134	0.0047
18	56.16	405.40	128.18	0.32	0.0138	0.0044
19	59.22	405.40	113.99	0.28	0.0142	0.0040
20	62.28	405.40	99.02	0.24	0.0146	0.0036
21	65.34	405.40	85.39	0.21	0.0150	0.0032
22	68.4	405.40	56.78	0.14	0.0153	0.0021
					Average	0.00147

Note that this average is the average from both the left and right side of Grids C and D, which is the average of the entire Z-direction yield drifts. This is done assuming a rigid movement of all floors in each direction. The same applies for the X direction.

The final step is calculating the stiffness in each direction. This is done by assuming each EBF full-height frame in one direction as a spring that is parallel to each other. A parallel assumption is taken due to the fact that the top floor of each EBF full-height frame must move the same amount in one direction. As such, the stiffness can be calculated as,

Example, Grid C stiffness,

$$K_e = \frac{M_o}{\theta_y h_{eff}^2}$$

$$K_e = \frac{13171.63\ kNm}{0.00148\ (47.2m)^{\,2}} = 4007618.82\ N/m$$

Calculating fundamental periods,

$$K_{C,L} = 4007618.82\ N/m \qquad K_{C,R} = 4806564.18\ N/m$$

$$K_{D,L} = 1436765.83\ N/m \qquad K_{D,R} = 4002101.46\ N/m$$

$$K_{e,Z} = K_{C,L} + K_{C,R} + K_{R,L} + K_{D,R} = 14253050\ N/m$$

$$K_2 = 11732413.8\ N/m$$

$$K_6 = 13765839.18\ N/m$$

$$K_{e,X} = K_2 + K_6 = 25498253\ N/m$$

Returning to equation A-1,

$$T = 2\pi\sqrt{\frac{m}{k}}$$

$$T_Z = 2\pi\sqrt{\frac{8036200\ kg}{14253050\ N/m}} = 4.72\ s\ (Model\ Period: 4.64s, 1.68\%)$$

$$T_X = 2\pi\sqrt{\frac{8036200\ kg}{25498253\ N/m}} = 3.53\ s\ (Model\ Period: 3.556, 0.81\%$$

.

Appendix B

SAP2000 Angle Modelling Results

Appendix B: SAP2000 angle modelling results is included to show the complete steps of the displacement controlled loading. In order to obtain the yield of the cladding connection, which was detailed as using an angle to support the top part of the panel, a SAP2000 (Wilson & Habibullah 2002) model of the angle was created. The details of the model are explained in section 4.3.2 and the complete results of the SAP model is listed in Table B-1 to Table B-6.

Table B-1. SAP2000 joint displacement results for angle model

Joint	Output Case	Case Type	Step Type	Step Num	U1	U2	U3	R1	R2	R3
					m	m	m	rad	rad	rad
9	DEAD	NonStatic	Step	0	0.00	0.00	0.00	0.00	0.00	0.00
9	DEAD	NonStatic	Step	1	0.00	0.00	0.00	0.00	0.00	0.00
9	DEAD	NonStatic	Step	2	0.00	0.00	0.00	0.00	0.00	0.00
9	DEAD	NonStatic	Step	3	0.00	0.00	0.00	0.00	0.00	0.00
9	DEAD	NonStatic	Step	4	0.00	0.00	0.00	0.00	0.00	0.00
9	DEAD	NonStatic	Step	5	0.00	0.00	0.00	0.00	0.00	0.00
9	DEAD	NonStatic	Step	6	0.00	0.00	0.00	0.00	0.00	0.00
9	DEAD	NonStatic	Step	7	0.00	0.00	0.00	0.00	0.00	0.00
9	DEAD	NonStatic	Step	8	0.00	0.00	0.00	0.00	0.00	0.00
9	DEAD	NonStatic	Step	9	0.00	0.01	0.00	0.00	0.00	0.00
9	DEAD	NonStatic	Step	10	0.00	0.01	0.00	0.00	0.00	0.00
9	DEAD	NonStatic	Step	11	0.00	0.01	0.00	0.00	0.00	0.00
9	DEAD	NonStatic	Step	12	0.00	0.01	0.00	0.00	0.00	0.00
9	DEAD	NonStatic	Step	13	0.00	0.01	0.00	0.00	0.00	0.00
9	DEAD	NonStatic	Step	14	0.00	0.01	0.00	0.00	0.00	0.00
9	DEAD	NonStatic	Step	15	0.00	0.01	0.00	0.00	0.00	0.00
9	DEAD	NonStatic	Step	16	0.00	0.01	0.00	0.00	0.00	0.00
9	DEAD	NonStatic	Step	17	0.00	0.01	0.00	0.00	0.00	0.00
9	DEAD	NonStatic	Step	18	0.00	0.01	0.00	0.00	0.00	0.00
9	DEAD	NonStatic	Step	19	0.00	0.01	0.00	0.00	0.00	0.00
9	DEAD	NonStatic	Step	20	0.00	0.01	0.00	0.00	0.00	0.00
9	DEAD	NonStatic	Step	21	0.00	0.01	0.00	0.00	0.00	0.00
9	DEAD	NonStatic	Step	22	0.00	0.24	0.00	0.00	0.00	0.00
9	DEAD	NonStatic	Step	23	0.00	0.43	0.00	0.00	0.00	-0.01
9	DEAD	NonStatic	Step	24	0.00	0.46	0.00	0.00	0.00	-0.01
9	DEAD	NonStatic	Step	25	0.00	0.49	0.00	0.00	0.00	-0.01
9	DEAD	NonStatic	Step	26	0.00	0.49	0.00	0.00	0.00	-0.01

Table B-2. SAP2000 joint displacement results for angle model (cont.)

Joint	Output Case	Case Type	Step Type	Step Num	U1	U2	U3	R1	R2	R3
					m	m	m	rad	rad	rad
10	DEAD	NonStatic	Step	0	0.00	0.00	0.00	0.00	0.00	0.00
10	DEAD	NonStatic	Step	1	0.00	0.00	0.00	-0.01	0.00	0.00
10	DEAD	NonStatic	Step	2	0.00	0.00	0.00	-0.01	0.00	0.00
10	DEAD	NonStatic	Step	3	0.00	0.00	0.00	-0.02	0.00	0.00
10	DEAD	NonStatic	Step	4	0.00	0.00	0.00	-0.03	0.00	0.00
10	DEAD	NonStatic	Step	5	0.00	0.00	0.00	-0.03	0.00	0.00
10	DEAD	NonStatic	Step	6	0.00	0.00	0.00	-0.04	0.00	0.00
10	DEAD	NonStatic	Step	7	0.00	0.00	0.00	-0.04	0.00	0.00
10	DEAD	NonStatic	Step	8	0.00	0.01	0.00	-0.05	0.00	0.00
10	DEAD	NonStatic	Step	9	0.00	0.01	0.00	-0.06	0.00	0.00
10	DEAD	NonStatic	Step	10	0.00	0.01	0.00	-0.06	0.00	0.00
10	DEAD	NonStatic	Step	11	0.00	0.01	0.00	-0.07	0.00	0.00
10	DEAD	NonStatic	Step	12	0.00	0.01	0.00	-0.08	0.00	0.00
10	DEAD	NonStatic	Step	13	0.00	0.01	0.00	-0.08	0.00	0.00
10	DEAD	NonStatic	Step	14	0.00	0.01	0.00	-0.09	0.00	0.00
10	DEAD	NonStatic	Step	15	0.00	0.01	0.00	-0.09	0.00	0.00
10	DEAD	NonStatic	Step	16	0.00	0.01	0.00	-0.10	0.00	0.00
10	DEAD	NonStatic	Step	17	0.00	0.01	0.00	-0.11	0.00	0.00
10	DEAD	NonStatic	Step	18	0.00	0.01	0.00	-0.11	0.00	0.00
10	DEAD	NonStatic	Step	19	0.00	0.01	0.00	-0.12	0.00	0.00
10	DEAD	NonStatic	Step	20	0.00	0.01	0.00	-0.13	0.00	0.00
10	DEAD	NonStatic	Step	21	0.00	0.01	0.00	-0.13	0.00	0.00
10	DEAD	NonStatic	Step	22	0.00	0.24	0.00	-2.42	0.00	0.00
10	DEAD	NonStatic	Step	23	0.00	0.43	0.00	-4.33	0.00	0.00
10	DEAD	NonStatic	Step	24	0.00	0.46	0.00	-4.61	0.00	0.00
10	DEAD	NonStatic	Step	25	0.00	0.49	0.00	-4.89	0.00	0.00
10	DEAD	NonStatic	Step	26	0.00	0.49	0.00	-4.94	0.00	0.00

Table B-3. SAP2000 joint displacement results for angle model (cont.)

Joint	Output Case	Case Type	Step Type	Step Num	U1	U2	U3	R1	R2	R3
					m	m	m	rad	rad	rad
11	DEAD	NonStatic	Step	0	0.00	0.00	0.00	0.00	0.00	0.00
11	DEAD	NonStatic	Step	1	0.00	0.00	0.00	-0.01	0.00	0.00
11	DEAD	NonStatic	Step	2	0.00	0.00	0.00	-0.01	0.00	0.00
11	DEAD	NonStatic	Step	3	0.00	0.00	0.00	-0.02	0.00	0.00
11	DEAD	NonStatic	Step	4	0.00	0.00	0.00	-0.03	0.00	0.00
11	DEAD	NonStatic	Step	5	0.00	0.00	0.00	-0.03	0.00	0.00
11	DEAD	NonStatic	Step	6	0.00	0.00	0.00	-0.04	0.00	0.00
11	DEAD	NonStatic	Step	7	0.00	0.00	0.00	-0.04	0.00	0.00
11	DEAD	NonStatic	Step	8	0.00	0.00	0.00	-0.05	0.00	0.00
11	DEAD	NonStatic	Step	9	0.00	0.00	0.00	-0.06	0.00	0.00
11	DEAD	NonStatic	Step	10	0.00	0.00	0.00	-0.06	0.00	0.00
11	DEAD	NonStatic	Step	11	0.00	0.00	0.00	-0.07	0.00	0.00
11	DEAD	NonStatic	Step	12	0.00	0.00	0.00	-0.08	0.00	0.00
11	DEAD	NonStatic	Step	13	0.00	0.00	0.00	-0.08	0.00	0.00
11	DEAD	NonStatic	Step	14	0.00	0.00	0.00	-0.09	0.00	0.00
11	DEAD	NonStatic	Step	15	0.00	0.00	0.00	-0.10	0.00	0.00
11	DEAD	NonStatic	Step	16	0.00	0.00	0.00	-0.10	0.00	0.00
11	DEAD	NonStatic	Step	17	0.00	0.00	0.00	-0.11	0.00	0.00
11	DEAD	NonStatic	Step	18	0.00	0.00	0.00	-0.11	0.00	0.00
11	DEAD	NonStatic	Step	19	0.00	0.00	0.00	-0.12	0.00	0.00
11	DEAD	NonStatic	Step	20	0.00	0.00	0.00	-0.13	0.00	0.00
11	DEAD	NonStatic	Step	21	0.00	0.00	0.00	-0.13	0.00	0.00
11	DEAD	NonStatic	Step	22	0.00	0.00	0.00	-2.43	0.00	0.00
11	DEAD	NonStatic	Step	23	0.00	0.00	0.00	-4.33	0.00	0.00
11	DEAD	NonStatic	Step	24	0.00	0.00	0.00	-4.61	0.00	0.00
11	DEAD	NonStatic	Step	25	0.00	0.00	0.00	-4.89	0.00	0.00
11	DEAD	NonStatic	Step	26	0.00	0.00	0.00	-4.94	0.00	0.00

Table B-4. SAP2000 joint force results for angle model

Joint	Output Case	Case Type	Step Type	Step Num	F1	F2	F3	M1	M2	M3
					KN	KN	KN	KN-m	KN-m	KN-m
9	DEAD	NonStatic	Step	0	0	0	0	0	0	0
9	DEAD	NonStatic	Step	1	-0.2	0	-0.1	0.05	0	0
9	DEAD	NonStatic	Step	2	-0.5	0	-0.1	0.09	0.1	0
9	DEAD	NonStatic	Step	3	-0.7	0	-0.2	0.14	0.1	0
9	DEAD	NonStatic	Step	4	-1	0	-0.2	0.19	0.1	0
9	DEAD	NonStatic	Step	5	-1.2	0	-0.3	0.24	0.2	0
9	DEAD	NonStatic	Step	6	-1.5	0	-0.3	0.28	0.2	0
9	DEAD	NonStatic	Step	7	-1.7	0	-0.4	0.33	0.2	0
9	DEAD	NonStatic	Step	8	-2	0	-0.4	0.38	0.3	0
9	DEAD	NonStatic	Step	9	-2.2	0	-0.5	0.42	0.3	0
9	DEAD	NonStatic	Step	10	-2.5	0	-0.5	0.47	0.3	0
9	DEAD	NonStatic	Step	11	-2.7	0	-0.6	0.52	0.4	0
9	DEAD	NonStatic	Step	12	-3	0	-0.6	0.57	0.4	0
9	DEAD	NonStatic	Step	13	-3.2	0	-0.7	0.61	0.4	0
9	DEAD	NonStatic	Step	14	-3.5	0	-0.7	0.66	0.5	0
9	DEAD	NonStatic	Step	15	-3.7	0	-0.8	0.71	0.5	0
9	DEAD	NonStatic	Step	16	-4	0	-0.9	0.76	0.5	0
9	DEAD	NonStatic	Step	17	-4.2	0	-0.9	0.8	0.6	0
9	DEAD	NonStatic	Step	18	-4.5	0	-1	0.85	0.6	0
9	DEAD	NonStatic	Step	19	-4.7	0	-1	0.9	0.6	0
9	DEAD	NonStatic	Step	20	-5	0	-1.1	0.94	0.7	0
9	DEAD	NonStatic	Step	21	-5.2	0	-1.1	0.99	0.7	0
9	DEAD	NonStatic	Step	22	-5.5	0	-1.2	1.04	0.7	0
9	DEAD	NonStatic	Step	23	-5.7	0	-1.2	1.08	0.8	0
9	DEAD	NonStatic	Step	24	-5.7	0	-1.2	1.08	0.8	0
9	DEAD	NonStatic	Step	25	-5.7	0	-1.2	1.09	0.8	0
9	DEAD	NonStatic	Step	26	-5.7	0	-1.2	1.09	0.8	0

Table B-5. SAP2000 joint force results for angle model (cont.)

Joint	Output Case	Case Type	Step Type	Step Num	F1	F2	F3	M1	M2	M3
					KN	KN	KN	KN-m	KN-m	KN-m
10	DEAD	NonStatic	Step	0	0	0	0	0	0	0
10	DEAD	NonStatic	Step	1	0	0	0	0	0	0.14
10	DEAD	NonStatic	Step	2	0	0	0	0	0	0.28
10	DEAD	NonStatic	Step	3	0	0	0	0	0	0.42
10	DEAD	NonStatic	Step	4	0	0	0	0	0	0.57
10	DEAD	NonStatic	Step	5	0	0	0	0	0	0.71
10	DEAD	NonStatic	Step	6	0	0	0	0	0	0.85
10	DEAD	NonStatic	Step	7	0	0	0	0	0	0.99
10	DEAD	NonStatic	Step	8	0	0	0	0	0	1.13
10	DEAD	NonStatic	Step	9	0	0	0	0	0	1.27
10	DEAD	NonStatic	Step	10	0	0	0	0	0	1.42
10	DEAD	NonStatic	Step	11	0	0	0	0	0	1.56
10	DEAD	NonStatic	Step	12	0	0	0	0	0	1.7
10	DEAD	NonStatic	Step	13	0	0	0	0	0	1.84
10	DEAD	NonStatic	Step	14	0	0	0	0	0	1.98
10	DEAD	NonStatic	Step	15	0	0	0	0	0	2.12
10	DEAD	NonStatic	Step	16	0	0	0	0	0	2.27
10	DEAD	NonStatic	Step	17	0	0	0	0	0	2.41
10	DEAD	NonStatic	Step	18	0	0	0	0	0	2.55
10	DEAD	NonStatic	Step	19	0	0	0	0	0	2.69
10	DEAD	NonStatic	Step	20	0	0	0	0	0	2.83
10	DEAD	NonStatic	Step	21	0	0	0	0	0	2.97
10	DEAD	NonStatic	Step	22	0	0	0	0	0	3.12
10	DEAD	NonStatic	Step	23	0	0	0	0	0	3.23
10	DEAD	NonStatic	Step	24	0	0	0	0	0	3.25
10	DEAD	NonStatic	Step	25	0	0	0	0	0	3.27
10	DEAD	NonStatic	Step	26	0	0	0	0	0	3.27

Table B-6. SAP2000 joint force results for angle model (cont.)

Joint	Output Case	Case Type	Step Type	Step Num	F1	F2	F3	M1	M2	M3
					KN	KN	KN	KN-m	KN-m	KN-m
11	DEAD	NonStatic	Step	0	0	0	0	0	0	0
11	DEAD	NonStatic	Step	1	0.2	-0.5	0.1	0	0	0
11	DEAD	NonStatic	Step	2	0.5	-0.9	0.1	0	0	0
11	DEAD	NonStatic	Step	3	0.7	-1.4	0.2	0	0	0
11	DEAD	NonStatic	Step	4	1	-1.9	0.2	0	0	0
11	DEAD	NonStatic	Step	5	1.2	-2.4	0.3	0	0	0
11	DEAD	NonStatic	Step	6	1.5	-2.8	0.3	0	0	0
11	DEAD	NonStatic	Step	7	1.7	-3.3	0.4	0	0.1	0
11	DEAD	NonStatic	Step	8	2	-3.8	0.4	0	0.1	0
11	DEAD	NonStatic	Step	9	2.2	-4.2	0.5	0	0.1	0
11	DEAD	NonStatic	Step	10	2.5	-4.7	0.5	0	0.1	0
11	DEAD	NonStatic	Step	11	2.7	-5.2	0.6	0	0.1	0
11	DEAD	NonStatic	Step	12	3	-5.7	0.6	0	0.1	0
11	DEAD	NonStatic	Step	13	3.2	-6.1	0.7	0	0.1	0
11	DEAD	NonStatic	Step	14	3.5	-6.6	0.7	0	0.1	0
11	DEAD	NonStatic	Step	15	3.7	-7.1	0.8	0	0.1	0
11	DEAD	NonStatic	Step	16	4	-7.6	0.9	0	0.1	0
11	DEAD	NonStatic	Step	17	4.2	-8	0.9	0	0.1	0
11	DEAD	NonStatic	Step	18	4.5	-8.5	1	0	0.1	0
11	DEAD	NonStatic	Step	19	4.7	-9	1	0	0.1	0
11	DEAD	NonStatic	Step	20	5	-9.4	1.1	0	0.2	0
11	DEAD	NonStatic	Step	21	5.2	-9.9	1.1	0	0.2	0
11	DEAD	NonStatic	Step	22	5.5	-10	1.2	0	0.2	0
11	DEAD	NonStatic	Step	23	5.7	-11	1.2	0	0.2	0
11	DEAD	NonStatic	Step	24	5.7	-11	1.2	0	0.2	0
11	DEAD	NonStatic	Step	25	5.7	-11	1.2	0	0.2	0
11	DEAD	NonStatic	Step	26	5.7	-11	1.2	0	0.2	0

Appendix C

Exterior Cladding Details and Earthquake Damage Drawings

Appendix C: Exterior Cladding Details and Earthquake Damage Drawings is included to provide a better understanding of the case study building's exterior cladding performance during the 2010 Canterbury earthquake. These drawings are taken from the construction data provided by the Christchurch City Council (Christchurch City Council 2016b). Some drawings are taken from the earthquake report obtained from the Christchurch City Council to highlight the damage on the claddings.

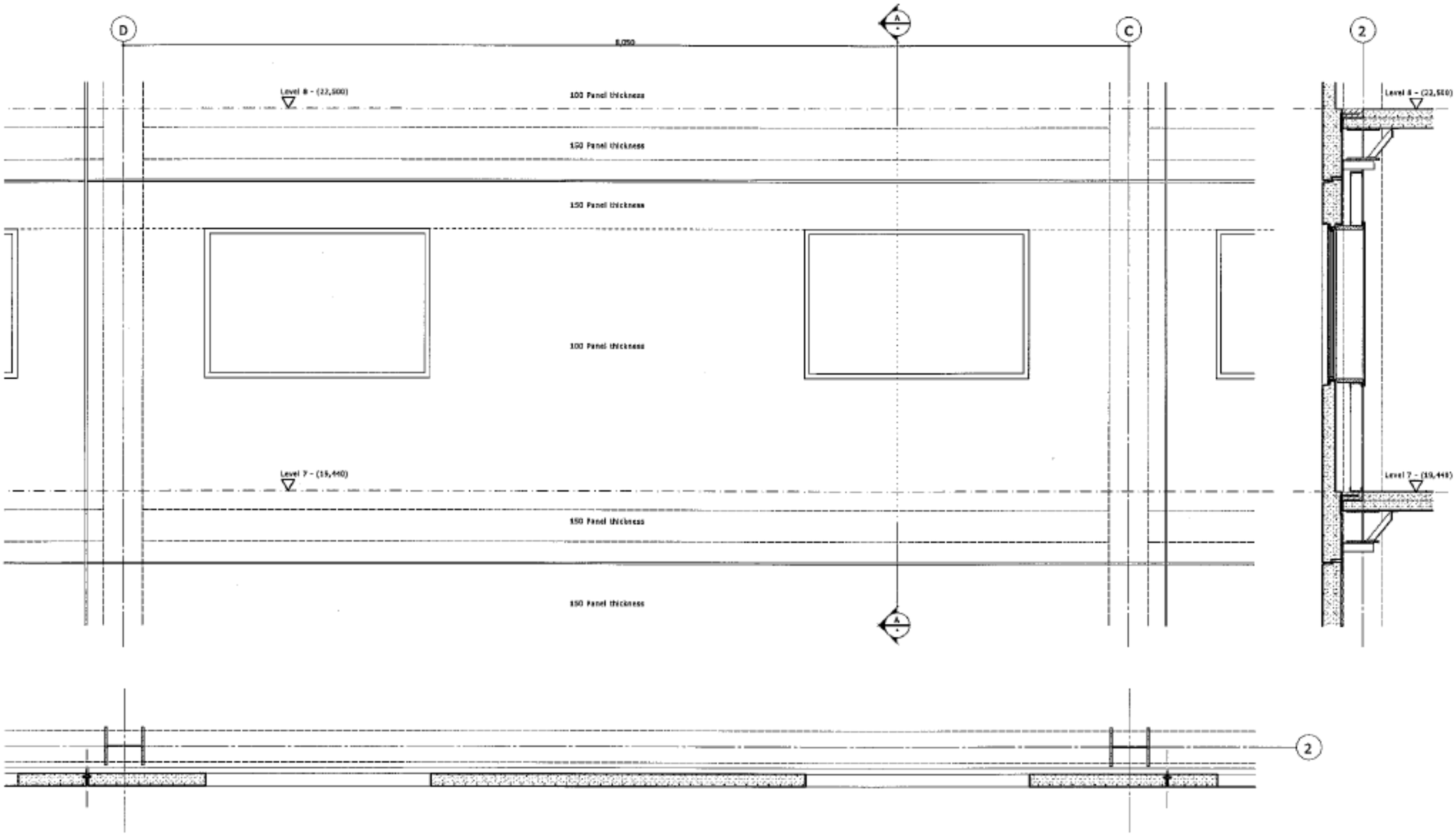

Figure C.1. Example of typical panel elevation, section and plan

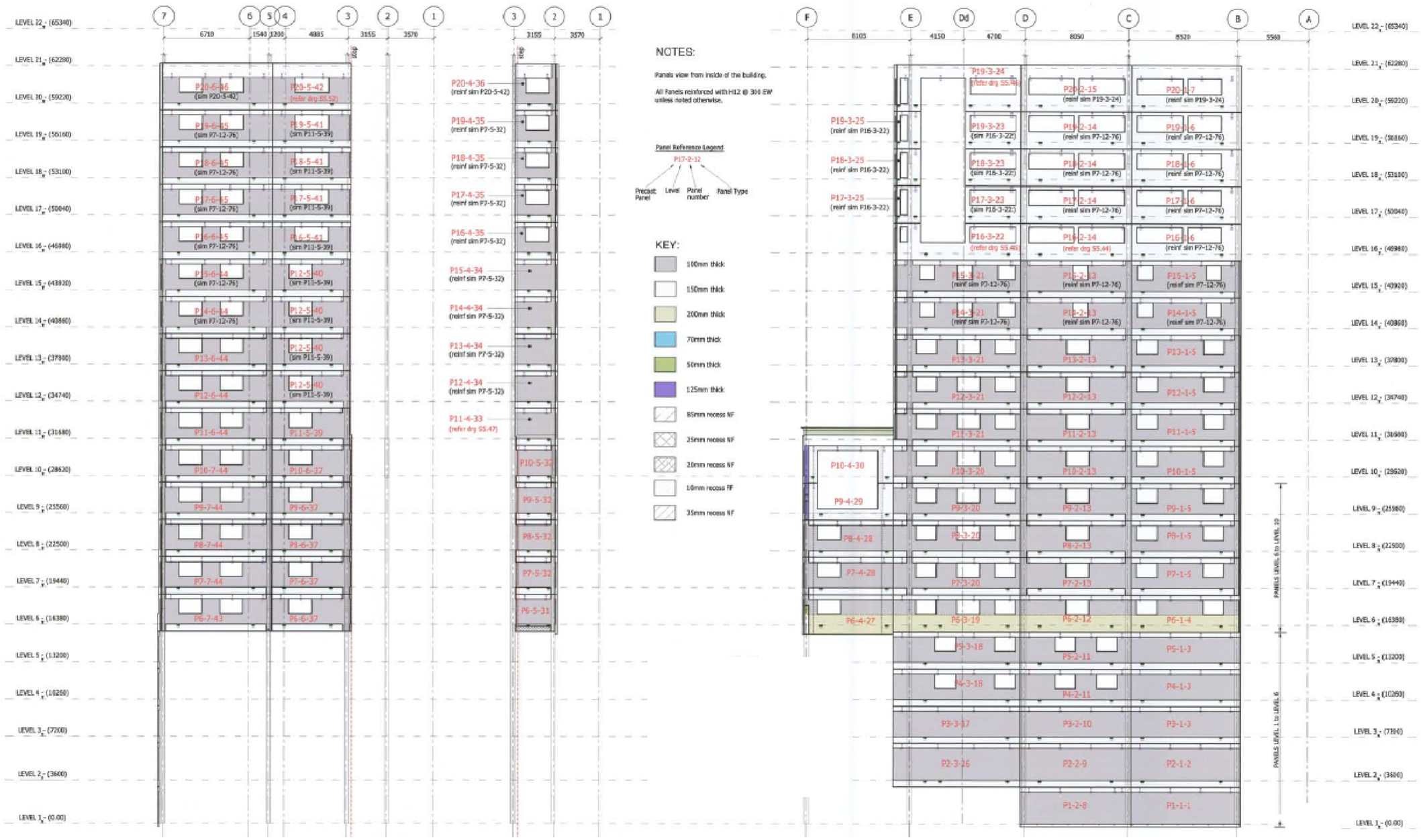

Figure C.2. South wall grid B, near grid B and East wall grid 7 panel elevation

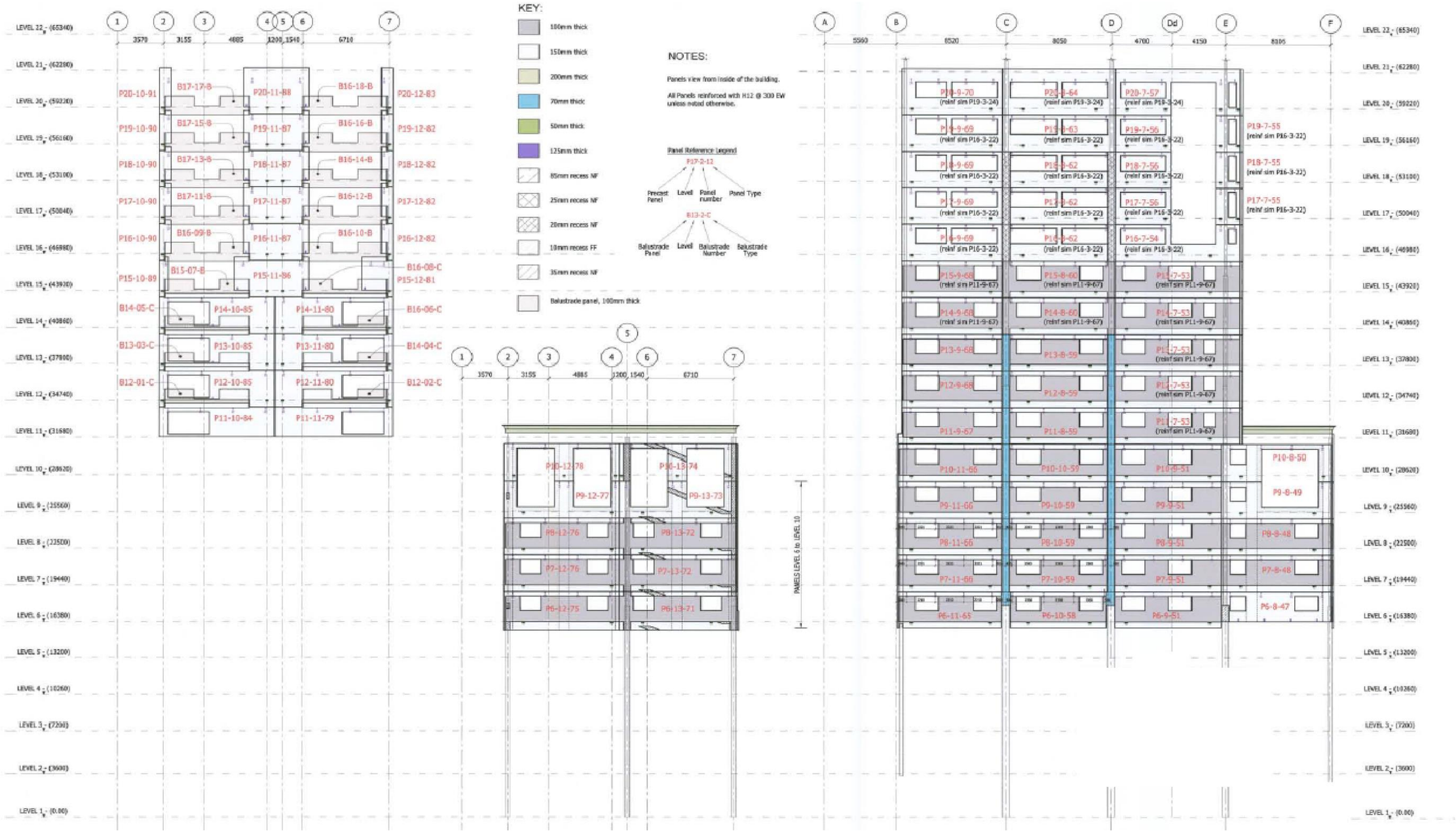

Figure C.3. North wall near grid E, grid F and West wall grid 2 panel elevation

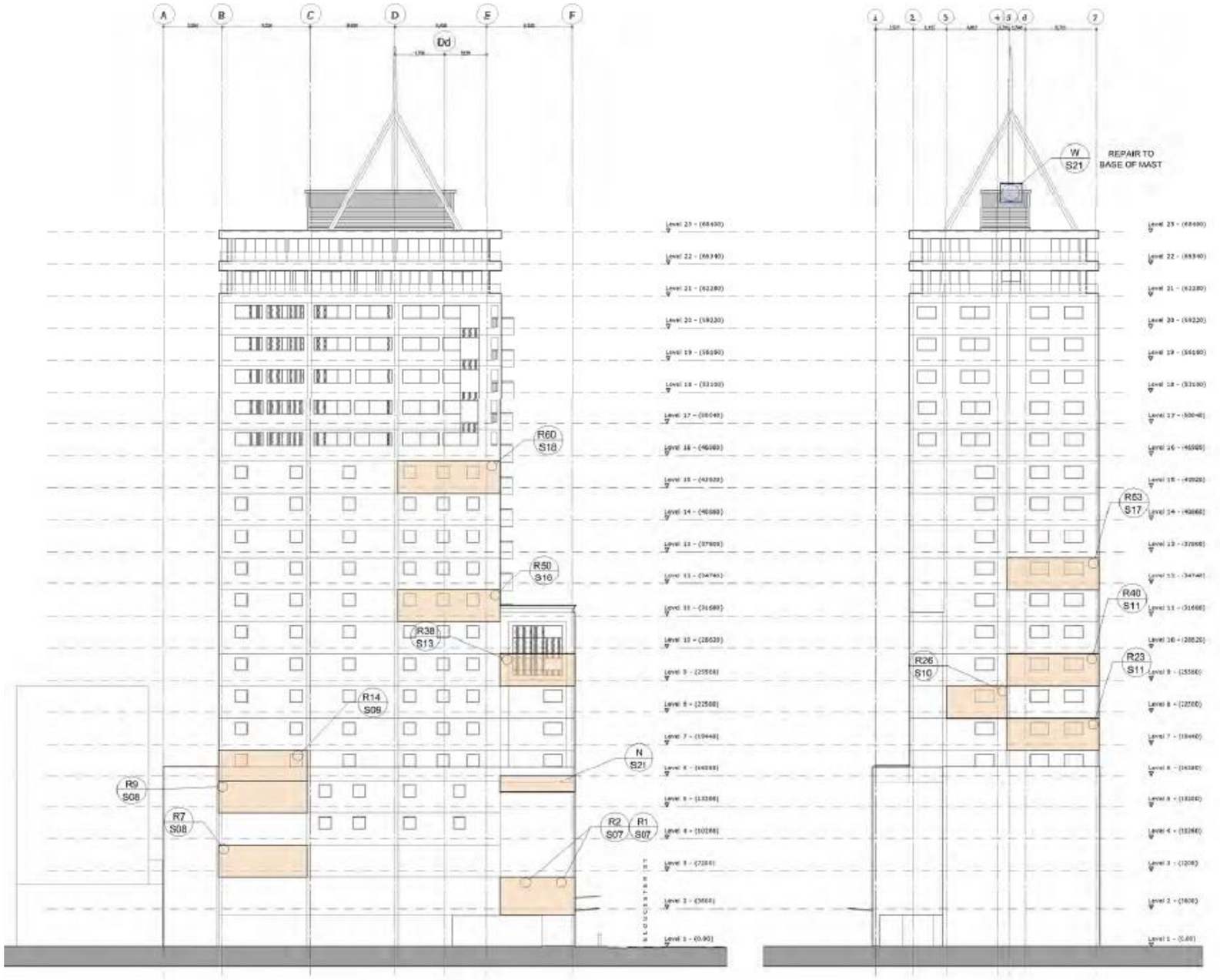

Figure C.4. Exterior Cladding damage on East elevation and South elevation

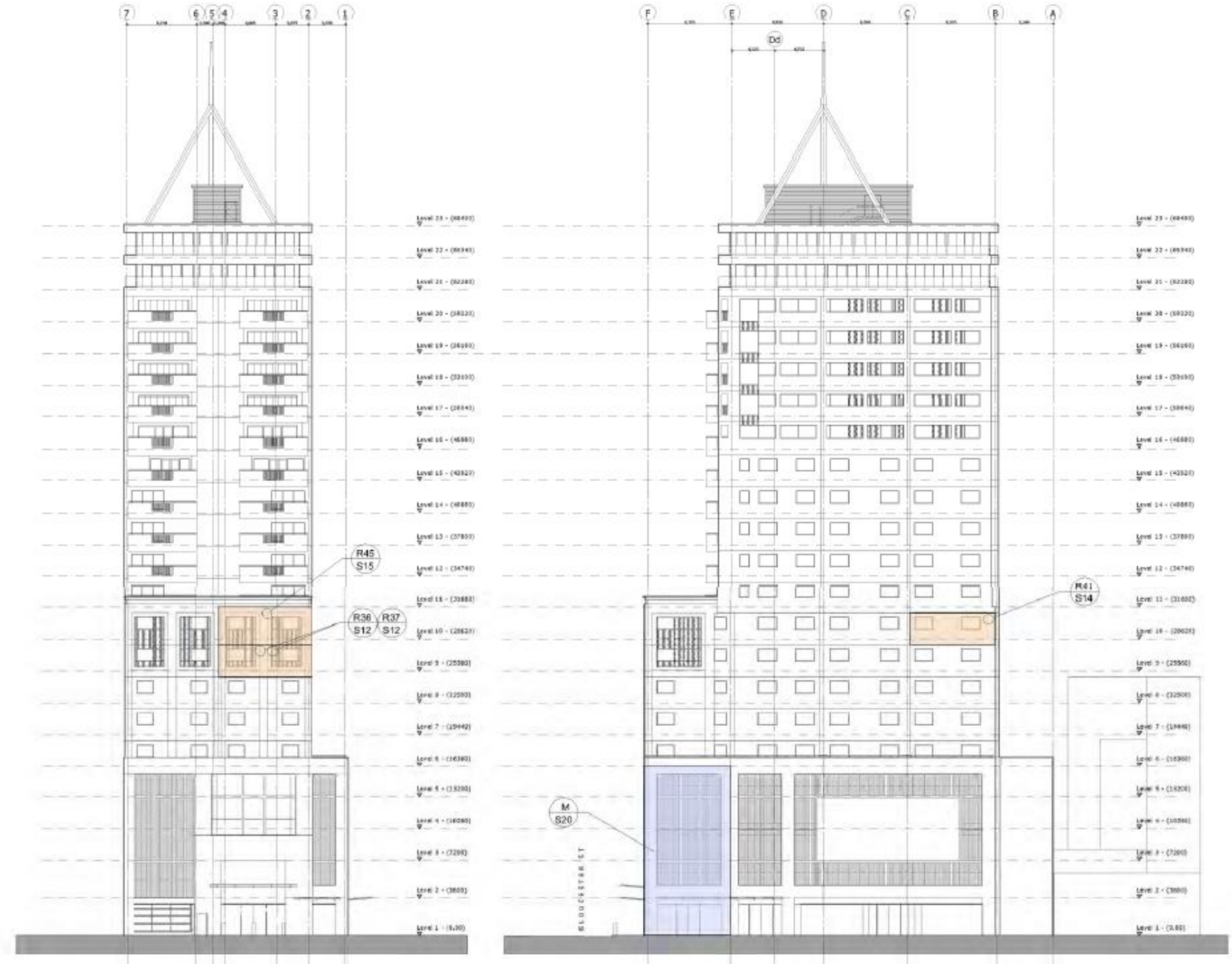

Figure C.5. Exterior Cladding damage on North elevation and West elevation

Appendix D

Strong Motion Site Records and Response Spectra

Appendix D: Strong motion sites records and response spectra for the 2010 Canterbury earthquake series is included to show the demand of the earthquake and to compare it with the New Zealand code level of design. As such, Figure D.1 to Figure D.3 present the ground motion records as recorded by three strong motion stations, CCCC (only three earthquakes were recorded at this site), CHHC and CBGS. In addition to the ground motions, the acceleration and displacement spectra are also included in Figure D.4 and Figure D.5, respectively.

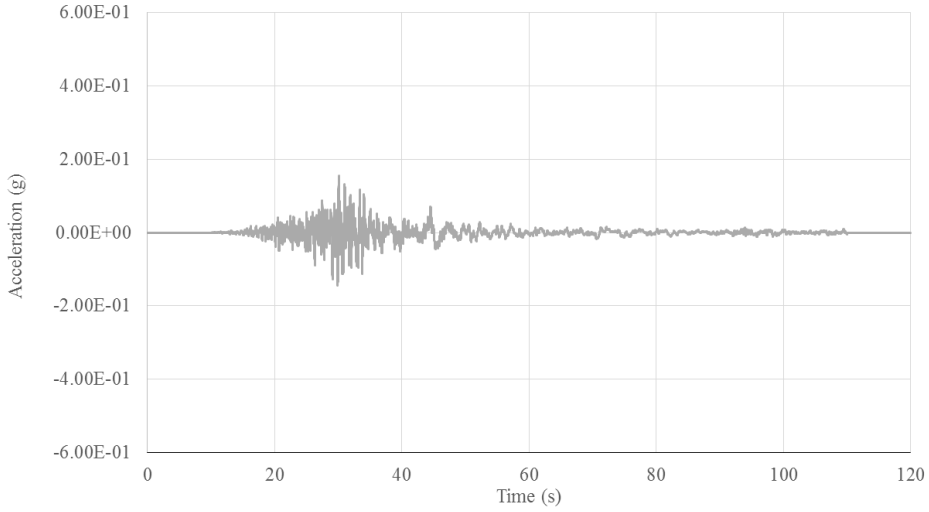

(a)

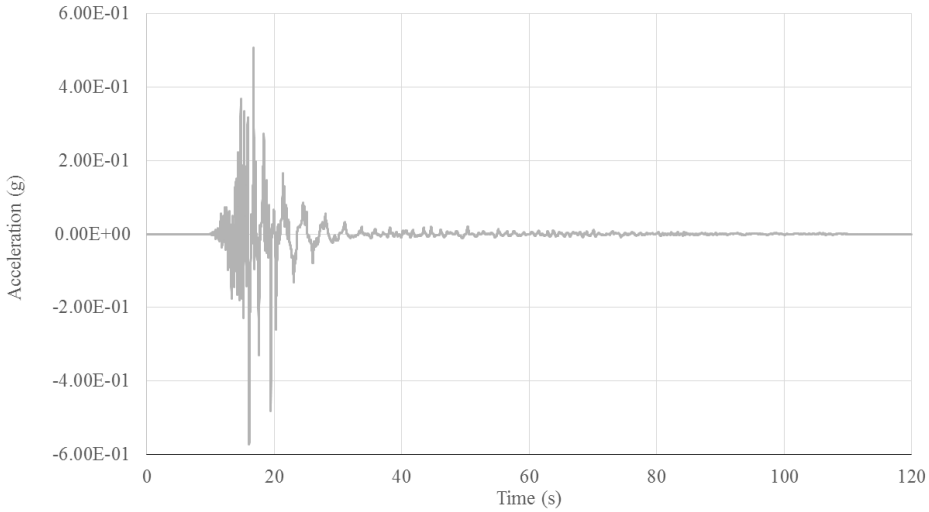

(b)

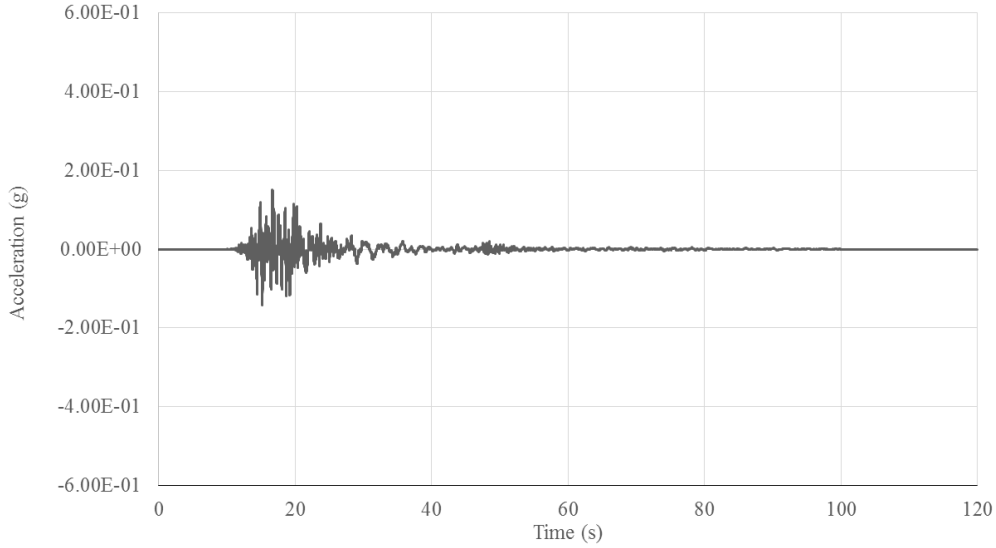

(c)

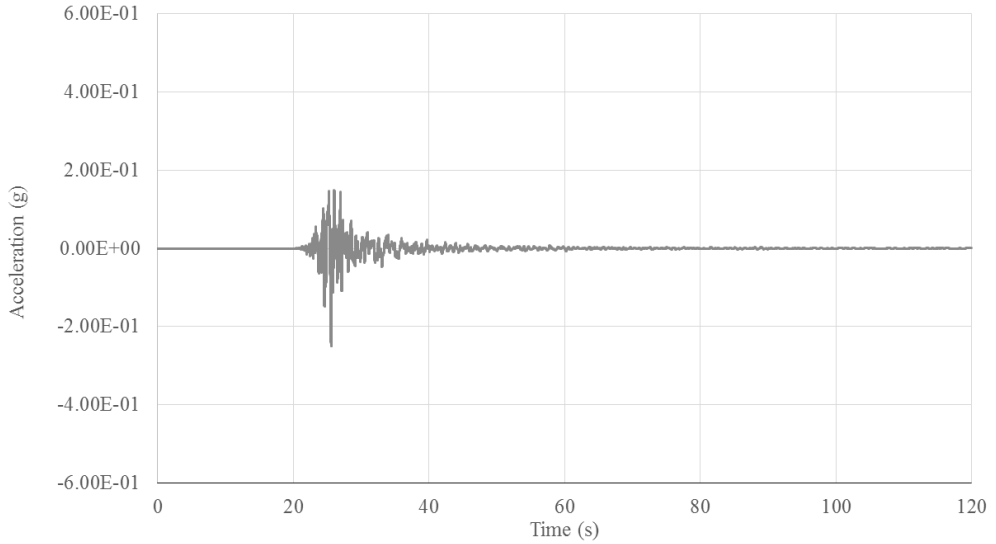

(d)

Figure D.1. Christchurch Botanical Gardens Station (CBGS) ground motion record for the (a) September 2010 (b) February 2011 (c) June 2011 (d) December 2011

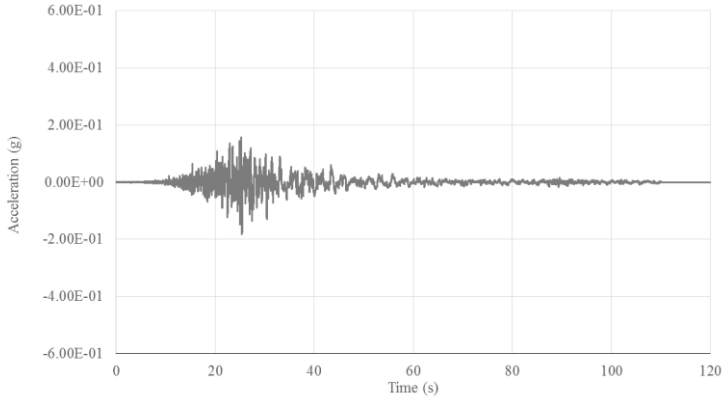

(a)

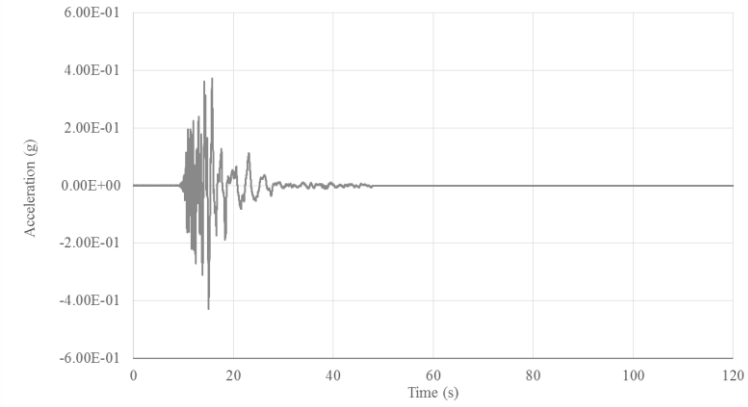

(b)

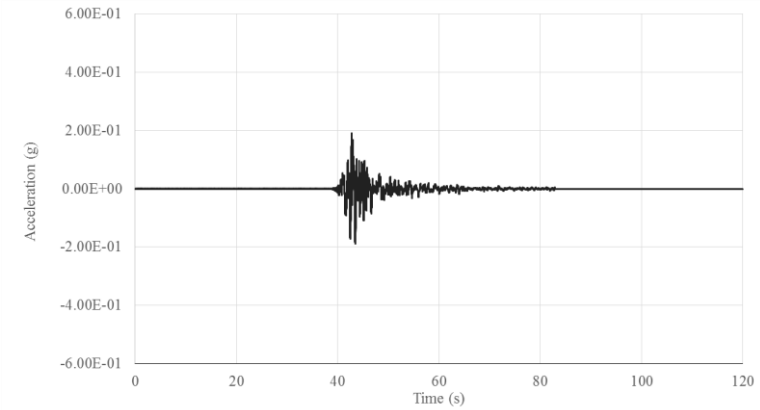

(c)

Figure D.2. Christchurch Catholic Cathedral College (CCCC) ground motion record for the (a) September 2010 (b) February 2011 (c) December 2011

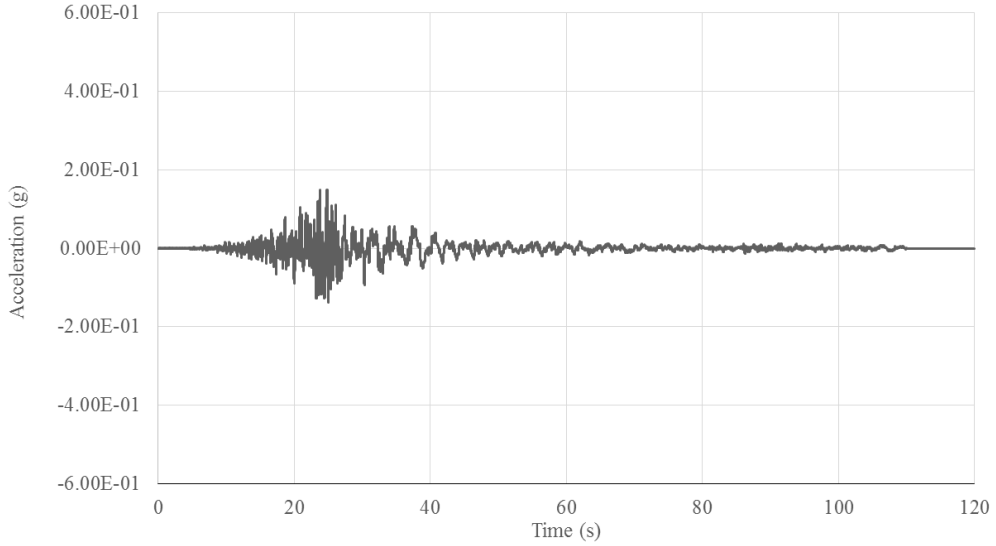
6.00E-01
4.00E-01
2.00E-01
0.00E+00
-2.00E-01
-4.00E-01
-6.00E-01
Acceleration (g)
0
20
40
60
80
100
120
Time (s)

(a)

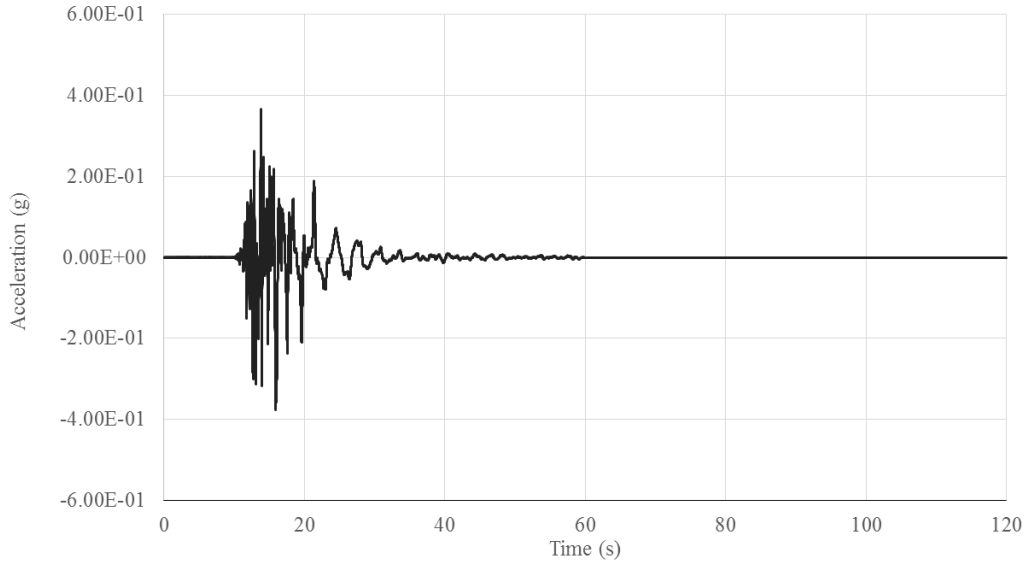
6.00E-01
4.00E-01
2.00E-01
0.00E+00
-2.00E-01
-4.00E-01
-6.00E-01
Acceleration (g)
0
20
40
60
80
100
120
Time (s)

(b)

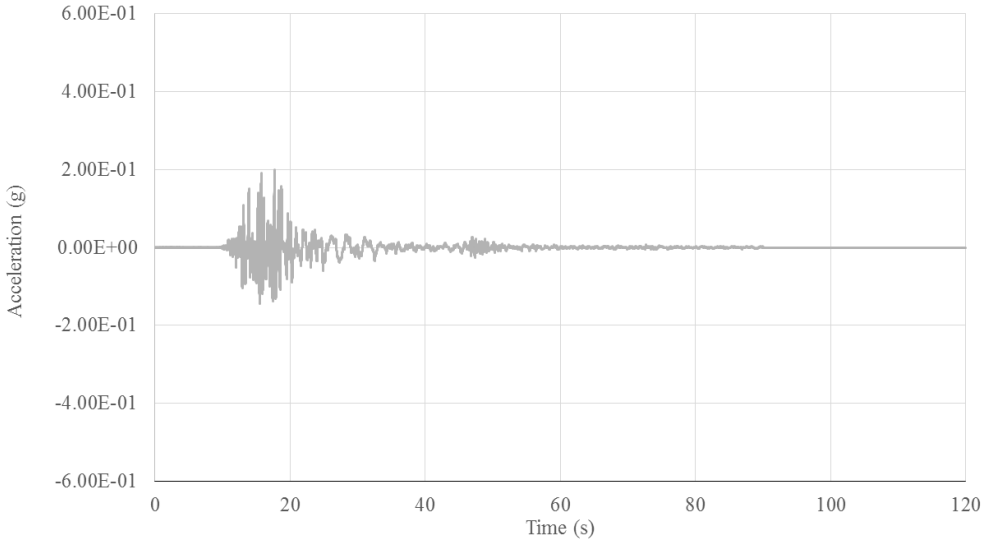

(c)

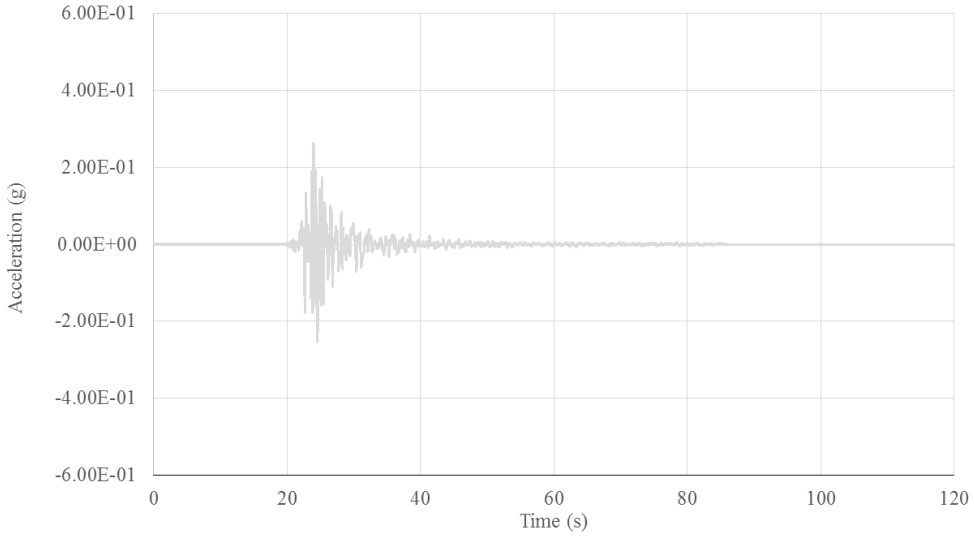

(d)

Figure D.3. Christchurch Hospital (CHHC) ground motion record for the (a) September 2010 (b) February 2011 (c) June 2011 (d) December 2011

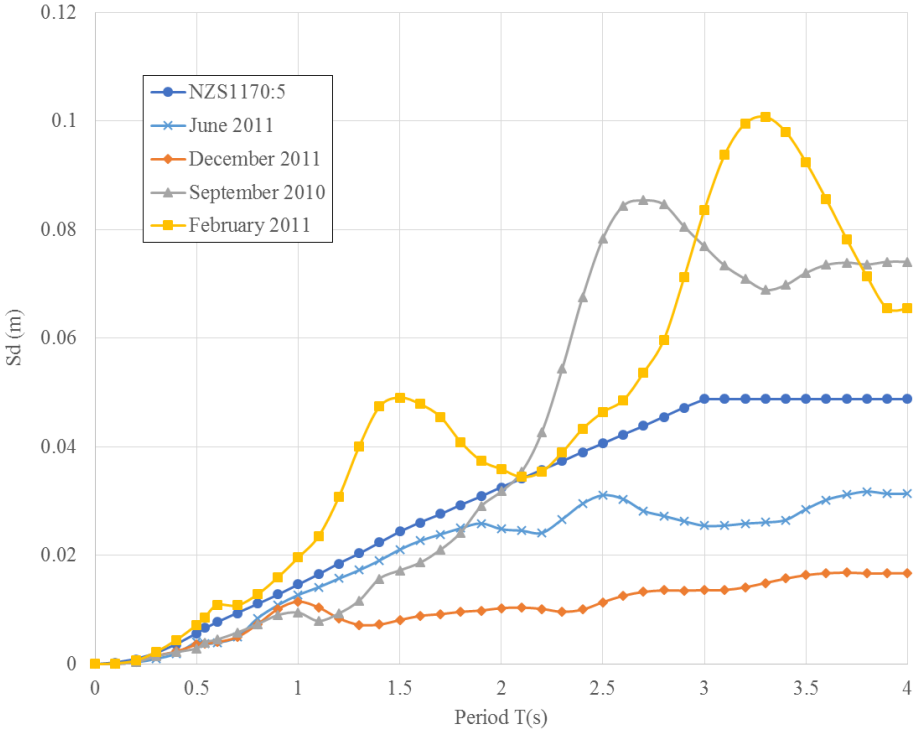

Figure D.4. Displacement response spectra for the recent Canterbury earthquakes

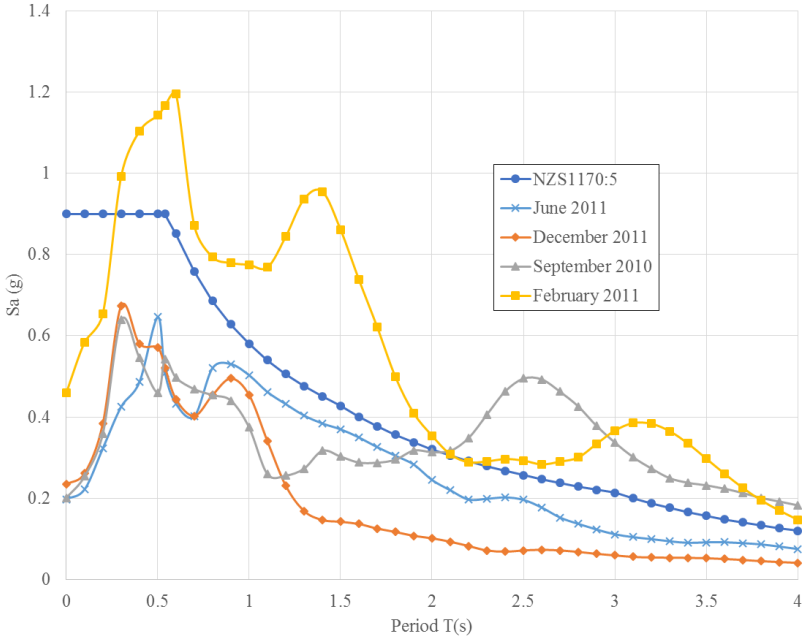

Figure D.5. Acceleration response spectra for the recent Canterbury earthquakes

Appendix E

Eccentrically Braced Frame Fragilities

Appendix E: EBF Fragilities is included as a reference for all the EBF fragilities developed for the Pacific Tower. These fragilities were derived using a MATLAB code provided in O'Reilly and Sullivan (2016).

Table E-1. Eccentrically braced frames fragility functions

Grid	Floor	Size	Link Length (m)	DS1 (rad)	β	DS2 (rad)	β	DS3 (rad)	β
1	1	310UC118	0.4	0.003	0.228	0.004	0.233	0.005	0.272
1	2	200UC60	0.4	0.004	0.198	0.004	0.208	0.006	0.253
1	3	200UC60	0.4	0.004	0.188	0.005	0.193	0.006	0.234
1	4	200UC60	0.4	0.005	0.176	0.005	0.184	0.006	0.217
1	5	200UC60	0.4	0.005	0.185	0.006	0.181	0.007	0.215
2	6	250UC90	1	0.009	0.193	0.011	0.209	0.013	0.253
2	7	250UC73	1	0.009	0.192	0.011	0.205	0.014	0.241
2	8	250UC73	1	0.010	0.194	0.012	0.205	0.014	0.247
2	9	250UC73	1	0.010	0.197	0.012	0.201	0.015	0.237
2	10	250UC73	1	0.011	0.190	0.013	0.193	0.015	0.235
2	11	250UC73	1	0.011	0.180	0.013	0.193	0.016	0.226
2	12	250UC73	1	0.012	0.188	0.014	0.198	0.016	0.227
2	13	250UC73	1	0.012	0.187	0.014	0.187	0.017	0.221
2	14	250UC73	1	0.013	0.185	0.015	0.191	0.017	0.223
2	15	250UC73	1	0.013	0.184	0.015	0.197	0.017	0.212
2	16	250UC73	1	0.014	0.194	0.016	0.189	0.018	0.209
2	17	250UC73	1	0.014	0.184	0.016	0.187	0.018	0.197
2	18	250UC73	1	0.015	0.182	0.017	0.196	0.019	0.209
2	19	250UC73	1	0.015	0.189	0.017	0.190	0.020	0.212
2	20	250UC73	1	0.015	0.195	0.017	0.188	0.020	0.210
4	21	250UC73	0.55	0.014	0.213	0.015	0.200	0.016	0.197
4	22	250UC73	0.55	0.014	0.220	0.015	0.201	0.017	0.199
6	1	310UC137	0.55	0.004	0.231	0.005	0.244	0.006	0.287
6	2	310UC137	0.55	0.005	0.204	0.006	0.224	0.007	0.258
6	3	310UC118	0.55	0.005	0.204	0.006	0.203	0.007	0.251
6	4	310UC118	0.55	0.005	0.185	0.006	0.210	0.008	0.255
6	5	310UC118	0.55	0.006	0.184	0.007	0.190	0.008	0.233
6	6	250UC90	0.55	0.006	0.177	0.008	0.185	0.009	0.229
6	7	250UC90	0.55	0.007	0.180	0.008	0.185	0.009	0.225
6	8	250UC90	0.55	0.007	0.180	0.008	0.184	0.010	0.216
6	9	250UC73	0.55	0.008	0.175	0.009	0.190	0.010	0.211
6	10	250UC73	0.55	0.008	0.187	0.009	0.191	0.011	0.208
6	11	250UC73	0.55	0.009	0.187	0.010	0.186	0.011	0.196
6	12	250UC73	0.55	0.009	0.188	0.010	0.193	0.012	0.197
6	13	250UC73	0.55	0.010	0.187	0.011	0.195	0.012	0.191

6	14	250UC73	0.55	0.010	0.195	0.011	0.188	0.013	0.194
6	15	250UC73	0.55	0.011	0.194	0.012	0.196	0.013	0.205
6	16	250UC73	0.55	0.011	0.196	0.012	0.182	0.014	0.211
6	17	250UC73	0.55	0.011	0.199	0.013	0.196	0.014	0.209
6	18	250UC73	0.55	0.012	0.199	0.013	0.197	0.015	0.201
6	19	250UC73	0.55	0.012	0.204	0.014	0.197	0.015	0.202
6	20	250UC73	0.55	0.013	0.198	0.014	0.202	0.016	0.200
6	21	250UC73	0.55	0.013	0.205	0.015	0.205	0.016	0.204
6	22	250UC73	0.55	0.014	0.207	0.015	0.198	0.017	0.202
C	1	327HCC222	0.75	0.015	0.247	0.020	0.261	0.025	0.299
C	2	327HCC222	0.75	0.017	0.227	0.022	0.241	0.027	0.272
C	3	310UC158	0.75	0.018	0.202	0.023	0.220	0.028	0.271
C	4	310UC158	0.75	0.019	0.200	0.024	0.219	0.030	0.255
C	5	310UC158	0.75	0.021	0.197	0.025	0.215	0.031	0.249
C	6	310UC158	0.75	0.023	0.187	0.027	0.208	0.033	0.237
C	7	310UC158	0.75	0.024	0.190	0.028	0.199	0.034	0.234
C	8	250UC90	0.75	0.025	0.186	0.030	0.194	0.036	0.229
C	9	250UC90	0.75	0.027	0.186	0.032	0.192	0.037	0.233
C	10	250UC90	0.75	0.028	0.188	0.033	0.189	0.039	0.222
C	11	200UC52	0.75	0.030	0.190	0.035	0.198	0.041	0.223
C	12	200UC52	0.75	0.031	0.192	0.036	0.194	0.043	0.218
C	13	200UC52	0.75	0.033	0.191	0.038	0.191	0.043	0.209
C	14	200UC52	0.75	0.034	0.195	0.040	0.188	0.045	0.209
C	15	200UC52	0.75	0.036	0.184	0.041	0.188	0.047	0.207
C	16	200UC46	0.75	0.038	0.204	0.041	0.197	0.049	0.209
C	17	200UC46	0.75	0.039	0.198	0.044	0.200	0.050	0.207
C	18	200UC46	0.75	0.040	0.201	0.045	0.193	0.052	0.198
C	19	200UC46	0.75	0.042	0.203	0.047	0.190	0.053	0.219
C	20	200UC46	0.75	0.044	0.204	0.048	0.194	0.055	0.210
C	21	200UC46	0.75	0.045	0.199	0.050	0.198	0.055	0.202
C	22	200UC46	0.75	0.046	0.199	0.051	0.199	0.057	0.201
C	1	310UC137	1.2	0.007	0.251	0.009	0.266	0.013	0.305
C	2	310UC137	1.2	0.008	0.233	0.010	0.256	0.013	0.285
C	3	310UC137	1.2	0.008	0.224	0.011	0.239	0.014	0.288
C	4	310UC137	1.2	0.009	0.223	0.011	0.225	0.014	0.265
C	5	310UC137	1.2	0.009	0.207	0.012	0.223	0.014	0.278
C	6	310UC118	1.2	0.010	0.203	0.012	0.217	0.015	0.259
C	7	310UC118	1.2	0.010	0.196	0.013	0.218	0.015	0.256
C	8	310UC118	1.2	0.011	0.198	0.013	0.197	0.016	0.244
C	9	310UC118	1.2	0.011	0.193	0.013	0.204	0.016	0.246
C	10	310UC118	1.2	0.012	0.189	0.014	0.211	0.017	0.240
C	11	250UC90	1.2	0.012	0.195	0.014	0.199	0.017	0.234
C	12	250UC90	1.2	0.012	0.187	0.015	0.194	0.018	0.237

C	13	250UC90	1.2	0.013	0.186	0.015	0.193	0.018	0.223
C	14	250UC90	1.2	0.013	0.188	0.016	0.194	0.018	0.233
C	15	250UC90	1.2	0.014	0.187	0.016	0.200	0.019	0.227
C	16	250UC73	1.2	0.014	0.186	0.017	0.197	0.020	0.215
C	17	250UC73	1.2	0.014	0.195	0.017	0.194	0.020	0.220
C	18	250UC73	1.2	0.015	0.191	0.017	0.196	0.021	0.224
C	19	250UC73	1.2	0.016	0.186	0.018	0.194	0.021	0.219
C	20	250UC73	1.2	0.016	0.190	0.019	0.189	0.022	0.206
D	1	310UC118	0.75	0.015	0.238	0.020	0.260	0.025	0.304
D	2	310UC118	0.75	0.017	0.229	0.022	0.231	0.028	0.278
D	3	250UC73	0.75	0.018	0.208	0.023	0.226	0.028	0.276
D	4	250UC73	0.75	0.019	0.203	0.024	0.222	0.030	0.251
D	5	250UC73	0.75	0.021	0.189	0.025	0.214	0.031	0.255
D	6	250UC73	0.75	0.022	0.191	0.027	0.206	0.033	0.237
D	7	250UC73	0.75	0.024	0.184	0.028	0.202	0.035	0.236
D	8	250UC73	0.75	0.025	0.185	0.030	0.203	0.036	0.237
D	9	250UC73	0.75	0.027	0.190	0.032	0.196	0.038	0.218
D	10	250UC73	0.75	0.028	0.189	0.033	0.195	0.040	0.221
D	11	200UC52	0.75	0.030	0.187	0.035	0.194	0.041	0.224
D	12	200UC52	0.75	0.032	0.190	0.036	0.192	0.042	0.212
D	13	200UC52	0.75	0.033	0.192	0.038	0.194	0.044	0.211
D	14	200UC52	0.75	0.034	0.195	0.039	0.192	0.045	0.210
D	15	200UC52	0.75	0.036	0.191	0.041	0.196	0.046	0.210
D	16	200UC46	0.75	0.037	0.199	0.042	0.197	0.048	0.219
D	17	200UC46	0.75	0.039	0.196	0.043	0.191	0.050	0.203
D	18	200UC46	0.75	0.040	0.207	0.045	0.198	0.051	0.208
D	19	200UC46	0.75	0.041	0.201	0.047	0.196	0.053	0.215
D	20	200UC46	0.75	0.043	0.205	0.048	0.195	0.054	0.211
D	21	200UC46	0.75	0.045	0.197	0.050	0.195	0.055	0.212
D	22	200UC46	0.75	0.046	0.205	0.052	0.204	0.058	0.196
D	11	250UC90	1.2	0.012	0.189	0.014	0.196	0.017	0.228
D	12	250UC90	1.2	0.013	0.189	0.015	0.198	0.018	0.243
D	13	250UC90	1.2	0.013	0.188	0.015	0.189	0.018	0.228
D	14	250UC90	1.2	0.013	0.182	0.016	0.192	0.019	0.221
D	15	250UC90	1.2	0.014	0.193	0.016	0.198	0.019	0.230
D	16	250UC73	1.2	0.014	0.195	0.017	0.189	0.020	0.216
D	17	250UC73	1.2	0.015	0.184	0.017	0.191	0.020	0.220
D	18	250UC73	1.2	0.015	0.185	0.017	0.197	0.021	0.219
D	19	250UC73	1.2	0.016	0.189	0.018	0.195	0.021	0.214
D	20	250UC73	1.2	0.016	0.191	0.019	0.192	0.022	0.210
F	1	310UC118	0.4	0.003	0.223	0.004	0.232	0.005	0.278
F	2	250UC90	1	0.007	0.227	0.009	0.234	0.011	0.294
F	3	250UC90	1	0.007	0.216	0.009	0.231	0.011	0.262

F	4	250UC90	1	0.008	0.209	0.010	0.217	0.012	0.267
F	5	250UC90	1	0.008	0.198	0.010	0.218	0.013	0.265
F	6	250UC73	1	0.009	0.200	0.010	0.206	0.013	0.248
F	7	250UC73	1	0.009	0.190	0.011	0.202	0.013	0.244
F	8	250UC73	1	0.010	0.187	0.011	0.198	0.014	0.235
F	9	250UC73	1	0.010	0.184	0.012	0.199	0.014	0.235
F	10	250UC73	1	0.010	0.190	0.012	0.192	0.015	0.238

Appendix F

PACT Inventory and Expected Annual Loss without Claddings Engineering Demand Parameters

Appendix F: PACT Inventory and Expected Annual Loss without Claddings Engineering Demand Parameters is included in order to present the complete inventory used for the loss analysis of the case study building as well as to show the EDP of one of the retrofit options, the re-detailing of the cladding connections as such that in the model the claddings can be "removed".

- Inventory of Damageable Components

Table F-1. Inventory of X-direction items in PACT

Floor	Height (ft.)	Floor Area (ft^2)	Direction 1 (X)			
			EBF Links (Each)	Cladding Panels (m^2 of Cladding)	Cladding Connections (# of Connections)	Drywall Partitions (Floor Area m^2)
1	11.81	8166.6	2	59.65	4	758.71
2	11.81	8166.6	2	91.51	6	758.71
3	10.04	3621	2	77.79	6	336.40
4	10.04	3788.9	2	74.73	6	351.96
5	10.04	3377.7	2	80.84	6	313.77
6	10.04	6082.7	1.5	205.17	16	565.15
7	10.04	5771.6	1.5	205.17	16	536.21
8	10.04	5771.6	1.5	205.17	16	536.21
9	10.04	5771.6	1.5	205.17	16	536.21
10	10.04	5771.6	1.5	205.17	16	536.21
11	10.04	5800.7	1.5	155.57	12	538.92
12	10.04	4524.1	1.5	155.57	12	420.25
13	10.04	4524.1	1.5	155.57	12	420.25
14	10.04	4524.1	1.5	155.57	12	420.25
15	10.04	4524.1	1.5	155.57	12	420.25
16	10.04	4510.1	1.5	155.57	12	419.05
17	10.04	4510.1	1.5	155.57	12	419.05
18	10.04	4510.1	1.5	155.57	12	419.05
19	10.04	4510.1	1.5	155.57	12	419.05
20	10.04	4510.1	1.5	155.57	12	419.05
21	10.04	4543.5	1.5	0	0	422.06
22	10.04	4543.5	1.5	0	0	422.06

Table F-2. Inventory of Z-direction items in PACT

Floor	Height (ft.)	Floor Area (ft^2)	Direction 2 (Z)			
			EBF Links (Each)	Cladding Panels (m^2 of Cladding)	Cladding Connections (# of Connections)	Drywall Partitions (Floor Area m^2)
1	11.81	8166.6	2	0	0	758.71
2	11.81	8166.6	2	0	0	758.71
3	10.04	3621	2	0	0	336.40
4	10.04	3788.9	2	0	0	351.96
5	10.04	3377.7	2	0	0	313.77
6	10.04	6082.7	2	107.04	10	565.15
7	10.04	5771.6	2	107.04	10	536.21
8	10.04	5771.6	2	107.04	10	536.21
9	10.04	5771.6	2	107.04	10	536.21
10	10.04	5771.6	2	107.04	10	536.21
11	10.04	5800.7	2	107.04	10	538.92
12	10.04	4524.1	2	107.04	10	420.25
13	10.04	4524.1	2	107.04	10	420.25
14	10.04	4524.1	2	107.04	10	420.25
15	10.04	4524.1	2	107.04	10	420.25
16	10.04	4510.1	2	107.04	10	419.05
17	10.04	4510.1	2	107.04	10	419.05
18	10.04	4510.1	2	107.04	10	419.05
19	10.04	4510.1	2	107.04	10	419.05
20	10.04	4510.1	2	107.04	10	419.05
21	10.04	4543.5	1	0	0	422.06
22	10.04	4543.5	1	0	0	422.06

Table F-3. Inventory of non-directional items in PACT

Floor	Height (ft.)	Floor Area (ft^2)	Non-directional							
			Elevators (Each)	Cold Water Piping (1000ft)	Cold Water Bracing (1000ft)	Hot Water Piping (1000ft)	Hot Water Bracing (1000ft)	Sanitary Waste Piping (1000ft)	Fire Sprinkler Water Piping (1000ft)	Fire Sprinkler Drop (1000ft)
1	11.81	8166.6	2	0.12	0.12	0.24	0.24	0.99	1.80	0.98
2	11.81	8166.6	0	0.12	0.12	0.24	0.24	0.99	1.80	0.98
3	10.04	3621	0	0.05	0.05	0.11	0.11	0.44	0.80	0.43
4	10.04	3788.9	0	0.06	0.06	0.11	0.11	0.46	0.83	0.45
5	10.04	3377.7	0	0.05	0.05	0.10	0.10	0.41	0.74	0.41
6	10.04	6082.7	0	0.09	0.09	0.18	0.18	0.74	1.34	0.73
7	10.04	5771.6	0	0.09	0.09	0.17	0.17	0.70	1.27	0.69
8	10.04	5771.6	0	0.09	0.09	0.17	0.17	0.70	1.27	0.69
9	10.04	5771.6	0	0.09	0.09	0.17	0.17	0.70	1.27	0.69
10	10.04	5771.6	0	0.09	0.09	0.17	0.17	0.70	1.27	0.69
11	10.04	5800.7	0	0.09	0.09	0.17	0.17	0.70	1.28	0.70
12	10.04	4524.1	0	0.07	0.07	0.14	0.14	0.55	1.00	0.54
13	10.04	4524.1	0	0.07	0.07	0.14	0.14	0.55	1.00	0.54
14	10.04	4524.1	0	0.07	0.07	0.14	0.14	0.55	1.00	0.54
15	10.04	4524.1	0	0.07	0.07	0.14	0.14	0.55	1.00	0.54
16	10.04	4510.1	0	0.07	0.07	0.14	0.14	0.55	0.99	0.54
17	10.04	4510.1	0	0.07	0.07	0.14	0.14	0.55	0.99	0.54
18	10.04	4510.1	0	0.07	0.07	0.14	0.14	0.55	0.99	0.54
19	10.04	4510.1	0	0.07	0.07	0.14	0.14	0.55	0.99	0.54
20	10.04	4510.1	0	0.07	0.07	0.14	0.14	0.55	0.99	0.54
21	10.04	4543.5	0	0.07	0.07	0.14	0.14	0.55	1.00	0.55
22	10.04	4543.5	0	0.07	0.07	0.14	0.14	0.55	1.00	0.55

- Engineering Demand Parameters for time-based analysis done with model without claddings

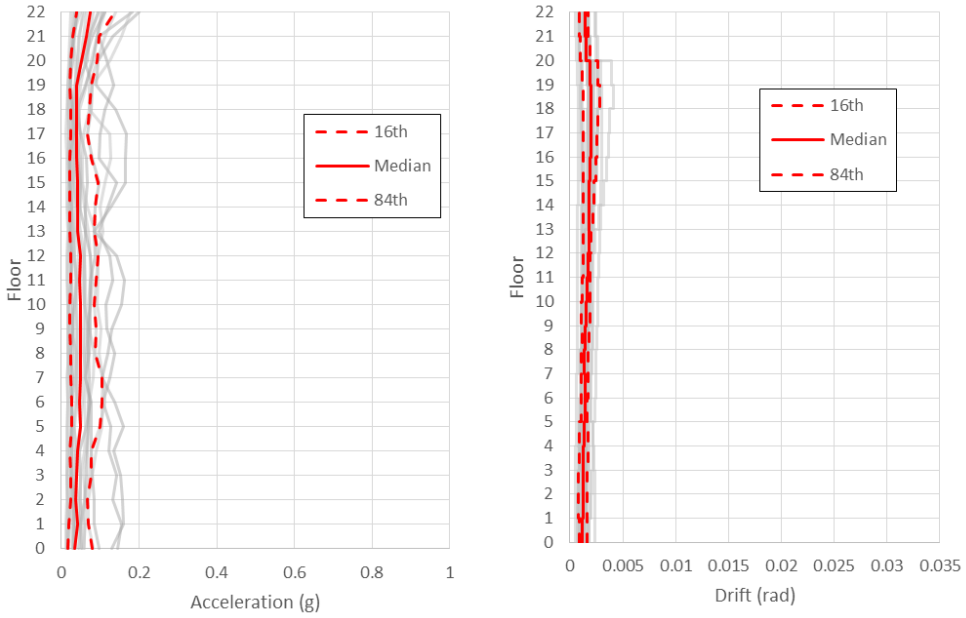

(a) (b)

Figure F.1. NS EDP for 80% in 50 years; Sa(4.0s) = 0.012g; (a) peak transient floor acceleration and (b) peak inter-storey drift

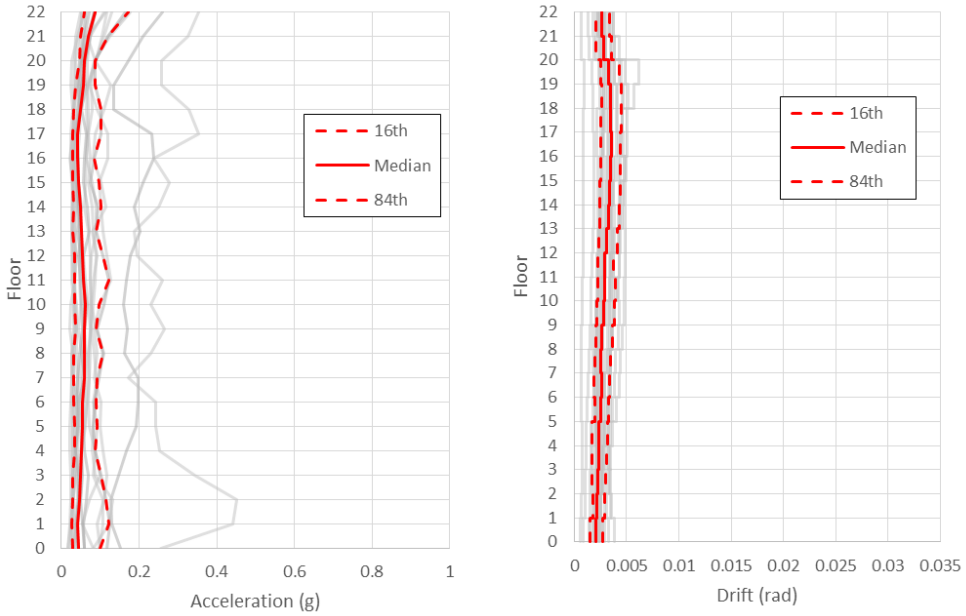

(a) (b)

Figure F.2. NS EDP for 50% in 50 years; Sa(4.0s) = 0.022g; (a) peak transient floor acceleration and (b) peak inter-storey drift

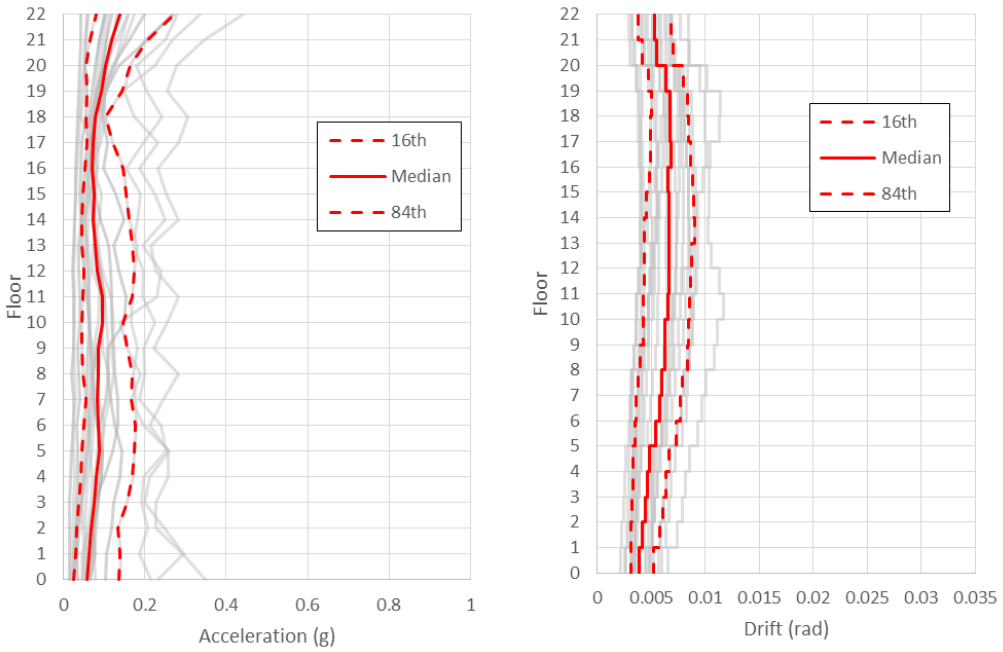

(a) (b)

Figure F.3. NS EDP for 20% in 50 years; Sa(4.0s) = 0.04g; (a) peak transient floor acceleration and (b) peak inter-storey drift

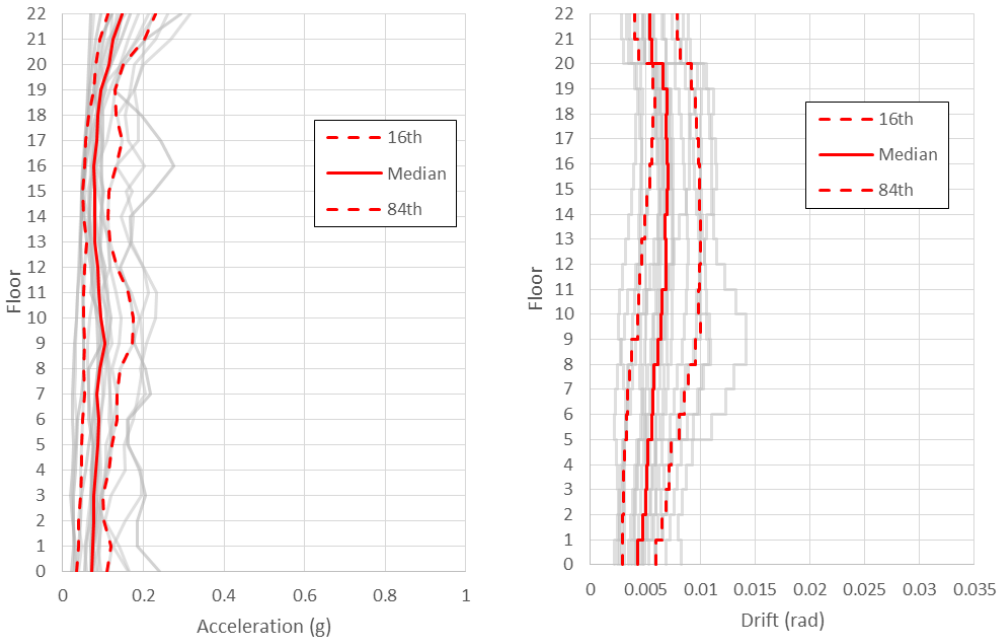

(a) (b)

Figure F.4. NS EDP for 10% in 50 years; Sa(4.0s) = 0.054g; (a) peak transient floor acceleration and (b) peak inter-storey drift

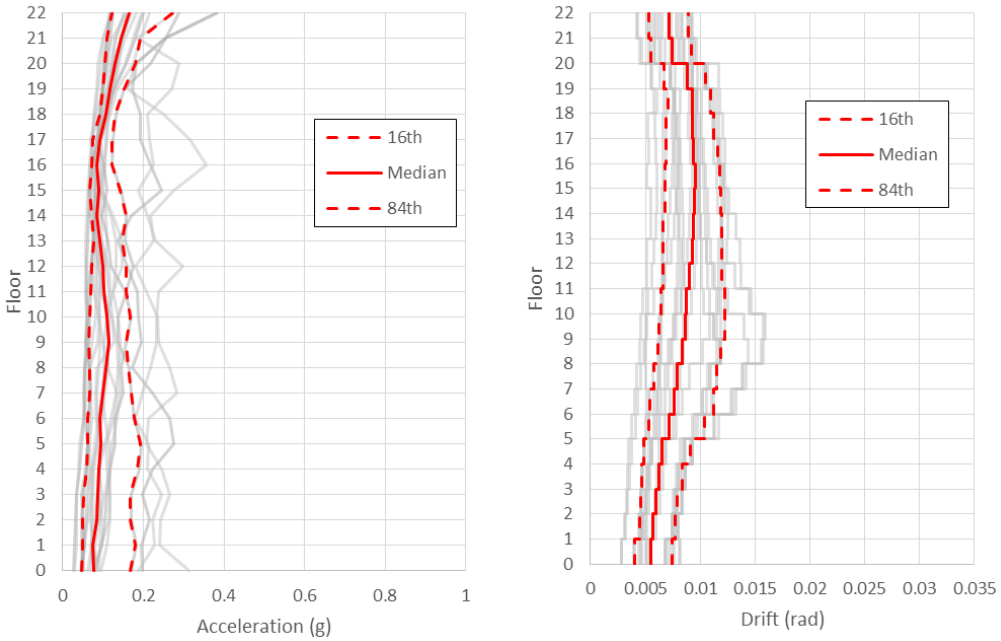

(a) (b)

Figure F.5. NS EDP for 5% in 50 years; Sa(4.0s) = 0.071g; (a) peak transient floor acceleration and (b) peak inter-storey drift

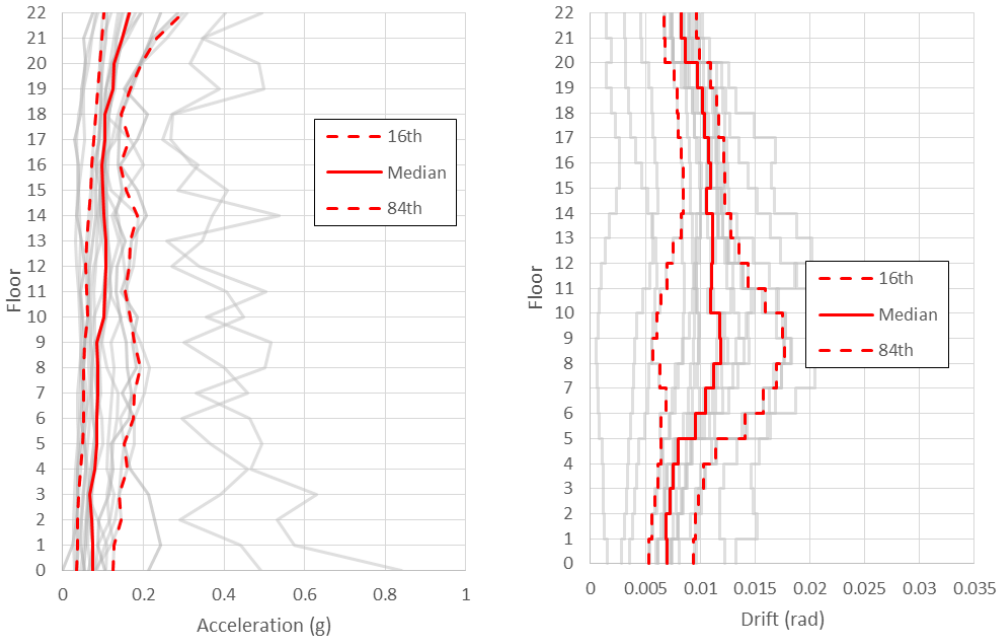

(a) (b)

Figure F.6. NS EDP for 2% in 50 years; Sa(4.0s) = 0.096g; (a) peak transient floor acceleration and (b) peak inter-storey drift

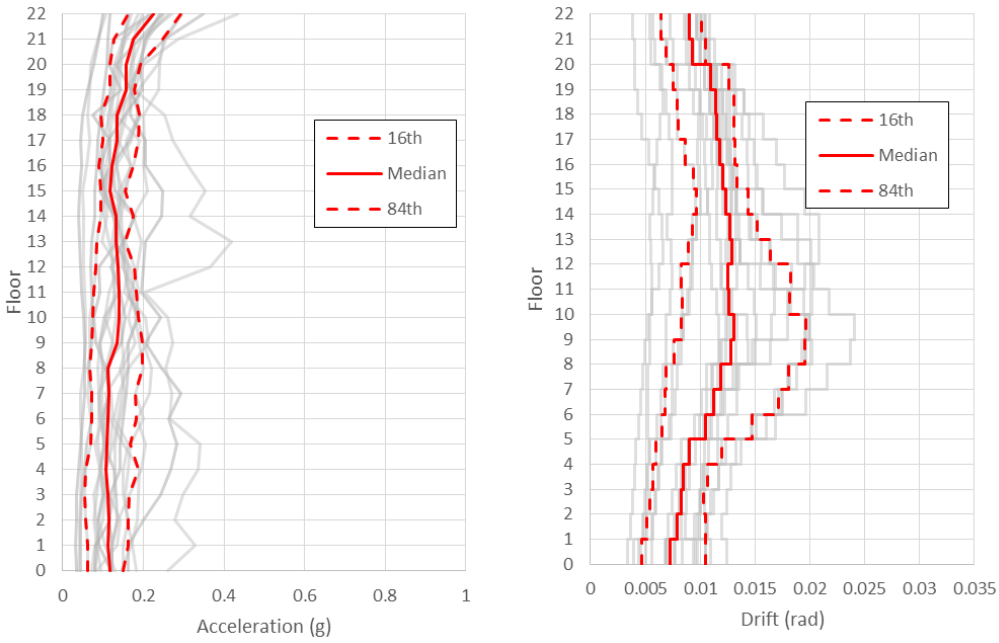

(a) (b)

Figure F.7. NS EDP for 1% in 50 years; Sa(4.0s) = 0.118g; (a) peak transient floor acceleration and (b) peak inter-storey drift

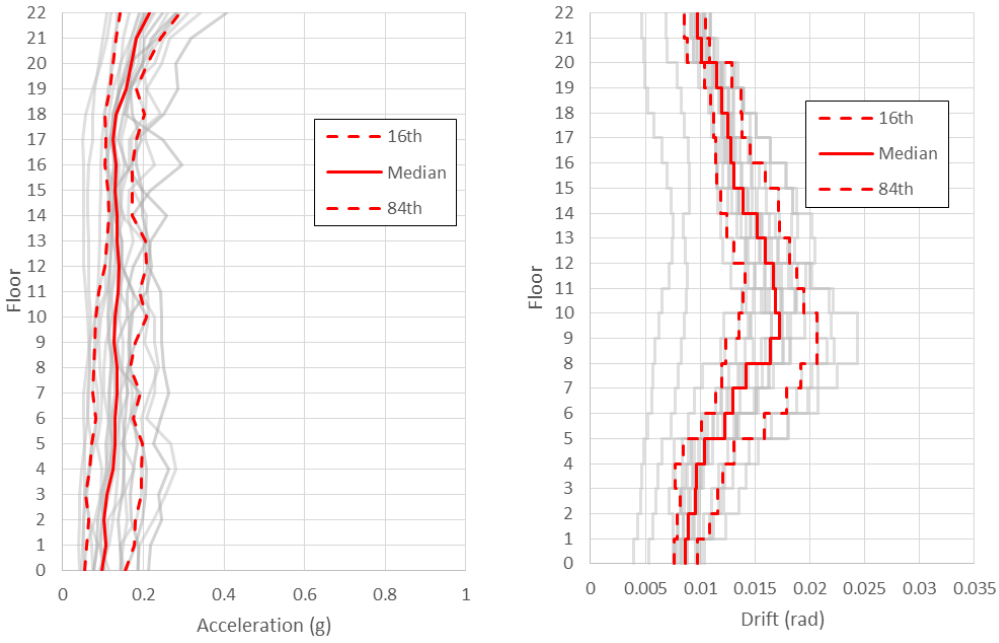

(a) (b)

Figure F.8. NS EDP for 0.5% in 50 years; Sa(4.0s) = 0.143g; (a) peak transient floor acceleration and (b) peak inter-storey drift

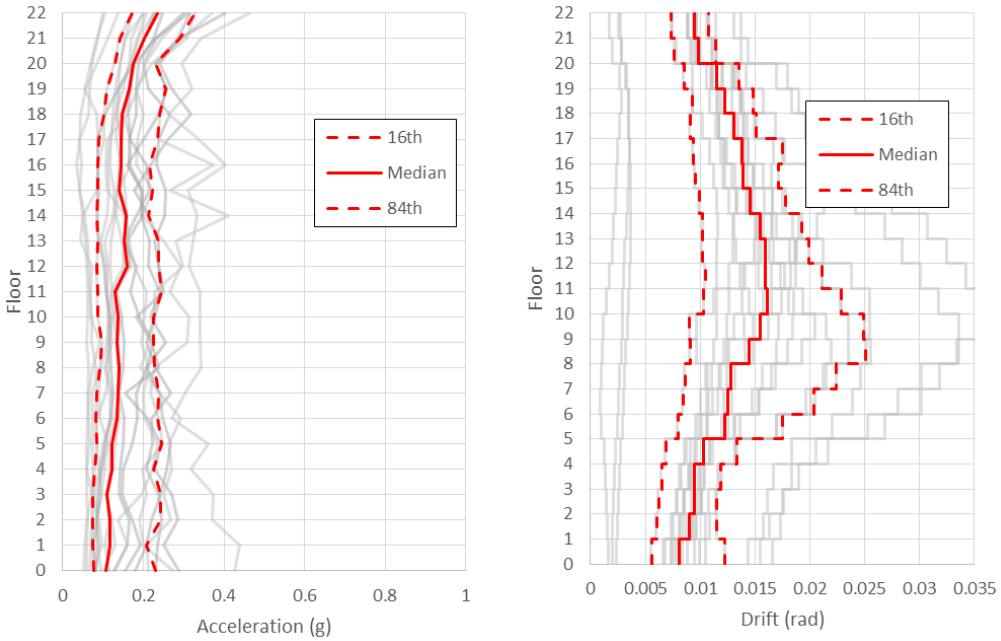

(a) (b)

Figure F.9. NS EDP for 0.2% in 50 years; Sa(4.0s) = 0.18g; (a) peak transient floor acceleration and (b) peak inter-storey drift

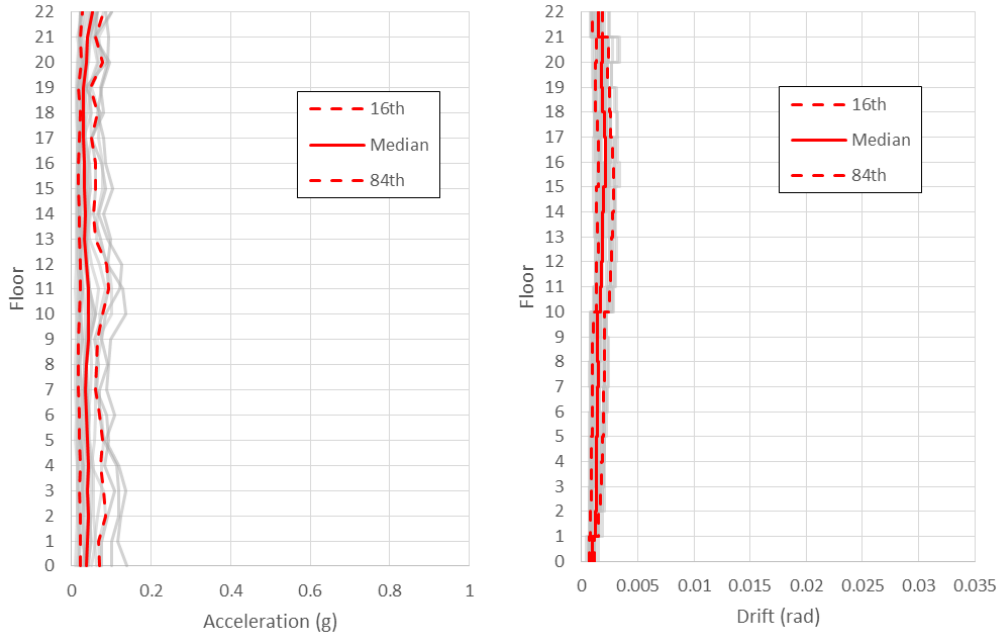

(a) (b)

Figure F.10. EW EDP for 80% in 50 years; Sa(4.0s) = 0.012g; (a) peak transient floor acceleration and (b) peak inter-storey drift

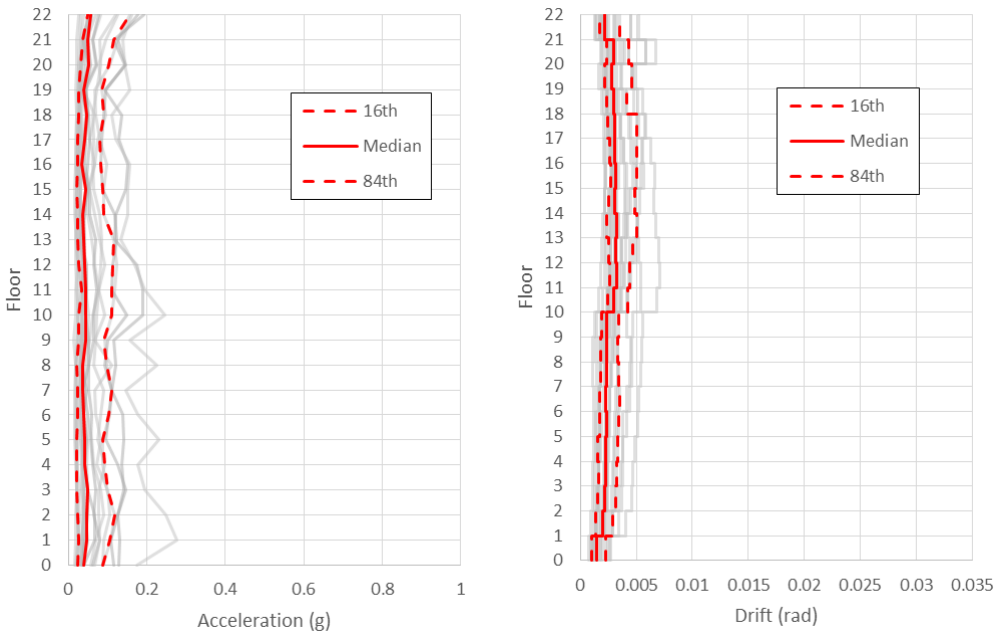

(a) (b)

Figure F.11. EW EDP for 50% in 50 years; Sa(4.0s) = 0.022g; (a) peak transient floor acceleration and (b) peak inter-storey drift

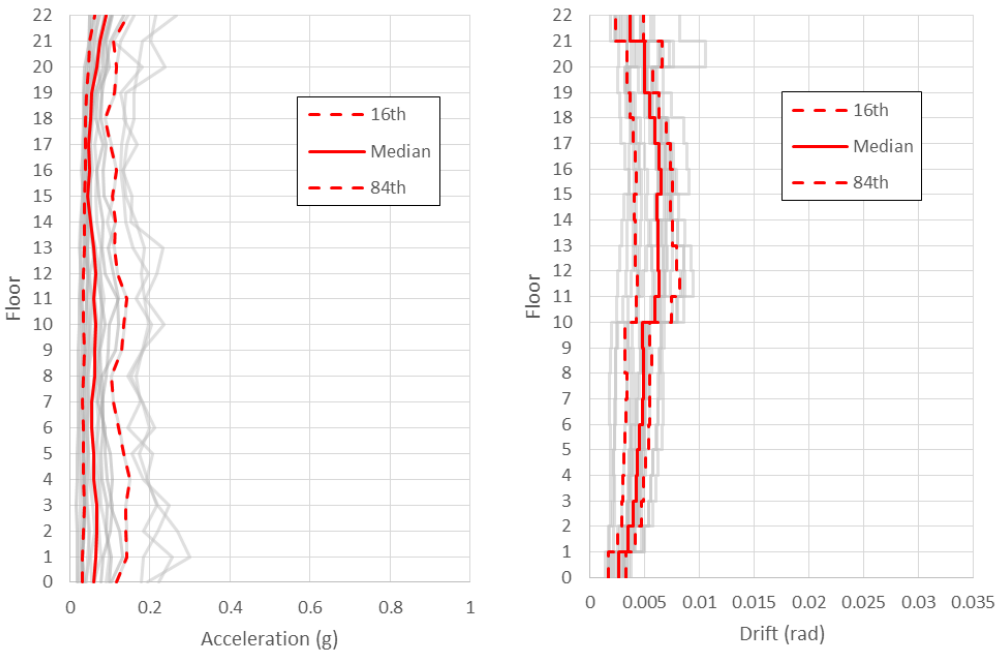

(a) (b)

Figure F.12. EW EDP for 20% in 50 years; Sa(4.0s) = 0.04g; (a) peak transient floor acceleration and (b) peak inter-storey drift

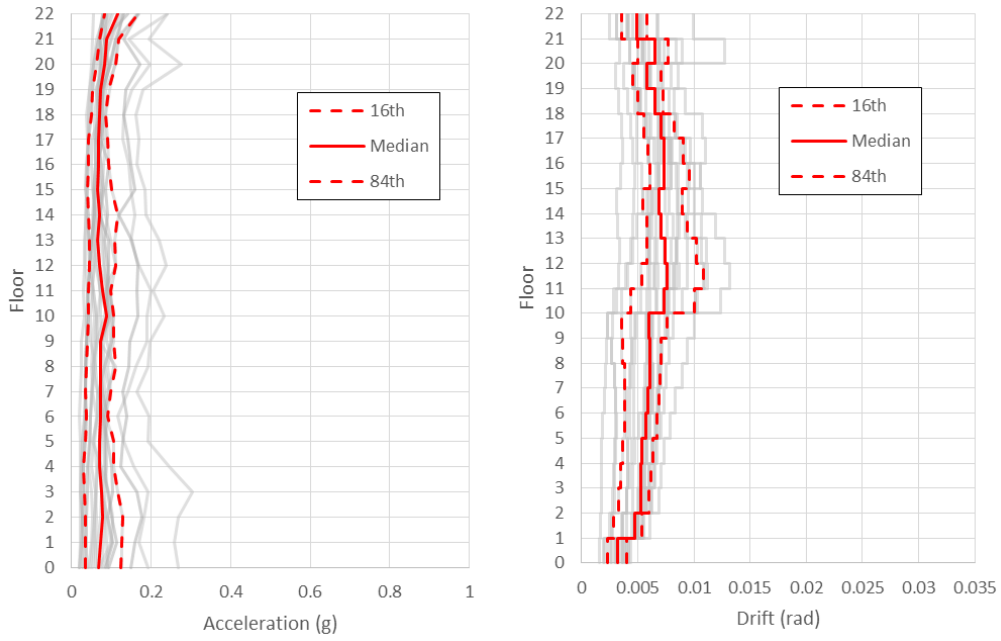

(a) (b)

Figure F.13. EW EDP for 10% in 50 years; Sa(4.0s) = 0.054g; (a) peak transient floor acceleration and (b) peak inter-storey drift

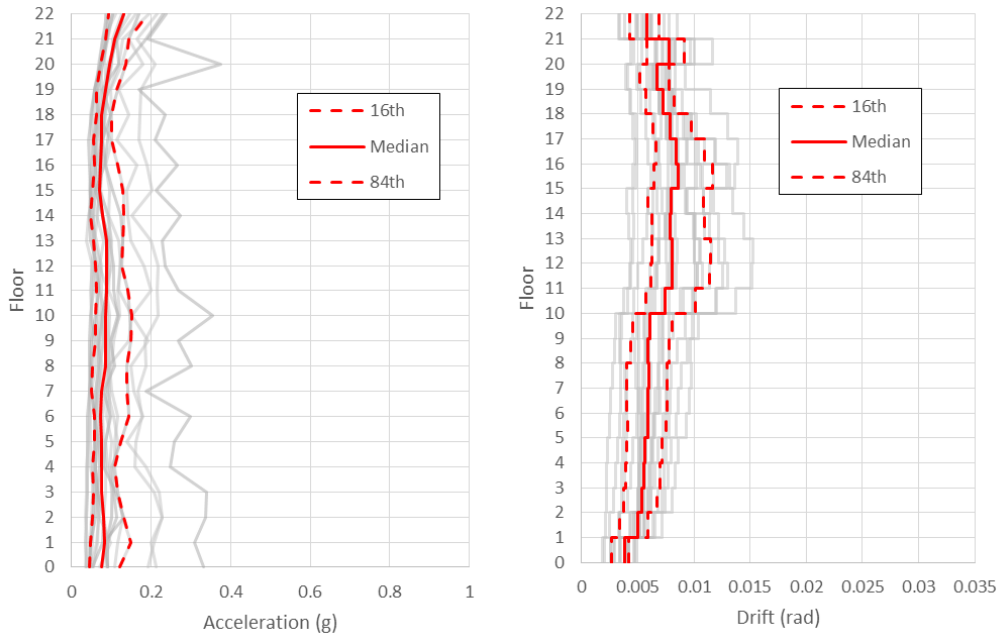

(a) (b)

Figure F.14. EW EDP for 5% in 50 years; Sa(4.0s) = 0.071g; (a) peak transient floor acceleration and (b) peak inter-storey drift

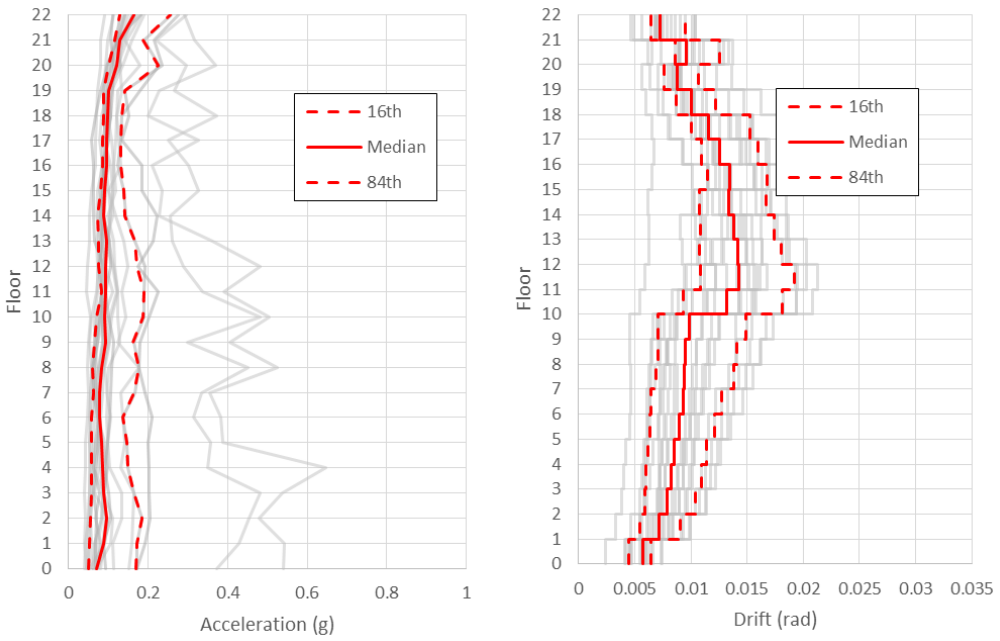

(a) (b)

Figure F.15. EW EDP for 2% in 50 years; Sa(4.0s) = 0.096g; (a) peak transient floor acceleration and (b) peak inter-storey drift

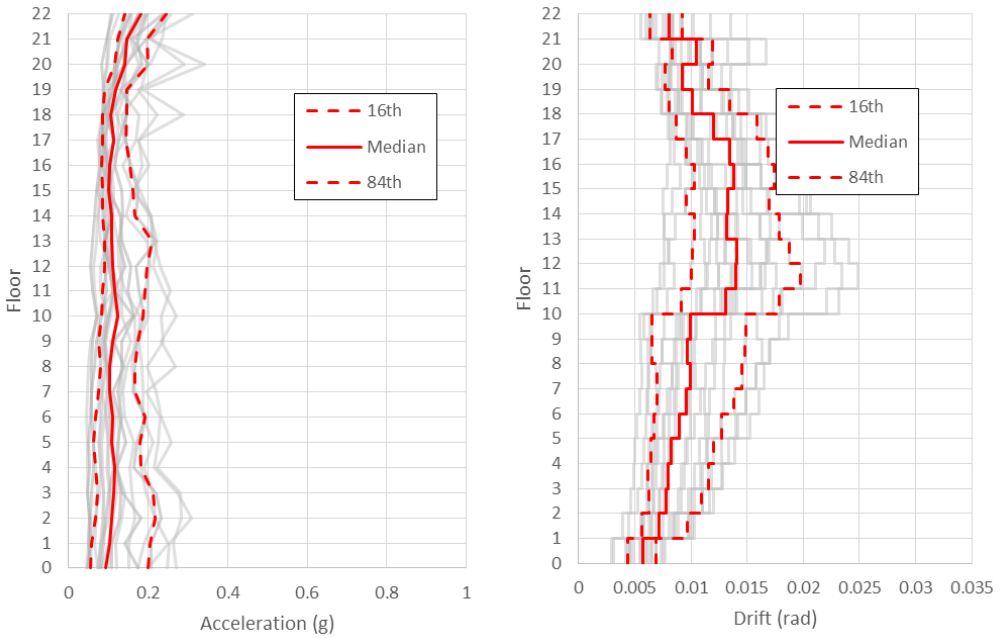

(a) (b)

Figure F.16. EW EDP for 1% in 50 years; Sa(4.0s) = 0.118g; (a) peak transient floor acceleration and (b) peak inter-storey drift

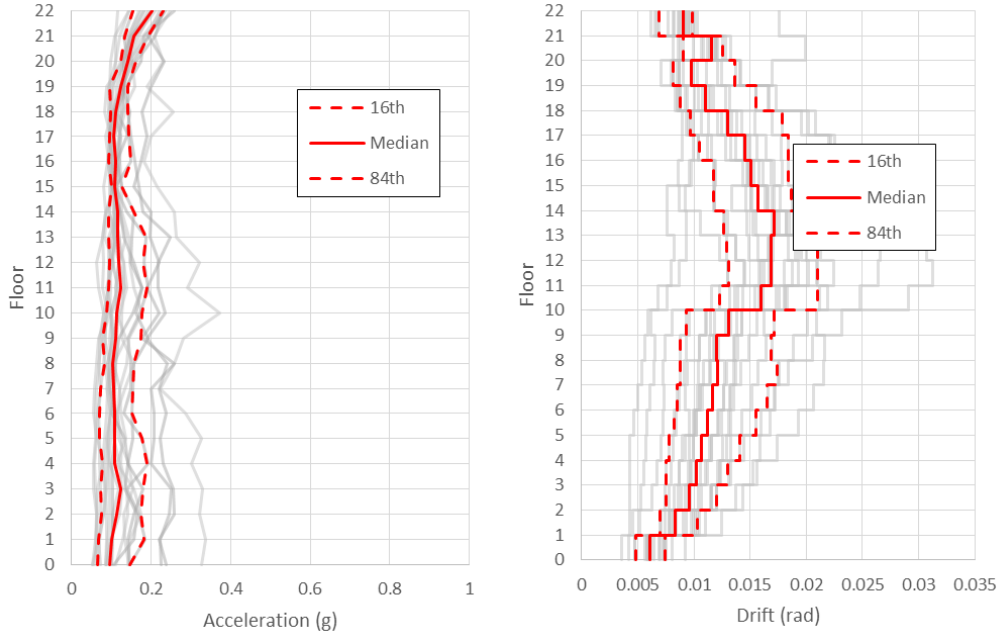

(a) (b)

Figure F.17. EW EDP for 0.5% in 50 years; Sa(4.0s) = 0.143g; (a) peak transient floor acceleration and (b) peak inter-storey drift

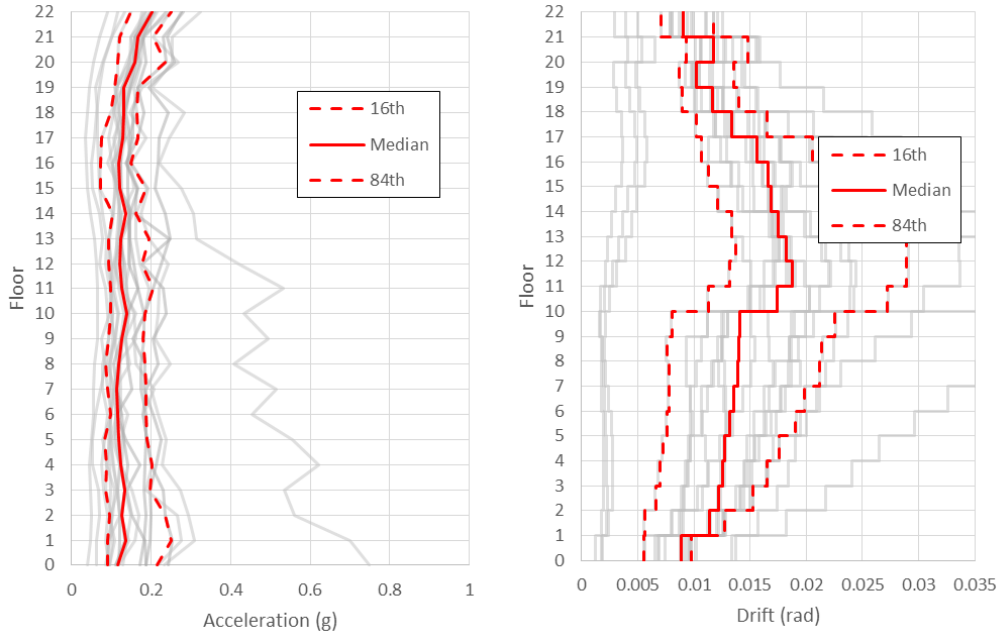

(a) (b)

Figure F.18. EW EDP for 0.2% in 50 years; Sa(4.0s) = 0.18g; (a) peak transient floor acceleration and (b) peak inter-storey drift

Appendix G

Structural Drawings

Appendix G: Structural drawings was included to provide a better understanding of the structural design of the case study building, the Pacific Tower. This drawings were obtained from the Christchurch City Council (Christchurch City Council 2016c).

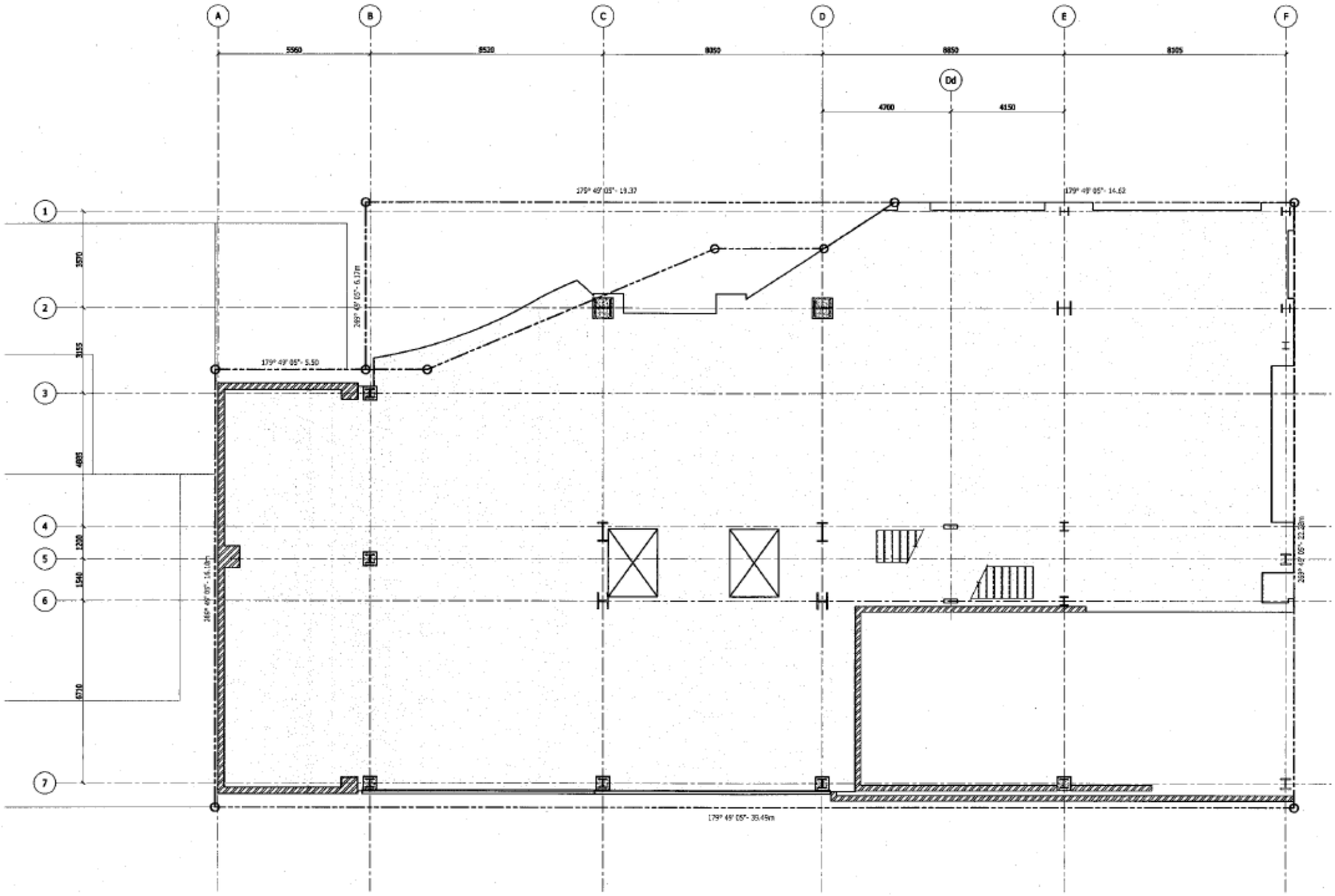

Figure G.1. Structural Plan Level 1 (Christchurch City Council 2016c)

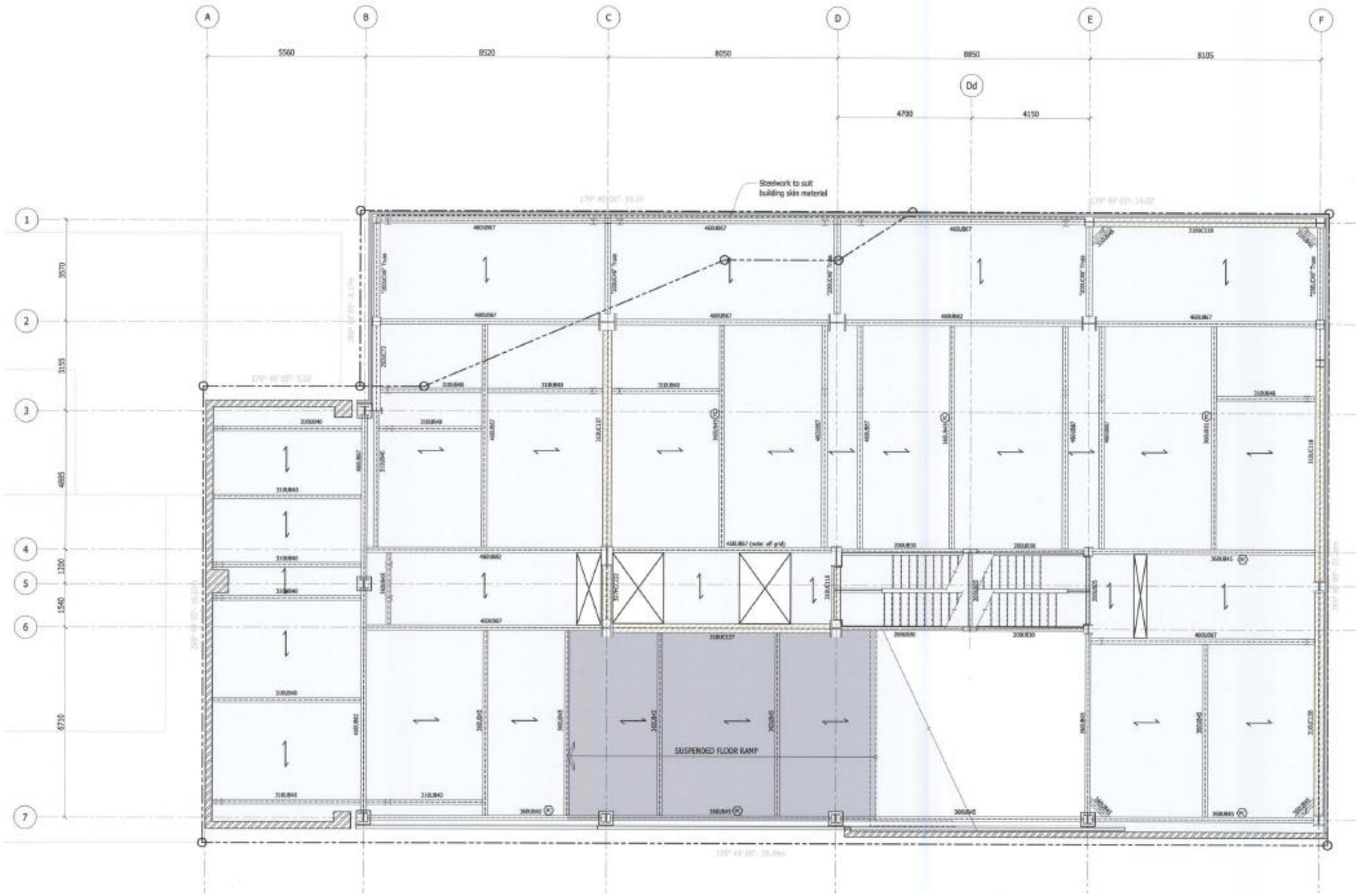

Figure G.2. Structural Plan Level 2 (Christchurch City Council 2016c)

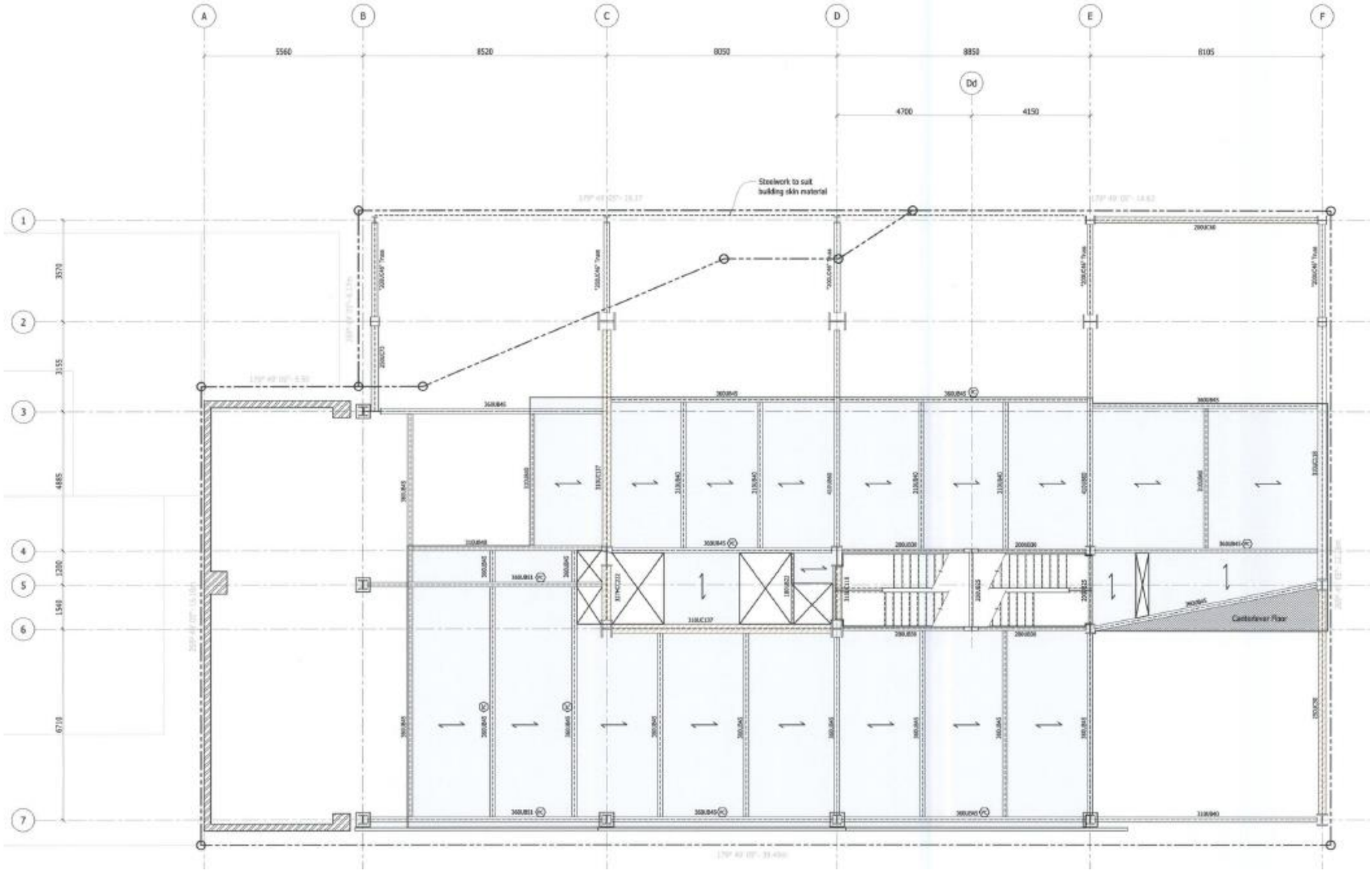

Figure G.3. Structural Plan Level 3 (Christchurch City Council 2016c)

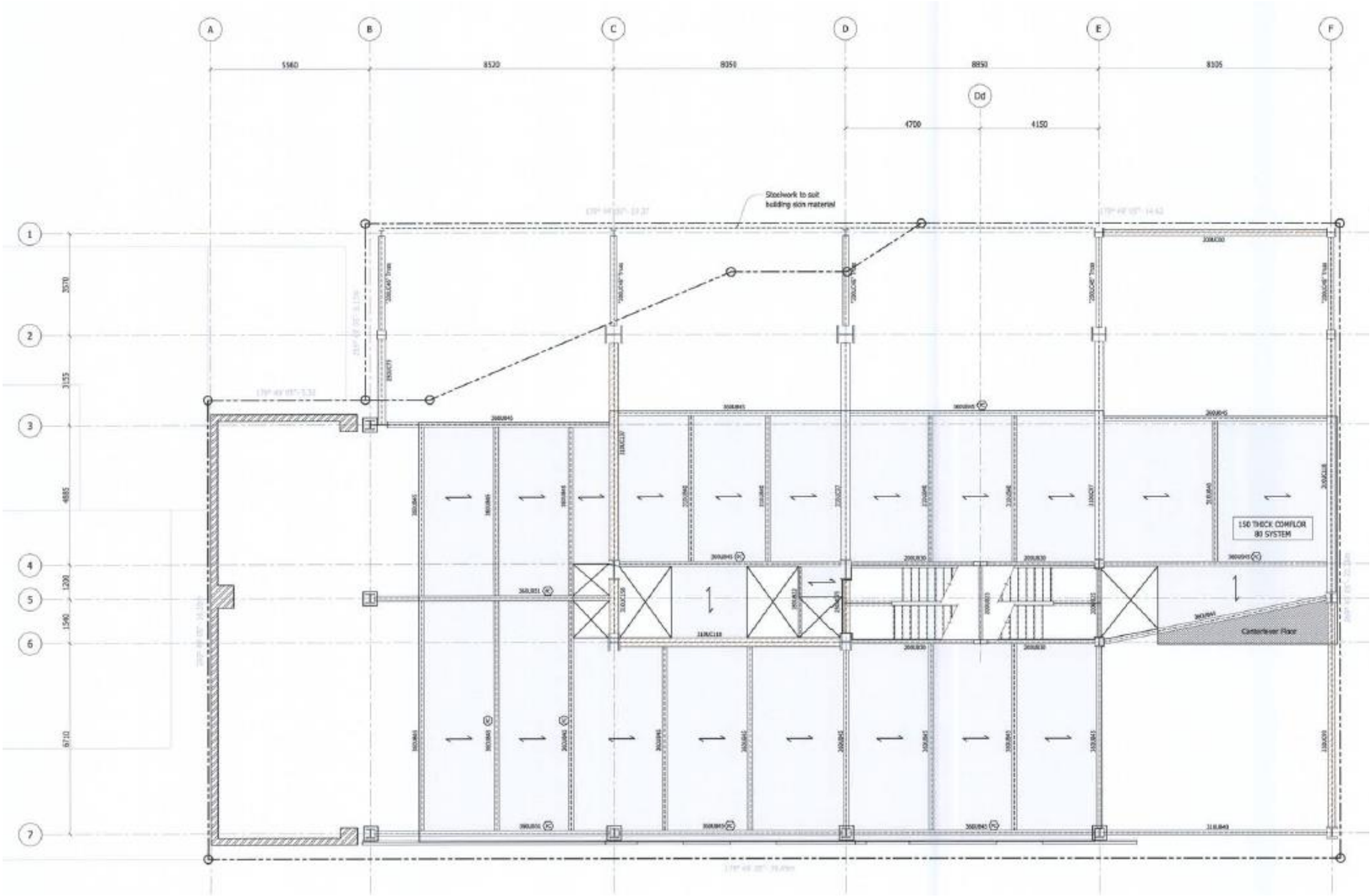

Figure G.4. Structural Plan Level 4 (Christchurch City Council 2016c)

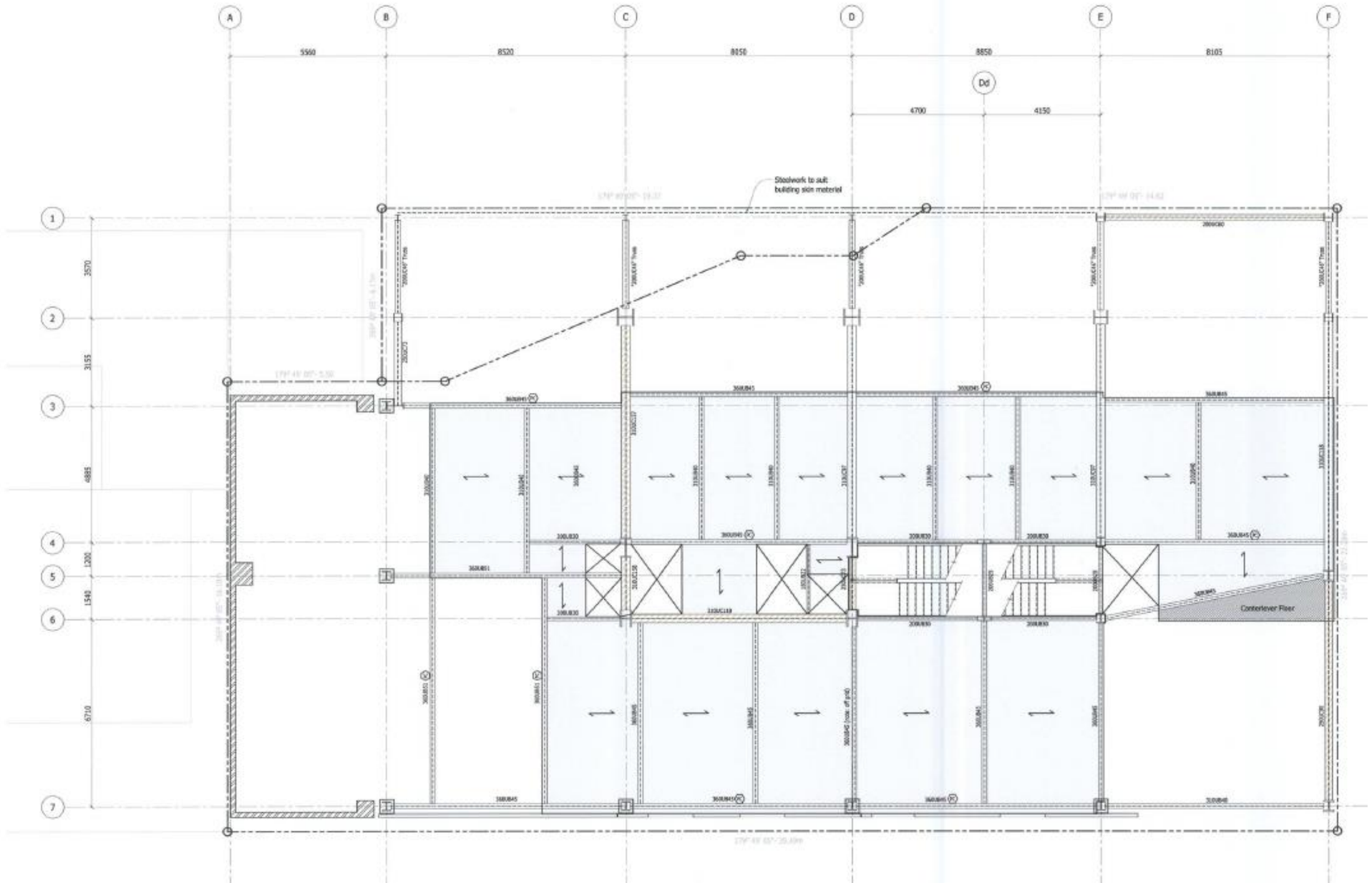

Figure G.5. Structural Plan Level 5 (Christchurch City Council 2016c)

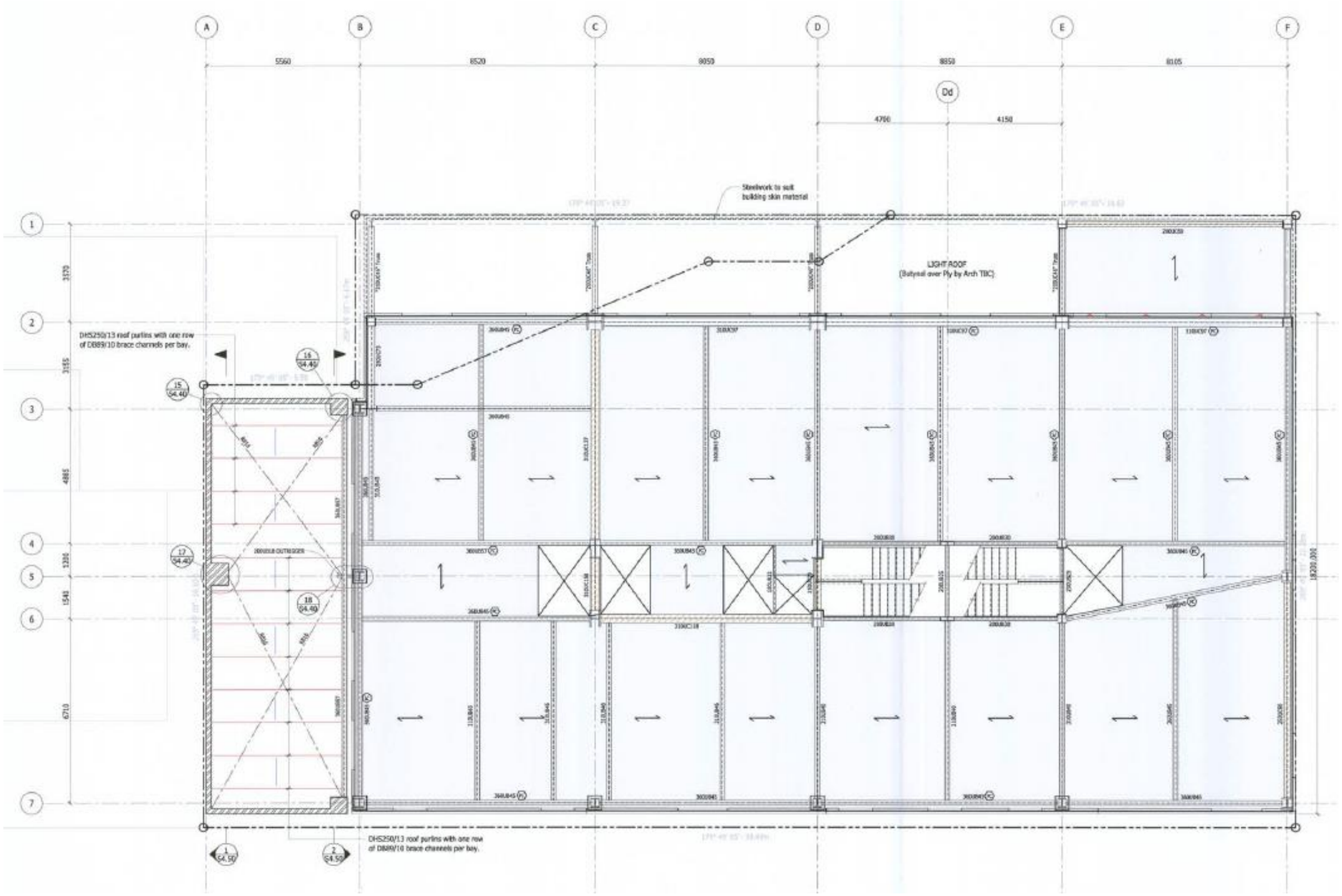

Figure G.6. Structural Plan Level 6 (Christchurch City Council 2016c)

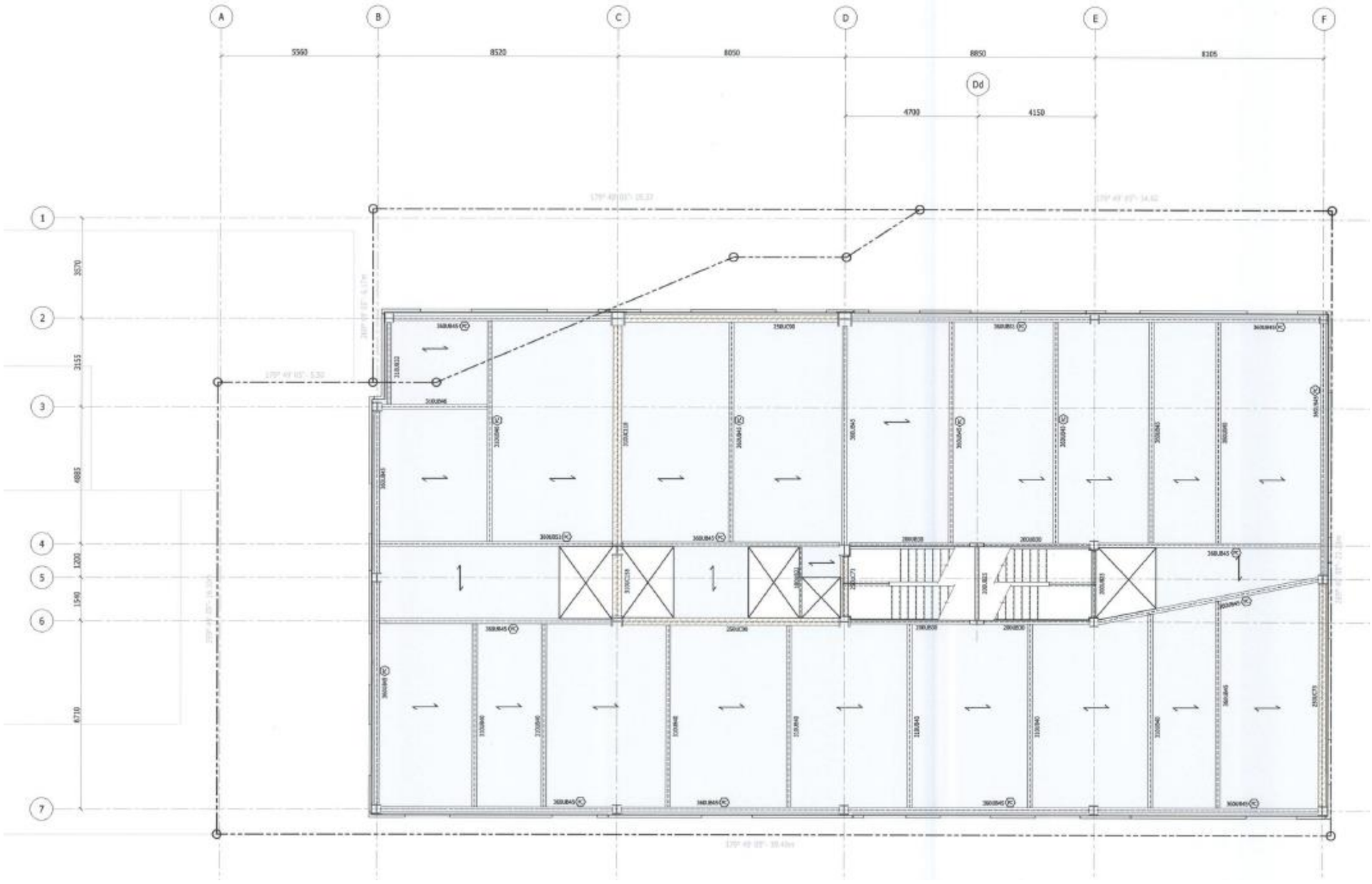

Figure G.7. Structural Plan Level 7 (Christchurch City Council 2016c)

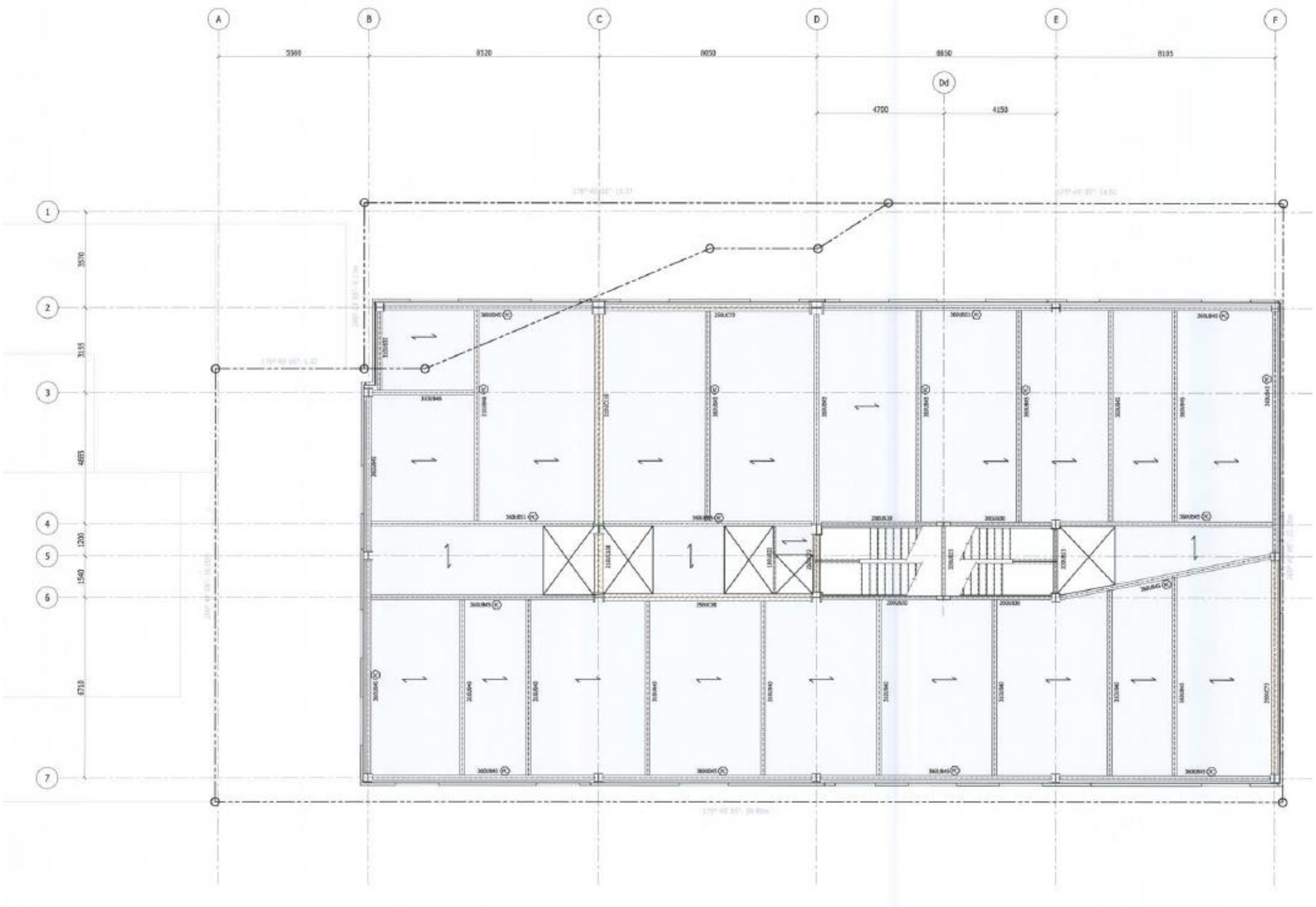

Figure G.8. Structural Plan Level 8 (Christchurch City Council 2016c)

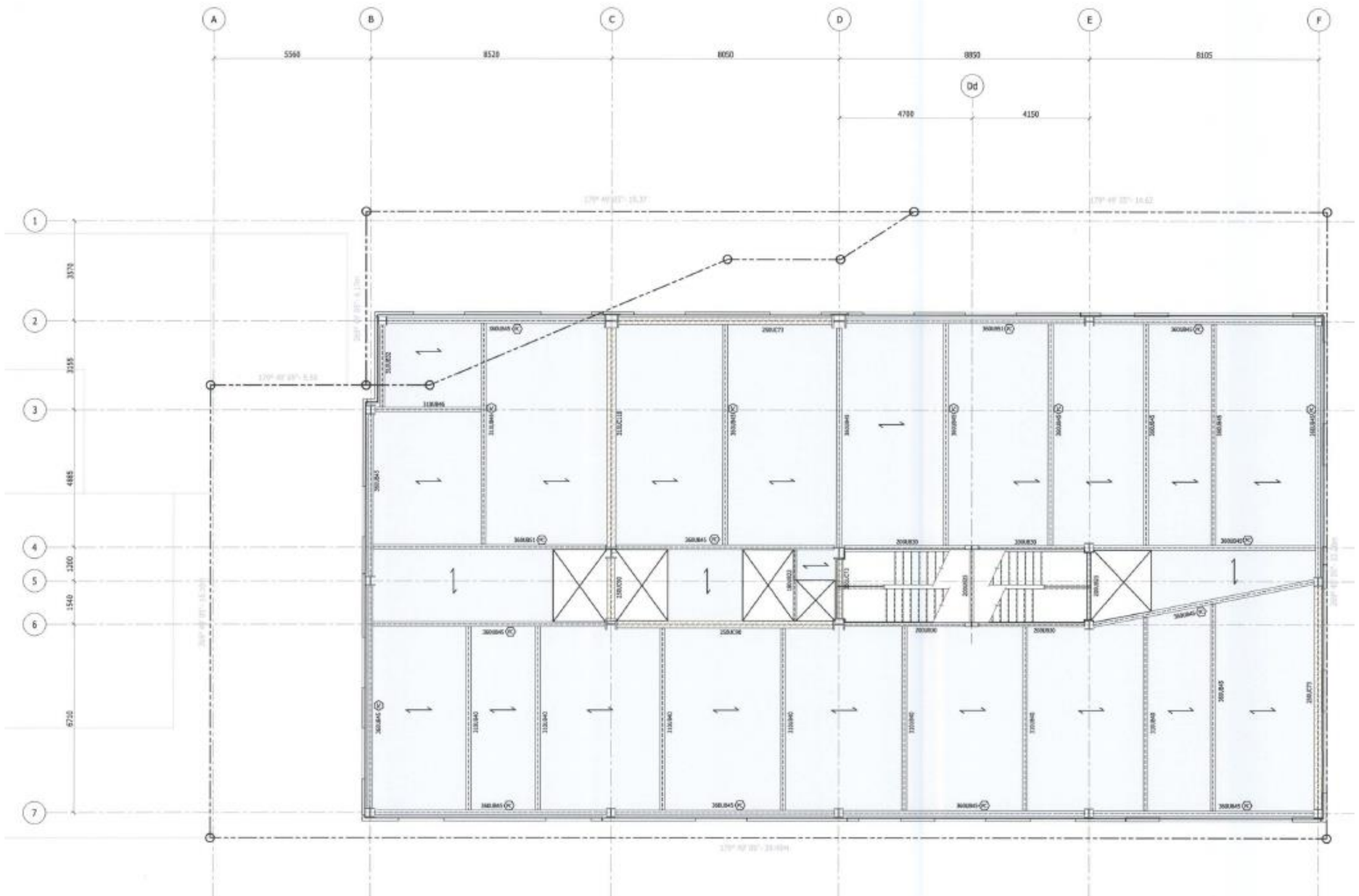

Figure G.9. Structural Plan Level 9 (Christchurch City Council 2016c)

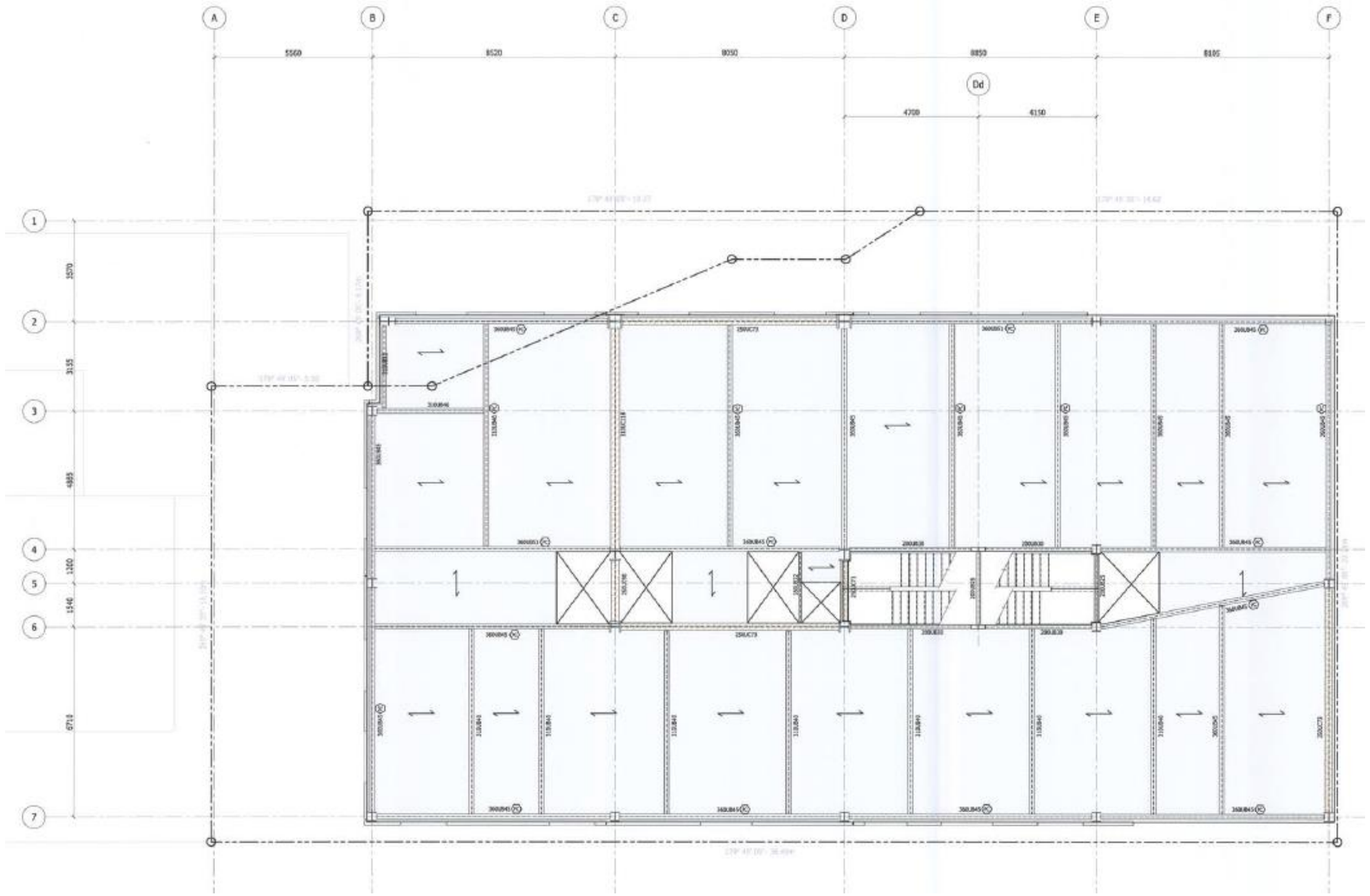

Figure G.10. Structural Plan Level 10 (Christchurch City Council 2016c)

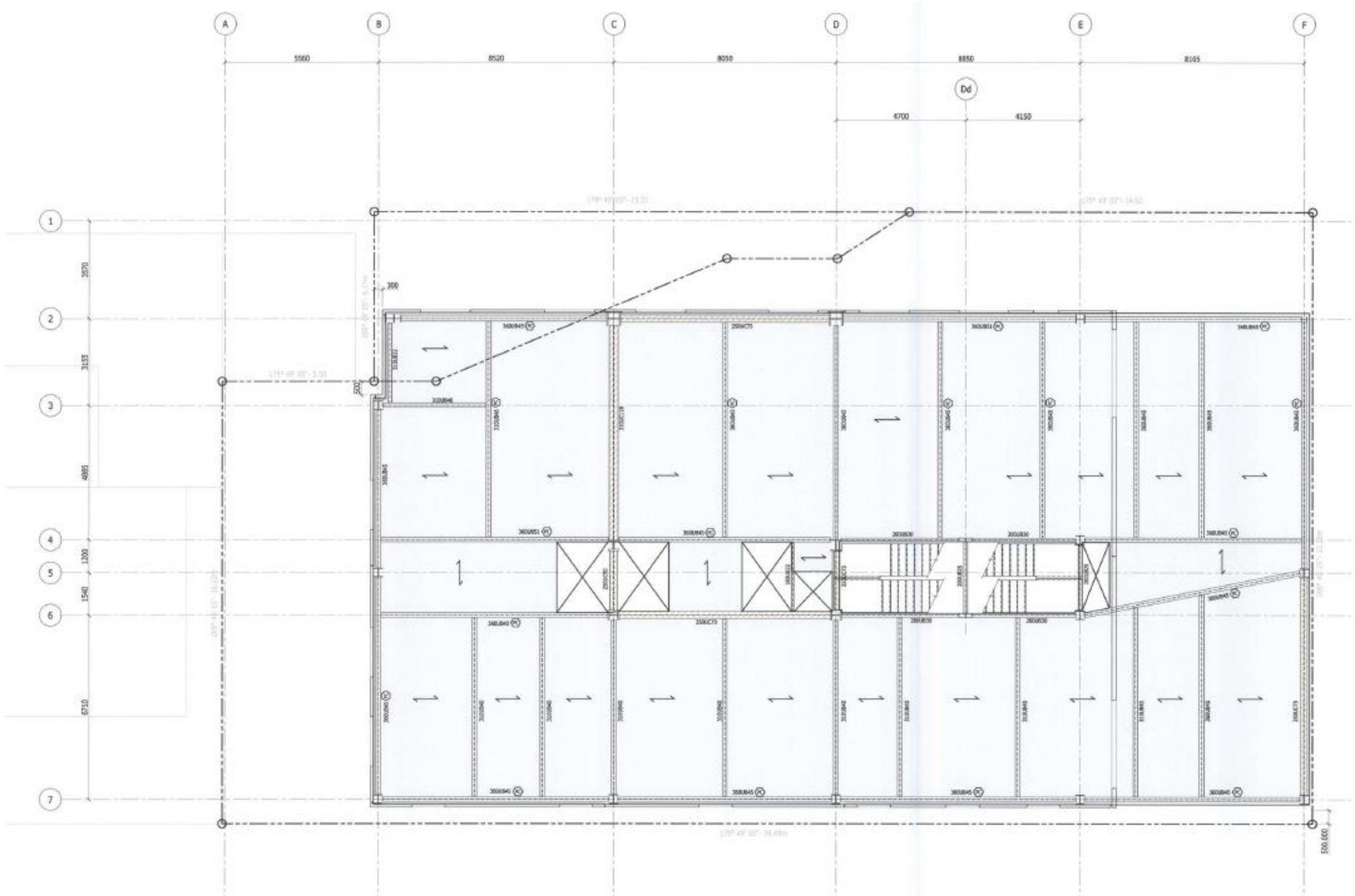

Figure G.11. Structural Plan Level 11 (Christchurch City Council 2016c)

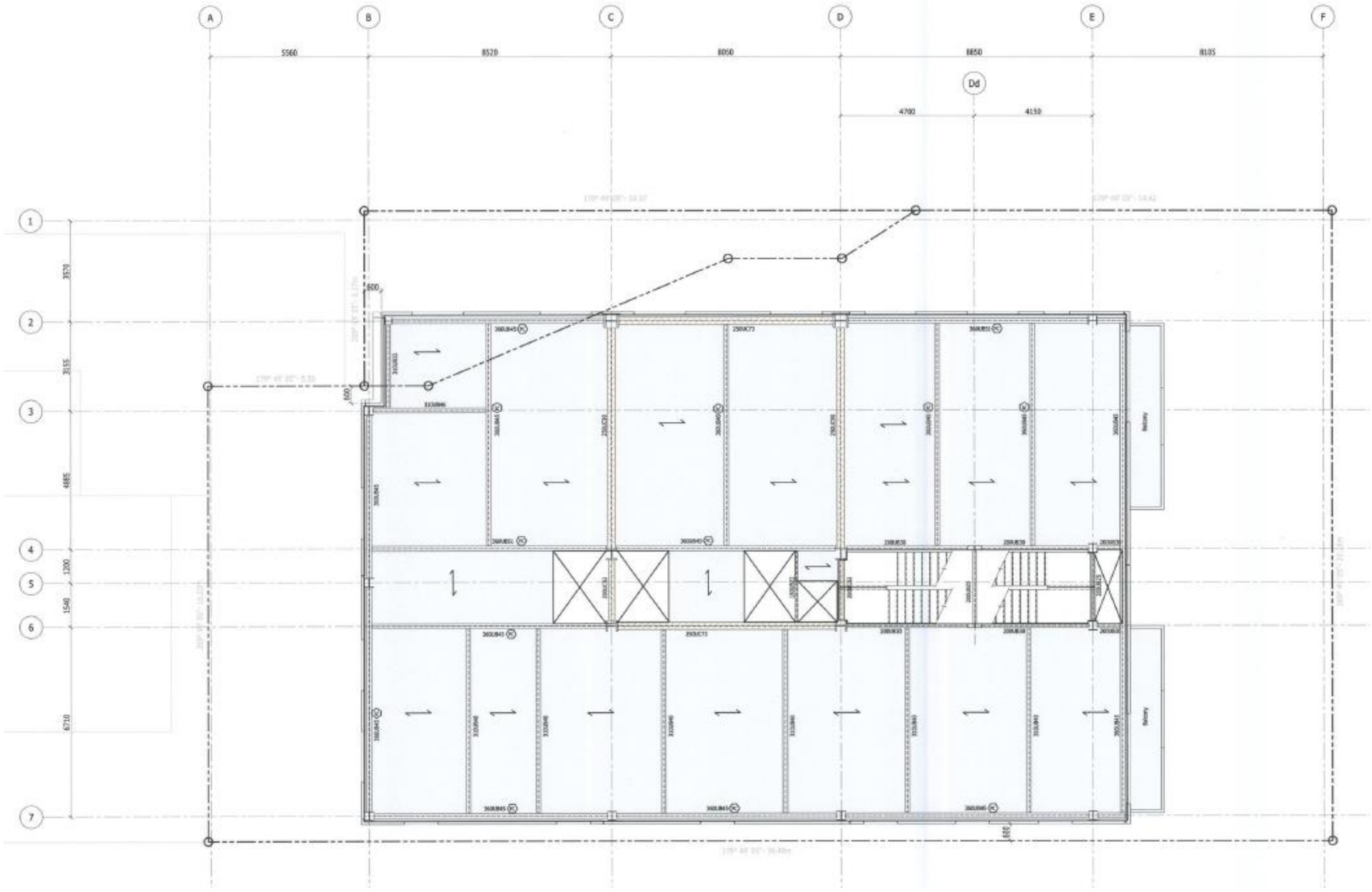

Figure G.12. Structural Plan Level 12 (Christchurch City Council 2016c)

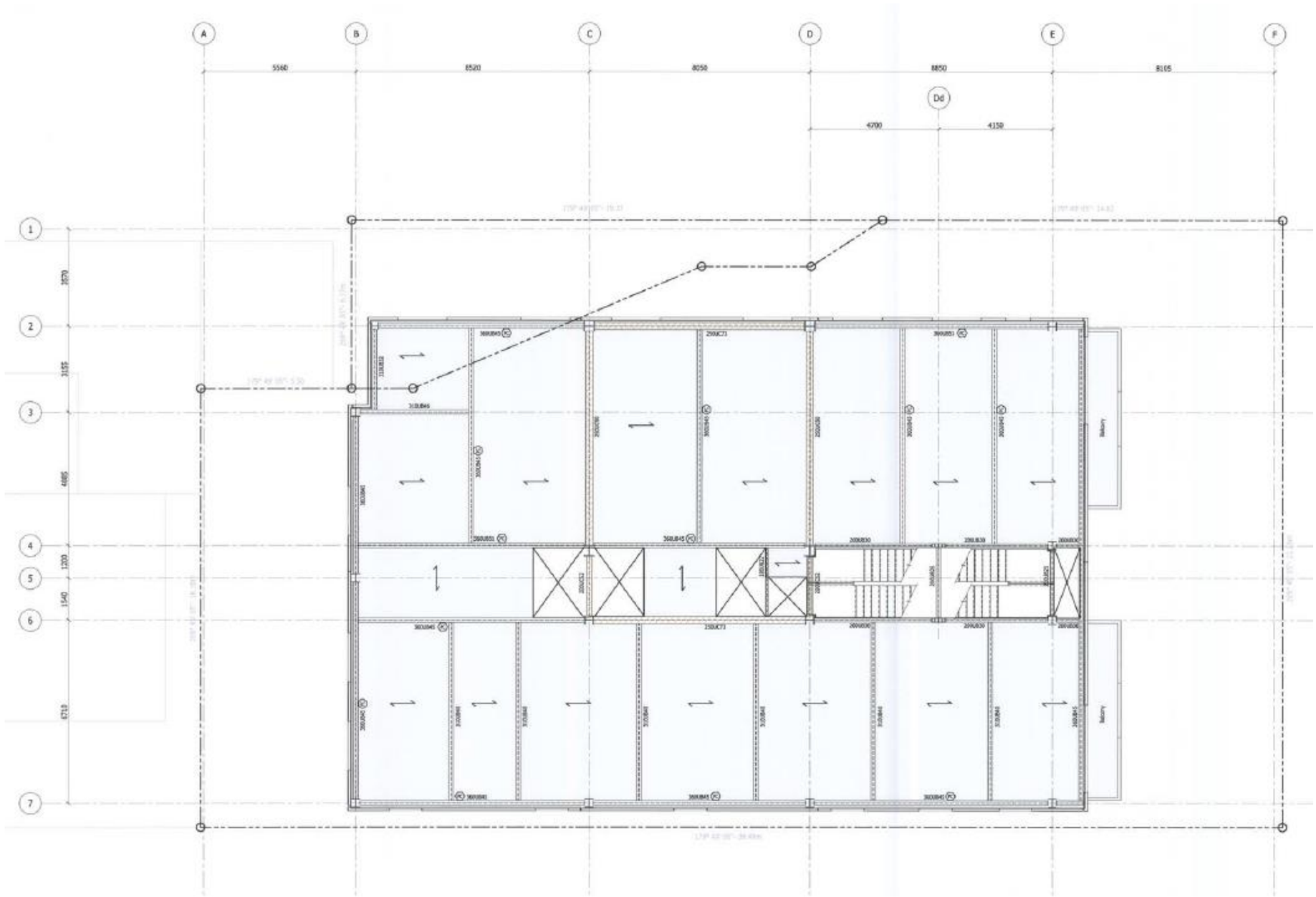

Figure G.13. Structural Plan Level 13 (Christchurch City Council 2016c)

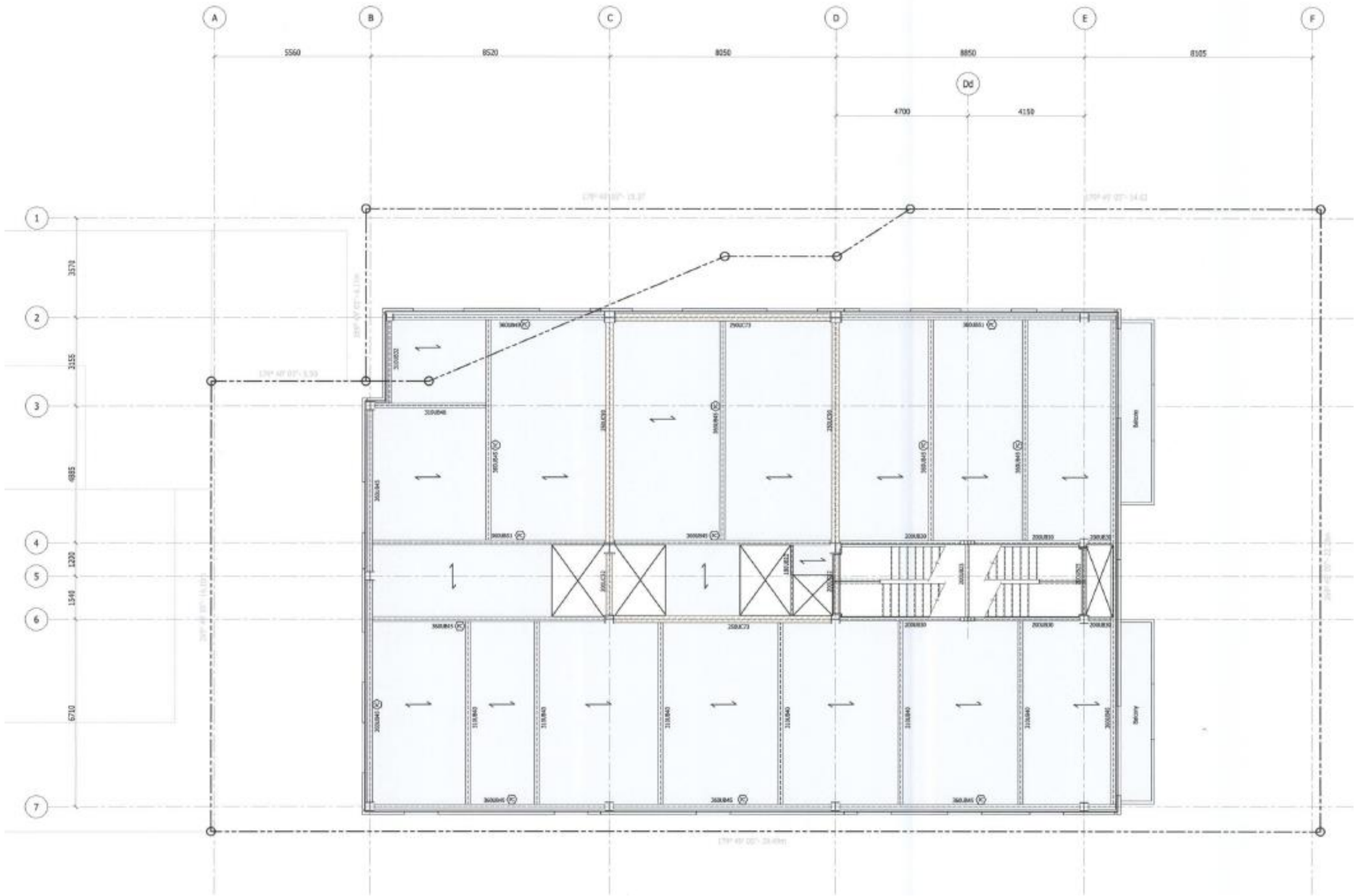

Figure G.14. Structural Plan Level 14 (Christchurch City Council 2016c)

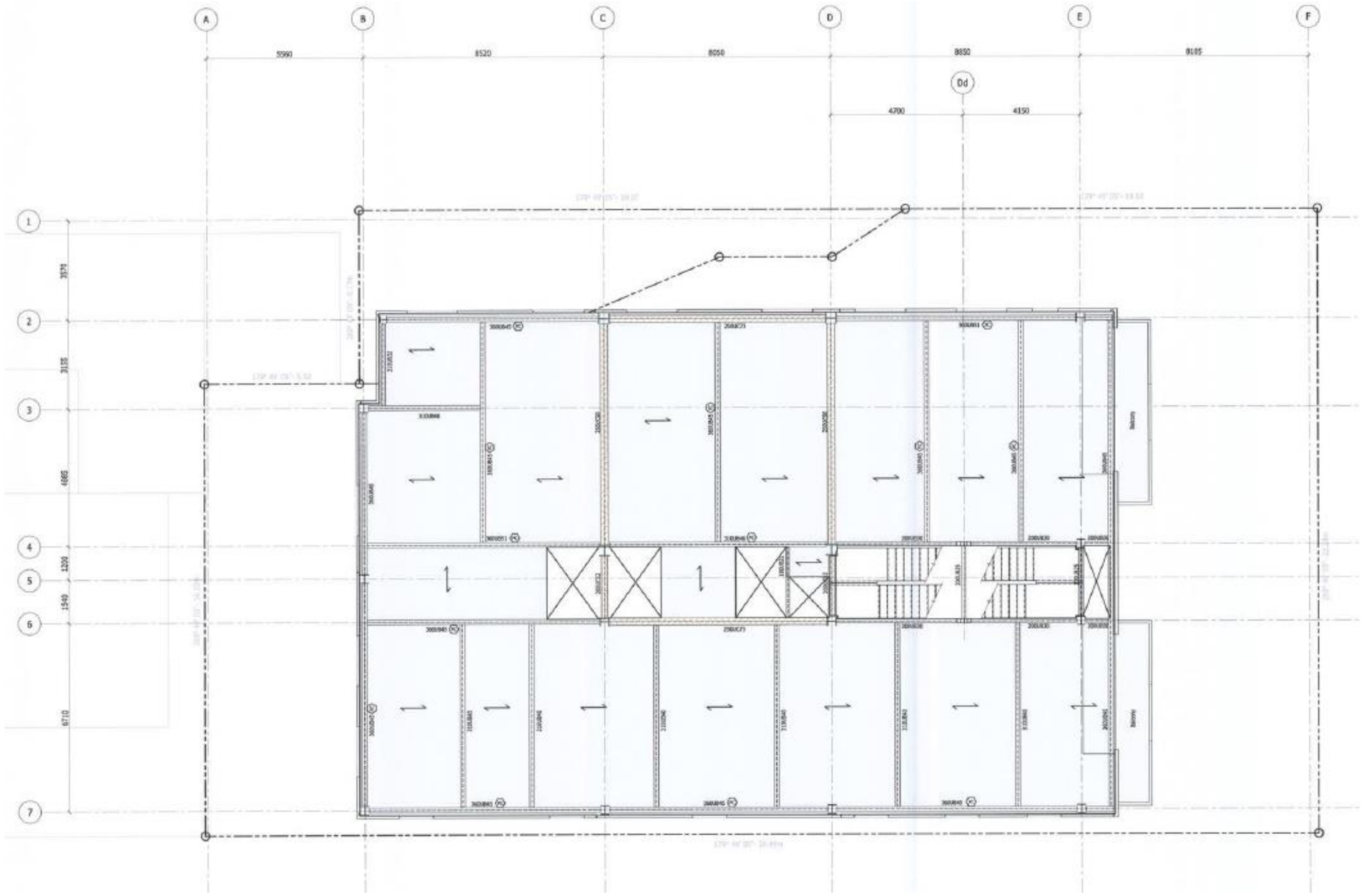

Figure G.15. Structural Plan Level 15 (Christchurch City Council 2016c)

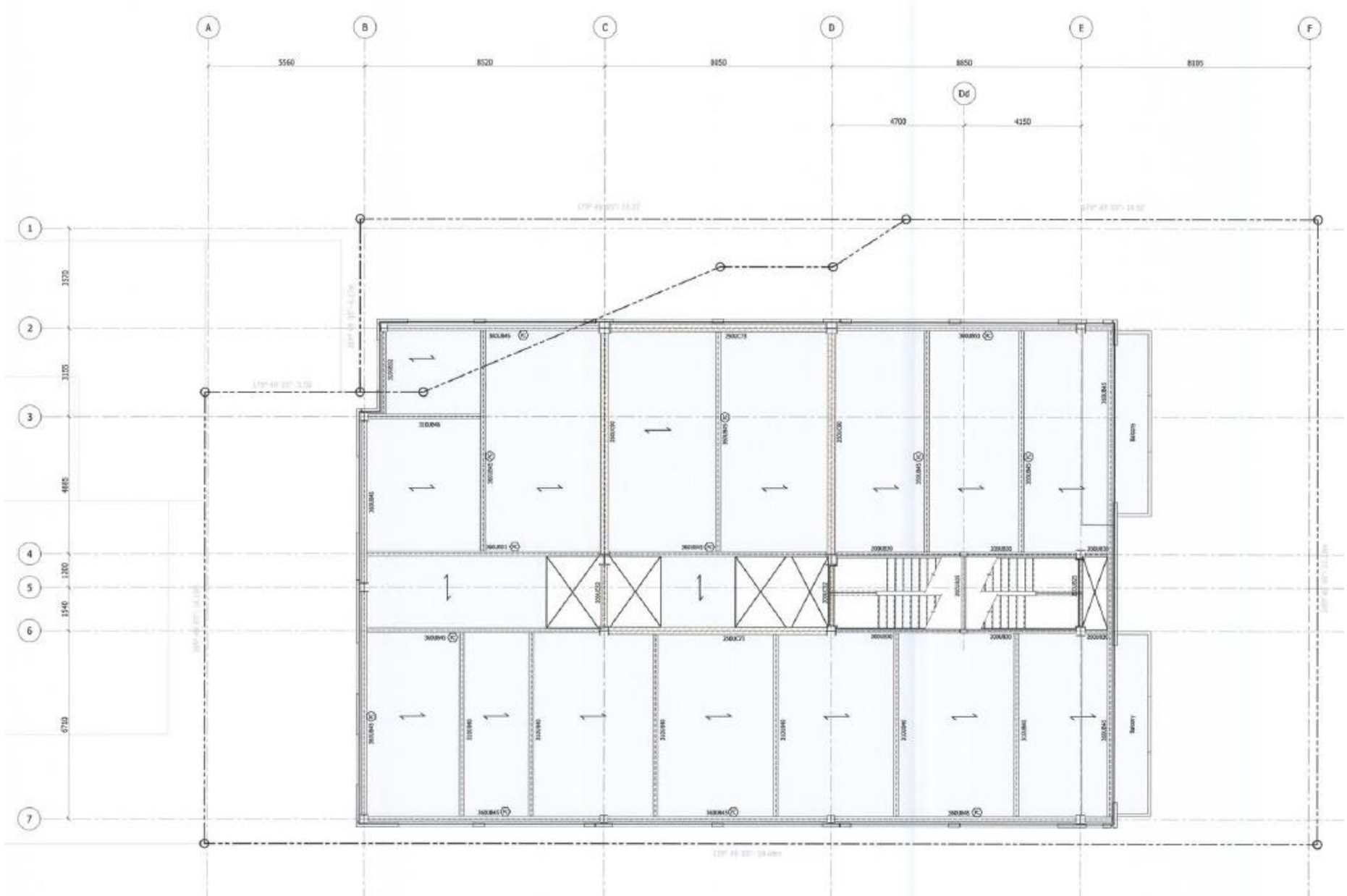

Figure G.16. Structural Plan Level 16 (Christchurch City Council 2016c)

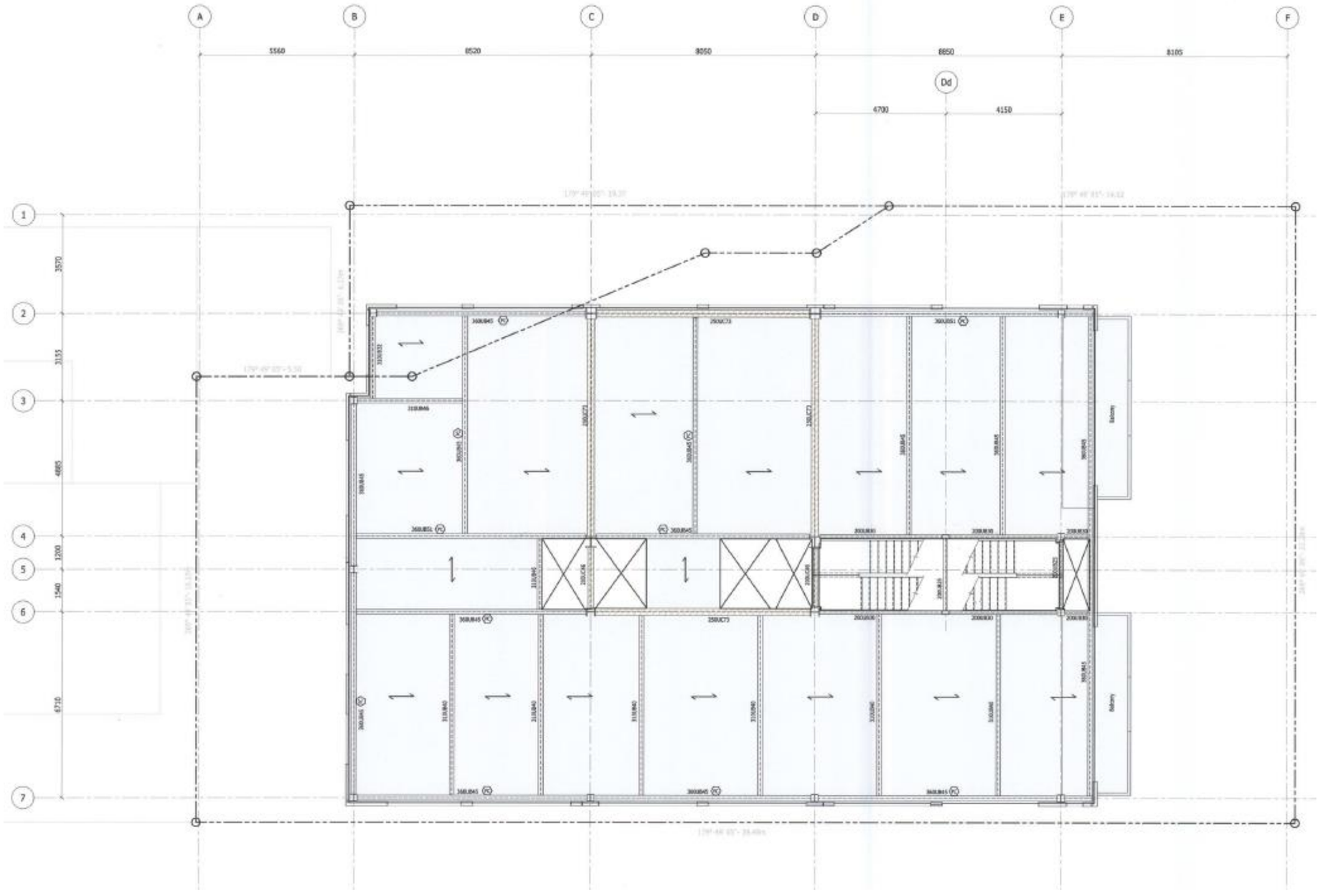

Figure G.17. Structural Plan Level 17 (Christchurch City Council 2016c)

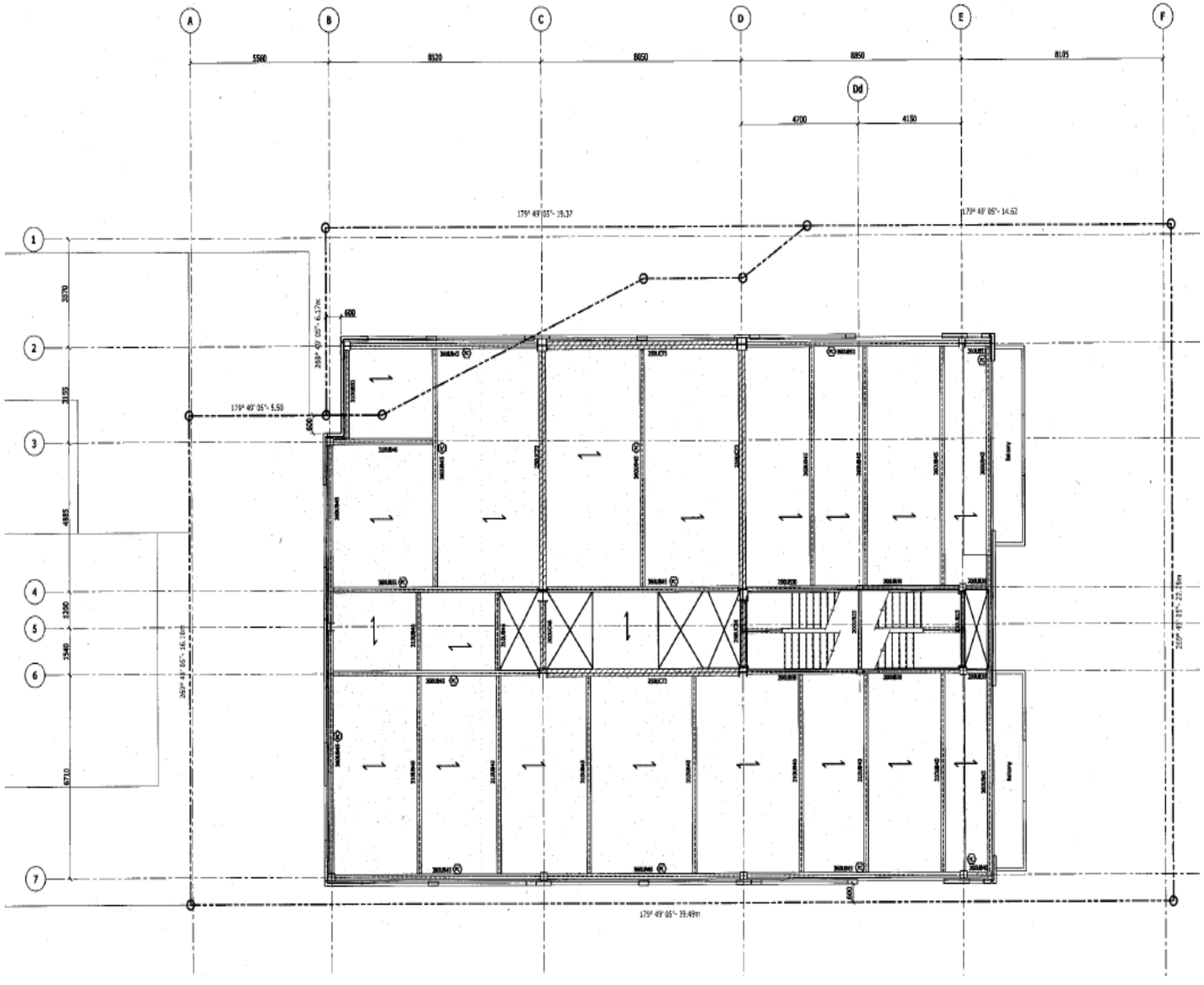

Figure G.18. Structural Plan Level 18 (Christchurch City Council 2016c)

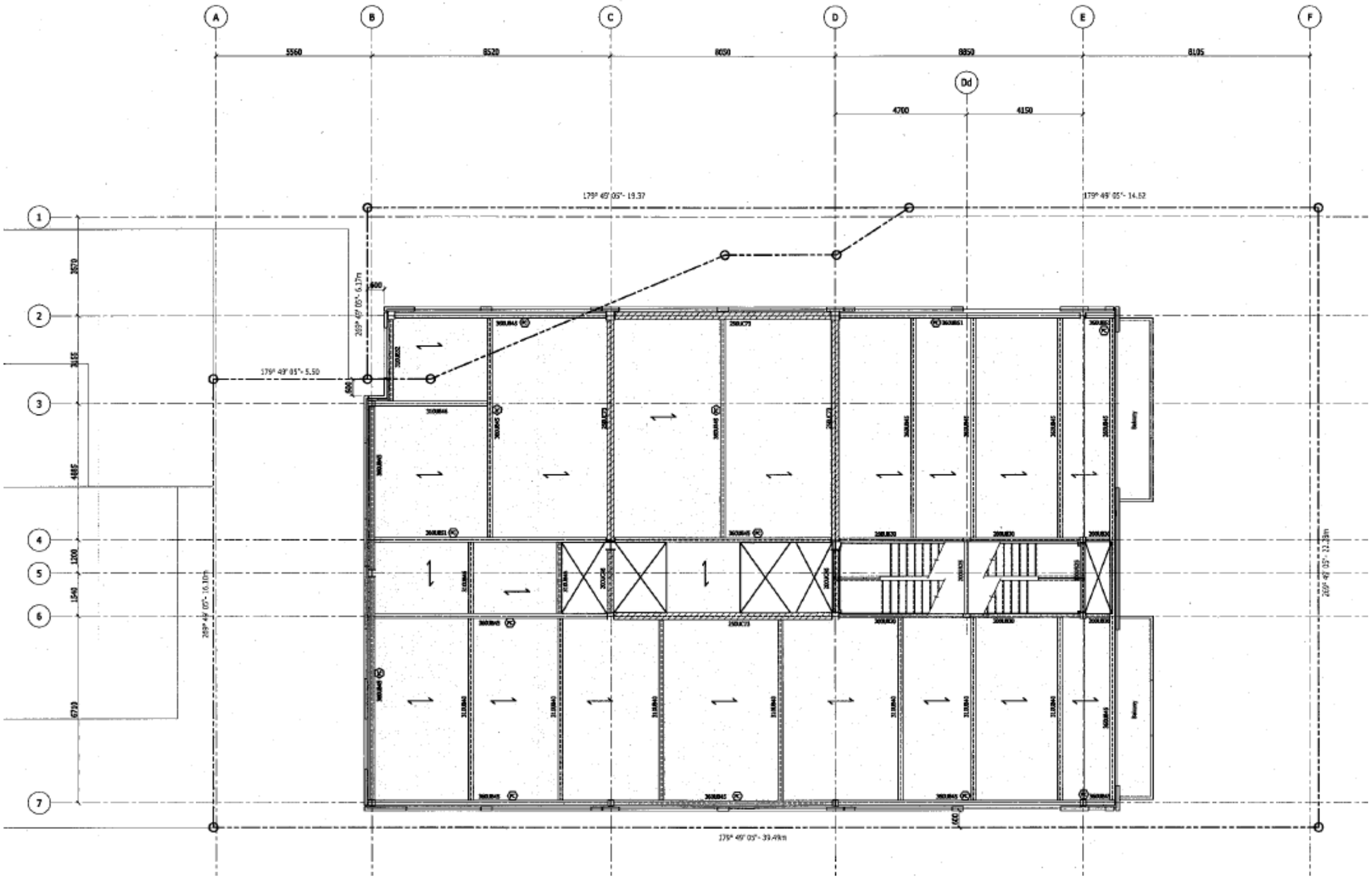

Figure G.19. Structural Plan Level 19 (Christchurch City Council 2016c)

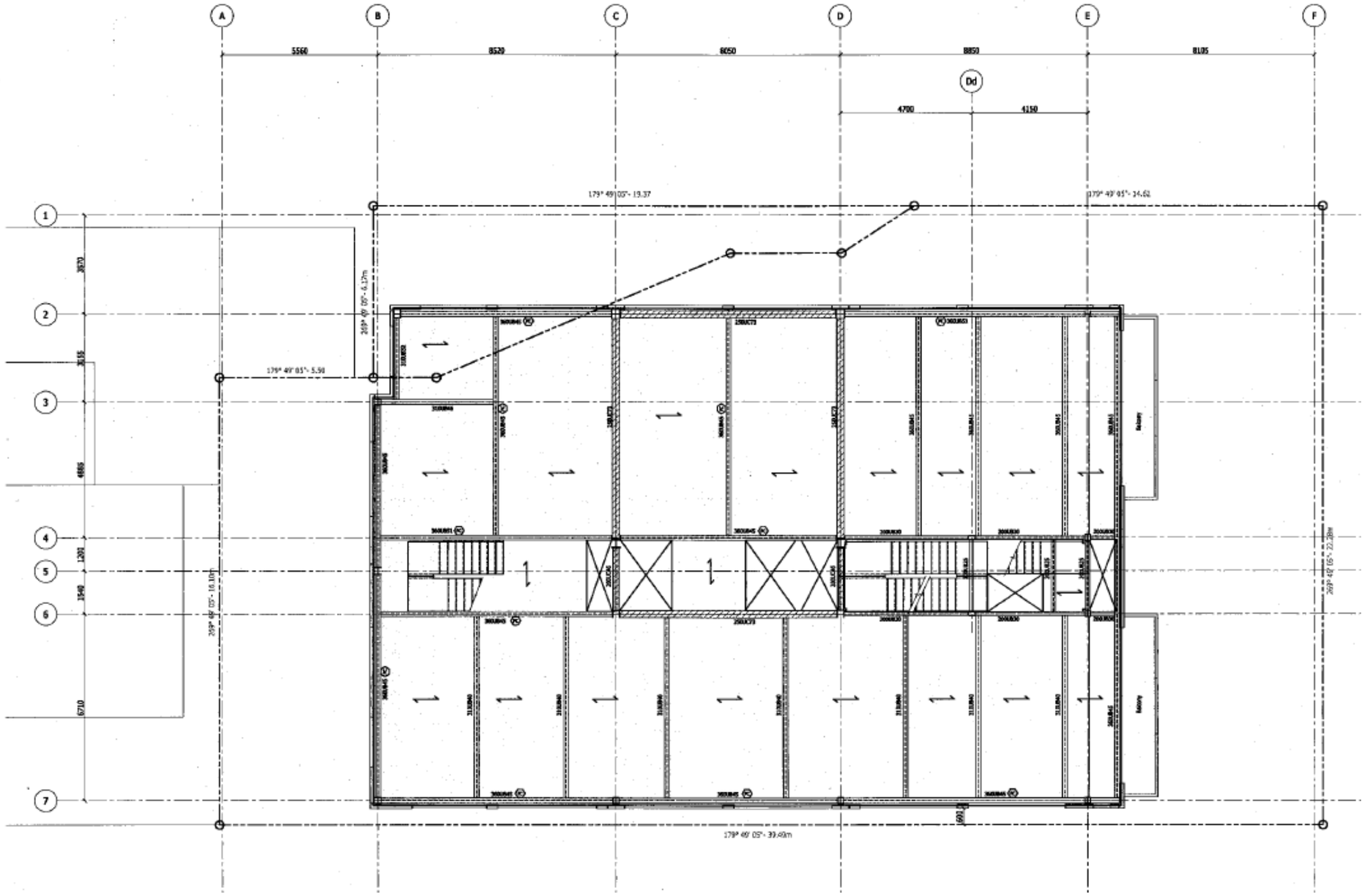

Figure G.20. Structural Plan Level 20 (Christchurch City Council 2016c)

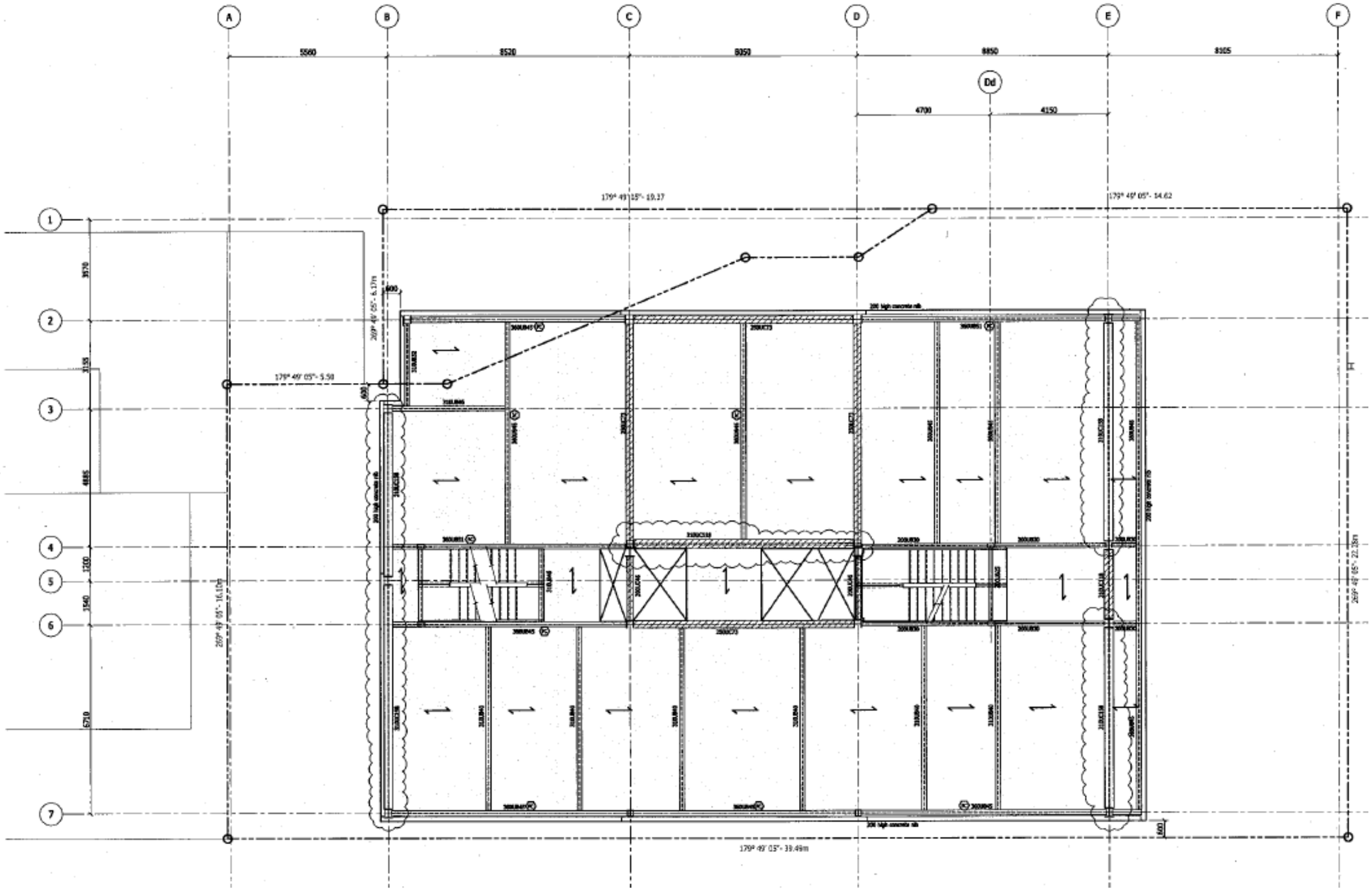

Figure G.21. Structural Plan Level 21 (Christchurch City Council 2016c)

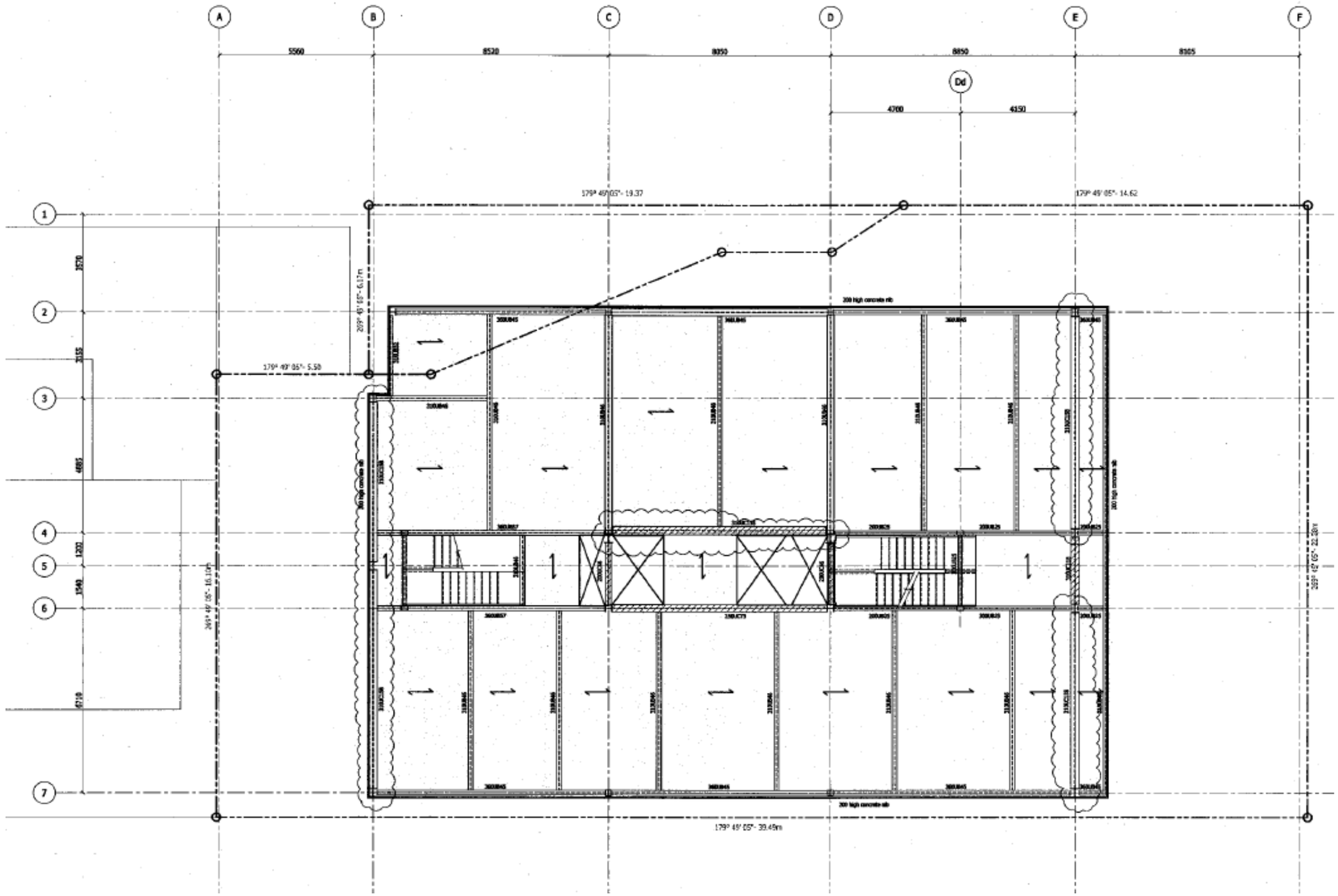

Figure G.22. Structural Plan Level 22 (Christchurch City Council 2016c)

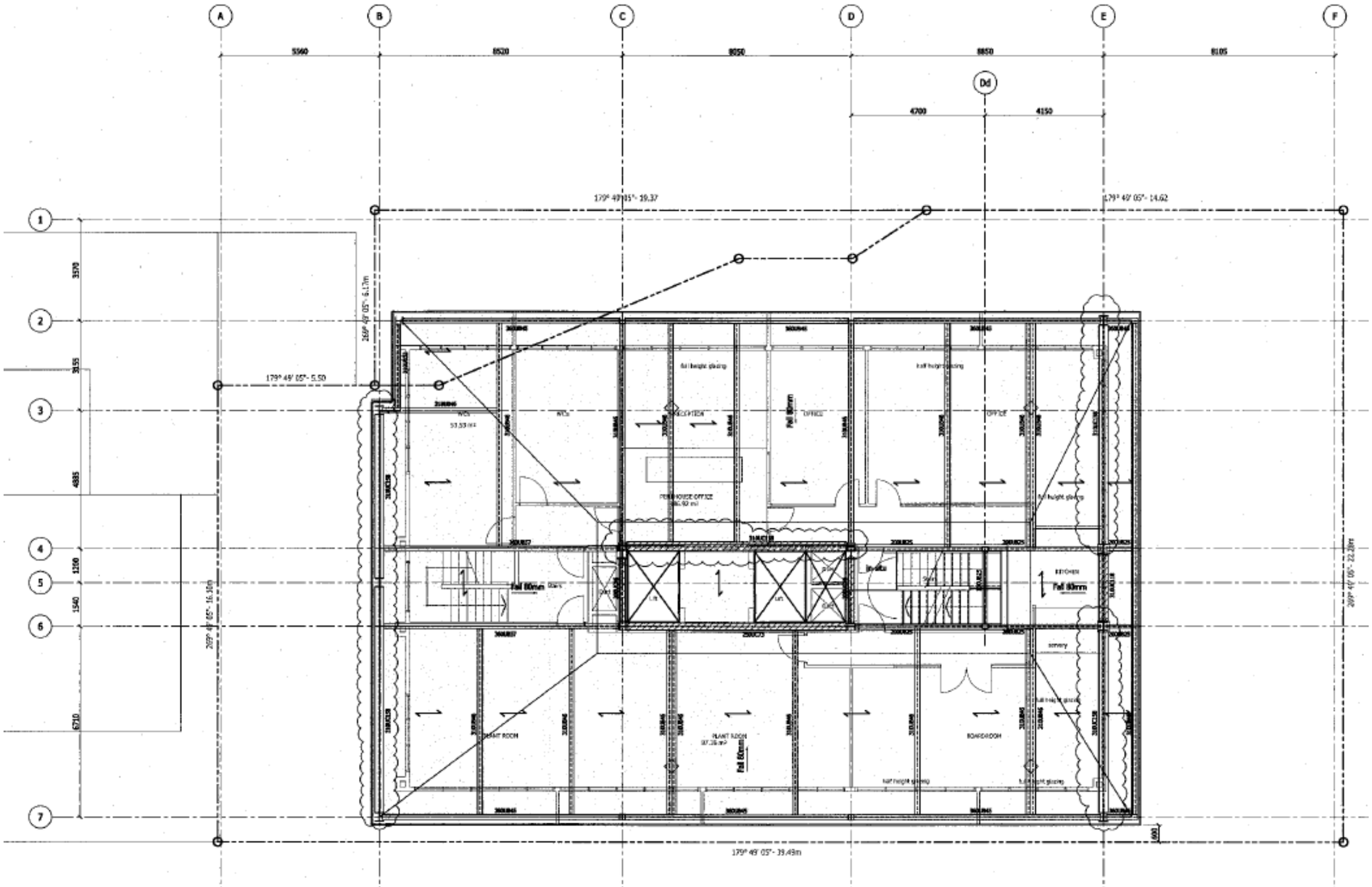

Figure G.23. Structural Plan – Rooftop (Christchurch City Council 2016c)

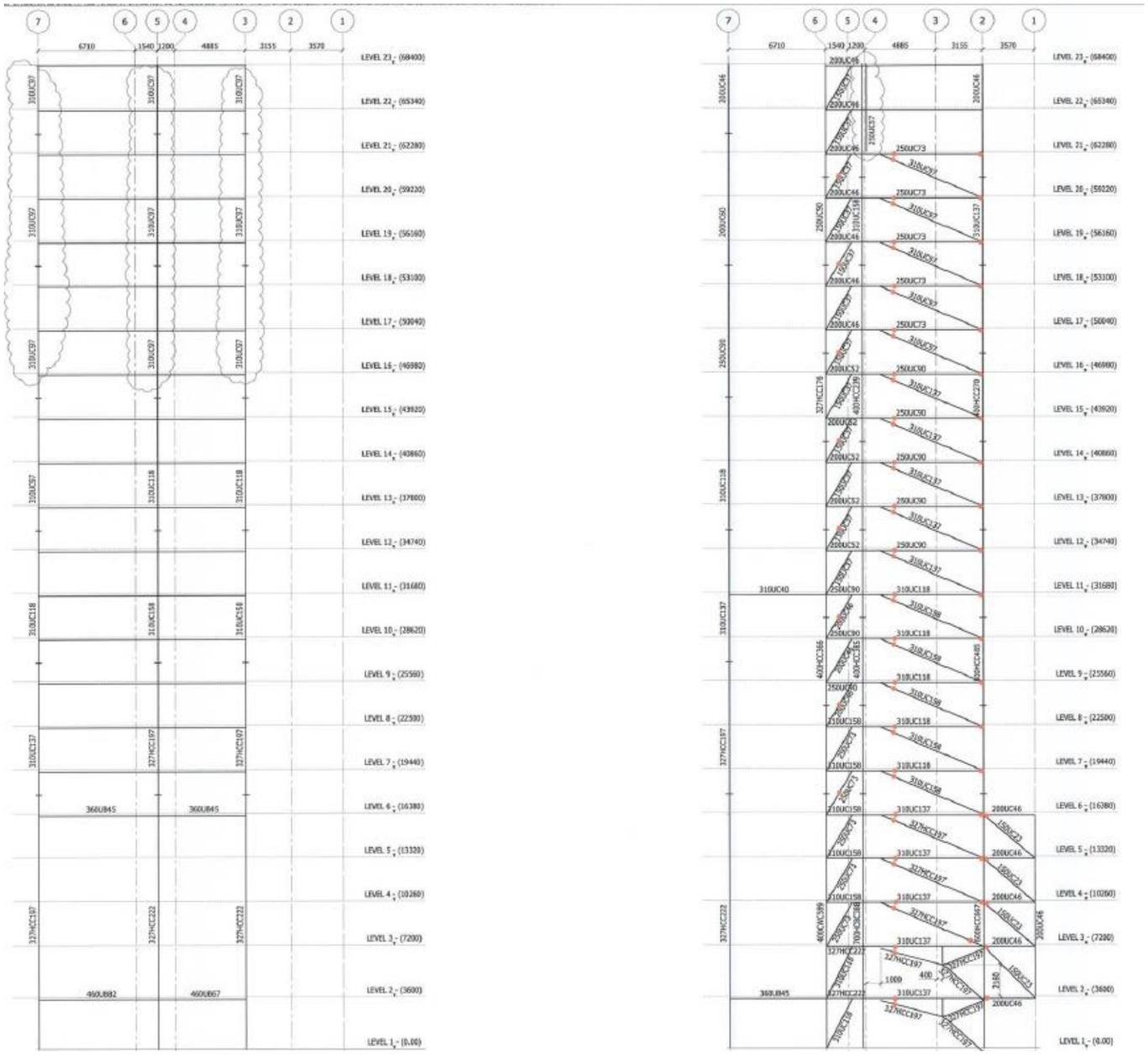

Figure G.24. Structural Elevation Grids B and C (Christchurch City Council 2016c)

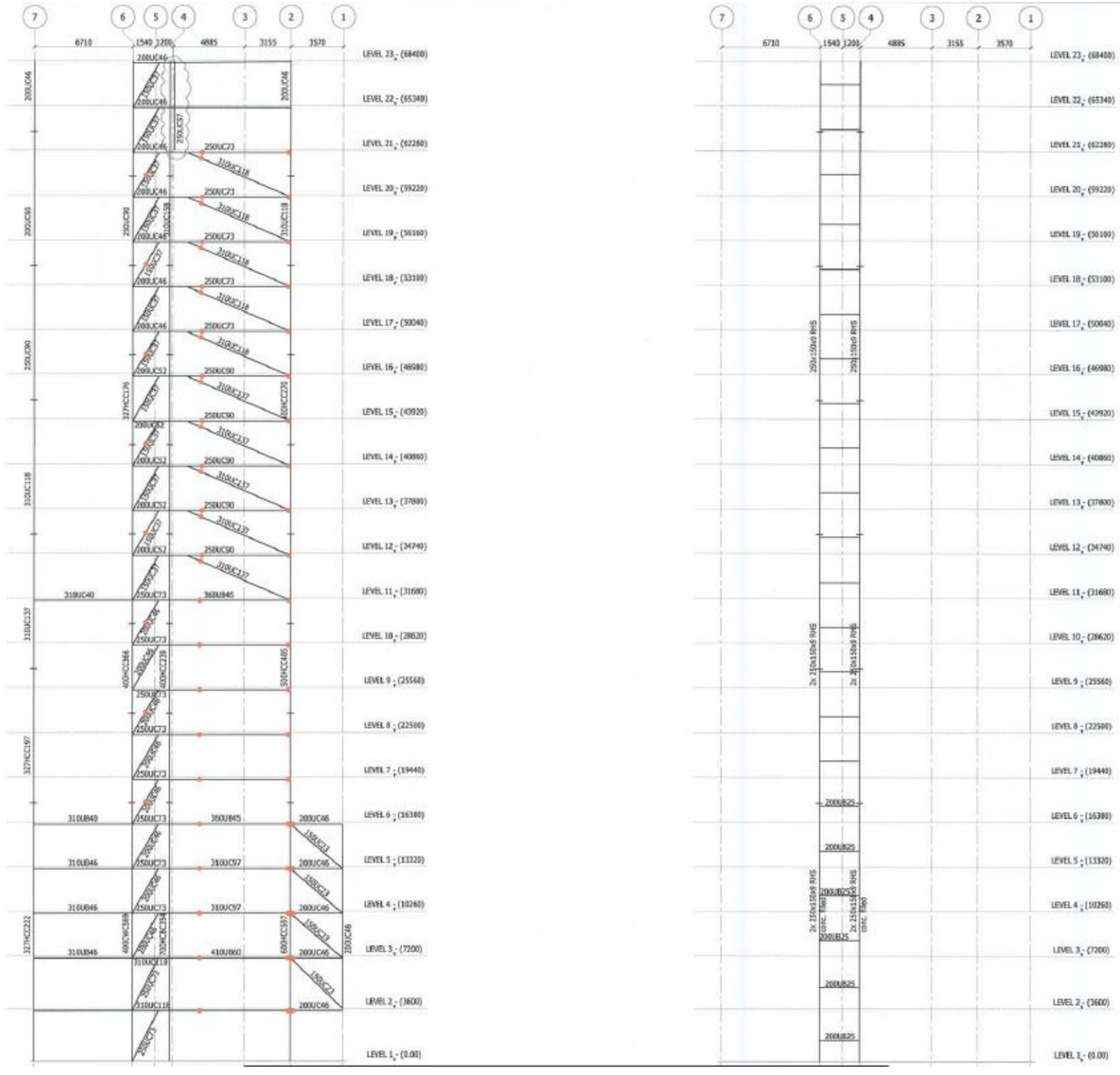

Figure G.25. Structural Elevation Grids D and Dd (Christchurch City Council 2016c)

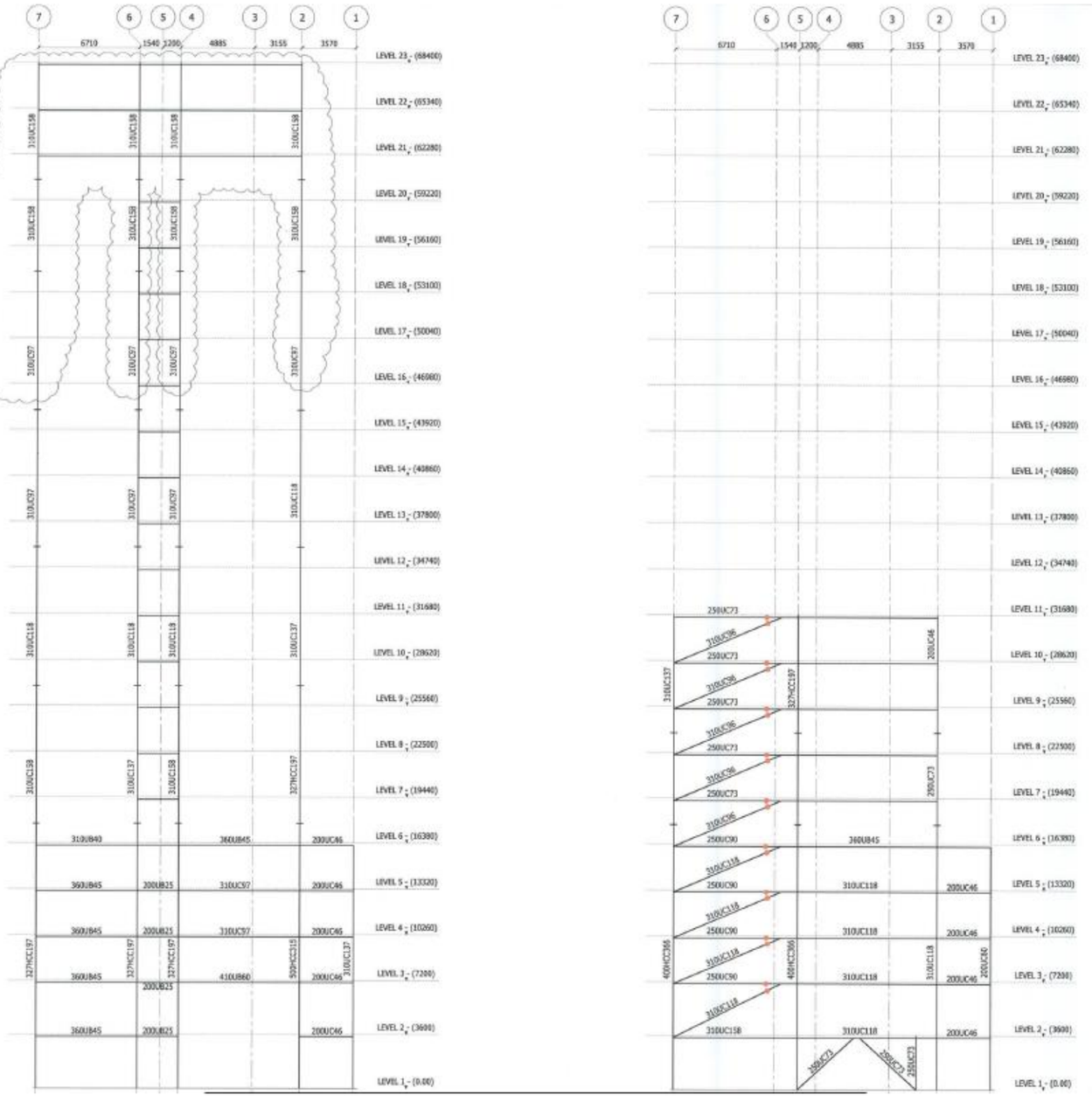

Figure G.26. Structural Elevation Grids E and F (Christchurch City Council 2016c)

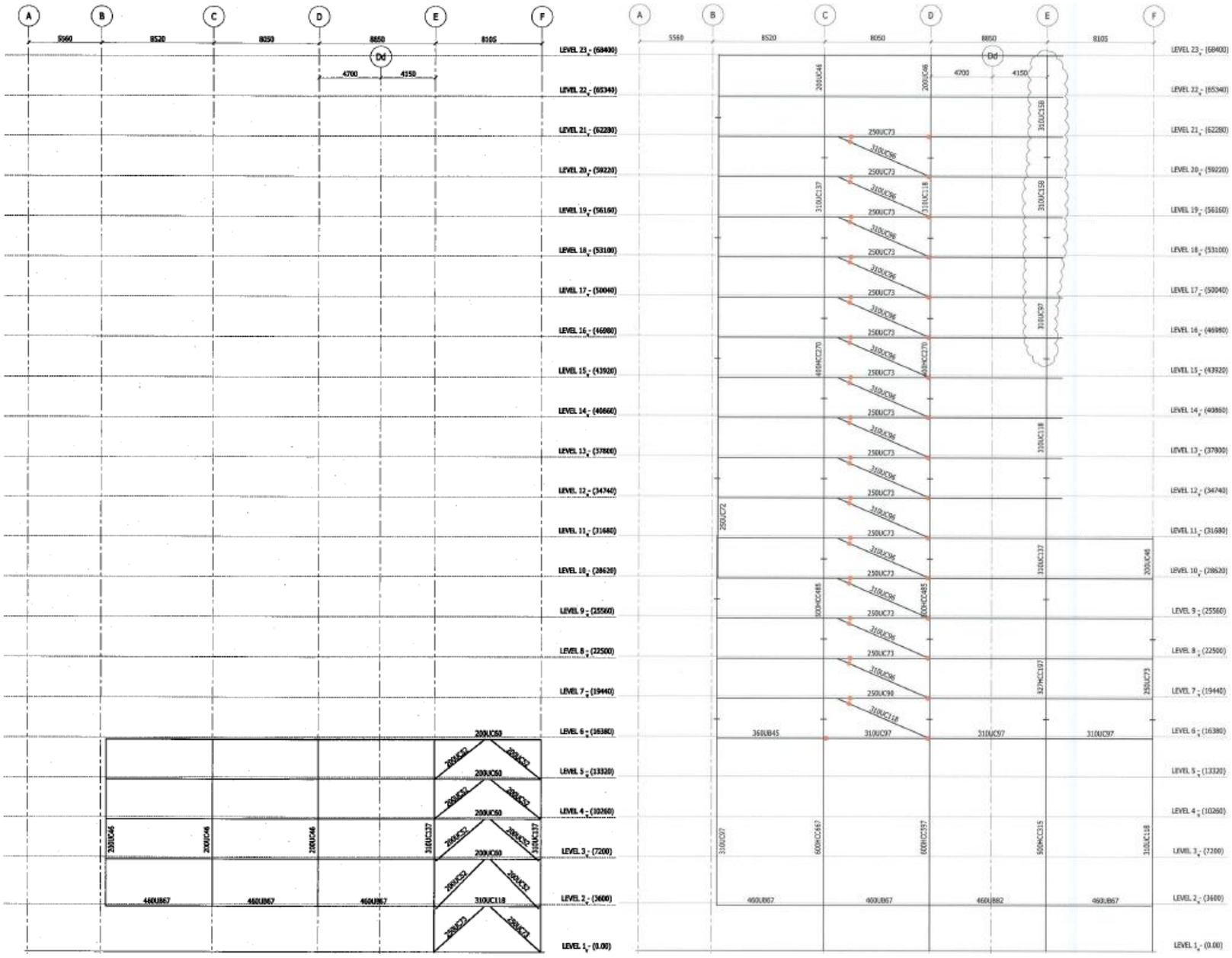

Figure G.27. Structural Elevation Grid 1 and 2 (Christchurch City Council 2016c)

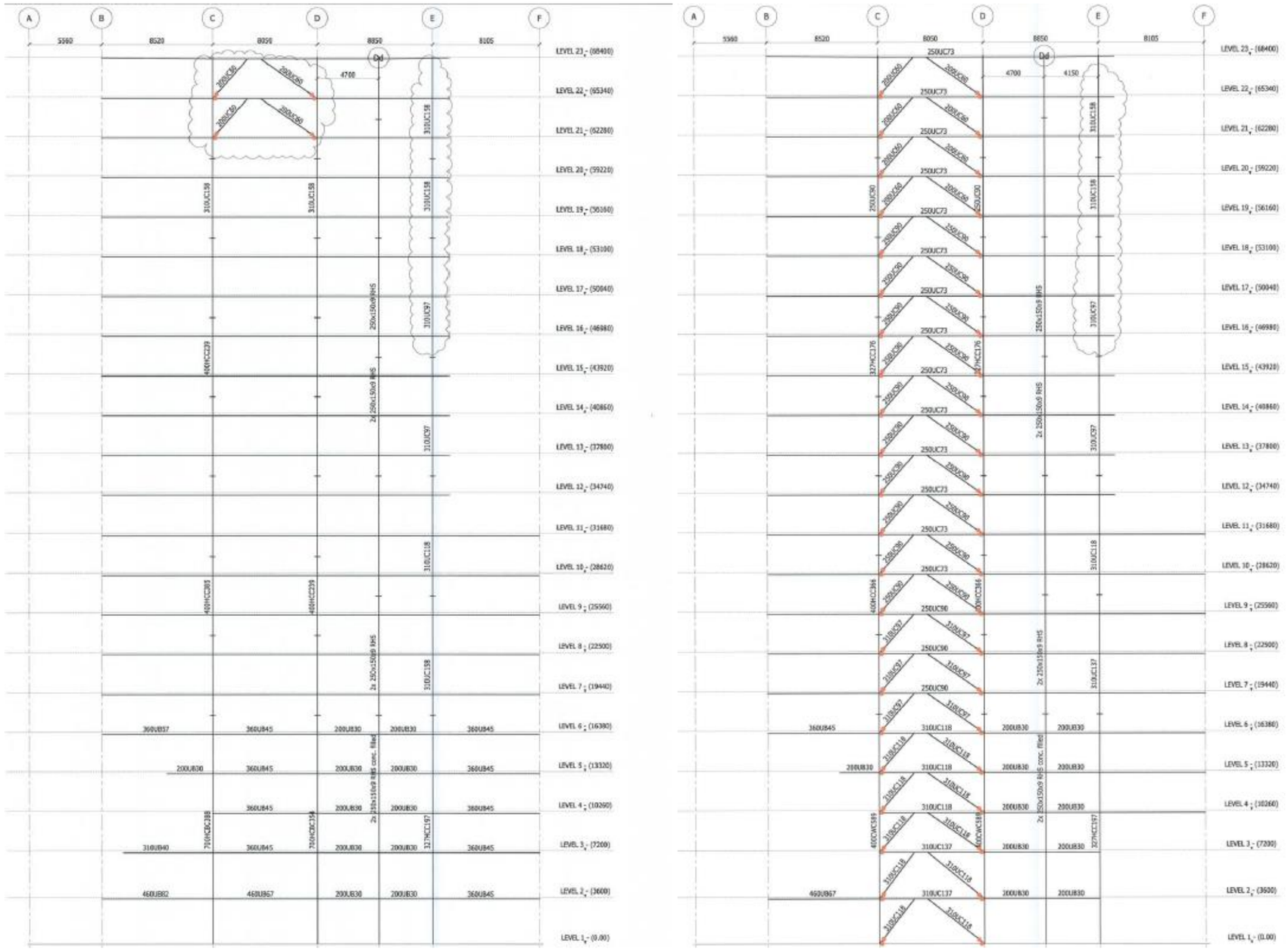

Figure G.28. Structural Elevation Grid 4 and 6 (Christchurch City Council 2016c)

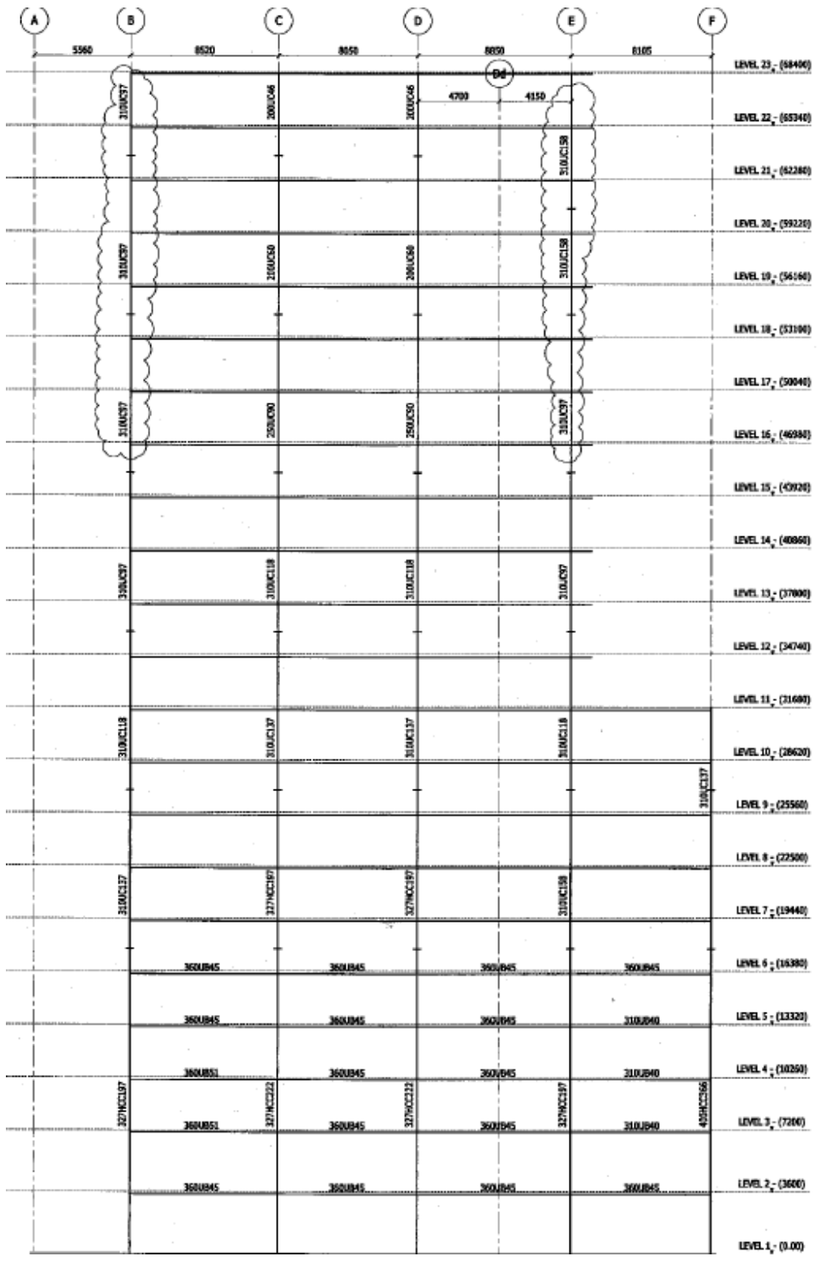

Figure G.29. Structural Elevation Grid 7 (Christchurch City Council 2016c)

References

Araya-Letelier, G., & Miranda, E. (2012). *Novel sliding/frictional connections for improved seismic performance of gypsum wallboard partitions.* Paper presented at the The 15th World Conference on Earthquake Engineering, Lisbon, Portugal.

Badillo-Almaraz, H., Whittaker, A. S., & Reinhorn, A. M. (2007). Seismic fragility of suspended ceiling systems. *Earthquake Spectra, 23*(1), 21-40.

Baird, A. (2014). *Seismic performance of precast concrete cladding systems.* (Master's Degree), University of Canterbury, New Zealand.

Baird, A., Palermo, A., & Pampanin, S. (2011). Facade damage assessment of multi-storey buildings in the 2011 Christchurch earthquake. *Bulletin of the New Zealand Society for Earthquake Engineering, 44*(4), 368-376.

Baker, J. W., & Cornell, C. A. (2006). Spectral shape, epsilon and record selection. *Earthquake Engineering & Structural Dynamics, 35*(9), 1077-1095.

Baker, J. W., & Gupta, A. (2016). Bayesian Treatment of Induced Seismicity in Probabilistic Seismic-Hazard Analysis. *Bulletin of the Seismological Society of America, 106*(3), 860-870. doi: 10.1785/0120150258

Beck, J. L., Porter, K. A., Shaikhutdinov, R., Au, S., Mizukoshi, K., Miyamura, M., Ishida, H., Moroi, T., Tsukada, Y., & Masuda, M. (2002). Impact of seismic risk on lifetime property values.

Bommer, J., Scott, S., & Sarma, S. (2000). Hazard-consistent earthquake scenarios. *Soil Dynamics and Earthquake Engineering, 19*(4), 219-231.

Bommer, J. J., & Crowley, H. (2006). The influence of ground-motion variability in earthquake loss modelling. *Bulletin of Earthquake Engineering, 4*, 231-248. doi: 10.1007/s10518-006-9008-z

Bosco, M., & Rossi, P. (2009). Seismic behaviour of eccentrically braced frames. *Engineering Structures, 31*(3), 664-674.

Bradley, B. A. (2010). A generalized conditional intensity measure approach and holistic ground-motion selection. *Earthquake Engineering & Structural Dynamics, 39*(12), 1321-1342. doi: 10.1002/eqe.995

Bradley, B. A., & Baker, J. W. (2015). Ground motion directionality in the 2010–2011 Canterbury earthquakes. *Earthquake Engineering & Structural Dynamics, 44*(3), 371-384. doi: 10.1002/eqe.2474

Bradley, B. A., Dhakal, R. P., Cubrinovski, M., MacRae, G. A., & Lee, D. S. (2008). Seismic loss estimation for efficient decision making.

Bruneau, M., Anagnostopoulou, M., MacRae, G., Clifton, C., & Fussell, A. (2010). Preliminary Report on Steel Building Damage from the Darfield Earthquake of September 4, 2010. *Bulletin of the New Zealand Society for Earthquake Engineering, 43*(4), 351-359.

Buchan, J. (2007). Internal report of non-structural and contents inventories for the Christchurch Council Chambers building. *Christchurch, New Zealand*.

Canterbury Earthquakes Royal Commission. (2011). The Performance of Christchurch CBD Buildings (Vol. 2).

Canterbury Earthquakes Royal Commission. (2012). *Final report: Volume 2: The performance of Christchurch CBD buildings*. See h ttp://canterbury. royalcommission. govt. nz/Final-Report.

Carr, A. (2004). RUAUMOKO 3D inelastic three-dimensional dynamic analysis program: User manual." University of Canterbury–Department of Civil Engineering, Christchurch, NZ.

Carr, A. (2017). 3D RUAUMOKO: inelastic three-dimensional dynamic analysis program. *Christchurch (NZ): University of Canterbury, Department of Civil Engineering*.

Christchurch City Council. (2016a). 166 Gloucester St. - Architectural Drawings.

Christchurch City Council. (2016b). 166 Gloucester St. - Construction Documents.

Christchurch City Council. (2016c). 166 Gloucester St. - Structural Drawings. Christchurch, New Zealand.

Civjan, S. A., Engelhardt, M. D., & Gross, J. L. (2000). Retrofit of pre-Northridge moment-resisting connections. *Journal of Structural Engineering*, *126*(4), 445-452.

Clifton, C., Bruneau, M., MacRae, G., Leon, R., & Fussell, A. (2011). Steel structures damage from the Christchurch earthquake series of 2010 and 2011. *Bulletin of the New Zealand Society for Earthquake Engineering*, *44*(4), 297-318.

Cornell, C. A. (1968). Engineering seismic risk analysis. *Bulletin of the Seismological Society of America*, *58*(5), 1583-1606.

Corus New Zealand. (2005). ComFlor 80 Composite Floor Decking. *Auckland, NZ*.

Crisafulli, F. J. (1997). Seismic behaviour of reinforced concrete structures with masonry infills.

Davies, R. D., Retamales, R., Mosqueda, G., & Filiatrault, A. (2011). Seismic Evaluation Parameterization and Effects of Steel Framed Gypsum Partition Walls on The Seismic Performance of an Essential Facility. New York.

Deierlein, G., Krawinkler, H., & Cornell, C. (2003). *A Framework for Performance-Based Earthquake Engineering.* Paper presented at the Pacific Conference on Earthquake Engineering.

Dhakal, R. P., Pourali, A., & Saha, S. K. (2016). SIMPLIFIED SEISMIC LOSS FUNCTIONS FOR SUSPENDED CEILINGS AND DRYWALL PARTITIONS. *Bulletin of the New Zealand Society for Earthquake Engineering*, *49*(1).

EERI. (2012). The 2010 Canterbury and 2011 Christchurch New Zealand Earthquakes and the 2011 Tohoku Japan Earthquake: Emerging Needs and Opportunities.

EERI. (2016). EERI Response to M7.0 Earthquake in Kumamoto, Japan on April 15, 2016.

FEMA. (2000). Commentary for the seismic rehabilitation of buildings, report FEMA-356. *Washington, DC: SAC Joint Venture for the Federal Emergency Management Agency*.

FEMA. (2011). E-74. *Reducing the Risks of Nonstructural Earthquake Damage: A Practical Guide*.

FEMA P-58.3. *FEMA P58.3: PACT*. Paper presented at the Proc., 15th World Conf. on Earthquake Engineering.

Fukuyama, H., & Sugano, S. (2000). Japanese seismic rehabilitation of concrete buildings after the Hyogoken-Nanbu Earthquake. *Cement and Concrete Composites, 22*(1), 59-79.

Gardiner, S. (2012). Post-Earthquake Assessment Detailed Engineering Evaluation and Repair Recommendations. Christchurch, New Zealand.

Gardiner, S., Clifton, G., & MacRae, G. (2013). *Performance, Damage Assessment and Repair of a Multistorey Eccentrically Braced Framed Building Following the Christchurch Earthquake Series.* Paper presented at the Steel Innovations Conference 2013.

Goda, K., & Taylor, C. A. (2012). Effects of aftershocks on peak ductility demand due to strong ground motion records from shallow crustal earthquakes. *Earthquake Engineering & Structural Dynamics, 41*(15), 2311-2330.

Google Street View. (2016). Pacific Tower.

Gupta, A. K. (1992). *Response spectrum method in seismic analysis and design of structures* (Vol. 4): CRC press.

Hanganu, A. D., Onate, E., & Barbat, A. H. (2002). A finite element methodology for local/global damage evaluation in civil engineering structures. *Computers & Structures, 80*(20), 1667-1687.

Hogg, K., MacRae, G. A., & Dhakal, R. (2011). Performance of ceilings in the February 2011 Christchurch earthquake.

Holmes, M. (1961). STEEL FRAMES WITH BRICKWORK AND CONCRETE INFILLING. *proceedings of the Institution of civil Engineers, 19*(4), 473-478. doi: 10.1680/iicep.1961.11305

Ibarra, L. F., Medina, R. A., & Krawinkler, H. (2005). Hysteretic models that incorporate strength and stiffness deterioration. *Earthquake Engineering & Structural Dynamics, 34*(12), 1489-1511.

Iervolino, I. (2017). Assessing uncertainty in estimation of seismic response for PBEE. *Earthquake Engineering & Structural Dynamics*.

Iervolino, I., Giorgio, M., & Chioccarelli, E. (2014). Closed-form aftershock reliability of damage-cumulating elastic-perfectly-plastic systems. *Earthquake Engineering & Structural Dynamics, 43*(4), 613-625.

Jalayer, F., & Ebrahimian, H. (2017). Seismic risk assessment considering cumulative damage due to aftershocks. *Earthquake Engineering & Structural Dynamics, 46*(3), 369-389.

Japan Building Disaster Prevention Association. (2011). *2011 Nen kaichōban - Taishin kaishū sokushin-hō no tame no kizon tekkotsudzukuri kenchiku-mono no taishin shindan oyobi taishin kaishū shishin - Dō kaisetsu [Earthquake-Resistant Diagnosis and Earthquake Retrofit Guidelines*

and Explanation for Existing Steel-Framed Buildings for Seismic Repair Promotion Law 2011 Revised Edition - The Same Commentary].

Jeon, J. S., DesRoches, R., Lowes, L. N., & Brilakis, I. (2015). Framework of aftershock fragility assessment–case studies: older California reinforced concrete building frames. *Earthquake Engineering & Structural Dynamics, 44*(15), 2617-2636.

Kappos, A. J., & Dimitrakopoulos, E. G. (2008). Feasibility of pre-earthquake strengthening of buildings based on cost-benefit and life-cycle cost analysis, with the aid of fragility curves. *Natural hazards, 45*(1), 33-54. doi: 10.1007/s11069-007-9155-9

Kappos, A. J., Penelis, G. G., & Drakopoulos, C. G. (2002). Evaluation of simplified models for lateral load analysis of unreinforced masonry buildings. *Journal of Structural Engineering, 128*(7), 890-897.

Lang, D. H., Singh, Y., & Prasad, J. (2012). Comparing empirical and analytical estimates of earthquake loss assessment studies for the city of Dehradun, India. *Earthquake Spectra, 28*(2), 595-619.

Li, Q., & Ellingwood, B. R. (2007). Performance evaluation and damage assessment of steel frame buildings under main shock–aftershock earthquake sequences. *Earthquake Engineering & Structural Dynamics, 36*(3), 405-427.

Luco, N., Bazzurro, P., & Cornell, C. A. (2004). *Dynamic versus static computation of the residual capacity of a mainshock-damaged building to withstand an aftershock.* Paper presented at the Proceedings of the 13th world conference on earthquake engineering.

Lupoi, G., Franchin, P., Lupoi, A., & Pinto, P. E. (2006). Seismic fragility analysis of structural systems. *Journal of Engineering Mechanics, 132*(4), 385-395.

MathWorks, I. (2005). *MATLAB: the language of technical computing. Desktop tools and development environment, version 7* (Vol. 9): MathWorks.

McGuire, R. K. (1995). Probabilistic seismic hazard analysis and design earthquakes: Closing the loop. *Bulletin of the Seismological Society of America, 85*(5), 1275-1284.

McGuire, R. K., Cornell, C. A., & Toro, G. R. (2005). The Case for Using Mean Seismic Hazard. *Earthquake Spectra, 21*(3), 879-886. doi: doi:10.1193/1.1985447

McVerry, G. H., Zhao, J. X., Abrahamson, N. A., & Somerville, P. G. (2006). New Zealand acceleration response spectrum attenuation relations for crustal and subduction zone earthquakes. *Bulletin of the New Zealand Society for Earthquake Engineering, 39*(1), 1-58.

Mitrani-Reiser, J. (2007). *An ounce of prevention: probabilistic loss estimation for performance-based earthquake engineering.* California Institute of Technology.

Naeim, F., & Lew, M. (1995). On the use of design spectrum compatible time histories. *Earthquake Spectra, 11*(1), 111-127.

National Research Council. (2003). *Living on an Active Earth: Perspectives on Earthquake Science*. Washington, DC: The National Academies Press.

National Research Institute for Earth Science and Disaster Resilience. (2017). *Strong-motion Seismograph Networks (K-Net and KiK-net)*.

Newman, A. (2001). *Structural renovation of buildings: Methods, details, and design examples*: McGraw-Hill.

NZS. (2002). 1170.1: 2002—structural design actions. *Wellington, New Zealand: Standards New Zealand*.

NZS. (2007). NZS3404 Part 1: and2 1997 (Incorporating Amendment 1 and 2). *Standards New Zealand, Wellington*.

O'Reilly, G. J., & Sullivan, T. J. (2016). Fragility functions for eccentrically braced steel frame structures. *Earthquakes and Structures, 10*(2), 367-388.

Oakley, J. (2008). Simpson Anchors Presentation.

Paganotti, G., MacRae, G., & Dhakal, R. (2011). *Development of typical NZ ceiling system seismic fragilities.* Paper presented at the Ninth Pacific Conference on Earthquake Engineering (PCEE).

Poland, C., Hill, J., & Sharpe, R. (1995). *Performance Based Seismic Engineering of Buildings* (J. Soulages Ed.). Sacramento, Calif: Structural Engineers Association of California.

Porter, K. A. (2003). *An overview of PEER's performance-based earthquake engineering methodology.* Paper presented at the Proceedings of Ninth International Conference on Applications of Statistics and Probability in Civil Engineering.

Porter, K. A., & Beck, J. L. (2004). *Simplified PBEE to Estimate Economic Seismic Risk for Buildings.* Paper presented at the Proceedings of the International Workshop on Performance-Based Seismic Design.

Porter, K. A., Kiremidjian, A. S., & LeGrue, J. S. (2001). Assembly-based vulnerability of buildings and its use in performance evaluation. *Earthquake Spectra, 17*(2), 291-312.

Priestley, M., Calvi, G., & Kowalsky, M. (2007). *Direct displacement-based seismic design of structures.* Paper presented at the 5th New Zealand Society for Earthquake Engineering Conference.

Priestley, M., & Paulay, T. (1992). Seismic design of reinforced concrete and masonry buildings. *New York: John Wiley & Sons, Inc*.

Ramset. (2017). Ramset TruBolt (TM) Stud Anchors Brochure.

Reiter, L. (1991). *Earthquake hazard analysis: issues and insights*: Columbia University Press.

Ricles, J. M., & Popov, E. P. (1987). *Experiments on eccentrically braced frames with composite floors*: Earthquake Engineering Research Center, University of California.

Ricles, J. M., & Popov, E. P. (1989). Composite action in eccentrically braced frames. *Journal of Structural Engineering, 115*(8), 2046-2066.

Ricles, J. M., & Popov, E. P. (1994). Inelastic Link Element for EBF Seismic Analysis. *Journal of Structural Engineering, 120*(2), 441-463. doi: doi:10.1061/(ASCE)0733-9445(1994)120:2(441)

Roy, N., Labossière, P., Proulx, J., St-Georges, É., & Paultre, P. (2009). FRP Wrapping of RC Structures Submitted to Seismic Loads *Seismic Risk Assessment and Retrofitting* (pp. 297-305): Springer.

Ruiz-García, J., & Negrete-Manriquez, J. C. (2011). Evaluation of drift demands in existing steel frames under as-recorded far-field and near-fault mainshock–aftershock seismic sequences. *Engineering Structures, 33*(2), 621-634.

Spence, R., Bommer, J., del Re, D., Bird, J., Aydinoğlu, N., & Tabuchi, S. (2003). Comparing Loss Estimation with Observed Damage: A Study of the 1999 Kocaeli Earthquake in Turkey. *Bulletin of Earthquake Engineering, 1*(1), 83-113. doi: 10.1023/a:1024857427292

Sullivan, T. J. (2013). Direct displacement-based seismic design of steel eccentrically braced frame structures. *Bulletin of Earthquake Engineering, 11*(6), 2197-2231. doi: 10.1007/s10518-013-9486-8

Welch, D., Sullivan, T., & Calvi, G. (2014). Developing direct displacement-based procedures for simplified loss assessment in performance-based earthquake engineering. *Journal of Earthquake Engineering, 18*(2), 290-322.

Williams, R. J., Gardoni, P., & Bracci, J. M. (2009). Decision analysis for seismic retrofit of structures. *Structural Safety, 31*(2), 188-196.

Wilson, E. L., & Habibullah, A. (2002). Structural analysis program SAP2000. *Computers and Structures Inc., California*.

Wilson, E. L., Hollings, J., & Dovey, H. H. (1979). *Etabs: Three dimensional analysis of building systems (extended version)*: National Information Service for Earthquake Engineering/Computer Applications, Earthquake Engineering Research Center, University of California.

Wotherspoon, L. M., Palermo, A., & Holden, C. (2017). THE 2016 MW7.8 KAIKŌURA EARTHQUAKE: AN INTRODUCTION *Bulletin of NZSEE, 50*(2).

Yeow, T., Orumiyehei, A., Sullivan, T., MacRae, G., Clifton, C., & Elwood, K. (2017). Seismic Performance of The Sliding Hinge Joint Considering Limit States. *Under Review*.

Yeow, T., & Sullivan, T. (2017). Development of Testbed Floor-plan Layout for Seismic Loss Estimation Studies. *In Progress*.

Yeow, T. Z., MacRae, G. A., & Dhakal, R. P. (2016). Wall building stiffness and strength effect on content sliding in Wellington seismic conditions. *Earthquake Engineering & Structural Dynamics*.

Zareian, F., & Krawinkler, H. (2006). *Simplified performance-based earthquake engineering.* Stanford University Stanford, CA, USA.